CHARACTERISATION OF PEDOT AND ITS DERIVATIVES IN ELECTROCHEMICAL SENSING APPLICATIONS

YUSRAN SULAIMAN

CHARACTERISATION OF PEDOT AND ITS DERIVATIVES IN ELECTROCHEMICAL SENSING APPLICATIONS

A thesis submitted for the partial fulfillment of the requirements for the degree of

Doctor of Philosophy

by

Yusran Sulaiman

Department of Chemistry
University of Durham

2012

ABSTRACT

The emergence of a new class of polymer, namely conducting polymers (CPs) in late 1970s, has attracted many physicists, chemists and materials researchers to study them in depth due to the unique properties and broad applications of this material. Poly (3,4-ethylenedioxythiophene) (PEDOT) has been found to be the most chemically stable CP to date. The aim of this project was to characterise PEDOT and its derivatives for applications in ion sensing. In this work, PEDOT and its derivatives *i.e.* poly(3,4-propylenedioxythiophene) (PProDOT) and poly(3,3-dibenzyl-3,4-propylenedioxythiophene) (PDBPD) doped with perchlorate (ClO_4^-) have been electrochemically synthesised on glassy carbon (GC) and indium-tin-oxide coated glass (ITO) electrodes in acetonitrile. PEDOTs were also prepared in aqueous solutions using perchlorate (ClO_4^-) and chloride (Cl^-) counterions as comparison. Scanning electron microscopy (SEM), atomic force microscopy (AFM), contact angle (CA) measurements and Raman spectroscopy have been used to characterise the physical properties of the polymer coated glassy carbon (GC) and ITO electrodes. PDBPD has shown to have the most compact morphology, roughest and least wettable surface. The electrochemical studies have shown that PEDOT has the highest capacitive current. The combination of this property and mixed electronic and ionic conductivity make the PEDOT suitable to be used as a solid contact (transducer) in all-solid-state ion-selective electrode (ASSISE). PEDOT doped with poly(sodium 4-styrenesulfonate) (PSS) was found to be superior to hyaluronic acid (HA) as a solid contact for ASS Ca^{2+}-, K^+- and Na^+-selective electrodes. Measurements of Ca^{2+} and K^+ upon plant stress using ion ion-selective microelectrodes have been demonstrated. Chiral electrodes based on electrodeposited PEDOT doped with chiral molecules (collagen, HA and hydroxypropyl cellulose) were shown to discriminate between (*R*)-(−)- and (*S*)-(+)-mandelic acid. The work carried out in this thesis has shown that PEDOT is one of the most versatile conducting polymers.

DECLARATION

The work described herein was carried out in the Department of Chemistry, University of Durham. All the work is my own unless otherwise stated and no part of it has been submitted for a degree at this or any other university.

Statement of Copyright

ACKNOWLEGEMENTS

In the name of Allah, the Most Gracious, the Most Merciful

'*Alhamdulillah*'. With the aid of the Almighty Allah, I have managed to accomplish the writing of this thesis. Thank God for the strength that has been bestowed upon me, without which this thesis might not have been completed.

I would like to take this opportunity to express my token of appreciation to those who have helped me a lot throughout this thesis. This thesis would not have been possible without the support of many people.

First of all, I would like to express my sincere thanks to my supervisor Dr. Ritu Kataky for her encouragement, help, excellent advice, guidance, constructive criticism and valuable suggestions besides sharing her knowledge with me. Thank you very much for being there with all the inspiration, wisdom and optimism that always helped me to see the bright side of things.

Special thanks also to all my labmates, Ruzniza, Rui, Paula, Alice, Darius, Rachael, Dr. Anil, Dr. Francisco, Dr. Ioana and Dr. Inderpreet, for their help, support, sharing the knowledge and useful discussion throughout this thesis. Thank you to people in School of Biological and Biomedical Science, particularly Prof. Marc Knight for the information and materials for *Arabidopsis thaliana*.

I would like to acknowledge Mr. Leon Bowen and Ms. Helen Riggs for the ESEM and FESEM measurements. I would also like to thank Dr. Richard Thompson for teaching me how to carry out AFM measurements and analyses.

I should also truly be thankful for much help from the mechanical and electrical workshop staff. They are Kelvin Appleby, Omer Ekinoglu, Barry T. Barker, Neil Holmes and Scott Ramsey. They have given their support when their help was needed. I cannot forget to thank to all the Malaysian communities in the United Kingdom, particularly in Durham for making the environment very welcoming to me.

I would also like to convey my thanks to Department of Chemistry, University of Durham for providing laboratory facilities and to my sponsor Ministry of Higher Education, Malaysia and Universiti Putra Malaysia (UPM) for the financial means. I would also like to express my sincere thanks to Graduate School and ITS, University of Durham for providing useful training courses.

Most importantly, I would like to express a huge debt of gratitude to my beloved wife, Siti Aisyah and my daughter Nur Amani for all the support and patience. They are the people who were on my side with tremendous perseverance at each and every difficult stage during this work. Your constant encouragement and motivations have made this period less stressful. Last but not least, I am thankful to family for their understanding, patience and endless support without seeking anything in return.

Once again

Thank you

DEDICATION

To my wife, Siti Aisyah and my daughter, Nur Amani…

PUBLICATIONS

1. Sulaiman, Y. and Kataky, R. (2012) Effect of Monomer Modifications on The Physical properties of Electropolymerised PEDOT Films (2012). *Journal of The Electrochemical Sociecty*. 159. F1-F9.

2. Sulaiman, Y. and Kataky, R. (2012) Chiral Acid Selectivity Displayed by PEDOT Electropolymerised in Presence of Chiral Molecules. *Analyst*. 137(10), 2386-2393.

3. Sulaiman, Y. and Kataky, R. (2012) Non-invasive Monitoring of Temperature Stress in *Arabidopsis Thaliana* roots, using Ion Amperometry. *Analytical Methods*. (accepted)

TABLE OF CONTENT

LIST OF SYMBOLS

Symbol	Meaning	Usual unit
a	activity	-
A	area	cm^2
C	capacitance	F
C	concentration	$M/mol\ dm^{-3}$
C_{dl}	double layer capacitance	F
D	diffusion coefficient	$cm^2\ s^{-1}$
E	electrode potential	V
$E^{0'}$	formal potential	V
E_g	band gap	eV
E_{pa}	anodic peak potential	V
E_{pc}	cathodic peak potential	V
$E_{p/2}$	half peak potential potential where $i = i_{p/2}$	V
$E_{1/2}$	half wave potential	V
E_F	Fermi level	eV
$E°$	standard electrode potential	V
f	frequency	s^{-1} / Hz
F	Farads	F
F	Faraday constant	$C\ mol^{-1}$
I_{pa}	anodic peak current	A
I_{pc}	cathodic peak current	A
I	current	A
k_o	heterogenous rate constant	$cm\ s^{-1}$
R	gas constant	$J\ K^{-1}\ mol^{-1}$
R_{ct}	resistance of charge transfer	Ω
R_s	resistance of solution	Ω
t	time	s

T	temperature	ºC
z	charge on an ion in signed units of electronic charge	
Z	Impedance	Ω
Z'	real impedance	Ω
Z''	imaginary impedance	Ω
Z_w	Warburg impedance	Ω
ºC	celcius	ºC
ϕ	phase angle between two sinusoidal signals	º
θ_a	advancing contact angle	º
θ_r	receding contact angle	º
γ	level of doping	
$\mathbf{\Delta}E_p$	peak separation (E_{pa} -E_{pc})	V
$\mathbf{\Delta\theta}$	contact angle hysteresis	º

LIST OF ABBREVIATIONS

Abbreviation	Meaning
A	ampere
ACN	acetonitrile
AFM	atomic force microscopy
Ag/AgCl	silver/silver chloride
ASS	all-solid-state
ASSISE	all-solid-state ion-selective electrode
C	Coulomb
CE	counter electrode
ClO_4^-	perchlorate anion
CNIn	5-cyanoindole
CP	conducting polymer
CPE	constant phase element
CTAB	cetyltrimethylammonium bromide
CV	cyclic voltammetry/voltammogram
CWE	coated-wire electrode
DBPD	3,3-dibenzyl-3,4-propylenedioxythiophene
DM	*N*-dodecyl-β-D-maltoside
EIS	electrochemical impedance spectroscopy
EDOT	3,4-ethylenedioxythiophene
ESEM	environmental scanning electron microscopy
FESEM	field emission scanning electron microscopy
FTP	3-(-4-fluorophenyl)thiophene
GC	glassy carbon
GC/PDBPD/$LiClO_4$(ACN)	PDBPD coated GC electrode prepared in acetonitrile containing $LiClO_4$
GC/PEDOT/HA	PEDOT coated GC electrode prepared in hyaluronic acid

GC/PEDOT/HA-Ca^{2+}	calcium membrane cover on PEDOT/HA/GC
GC/PEDOT/HA-K^{+}	potassium membrane cover on PEDOT/HA/GC
GC/PEDOT/HA-Na^{+}	sodium membrane cover on PEDOT/HA/GC
GC/PEDOT/KCl(Aq)	PEDOT coated GC electrode prepared in aqueous solution containing KCl
GC/PEDOT/$LiClO_4$(ACN)	PEDOT coated GC electrode prepared in acetonitrile containing $LiClO_4$
GC/PEDOT/$LiClO_4$(Aq)	PEDOT coated GC electrode prepared in aqueous solution containing $LiClO_4$
GC/PEDOT/PSS	PEDOT coated GC electrode prepared in NaPSS
GC/PEDOT/PSS-Ca^{2+}	calcium membrane cover on PEDOT/PSS/GC
GC/PEDOT/PSS-K^{+}	potassium membrane cover on PEDOT/PSS/GC
GC/PEDOT/PSS-Na^{+}	sodium membrane cover on PEDOT/PSS/GC
GC/PProDOT/$LiClO_4$(ACN)	PProDOT coated GC electrode prepared in acetonitrile containing $LiClO_4$
HA	hyaluronic acid
HPC	hydroxypropyl cellulose
Hz	Hertz
ISE	ion-selective electrode
ISM	ion-selective membrane
ITO	indium-tin-oxide coated glass
ITO/PDBPD/$LiClO_4$(ACN)	PDBPD coated ITO electrode prepared in acetonitrile containing $LiClO_4$
ITO/PEDOT/KCl(Aq)	PEDOT coated ITO electrode prepared in aqueous solution containing KCl
ITO/PEDOT/$LiClO_4$(ACN)	PEDOT coated ITO electrode prepared in acetonitrile containing $LiClO_4$
ITO/PEDOT/$LiClO_4$(Aq)	PEDOT coated ITO electrode prepared in aqueous solution containing $LiClO_4$
ITO/PProDOT/$LiClO_4$(ACN)	PProDOT coated ITO electrode prepared in acetonitrile containing $LiClO_4$

KCl	potassium chloride
$LiClO_4$	lithium perchlorate
LOD	limit of detection
M	molar
MS	Murashige and Skoog medium
mM	milimolar
mV	millivolt
NaPSS	poly(sodium 4-styrenesulfonate)
nm	nanometer
PA	polyacetylene
PAn	polyaniline
PCDM	poly (4-(dicyanomethylene)-4*H*-cyclopenta bydithiophene)
PCln	PCln : poly (5-cyanoindole)
PDBPD	poly(3,3-dibenzyl-3,4-propylenedioxythiophene)
PEDOT	poly(3,4-ethylenedioxythiophene)
PEDOT/collagen	PEDOT doped with collagen
PEDOT/HA	PEDOT doped with hyaluronic acid
PEDOT/HPC	PEDOT doped with hydroxypropyl cellulose
PEDOT/PSS	PEDOT doped with polystrenesulfonate
PEDTM	poly (2,3-dihydrothieno[3,4-*b*]-1,4-dioxyn-2-yl methanol)
PNTP	poly (1-(4-nitrophenyl)-2,5-di(2-thienyl)-1H-pyrrole)
PProDOT	poly(3,4-propylenedioxythiophene)
PPy	polypyrrole
ProDOT	3,4-propylenedioxythiophene
PSS	polystyrene sulfonate
PTh	polythiophene
Pt	platinum

r.m.s	root mean square
RE	reference electrode
RSD	relative standard deviation
SCE	saturated calomel electrode
SD	standard deviation
SDBS	sodium dodecylbenzenesulfate
SDS	sodium dodecylsulfate
SEM	scanning electron microscopy
TBAP	tetrabutylammonium perchlorate
Triton X-100	polyethylene glycol octylphenyl ether
V	volts
WE	working electrode

LIST OF FIGURES

LIST OF TABLES

CHAPTER 1

INTRODUCTION

1.1 General Introduction

Conducting polymers (CPs) also known as 'synthetic metals' are materials discovered about 35 years ago that have emerged as one of the most exciting and interdisciplinary areas in science and engineering. The knowledge in this field has grown rapidly and many CPs based on polyanilines, polypyrroles and polythiophenes have been synthesised (Cadogan *et al.*, 1992, Hiller *et al.*, 1996, Hwang *et al.*, 2003). Of the many CPs, poly(3,4-ethylenedioxythiophene) (PEDOT), a derivative of polythiophene, possesses some advantages such as very high conductivity (ca. 300 S/m), good optical transparency in the visible spectral region and very high stability in the oxidised state. As a result, many applications of PEDOT have been rapidly developed such as electrochromic devices, solid state capacitors and electrochemical sensors (Groenendaal *et al.*, 2000). However, in depth studies of physical and electrochemical properties of PEDOT derivatives are still lacking. This has prompted us to study more detail of the PEDOT derivatives namely, poly(3,4-propylenedioxythiophene) (PProDOT) and poly(3,3-dibenzyl-3,4-propylenedioxythiophene) (PDBPD).

The growing demands for developing fast, robust and easy to miniaturise devices for monitoring analyte particularly ions make CPs good candidates for developing electrochemical sensors. One of the important subgroup of electrochemical sensors is potentiometric ion sensors, also known as ion-selective electrodes (ISE). Due to mixed electronic and ionic conductivity, CPs can be used as ion-to-electron transducers between the electronic conductor and the ion-selective membrane. This configuration will eliminate the use of filling solution that is commonly use in conventional ISEs and results

in an all-solid-state ISE (ASSISE). PEDOT has shown to be prominent in this type of sensors due to high potential stability (Bobacka, 1999).

Furthermore, the properties of conducting polymers can be tailored via functionalisation, for instance, by covalent bonding of side groups to the conjugated polymer backbone (Elsenbaumer *et al.*, 1985) and by the incorporation of different doping anions during the electropolymerisation process (Goto and Akagi, 2006). This important feature makes CPs suitable as chiral selectors. It is known that many of the most important molecules in living systems are chiral e.g. proteins, amino acids, sugars and nucleic acids. In nature, these molecules exist in only one of two possible enantiomeric forms (Crossley, 1995). In most cases, only one enantiomer of a chiral molecule is desired. In the case of chiral drug, one enantiomer may perform the task in living systems, the other may be inactive or even toxic. Therefore, fabrication of chiral sensors is important.

1.2 Aim of Research

Poly(3,4-ethylenedioxythiophene) (PEDOT) which is a derivative of polythiophene has been chosen for the study in this research as this conducting polymer is the most chemically stable to date (Groenendaal *et al.*, 2000) due to the presence of two O-electron donating groups at the position 3 and 4 of thiophene that stabilise the structure of PEDOT. Due to the intrinsic features of PEDOT, the ultimate goal of this research is to use PEDOT modified electrodes as a platform for ion sensing.

The objectives of the present thesis are as follows:

(i) To electropolymerise PEDOT and its derivatives *i.e.* poly (3,4-propylenedioxythiophene) (PProDOT) and poly(3,3-dibenzyl-3,4-propylenedioxythiophene) (PDBPD) doped with perchlorate ion (ClO_4^-) on glassy carbon and ITO electrodes in acetonitrile.

(ii) To electropolymerise PEDOT in aqueous solution containing chloride (Cl^-) and ClO_4^- on glassy carbon and ITO electrodes.

(iii) To characterise, analyse and compare the physical properties of conducting polymers prepared in (i) and (ii) by various techniques, namely scanning electron microscopy, atomic force microscopy, contact angle measurements and Raman spectroscopy.

(iv) To understand and evaluate the electrochemical properties of conducting polymers prepared in (i) and (ii) by means of cyclic voltammetry (CV) and electrochemical impedance spectroscopy (EIS).

(v) To fabricate and characterise all-solid-state calcium-, potassium- and sodium-selective electrodes based on PEDOT doped with poly(styrenesulfonate) (PSS) and hyaluronic acid (HA).

(vi) To demonstrate the application of all-solid-state ion-selective microelectrodes as chemical sensors to detect calcium and sodium in real samples.

(vii) To fabricate chiral selectors based on PEDOT and demonstrate chiral discrimination between enantiomers of mandelic acid.

1.3 Overview of Thesis

This thesis comprises of nine chapters. The first chapter (**Chapter 1**) provides a brief introduction and the motivation to do the work describe in this thesis. The objectives of the study are outlined.

Chapter 2 explains the background and general properties of conducting polymers. Some literature related to the synthesis and applications of PEDOT are also discussed. **Chapter 3** describes electrochemical sensors particularly potentiometric sensors and chiral sensors. The experimental techniques used in this work and the fundamental principles of electrochemistry are explained in **Chapter 4**.

In **Chapter 5**, the focus is on the preparation and physical characterisation of PEDOT and its derivatives. PEDOT and its derivatives (PProDOT and PDBPD) were synthesised by potentiodynamic methods and characterised by means of environmental scanning electron microscopy (ESEM), scanning electron microscopy (SEM), atomic force microscopy (AFM), contact angle measurement (CA) and Raman spectroscopy.

The electrochemical characteristics of the conducting polymer films (PEDOT, PProDOT and PDBPD) coated on GC and ITO glass electrodes are discussed in **Chapter 6**. PEDOT doped with bulky dopants *i.e.* poly(styrenesulfonate) (PSS) and hyaluronic acid (HA) used for cationic potentiometric ion sensing measurements are described in **Chapter 7**. The applications of the all-solid-state ion selective microelectrodes to monitor cellular activity are also discussed. Discrimination between (*R*)-(−)- and (*S*)-(+)-mandelic acid using chiral sensors based on PEDOT doped with chiral molecules is demonstrated in **Chapter 8**. Finally, **Chapter 9** summarises all the major conclusions of the present study. Some recommendations for future studies are also included.

References

Bobacka, J. (1999) Potential Stability of All-Solid-State Ion-Selective Electrodes Using Conducting Polymers As Ion-to-Electron Transducers. *Analytical Chemistry.* 71**.** 4932-4937.

Cadogan, A., Lewenstam, A. and Ivaska, A. (1992) Anionic Responses of Electrochemically Synthesized Polypyrrole Films. *Talanta.* 39**.** 617-620.

Crossley, R. J. (1995) *Chirality and The Biological Activity of Drugs.* Boca Raton, CRC-Press.

Elsenbaumer, R. L., Eckhardt, H., Iqbal, Z., Toth, J. and Baughman, R. H. (1985) Chiral Metals: Synthesis and Properties of a New Class of Conducting Polymers *Molecular Crystals and Liquid Crystals.* 118**.** 111-116.

Goto, H. and Akagi, K. (2006) Optically Active Electrochromism of Poly(3,4-Ethylenedioxythiophene) Synthesized by Electrochemical Polymerization in Lyotropic Liquid Crystal of Hydroxypropyl Cellulose/Water: Active Control of Optical Activity. *Chemistry of Materials.* 18**.** 255-262.

Groenendaal, B. L., Jonas, F., Freitag, D., Pielartzik, H. and Reynolds, J. R. (2000) Poly(3,4-Ethylenedioxythiophene) and Its Derivatives: Past, Present, and Future. *Advanced Materials.* 12**.** 481-494.

Hiller, M., Kranz, C., Huber, J., Bauerle, P. and Schuhmann, W. (1996) Amperometric Biosensors Produced by Immobilization of Redox Enzymes at Polythiophene-Modified Electrode Surfaces. *Advanced Materials.* 8**.** 219-222.

Hwang, B.-J., Santhanam, R., Wu, C.-R. and Tsai, Y.-W. (2003) Nucleation and growth mechanism for the electropolymerization of aniline in trifluoroacetic acid/lithium perchlorate/propylene carbonate medium. *Journal of Solid State Electrochemistry.* 7**.** 678-683.

CHAPTER 2

POLY(3,4-ETHYLENEDIOXYTHIOPHENE) (PEDOT)

2.1 Background

Polymers are macromolecules that are built from basic repeating units called monomers which are connected to each other by covalent bonds. It has been known for ages that many polymers are excellent insulators (e.g. polystyrene, polypropylene and polyethylene) that have significant advantages for many applications. The advantages include the flexibility of the polymer to make plastics and resist the flow of a current. However, a new concept of conducting or semiconducting polymers has been established since the first breakthrough by Shirakawa and co-workers (Shirakawa *et al.*, 1977), in which polyacetylene (PA) become conducting polymer when it was doped by iodine. This finding occurred accidentally when a student added one thousand times more catalyst in the production of acetylene and a beautiful silvery film was formed on the surface of the liquid in the vessel. Based on this finding, they found out that the film had very high conductivity (~ 10^3 S cm^{-1}) when it was doped with iodine in comparison to the undoped acetylene (10^{-5} S cm^{-1}). Due to the extensive research by Shirakawa and his co-workers in conducting polymers (CPs), they received the award of the Nobel Prize in 2000 in Chemistry.

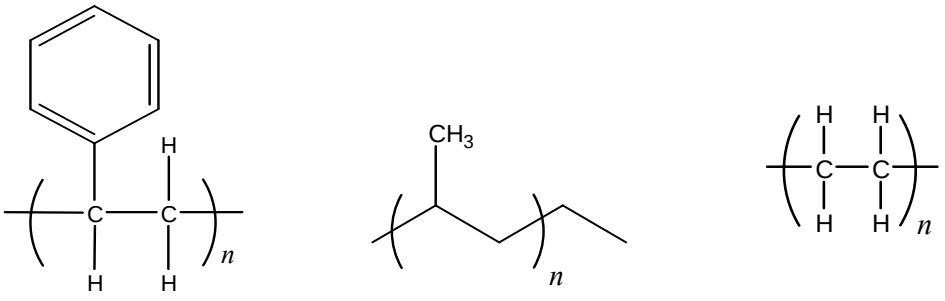

(a) (b) (c)

Figure 2.1: Insulating polymers: (a) polystyrene (b) polypropylene and (c) polyethylene.

Generally, CPs (also known as 'synthetic metals') are organic polymer semiconductors or organic semiconductors that can conduct electricity. Since the discovery of CPs, research in this field has received great attention and many other organic conductive polymers such as polypyrrole (PPy), polythiophene (PTh), polyaniline (PAn), polyfuran, poly(*p*-phenylene), poly(*p*-phenylene vinylene) and poly(heterocycle vinylene) (Cadogan *et al.*, 1992, Hiller *et al.*, 1996, Hwang *et al.*, 2003) (**Figure 2.2**) based polymers have been synthesised. Among the CPs, PAn has been produced in large amounts due to its ability to form processable conductive form at relatively low cost (Alan, 1993, Roncali, 1997, Roncali, 1999). Due to the possible presence of toxic compound (benzidine) in the structure upon degradation, the studies of PAn have been limited among industrial companies and academics groups. Since that, the focus has shifted to more environmentally friendly polymers such as PTh and this polymer has rapidly become the subject of considerable interest.

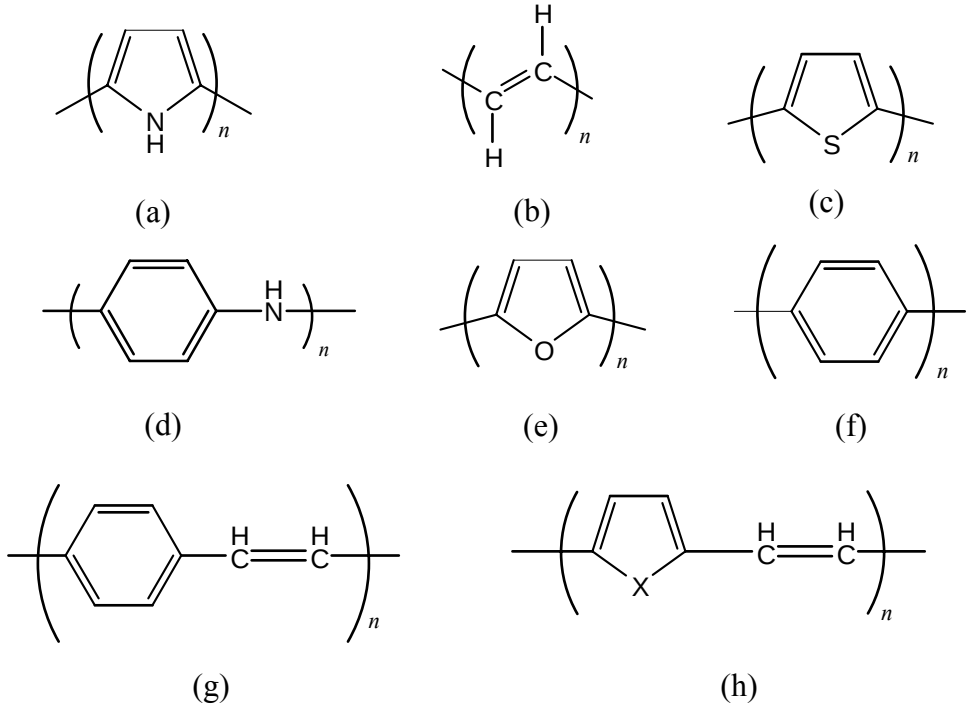

Figure 2.2: Conducting polymers: (a) polypyrrole, (b) polyacetylene, (c) polythiophene, (d) polyaniline, (e) polyfuran, (f) poly(*p*-phenylene), (g) poly(*p*-phenylene vinylene) and (h) poly(heterocycle vinylene) (*n* is number of coupled monomers).

In this chapter, general information about conducting polymers is given. The basic structure, properties and various studies already reported in the literature on conducting polymers particularly poly(3,4-ethylenedioxythiophene), PEDOT are discussed. Since PEDOT is a derivative of PTh, the basic features of PThs are also described. The syntheses of PEDOT using electropolymerisation methods and the advantages of PEDOT are also described. Finally, some literature on the derivatives of PEDOT used in this work, namely poly(3,4-propylenedioxythiophene) (PProDOT) and poly(3,3-dibenzyl-3,4-propylenedioxythiophene) (PDBPD) are explained and the potential applications of PEDOT are given.

2.2 Synthesis of Conducting Polymers

Conducting polymers can be synthesised by chemical and electrochemical techniques (Heinze, 1990). However, the electropolymerisation method is much preferred due to a better control of film thickness and quality. Each technique has advantages and disadvantages as summarised in **Table 2.1**.

The chemically synthesised polymer is usually produced in its undoped insulating state. The undoped polymer can be doped chemically or electrochemically to its conducting state. This concept will be explained in **Section 2.4**. Chemical oxidation can produce conducting polymers in bulk quantities, however usually the polymers are of poor quality with structural defects and/or impurities. The use of a strong oxidising agent could also result in overoxidation and decomposition of the polymer.

In contrast, a polymer obtained from an electrochemical process is readily formed in its oxidised conducting state and the thickness is well controlled by parameters such as time, number of cycles and the electrochemical techniques used. The polymer can be reduced chemically or electrochemically to its semiconducting state. In addition, impurities due to the supporting electrolytes have not been observed in the structure of the polymer resulting in a high purity of polymer. Thus, the

electropolymerisation method is generally much more preferred compared to chemical oxidation. However, the drawbacks of electrochemical techniques are that the polymer is produced in small quantities and there is difficulty in removing the polymer film from the electrode surface. This problem has resulted in difficulties in characterising the polymer using standard analytical techniques such as NMR spectroscopy and chromatography. Even though this technique is not a choice for bulk industrial production, it is of the utmost importance for fundamental studies. Various electrochemical techniques can be used to synthesise conducting polymers including potentiodynamic (potential scanning), potentiostatic (constant potential) and galvanostatic (constant current) methods (Doblhofer and Rajeshwar, 1998). Potentiostatic and galvanostatic methods are commonly used to investigate the nucleation mechanism and macroscopic growth due to the applicability of these techniques to such quantitative measurements. However, a potentiodynamic technique is needed to obtain qualitative information about the redox processes involved in the early stage of electropolymerisation (Lyons, 1997).

Table 2.1: Advantages and disadvantages of chemical and electrochemical polymerisation techniques.

Polymerisation techniques	Chemical polymerisation	Electrochemical polymerisation
Advantages	▪ Large scale production ▪ Post-covalent modification of bulk CP possible ▪ More options to modify CP backbone covalently	▪ Thin film synthesis possible ▪ Easy to synthesis ▪ Entrapment of molecules in CP ▪ Doping is simultaneous (doped state) ▪ Thickness of film can be controlled ▪ High purity
Disadvantages	▪ Cannot make thin film ▪ Synthesis more complicated ▪ Undoped state ▪ Poor quality/impurities ▪ Use of oxidizing agent can cause overoxidation and decomposition	▪ Difficult to remove film from electrode surface ▪ Post-covalent modification of bulk CP is difficult ▪ Small quantity

2.3 Growth Mechanism of Conducting Polymers

Electropolymerisation of conducting polymers is a unique process and is still a controversial subject due to the different mechanisms proposed to date such as Kim's mechanism (Kim *et al.*, 1988), Diaz's mechanism (Genies *et al.*, 1983) Pletcher's mechanism (Asavapiriyanont *et al.*, 1984) and Reynolds's mechanism (Qiu and Reynolds, 1992). However, Diaz's mechanism (Genies *et al.*, 1983) is most commonly found in the literature. In this mechanism, the charged species of the precursor must be produced by oxidation of the monomer at the anode surface to form a radical cation (monomer$^{+\cdot}$). The further step can proceed by various electrochemical and chemical reactions that are possible, resulting in a complex mechanism which is difficult to elucidate. The difference in various mechanisms lies in the coupling process, in which, the Diaz's mechanism involves radical cation coupling whereas Pletcher suggests radical cation monomer coupling. . An important aspect of the electropolymerisation reaction is that it occurs with electrochemical stoichiometry, with an *n* value in the range of 2.07 – 2.5 Faradays/mol (Waltman and Bargon, 1984). Two electrons per molecule are required to oxidise the monomer and the excess charge corresponds to the reversible oxidation or doping of the polymer.

As illustrated in **Figure 2.3**, the first step refers to an electrochemical step (E) in which the monomer is oxidised to its radical cation. As the electron transfer is usually much faster than the diffusion of the monomer to the electrode, a high concentration of radicals is continuously formed near the electrode surface. Two radical cations are coupled forming a dimer dication, consequently produce a dimer after losing two protons and rearomatisation. This rearomatisation constitutes a chemical reaction (C). The extended conjugation in the structure of dimer results in a lowering of the oxidation potential compared to the monomer. Therefore, the synthesis and doping of the polymer occurs simultaneously. The dimer can proceed to produce a dimer radical cation (electrochemical step (E)) and reacts with another radical cation to form a trimer. The electropolymerisation continues through successive electrochemical and chemical steps

according to the general $E(CE)_n$ scheme until the oligomer/polymer precipitates onto the electrode surface as it becomes insoluble in the electrolytic medium. The precipitation occurs due to the lower solubility of polymer compared to monomer or oligomers.

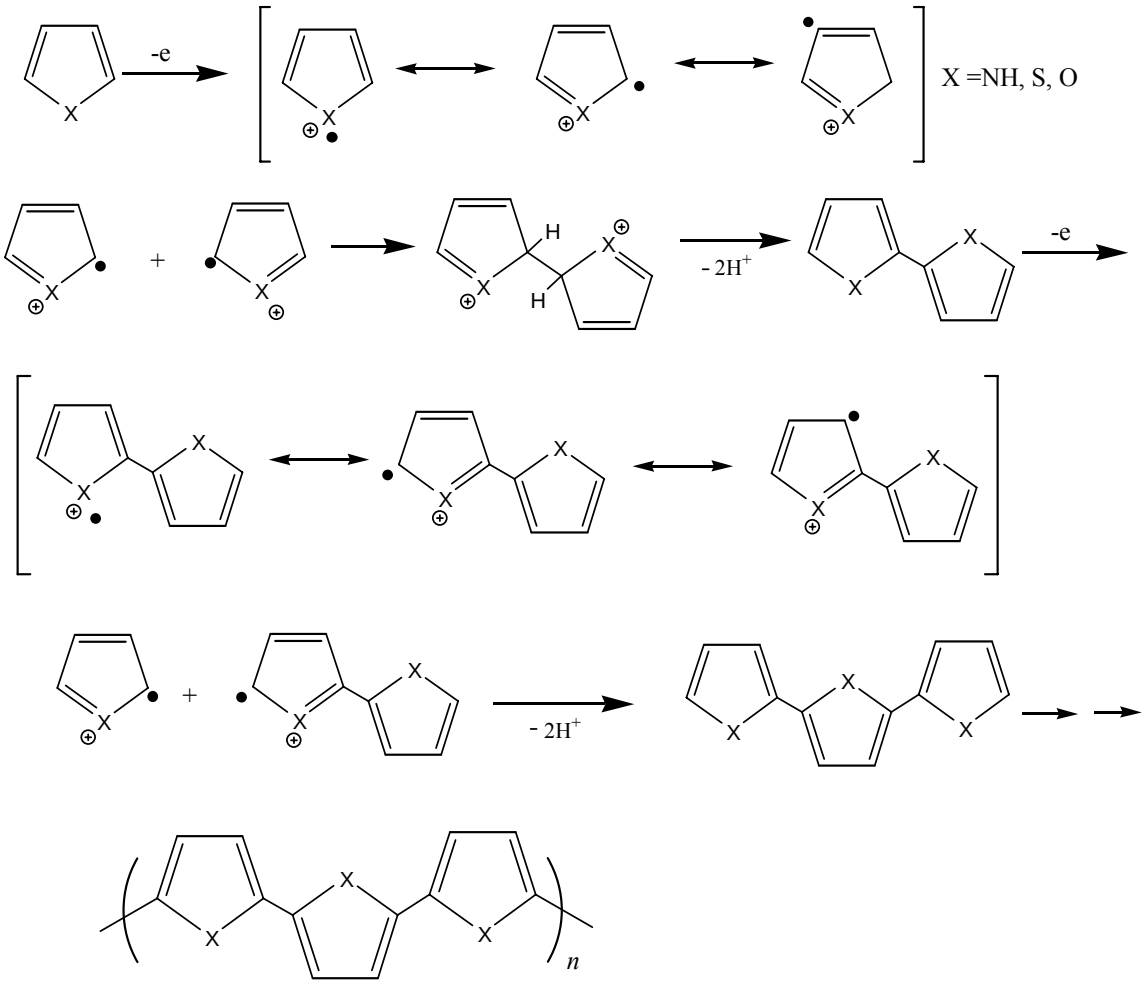

Figure 2.3: Mechanism of electropolymerisation of five-membered heterocycles (Ansari, 2006, Genies *et al.*, 1983).

Diaz's mechanism is mostly accepted due to the following reasons. Firstly, the electron paramagnetic resonance (EPR) or electron spin resonance (ESR) revealed the existence of a p-type radical (Street, 1986). An electron spin is an intrinsic property of electrons that related to its spin about an axis. Two electron spin states are allowed, which are described by the quantum number m_s, with values of +½ or -½. The existence of spin electron was shown by Stern-Gerlach experiment, which a beam can be split into two beams by magnetic field (Friedrich and Herschbach, 2003). In addition, the chronoabsorption studies have shown that the rate of film formation is dependent on t and not $t^{1/2}$. This observation is in agreement with the rate determining step (the slowest step), which is the radical coupling step not the diffusion of the monomer to the electrode surface (Genies *et al.*, 1983). However, in Kim's mechanism, the rate determining step of the reaction is removal of two electrons from monomer (Kim *et al.*, 1988).

2.4 Transport in Conducting Polymers

Intrinsic electronic conductivity in organic materials is due to the delocalised electronic structure along the conjugated backbone. In insulator polymers, there is no mobile electron to participate in the electrical transport. For instance, all valence electrons in the carbon atom of polyethylene (**Figure 2.1c**) take part in chemical bonding. In CPs (**Figure 2.2**), the electronic conduction is based on delocalisation of π-electrons along the backbone which plays important roles in the electrical and optical properties of conducting polymers.

The electronic conductivity of polymers is also related to their oxidation states (Bockris and Miller, 1987). CPs in their neutral state behave as insulators or semiconductors in which they have a wide gap between valence and conduction bands. In order to make them behave as metallic conductors, they have to be doped by a dopant during the doping process. Doping is a process of addition of electrons (reduction) or removal of electrons (oxidation) from the polymer chain. The charged species formed are able to move along the carbon chain (delocalisation) allowing electron transport and thus

giving an electronically conductive material (Lyons, 1997). When CPs are oxidised or reduced, their conductivity increases dramatically. This oxidation or reduction may be achieved chemically or electrochemically but in either case, electroneutrality within the material requires insertion of counter ions of the opposite charge into the material. In chemical doping, electron acceptors (p-doping) need to be added to the solution in order to allow the doping reaction to take place. On the other hand, electrochemical doping can be carried out by applying potential across the film in the presence of counter ions. This process is analogous to a semiconductor which can be made n-type (reduction) or p-type (oxidation) as a result of doping.

Once doping has occurred, the charge carrying species in the delocalised π system have the mobility to move along the backbone chain. From a macroscopic perspective, conduction through a CP takes place by charge hopping both along the polymer chains and also between the macromolecules that make up individual fibres and between the fibres themselves. Conduction in a CP can also be explained by band theory. Basically there are two bands called the valence band and the conduction band (**Figure 2.4**). A band consists of a group of molecular orbitals that are very close in energy level. The valence band contains the highest occupied molecular orbital (HUMO) and the conduction band contains the lowest unoccupied molecular orbital (LUMO). These two bands have a relatively large difference in energy level and are separated by a band gap (E_g) (Atkins, 1998).

In a metal, the valence and conduction bands have no gap between them and the band of energy levels is only partly filled, where the highest filled level at absolute zero is called the Fermi level (**Figure 2.4**). In this case, electrons can flow even when a tiny electrical potential difference is applied. The conductivity of metal decreases as the temperature is raised (Atkins, 1998) due to greater random motion of atoms which hinders electron movement.

If an electron could be promoted from valence band to the conduction band in a substance like diamond, metal-like properties could be observed. However, diamonds are insulators because the band gap between valence and conduction band is large, on the order of 5 eV and it is difficult to promote electrons to the conduction band. Semiconductors, on the other hand, usually have band gaps in the range 0.5 to 3.0 eV. At least a few electrons can be promoted to the conduction band by the input of modest of energy, so electrical conduction can occur. Thermally excited electrons can cross the gap, allowing a small current to flow. Thus, in contrast to a conductor, the conductivity of a semiconductor increases when it is heated (Atkins, 1998).

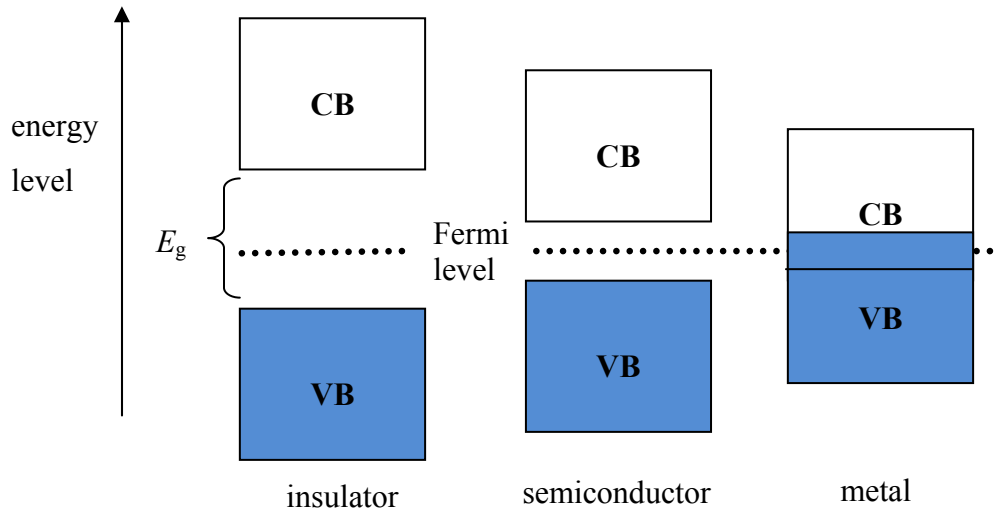

Figure 2.4: Conduction band (CB) and valence band (VB) in insulator, semiconductor and metal.

In a semiconductor, the doping process produces an acceptor level close to the valence band or a donor energy level close to the conduction band. However, this phenomenon does not occur in conducting polymer.

The mechanism of electronic conduction in CP is due to the continuous system of a large number of strongly interacting atomic orbitals leading to the formation of electronic band structure. When an electron is removed from the system of a conjugated polymer, a free radical and a positive charged are formed. The radical and the cation are

coupled to each other via local resonance of the charge and the radical. The combination of a charge site and a radical is called as polaron (**Figure 2.5**). Polarons can also be defined as a radical cation (spin ½) which is partially delocalised over some of polymer segment and is stabilised by polarising the medium around it. Polaron can move over several double bonds by rearrangement along the conjugated chain (Kanatzidis, 1990). The formation of polaron creates new localised electronic states in the band gap between conduction and valence band as shown in **Figure 2.6**. The lower energy state is occupied by a single unpaired electron. This phenomenon is different from conventional semiconductor in which the electron goes to the conduction band when an electron is added.

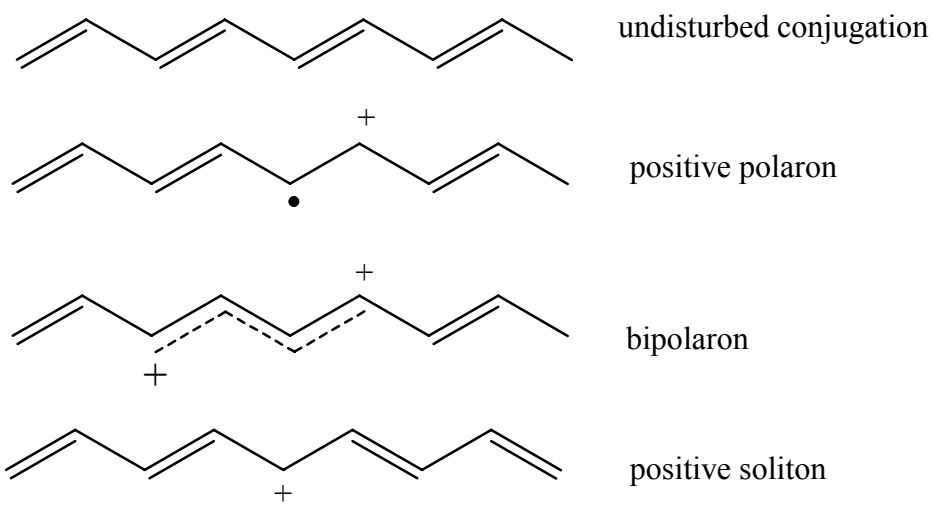

Figure 2.5: Structure of undisturbed conjugation, positive polaron, bipolaron and positive soliton.

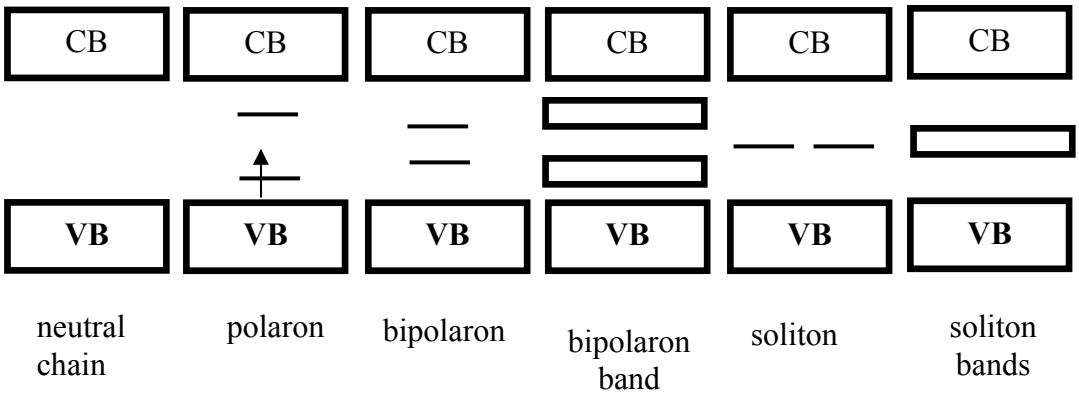

Figure 2.6: Representation of polaron, bipolaron and polaron bands.

At low oxidation levels, two polarons are kept away from each other by coulombic repulsion. With the oxidation level increases, the polarons become crowded and begin to interact when they get closer on the conjugated π-backbone. A bipolaron is formed when two polarons are combined due to further oxidation. It is defined as a pair of like charges (dication) associated with a strong local lattice distortion and it is spinless. The bipolaron has lower energy level and is more stable in comparison to a polaron. The bipolaron in non-degenerate conducting polymers may not be stable because of the Coulomb repulsion of the two polarons which constitute the bipolaron. However, the presence of dopant ions in the neighbourhood can stabilise the bipolaron (Brazovskii *et al.*, 1998). At higher doping levels, bipolarons form a bipolaron band (**Figure 2.6**). It is possible for a heavily doped conducting polymer that the upper and lower bipolaron bands will combine with the CB and VB respectively, forming a partially filled band similar to a metal. The same phenomenon occurs when electrons are added, in which the negative polaron (radical anion) and bipolaron (dianion) are formed. The remaining positive charges in the structure of bipolaron are free to move along the conjugated chains. Electronic conductivity arises from the mobility of polaron and bipolaron charge carriers.

Another mechanism is slightly different when two degenerate ground states are present as in *trans*-polyacetylene. In this condition, the charged cations are not bound to each other and can freely separate along the chain. This means that the charge defects are independent of one another and can form two separate phases having identical energy level called soliton (**Figure 2.5**). At higher doping levels, the solitons interact with each other to form a soliton band and give metal-like behaviour (Bredas and Street, 1985). Solitons can be positive and negative when the polymer is doped. In the undoped polymer, the soliton is neutral (Bredas and Street, 1985).

2.5 Polythiophene (PTh)

Heterocyclic compounds are cyclic compounds containing a heteroatom (other than carbon and hydrogen atoms. The structure of the five-membered poly(heterocyclic) product corresponds to the coupling of monomeric unit in 2,5-positions. Thiophene (**Figure 2.7**) is one of these five-membered aromatic ring compounds and it exists as a colourless liquid at room temperature. Thiophene has a relatively high oxidation potential (+1.6 V *vs* SCE) compared to pyrrole (+0.8 V *vs* SCE) (Tourillon, 1986). Polythiophene (PTh) and its derivatives can be chemically or electrochemically synthesised. The electrical conductivity of the PTh film can be varied over 12 orders of magnitude, with properties ranging from insulator (~ 10^{-10} S cm^{-1}) to semiconductor and to metal (~ 10^{2} S cm^{-1}). PTh was the first class of polymers which is chemically and electrochemically stable in air and moisture in both doped and undoped states (Osterholm *et al.*, 1987). During the polymerisation, either α-α' coupling or α-β' coupling can occur. However, α-α' coupling in PTh and its derivatives is dominant as confirmed by ^{13}C nuclear magnetic resonance (NMR) spectrum analysis. There was a sharp absorption band at 120 and 127 ppm for PTh and at 136 ppm for poly(3-methylthiophene) due to the C_{β}-H bonding (Arbizzani *et al.*, 1992).

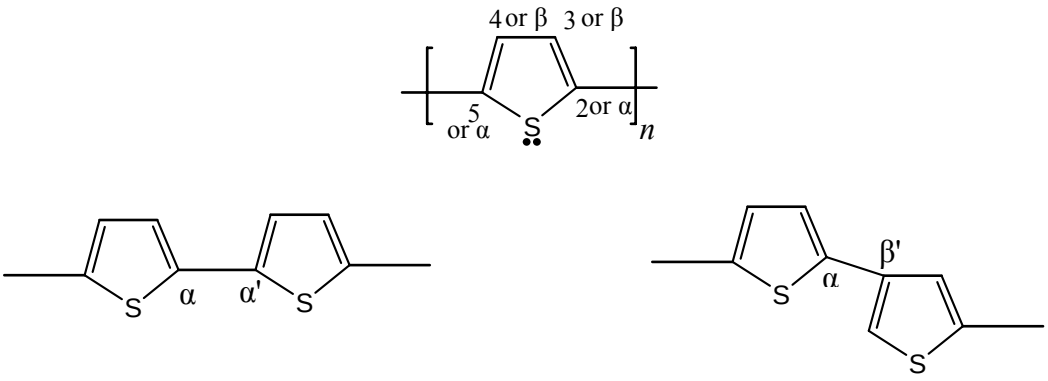

Figure 2.7: Bonding in polythiophene.

2.5.1 Poly(mono substituted thiophenes)

Substitution of H at the position 3 of PTh by a strong electron withdrawing group to give 3-thiophenecarboxylic acid, 3-thiophenecarboxaldehyde, 3-cyanothiophene and 3-nitrothiophene has shown that the oxidation potential increased by approximately 0.5 – 0.7 V compared to thiophene. (Kagan and Arora, 1983, Waltman and Bargon, 1986). The electropolymerisation of 3-thiopheneacetic acid proceeds with low current efficiency (less than 1) and requires high anodic potentials (+1.6 V *vs* Ag/Ag^{+}) (Albery *et al.*, 1991). Halogen substituted thiophene *i.e.* 3-choloro-, 3-bromo-, 3-iodo-thiophene have also been reported to have great difficulty to electropolymerise and led to form poor conducting polymers with high oxidation potentials (Lemaire *et al.*, 1990, Shi *et al.*, 1989, Tourillon and Garnier, 1984a, Waltman *et al.*, 1983). The difficulty to electropolymerise the monosubstituted thiophene with electron withdrawing groups has been attributed to the high reactivity of the corresponding radicals that undergoes rapid reactions with the solvent or anions to form soluble products instead of promoting electropolymerisation (Waltman and Bargon, 1986).

On the other hand, substitution of thiophene by electron donating groups produces a decrease in oxidation potentials and stabilisation of the corresponding radicals. Attempts to electropolymerise 3-(methylthiophene)- and 3-(ethylthiophene)- were

unsuccessful (Ruiz *et al.*, 1989) or led to the formation of soluble oligomers (Tanaka *et al.*, 1988). This was attributed to the spin density in the radicals being maximum on the sulphur and not on the α-position of the thiophene ring, which is the main required condition for electropolymerisation. Conductivity and electrochemical stability of thiolalkyl-substituted polymer synthesised chemically are significantly lower than unsubstituted PTh (Ruiz *et al.*, 1989, Tsai *et al.*, 1989). In the case of alkoxy groups, the electron donating effect from oxygen does decrease the oxidation potential and favours the formation of soluble short-chain oligomers. The degree of polymerisation of 3-methoxythiophene has been reported differently by authors, ranging from 5-10 monomers (Chang *et al.*, 1987, Dian *et al.*, 1986, Lowen *et al.*, 1989) to 80 (Tanaka *et al.*, 1988) and the oxidation potentials as different as +0.28 V ((Dian *et al.*, 1986) and -0.2 V (Tanaka *et al.*, 1988) *vs* Ag/Ag^{+}. It seems that the electronic effect gives an effect on the reactivity of the substituted thiophenes and to obtain high quality PThs-based polymer, the reactivity of the monomer radical cation should be kept within defined limits.

2.5.2 Poly(3,4-disubstituted thiophenes)

The simplest disubstituted thiophene is obtained by the introduction of alkyl groups at the position of 3 and 4 of thiophene. It has been reported that a methyl group at β-position has led to a significant increase in conductivity and conjugation (Tourillon and Garnier, 1983, Waltman *et al.*, 1983). This observation was attributed to the decline of the number of α-β' couplings and the oxidation potential (ca 0.2 V) caused by the inductive effect of the methyl group. A new strategy was discovered by Tourillon and Garnier (1984b) to synthesise disubstituted at the β-β position to produce stereoregular polymer. By having this structure, the α-β' coupling was suppressed. However, this strategy produces less effective conjugation due to the steric hindrance between substituents grafted on the consecutive monomers that distort the π conjugation system. It is also found that poly(3,4-dialkylthiophenes) have higher oxidation potentials, optical band gaps and lower conductivities compared to monosubstituted polymers (Tourillon and Garnier, 1984c).

The mono and disubstitution of thiophene by alkoxy (Daoust and Leclerc, 1991) and thioalkyl groups (Tsai *et al.*, 1989) also reveal significant steric effect. In contrast, unsymmetrically disubstituted polymer such as poly(3-methoxy-4-methyl-thiophene) and poly(3-butoxy-4-methyl-thiophene) showed lower oxidation potentials and smaller band gaps compared to their monosubstituted or symmetrically disubstituted analogue (Daoust and Leclerc, 1991, Feldhues *et al.*, 1989). However, a precise evaluation of the reduction of steric hindrance of alkoxy groups is difficult due to the electronic effect. Interestingly, Jonas and Schrader (1991) have synthesised poly(3,4-ethylenedioxythiophene) (PEDOT) for the first time anodically. This polymer represents interesting approach for the reduction of steric hindrance in 3,4-disubstituted PThs.

2.5.3 Poly(3,4-ethylenedioxythiophene) (PEDOT)

In the 1980s, scientist at Bayer AG research in Germany developed a new PTh derivative called poly (3,4-ethylenedioxythiophene) (PEDOT) and known under the trade name Baytron. Indeed, Heywang and Jonas (1992) were the first to report the electrochemical synthesis of PEDOT. The monomer of PEDOT, called 3,4-ethylenedioxythiophene (EDOT) presented some specific physical and chemical properties. EDOT has a boiling point of 225 °C and it will slowly turn to dark upon exposure to air and light because of partial oxidation. Substitution of the H on position 3 and 4 of thiophene by an O-electron donor (**Figure 2.8**), significantly lowers the oxidation of EDOT compared to thiophene (Groenendaal *et al.*, 2003). These donating groups also stabilise the positive charge generated in doped PEDOT (Groenendaal *et al.*, 2003).

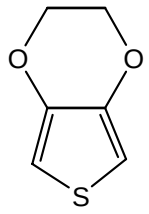

Figure 2.8: Chemical structure of EDOT.

Due to these intrinsic features, PEDOT has become one of the most popular conducting polymers being studied by many scientific research groups (Asami *et al.*, 2006, Chen *et al.*, 2008, Park *et al.*, 2008). Among a number of conjugated polymers (conducting polymers), PEDOT has shown some advantages. PEDOT shows better properties such as high conductivity (ca. 300 S/cm), environmental stability, high transparency (Groenendaal *et al.*, 2000), low oxidation potential, relatively low band gap (Dietrich *et al.*, 1994, Kirchmeyer and Reuter, 2005), good chemical and electrochemical properties (Groenendaal *et al.*, 2003). However, EDOT and PEDOT have a drawback of being water insoluble/partially soluble (2.1 g L^{-1} at 20 °C) both in neutral and doped forms (Skotheim *et al.*, 1998). This problem has been overcome by introducing polystyrene sulfonate (PSS) during polymerisation to obtain EDOT/PSS. PSS is water soluble polyelectrolyte that acts as charge-balancing dopant (Groenendaal *et al.*, 2000, Groenendaal *et al.*, 2003).

2.6 Synthesis of PEDOT

PEDOT and its derivatives can be synthesised in three ways *i.e.* oxidative chemical polymerisation, electrochemical polymerisation and transition metal-mediated coupling of derivatives of EDOT. The following section will only explain electrochemical polymerisation methods. Different electrochemical techniques such as cyclic voltammetry, chronoamperometry and chronopotentiometry were used to synthesise PEDOT and copolymer based EDOT (Sakmeche *et al.*, 1999). By using these electroanalytical techniques, only short time of polymerisation is needed and only a small amount of monomer is required.

2.6.1 Synthesis in Organic and Aqueous Media via Electrochemical Methods

Most PEDOT and copolymer PEDOT films have been prepared in organic media such as acetonitrile (ACN) containing $LiClO_4$ (Park *et al.*, 2006), tetrabutylammonium perchlorate (TBAP) (Han *et al.*, 2006) and propylene carbonate containing tetra(n-butyl) ammonia hexafluorophosphate ($TBAPF_6$) (Wang and Wong, 2006) due to their limited solubility in aqueous media. In organic media, EDOT monomers were well dispersed and yielded rough films without regularity. This was attributed to the better solubility of oligo-EDOT that resulted in precipitation of flocculating powder on the electrode surface (Groenendaal *et al.*, 2000, Groenendaal *et al.*, 2003). On the other hand, electropolymerisation of thiophene in such media requires potentials above 1.6 V *vs* SCE. The high potentials (above 1.45 – 1.55 V) can irreversibly damage the conjugated system, due to overoxidation (Gratzl *et al.*, 1990, Krische and Zagorska, 1989).

Recently, Yang *et al*. (2007) synthesised PEDOT nanofibrils under galvanostatic conditions on microfabricated neural prosthetic devices from aqueous solution containing polyacrylic acid (PAA). The size of PEDOT nanofibrils ranged from 100 to 1000 nm and it was claimed that the nanofibrils had lower electrical impedance due the high surface area. El Moustafid *et al.* (2003) has also reported that the anion of the electrolyte has a major effect on the conductivity of the PEDOT deposited.

By adding surfactant in aqueous solution, the solubility of EDOT and the deposition current were increased and the oxidation potential could be decreased (El Moustafid *et al.*, 2003). The surfactant can also stabilise charged species such as anion and cation radicals during the polymerisation (El Moustafid *et al.*, 2003, Zhang *et al.*, 2006). A number of surfactants have been used such as SDS[1] (Manisankar *et al.*, 2007, Sakmeche *et al.*, 1999), CTAB[2] (Manisankar *et al.*, 2007), SDBS[3], Triton X-100[4], DM[5]

[1] SDS: sodium dodecylsulfate
[2] CTAB : cetyltrimethylammonium bromide
[3] SDBS : sodium dodecylbenzenesulfate
[4] Triton X-100 : polyethylene glycol octylphenyl ether

and polyethylene glycol (Nien *et al.*, 2006). It was found that the production of radical cations in the media containing surfactants was faster but the coupling of these radical cations was slower due to the interaction of surfactants and the monomers or the radical cations. For example, hydroxyl group in DM can act as a mediator to facilitate the electron transfer from monomer to monomer$^{+\cdot}$ (Zhang *et al.*, 2006). This phenomenon affects the polymerisation rate and high quality CP films can be produced at low polymerisation rate (Zhang *et al.*, 2006).

Interestingly, Asami *et al*. (2006) have shown that good quality of PEDOT could be produced in aqueous solution without adding any surfactant by using an acoustic emulsification method *i.e.* ultrasonic irradiation. This technique has proven to provide a stable emulsion. They have also shown that Li^+ ion in $LiClO_4$ (supporting electrolyte in aqueous) contributed to the formation of an electric bilayer inside the droplet of EDOT monomer (**Figure 2.9**) in order to form PEDOT. The Li^+ ion was detected by inductively couple plasma spectrometry (ICP) and this phenomenon only found in $LiClO_4$ if compared to $LiNO_3$ and Li_2SO_4 electrolytes, due to the fact that $LiClO_4$ is relatively lipophilice in organic media. Based on this observation, it was likely that the electron transfer takes place between the electrode and droplets of the monomer but not the monomer dissolved in aqueous phase. The advantage of electropolymerising in aqueous solution is to avoid the possible interference of surfactants or organic solvents, leading to a resulting polymer that is more suitable for key applications such as biosensors.

[5] DM : N-dodecyl-β-D-maltoside

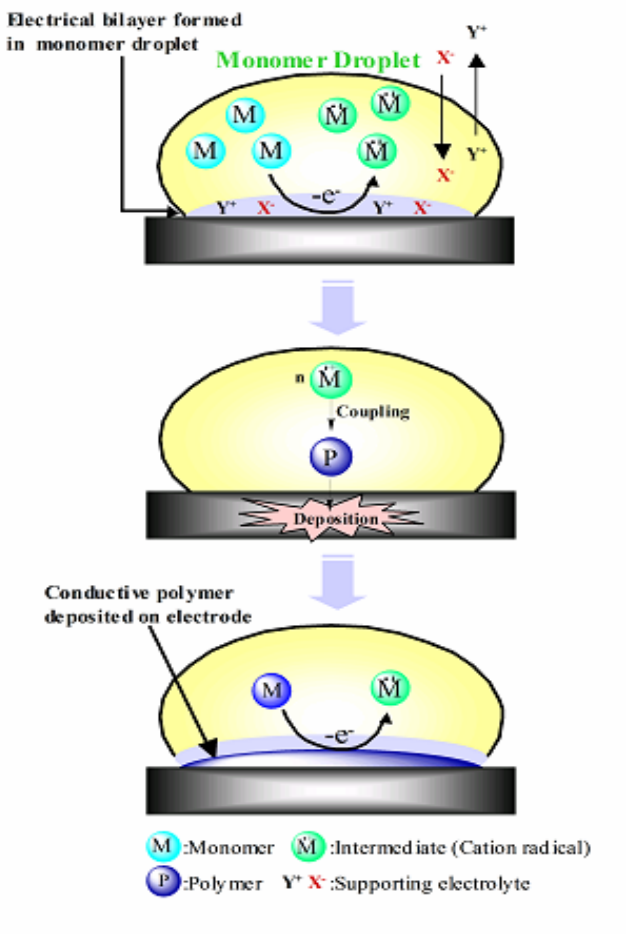

Figure 2.9: Schematic illustration of the electropolymerisation of a water-insoluble monomer in an aqueous solution (Asami *et al.*, 2006).

2.6.2 Copolymerisation of Other Monomers with EDOT

Many studies have been carried out on the synthesis of copolymers, in which one of the monomers is EDOT. The purpose is to combine the advantages of both monomers in order to get better quality of polymer. By having copolymer, the highest occupied molecular orbital (HOMO) and the lowest unoccupied molecular orbital (LUMO) levels of PEDOT were altered and subsequently the optical properties and electronic structure were changed as well (Groenendaal *et al.*, 2000, Roncali *et al.*, 2005). The copolymer synthesis was based on the fact that the oxidation potential of both monomers are close to each other which is required to make successful copolymer (Wan *et al.*, 1999).

The small difference of indole and EDOT oxidation potentials (0.08 V) makes the copolymerisation feasible (Xu *et al.*, 2005). Potential of +1.1 V (*vs* platinum wire ((Xu *et al.*, 2005)) and 1.5 V (*vs* SCE) proved to be the best condition for obtaining copolymers of indole/EDOT and CNIn[6]/EDOT, respectively (Nie *et al.*, 2008a, Xu *et al.*, 2005). Sezer *et al*. (2003) have synthesised 3,6 bis(3,4-ethylenedioxythiophenyl)-9-ethyl (EDOT-ECZ-EDOT) on a carbon fibre electrode (CF). A simple alternative method was suggested for determining the thickness of polymer deposited on CF by comparing with unmodified CF. Indeed, the polymer deposited on CF remained stable even at high potential (+1.2 V *vs* silver wire). Some other attempts to electrochemically synthesise copolymers such as PEDOT/PPy (Wang *et al.*, 2007, Xu *et al.*, 2006), PEDOT/PTh (Chang *et al.*, 2005), PEDOT/PEDTM[7] (Doherty *et al.*, 2006), PCDM[8]/PEDOT (Huang and Pickup, 1998), PCln[9]/PEDOT (Nie *et al.*, 2008a) and PNTP[10]/PEDOT (Varis *et al.*, 2007) have also been reported.

There are also some studies to produce copolymer in which both monomers have significant differences in their oxidation potentials. Wei *et al*. (2006) have successfully synthesised copolymer, FPT[11]/EDOT in acetonitrile containing 0.1 M tetrabutylammonium tetrafluoroborate as supporting electrolyte by direct anodic oxidation of the monomer mixtures on platinum or stainless steel electrodes. They used diffusion method strategy (Kuwabata *et al.*, 1988) by employing different ratios of monomers. The copolymer exhibited high conductivity and excellent ambient stability. It was found that the electrical conductivity of copolymer, 5-methylindole/PEDOT has improved in comparison with 5-methylindole (Nie *et al.*, 2008b). Modified features or characteristics such as decreased band gaps (Ak *et al.*, 2008), varied electrochromic parameters (Manisankar *et al.*, 2006), electrooptical properties (Doherty *et al.*, 2006) and multichromism properties (Camurlu *et al.*, 2008) were also found in copolymers.

[6] CNln : 5-cyannoindole
[7] PEDTM: poly (2,3-dihydrothieno[3,4-*b*]-1,4-dioxyn-2-yl methanol)
[8] PCDM: poly (4-(dicyanomethylene)-4*H*-cyclopenta[2,1-*b*:3,4-*b'*]dithiophene)
[9] PCln : poly (5-cyanoindole)
[10] PNTP : poly (1-(4-nitrophenyl)-2,5-di(2-thienyl)-1H-pyrrole)
[11] FTP: 3-(-4-fluorophenyl)thiophene

2.7 PProDOT and PDBPD

A number of derivatives of EDOT monomer have been synthesised by various research groups (Groenendaal *et al.*, 2000). 3,4-propylenedioxythiophene (ProDOT) monomer was initially prepared by Heywang and Jonas (1992) who found that the polymer, PProDOT, exhibits a reproducibly higher conductivity than PEDOT (Kumar *et al.*, 1998). This is due to the fact that ProDOT monomer is a crystalline solid and could be easily obtained, stored and handled in a highly pure state. In contrast, EDOT requires purification and as a liquid, it is slightly reactive allowing the formation of small impurities during storage (Kumar *et al.*, 1998). Huang *et al.* (2008) have demonstrated that PProDOT is an ideal as a hole collection layer (HCL) for photovoltaic devices due to its high porosity and reasonable series resistance.

A new derivative of PEDOT *i.e.* 3,3-dibenzyl-3,4-propylenedioxythiophene (PDBPD), synthesised by Anil Kumar and co-worker (Krishnamoorthy *et al.*, 2001) exhibited much higher (89%) electrochromic contrast compared to tetradecyl substituted polyethylenedioxythiophene derivative (68%) and dimethyl substituted ProDOT derivative (78%). This is due to an increase in the interchain separation caused by the incorporation of a rigid/bulky side chain (Kumar *et al.*, 1998). PDBPD also shows high coloration efficiency (575 cm^2/C) compare to PProDOT (285 cm^2/C) and PEDOT (183 cm^2/C) (Gaupp *et al.*, 2002, Krishnamoorthy *et al.*, 2001).

Most of the studies carried out for PProDOT and PDBPD are focused on the fabrication of electrochromic devices. However, so far, the physical and electrochemical properties of these two conducting polymers, PProDOT and PDBPD have not been fully explored. Thus, one of the aims of this work is to prepare PProDOT and PDBPD electrochemically and comparatively investigate the characteristics of the polymer films. This work will be discussed in **Chapter 5** and **Chapter 6**.

2.8 Applications of PEDOT

CPs are electroactive materials, thus the properties depend on the degree of oxidation (p-doping) and reduction (n-doping) of the conjugated backbone. In the undoped state, CPs are organic semiconductors with a suitable band gap to transform electricity into light and vice versa. These features make the CP suitable for photovoltaics devices (solar cells) and hole injection layer in light-emitting diodes based organic materials (OLED).

Among the CPs, polypyrrole and polyaniline can be easily synthesised by chemical and electrochemical polymerisations but the poor stability of these polymers is an obstacle for potential applications (McCullough, 1998, Skotheim *et al.*, 1998). On the other hand, polythiophene is a relatively stable conducting polymer but the synthesis by electrochemical method is very tricky because of the high oxidation potential of thiophene (+1.60 V *vs* SCE) (Roncali, 1997, Tourillon, 1986). This problem has been overcome by the discovery of new monomer, EDOT. Due to the salient features exhibited by PEDOT, it can be used in the field of anti-static coating (Meng *et al.*, 2003), electrochromic devices (Welsh *et al.*, 1999), as a matrix to entrap the enzyme (Krishnamoorthy *et al.*, 2004, Nien *et al.*, 2006), solid state capacitors, electroluminescent devices, and as underlayers for metallization of printed circuit boards (Kirchmeyer and Reuter, 2005). Sirringhaus *et al.* (2000) have shown that CP can also be used to fabricate low cost all-polymer transistor circuits by high-resolution inkjet printing.

CPs can be also synthesised in aqueous solutions (Bobacka *et al.*, 2000, Schweiss *et al.*, 2005). Avoiding the use of non-aqueous solvents renders the conjugated polymers biocompatible and therefore, CPs produced can be extensively used in the fabrication of inexpensive devices for development of biocompatible electrochemical sensors and biosensors in the medical diagnostic laboratories. Chemical sensors are miniaturised analytical devices, which can deliver real-time and on-line information about the

presence of specific compounds or ions in samples. In chemical sensor, initially, ion recognition process takes place followed by the conversion of the chemical signal into an electrical signal by transducer. CPs seem to be a good candidate to fulfill this feature for the production of all-solid-state potentiometric ion sensor, which is also known as all-solid-state ion-selective electrode (ASSISE) due to mixed electronic and ionic conductivity properties of CP. PEDOT has shown to be useful as ion-to electron transducers in ASSISE due to the high potential stability (Bobacka, 1999). This approach will be explained in more detail in **Chapter 7**.

The properties of CP can be tailored for specific application by incorporation of a various types of dopants (counterions) from relatively small to bulky biological molecules into the conducting polymer during electrochemical polymerisation. One of the possible applications using this approach is the fabrication of chiral electrodes. PEDOT deposited on electrode becomes chiral PEDOT by doping with chiral dopants (Goto and Akagi, 2006, Kawashima and Goto, 2011) and can be used as chiral selectors (**Chapter 8**).

References

Ak, M., Sahmetlioglu, E. and Toppare, L. (2008) Synthesis, Characterization and Optoelectrochemical Properties of Poly(1,6-bis(2,5-di(thiophen-2-yl)-1H-pyrrol-1-yl)hexane) and Its Copolymer with EDOT. *Journal of Electroanalytical Chemistry.* 621**.** 55-61.

Alan, J. H. (1993) Polyaniline with surfactant counterions: Conducting polymer materials which are processible in the conducting form. *Synthetic Metals.* 57**.** 3471-3482.

Albery, W. J., Li, F. and Mount, A. R. (1991) Electrochemical Polymerization of Poly(thiophene-3-acetic acid), Poly(thiophene-co-thiophene-3-acetic acid) and Determination of Their Molar Mass. *Journal of Electroanalytical Chemistry and Interfacial Electrochemistry.* 310**.** 239-253.

Ansari, R. (2006) Polypyrrole Conducting Electroactive Polymers: Synthesis and Stability Studies *E-Journal of Chemistry.* 3(4)**.** 186- 201

Arbizzani, C., Barbarella, G., Bongini, A., Mastragostino, M. and Zambianchi, M. (1992) Electrochemical and optical properties of poly(3-methylthiophenes) electrosynthesized by 3,3′-, 3,4′- and 4,4′-dimethyl-2,2′-bithiophenes. *Synthetic Metals.* 52**.** 329-339.

Asami, R., Fuchigami, T. and Atobe, M. (2006) Development of A Novel Environmentally Friendly Electropolymerization of Water-Insoluble Monomers in Aqueous Electrolytes Using Acoustic Emulsification. *Langmuir.* 22**.** 10258-10263.

Asavapiriyanont, S., Chandler, G. K., Gunawardena, G. A. and Pletcher, D. (1984) The Electrodeposition of Polypyrrole Films From Aqueous-Solutions. *Journal of Electroanalytical Chemistry.* 177**.** 229-244.

Atkins, P. W. (1998) *Physical Chemistry.* Oxford Melbourne Tokyo, OUP Oxford.

Bobacka, J. (1999) Potential Stability of All-Solid-State Ion-Selective Electrodes Using Conducting Polymers As Ion-to-Electron Transducers. *Analytical Chemistry.* 71**.** 4932-4937.

Bobacka, J., Lewenstam, A. and Ivaska, A. (2000) Electrochemical Impedance Spectroscopy of Oxidized Poly(3,4-Ethylenedioxythiophene) Film Electrodes in Aqueous Solutions. *Journal of Electroanalytical Chemistry.* 489**.** 17-27.

Bockris, J. O. and Miller, D. (1987) Conducting Polymers:Special Applications. IN ALCACER, L. (Ed.). D. Reidel, Dordrecht.

Brazovskii, S., Kirova, N., Yu, Z. G., Bishop, A. R. and Saxena, A. (1998) Stability of Bipolarons in Conjugated Polymers. *Optical Materials.* 9**.** 502-506.

Bredas, J. L. and Street, G. B. (1985) Polarons, Bipolarons, and Solitons in Conducting Polymers. *Accounts of Chemical Research.* 18**.** 309-315.

Cadogan, A., Lewenstam, A. and Ivaska, A. (1992) Anionic Responses of Electrochemically Synthesized Polypyrrole Films. *Talanta.* 39**.** 617-620.

Camurlu, P., Tarkuç, S., Sahmetlioglu, E., Akhmedov, I. M., Tanyeli, C. and Toppare, L. (2008) Multichromic Conducting Copolymer of 1-Benzyl-2,5-Di(thiophen-2-yl)-1H-Pyrrole with EDOT. *Solar Energy Materials and Solar Cells.* 92**.** 154-159.

Chang, A. C., Blankespoor, R. L. and Miller, L. L. (1987) Characterization and Spectroelectrochemical Studies of Soluble Polymerized 3-Methoxythiophene. *Journal of Electroanalytical Chemistry.* 236**.** 239-252.

Chang, C. C., Her, L. J. and Hong, J. L. (2005) Copolymer From Electropolymerization of Thiophene and 3,4-Ethylenedioxythiophene and Its Use as Cathode for Lithium Ion Battery. *Electrochimica Acta.* 50**.** 4461-4468.

Chen, J. H., Dai, C. A. and Chiu, W. Y. (2008) Synthesis of Highly Conductive EDOT Copolymer Films via Oxidative Chemical In Situ Polymerization. *Journal of Polymer Science Part A-Polymer Chemistry.* 46**.** 1662-1673.

Daoust, G. and Leclerc, M. (1991) Structure-Property Relationships in Alkoxy-Substituted Polythiophenes. *Macromolecules.* 24**.** 455-459.

Dian, G., Barbey, G. and Decroix, B. (1986) Electrochemical Synthesis of Polythiophenes and Polyselenophenes. *Synthetic Metals.* 13**.** 281-289.

Dietrich, M., Heinze, J., Heywang, G. and Jonas, F. (1994) Electrochemical and Spectroscopic Characterization of Polyalkylenedioxythiophenes. *Journal of Electroanalytical Chemistry.* 369**.** 87-92.

Doblhofer, K. and Rajeshwar, K. (1998) Electrochemistry of Conducting Polymer. IN SKOTHEIM, T. A., ELSENBAUMER, R. L. & REYNOLDS, J. R. (Eds.) *Handbook of Conducting Polymers.* 2nd ed. New York. Marcel Decker

Doherty, W. J., Wysocki, R. J., Armstrong, N. R. and Saavedra, S. S. (2006) Electrochemical Copolymerization and Spectroelectrochemical Characterization of 3,4-Ethylenedioxythiophene and 3,4-Ethylenedioxythiophene-Methanol Copolymers on Indium-Tin Oxide. *Macromolecules.* 39**.** 4418-4424.

El Moustafid, T., Gregory, R. V., Brenneman, K. R. and Lessner, P. M. (2003) Electrochemical Deposition and Characterization of Poly(3,4-ethylenedioxythiophene) from Aqueous Solutions. *Synthetic Metals.* 135-136**.** 435-436.

Feldhues, M., Kampf, G., Litterer, H., Mecklenburg, T. and Wegener, P. (1989) Polyalkoxythiophenes Soluble Electrically Conducting Polymers. *Synthetic Metals.* 28**.** C487-C493.

Friedrich, B. and Herschbach, D. (2003) Stern and Gerlach: How a bad cigar helped reorient atomic physics. *Physics Today.* 56**.** 53-59.

Gaupp, C. L., Welsh, D. M., Rauh, R. D. and Reynolds, J. R. (2002) Composite Coloration Efficiency Measurements of Electrochromic Polymers Based on 3,4-Alkylenedioxythiophenes. *Chemistry of Materials.* 14**.** 3964-3970.

Genies, E. M., Bidan, G. and Diaz, A. F. (1983) Spectroelectrochemical Study of Polypyrrole Films. *Journal of Electroanalytical Chemistry.* 149**.** 101-113.

Goto, H. and Akagi, K. (2006) Optically Active Electrochromism of Poly(3,4-Ethylenedioxythiophene) Synthesized by Electrochemical Polymerization in Lyotropic Liquid Crystal of Hydroxypropyl Cellulose/Water: Active Control of Optical Activity. *Chemistry of Materials.* 18**.** 255-262.

Gratzl, M., Hsu, D. F., Riley, A. M. and Janata, J. (1990) Electrochemically Deposited Polythiophene. 1. Ohmic Drop Compensation and The Polythiophene Paradox. *Journal of Physical Chemistry.* 94**.** 5973-5981.

Groenendaal, B. L., Jonas, F., Freitag, D., Pielartzik, H. and Reynolds, J. R. (2000) Poly(3,4-Ethylenedioxythiophene) and Its Derivatives: Past, Present, and Future. *Advanced Materials.* 12**.** 481-494.

Groenendaal, L., Zotti, G., Aubert, P. H., Waybright, S. M. and Reynolds, J. R. (2003) Electrochemistry of Poly(3,4-Alkylenedioxythiophene) Derivatives. *Advanced Materials.* 15**.** 855-879.

Han, D. H., Kim, J. W. and Park, S. M. (2006) Electrochemistry of Conductive Polymers 38. Electrodeposited Poly(3,4-Ethylenedioxy-Thiophene) Studied by Current Sensing Atomic Force Microscopy. *Journal of Physical Chemistry B.* 110**.** 14874-14880.

Heinze, J. (1990) Electronically Conducting Polymers. *Topics in Current Chemistry* 152**.** 1-47.

Heywang, G. and Jonas, F. (1992) Poly (alkylenedioxythiophene)s: New, Very Stable Conducting Polymers. *Advanced Materials.* 4**.** 116-118.

Hiller, M., Kranz, C., Huber, J., Bauerle, P. and Schuhmann, W. (1996) Amperometric Biosensors Produced by Immobilization of Redox Enzymes at Polythiophene-Modified Electrode Surfaces. *Advanced Materials.* 8**.** 219-222.

Huang, H. and Pickup, P. G. (1998) A Donor-Acceptor Conducting Copolymer with a Very Low Band Gap and High Intrinsic Conductivity. *Chemistry of Materials.* 10**.** 2212-2216.

Huang, J. H., Ho, Z. Y., Kekuda, D., Chu, C. W. and Ho, K. C. (2008) Controlled Growth of Nanofiber Network Hole Collection Layers with Pore Structure for Polymer-Fullerene Solar Cells. *Journal of Physical Chemistry C.* 112**.** 19125-19130.

Hwang, B.-J., Santhanam, R., Wu, C.-R. and Tsai, Y.-W. (2003) Nucleation and growth mechanism for the electropolymerization of aniline in trifluoroacetic acid/lithium perchlorate/propylene carbonate medium. *Journal of Solid State Electrochemistry.* 7**.** 678-683.

Jonas, F. and Schrader, L. (1991) Conductive Modifications of Polymers with Polypyrrole and Polythiophene. *Synthetic Metals.* 41**.** 831-836.

Kagan, J. and Arora, S. K. (1983) The Synthesis of Alpha-Thiophene Oligomers via Organoboranes. *Tetrahedron Letters.* 24**.** 4043-4046.

Kanatzidis, M. G. (1990) Conductive Polymers. *Chemical & Engineering News.* 68**.** 36-54.

Kawashima, H. and Goto, H. (2011) Synthesis and Properties of a Chiroptically Active Oligomer from 3,4-Ethylenedioxythiophene and (–)-Myrtenal. *Materials.* 4**.** 1013-1022.

Kim, K. J., Song, H. S., Kim, J. D. and Chon, J. K. (1988) Mechanism of Electropolymerization of Pyrrole in Acidic Aqueous Solutions. *Bulletin of the Korean Chemical Society.* 9**.** 248-251.

Kirchmeyer, S. and Reuter, K. (2005) Scientific Importance, Properties and Growing Applications of Poly(3,4-Ethylenedioxythiophene). *Journal of Materials Chemistry.* 15**.** 2077-2088.

Krische, B. and Zagorska, M. (1989) Overoxidation In Conducting Polymers. *Synthetic Metals.* 28**.** C257-C262.

Krishnamoorthy, K., Ambade, A. V., Kanungo, M., Contractor, A. Q. and Kumar, A. (2001) Rational Design of an Electrochromic Polymer with High Contrast in the Visible Region: Dibenzyl Substituted Poly(3,4-Propylenedioxythiophene). *Journal of Materials Chemistry.* 11**.** 2909-2911.

Krishnamoorthy, K., Gokhale, R. S., Contractor, A. Q. and Kumar, A. (2004) Novel Label-Free DNA Sensors Based on Poly(3,4-Ethylenedioxythiophene). *Chemical Communications.* 820-821.

Kumar, A., Welsh, D. M., Morvant, M. C., Piroux, F., Abboud, K. A. and Reynolds, J. R. (1998) Conducting Poly(3,4-Alkylenedioxythiophene) Derivatives as Fast Electrochromics with High-Contrast Ratios. *Chemistry of Materials.* 10**.** 896-902.

Kuwabata, S., Ito, S. and Yoneyama, H. (1988) Copolymerization of Pyrrole and Thiophene by Electrochemical Oxidation and Electrochemical-Behavior of the Resulting Copolymers. *Journal of the Electrochemical Society.* 135**.** 1691-1695.

Lemaire, M., Buchner, W., Garreau, R., Hoa, H. A., Guy, A. and Roncali, J. (1990) Synthesis of Organic Conductors Using Electrodesilylation. *Journal of Electroanalytical Chemistry.* 281**.** 293-298.

Lowen, S. V., Macinnes, D. and Funt, B. L. (1989) The Electrochemical Preparation of Soluble Electrically Conducting Polymers of 3-Methoxythiophene with Narrow Distributions of Molecular Weight. *Journal of Polymer Science Part a-Polymer Chemistry.* 27**.** 4087-4097.

Lyons, M. E. G. (1997) Transport and Kinetics in Electroactive Polymers. IN PRIGOGINE, I. & S. A. RICE (Eds.) *Advances in Chemical Physics, Polymeric Systems*. New York. John Wiley & Sons.

Manisankar, P., Vedhi, C., Selvanathan, G. and Prabu, H. G. (2006) Electrochemical Synthesis and Characterization of Novel Electrochromic Poly (3,4-Ethylenedioxythiophene-co-Diclofenac) with Surfactants. *Electrochimica Acta.* 51**.** 2964-2970.

Manisankar, P., Vedhi, C., Selvanathan, G. and Prabu, H. G. (2007) Influence of Surfactants on the Electrochromic Behavior of Poly (3,4-Ethylenedioxythiophene). *Journal of Applied Polymer Science.* 104**.** 3285-3291.

Mccullough, R. D. (1998) The Chemistry of Conducting Polythiophenes. *Advanced Materials.* 10**.** 93-116.

Meng, H., Perepichka, D. F., Bendikov, M., Wudl, F., Pan, G. Z., Yu, W. J., Dong, W. J. and Brown, S. (2003) Solid-State Synthesis of a Conducting Polythiophene via an Unprecedented Heterocyclic Coupling Reaction. *Journal of the American Chemical Society.* 125**.** 15151-15162.

Nie, G. M., Qu, L. Y., Xu, J. K. and Zhang, S. S. (2008a) Electrosyntheses and Characterizations of a New Soluble Conducting Copolymer of 5-Cyanoindole and 3,4-Ethylenedioxythiophene. *Electrochimica Acta.* 53**.** 8351-8358.

Nie, G. M., Qu, L. Y., Zhang, Y., Xu, J. K. and Zhang, S. S. (2008b) Electrochemical Copolymerization of 3,4-Ethylenedioxythiophene and 5-Methylindole and Characterizations of the Copolymers. *Journal of Applied Polymer Science.* 109**.** 373-381.

Nien, P. C., Tung, T. S. and Ho, K. C. (2006) Amperometric Glucose Biosensor Based on Entrapment of Glucose Oxidase in a Poly(3,4-ethylenedioxythiophene) Film. *Electroanalysis.* 18**.** 1408-1415.

Osterholm, J. E., Passiniemi, P., Isotalo, H. and Stubb, H. (1987) Synthesis and Properties of $FeCl_4$-Doped Polythiophene. *Synthetic Metals.* 18**.** 213-218.

Park, J., Kim, H. K. and Son, Y. (2008) Glucose Biosensor Constructed from Capped Conducting Microtubules of PEDOT. *Sensors and Actuators B-Chemical.* 133**.** 244-250.

Park, J., Kim, J. and Son, Y. (2006) Conducting Polymer Micro-Tubules Hosting Electroactive Species without Guest Modification. *Synthetic Metals.* 156**.** 714-720.

Qiu, Y. J. and Reynolds, J. R. (1992) Electrochemically Initiated Chain Polymerization of Pyrrole in Aqueous Media. *Journal of Polymer Science Part A-Polymer Chemistry.* 30**.** 1315-1325.

Roncali, J. (1997) Synthetic Principles for Bandgap Control in Linear pi-Conjugated Systems. *Chemical Reviews.* 97**.** 173-205.

Roncali, J. (1999) Electrogenerated Functional Conjugated Polymers as Advanced Electrode Materials. *Journal of Materials Chemistry.* 9**.** 1875-1893.

Roncali, J., Blanchard, P. and Frere, P. (2005) 3,4-Ethylenedioxythiophene (EDOT) as a Versatile Building Block for Advanced Functional p-Conjugated Systems. *Journal of Materials Chemistry.* 15**.** 1589-1610.

Ruiz, J. P., Nayak, K., Marynick, D. S. and Reynolds, J. R. (1989) Soluble Ethylmercapto-Substituted Polythiophenes. *Macromolecules.* 22**.** 1231-1238.

Sakmeche, N., Aeiyach, S., Aaron, J. J., Jouini, M., Lacroix, J. C. and Lacaze, P. C. (1999) Improvement of the Electrosynthesis and Physicochemical Properties of Poly(3,4-ethylenedioxythiophene) Using a Sodium Dodecyl Sulfate Micellar Aqueous Medium. *Langmuir.* 15**.** 2566-2574.

Schweiss, R., Lubben, J. F., Johannsmann, D. and Knoll, W. (2005) Electropolymerization of Ethylene Dioxythiophene (EDOT) in Micellar Aqueous Solutions Studied by Electrochemical Quartz Crystal Microbalance and Surface Plasmon Resonance. *Electrochimica Acta.* 50**.** 2849-2856.

Sezer, E., Sarac, A. H. S. and Parlak, E. A. (2003) Electrochemical Synthesis of EDOT-ECZ-EDOT Copolymer on Carbon Fiber Micro-Electrodes. *Journal of Applied Electrochemistry.* 33**.** 1233-1237.

Shi, L. H., Roncali, J. and Garnier, F. (1989) Electrochemical Synthesis of Poly(3-bromo thiophene). *Journal of Electroanalytical Chemistry.* 263**.** 155-161.

Shirakawa, H., Louis, E. J., Macdiarmid, A. G., Chiang, C. K. and Heeger, A. J. (1977) Synthesis of Electrically Conducting Organic Polymers: Halogen Derivatives of Polyacetylene, $(CH)_x$. *Journal of the Chemical Society-Chemical Communications.* 578-580.

Sirringhaus, H., Kawase, T., Friend, R. H., Shimoda, T., Inbasekaran, M., Wu, W. and Woo, E. P. (2000) High-Resolution Inkjet Printing of All-Polymer Transistor Circuits. *Science.* 290**.** 2123-2126.

Skotheim, T. A., Elsenbaumer, R. L. and Reynolds, J. R. (1998) *Handbook of Conducting Polymers.* (2nd ed.). New York, Marcel Dekker, Inc.

Street, G. B. (1986) Polypyrrole: From Powders to Platics. IN J., T. & SKOTHEIM, T. A. (Eds.) *Handbook of Conducting Polymers.* 1st ed. New York. Marcel Dekker.

Tanaka, S., Sato, M. and Kaeriyama, K. (1988) Electrochemical Preparation and Properties of Poly (3-methoxy-2, 5-thiophenediyl) and Poly (3-methylthio-2, 5-thiophenediyl). *Synthetic Metals.* 25**.** 277-288.

Tourillon, G. (1986) Polythiophene and Its Derivatives. IN SKOTHEIM, T. A. (Ed.) *Handbook of Conducting Polymers.* New York. Marcel Dekker, Inc.

Tourillon, G. and Garnier, F. (1983) Effect of Dopant on the Physicochemical and Electrical Properties of Organic Conducting Polymers. *Journal of Physical Chemistry.* 87**.** 2289-2292.

Tourillon, G. and Garnier, F. (1984a) Structural Effect on Electrochemical Properties of Polythiophene and Derivatives. *Journal of Electroanalytical Chemistry.* 161**.** 51-58.

Tourillon, G. and Garnier, F. (1984b) Structural Effect on the Electrochemical Properties of Polythiophene and Derivatives. *Journal of Electroanalytical Chemistry and Interfacial Electrochemistry.* 161**.** 51-58.

Tourillon, G. and Garnier, F. (1984c) Structural Effect on the Electrochemical Properties of Polythiophene Derivatives. *Journal of Electroanalytical Chemistry.* 161**.** 51-58.

Tsai, E. W., Basak, S., Ruiz, J. P., Reynolds, J. R. and Rajeshwar, K. (1989) Electrochemistry of Some β-Substituted Polythiophenes. Anodic Oxidation, Electrochromism, and Electrochemical Deactivation. *Journal of the Electrochemical Society.* 136**.** 3683-3689.

Varis, S., Ak, M., Akhmedov, I. M., Tanyeli, C. and Toppare, L. (2007) A Novel Multielectrochromic Copolymer Based on 1-(4-nitrophenyl)-2,5-di(2-thienyl)-1H-Pyrrole and EDOT. *Journal of Electroanalytical Chemistry.* 603**.** 8-14.

Waltman, R. J. and Bargon, J. (1984) Reactivity/Structure Correlations for the Electropolymerization of Pyrrole: An INDO/CNDO Study of the Reactive Sites of Oligomeric Radical Cations. *Tetrahedron.* 40**.** 3963-3970.

Waltman, R. J. and Bargon, J. (1986) Electrically Conducting Polymers: A Review of the Electropolymerization Reaction, of the Effects of Chemical Structure on Polymer Film Properties, and of Applications Towards Technology. *Canadian Journal of Chemistry-Revue Canadienne De Chimie.* 64**.** 76-95.

Waltman, R. J., Bargon, J. and Diaz, A. F. (1983) Electrochemical Studies of Some Conducting Polythiophene Films. *Journal of Physical Chemistry.* 87**.** 1459-1463.

Wan, X. B., Zhang, W., Jin, S., Xue, G., You, Q. D. and Che, B. (1999) The Electrochemical Copolymerization of Pyrrole and Furan in a Novel Binary Solvent System. *Journal of Electroanalytical Chemistry.* 470**.** 23-30.

Wang, J., Xu, Y. L., Chen, X. and Du, X. F. (2007) Electrochemical Supercapacitor Electrode Material Based on Poly(3,4-ethylenedioxythiophene)/Polypyrrole Composite. *Journal of Power Sources.* 163**.** 1120-1125.

Wang, X. J. and Wong, K. Y. (2006) Effects of a Base Coating Used for Electropolyrnerization of Poly(3,4-ethylenedioxythiophene) on Indium Tin Oxide Electrode. *Thin Solid Films.* 515**.** 1573-1578.

Wei, Z. H., Xu, J. K., Hou, J., Zhou, W. Q. and Pu, S. Z. (2006) Electrochemical and Spectroscopic Characteristics of Copolymers Electrochemically Synthesized from

3-(4-fluorophenyl)thiophene and 3,4-Ethylenedioxythiophene. *Journal of Materials Science.* 41**.** 3923-3930.

Welsh, D. M., Kumar, A., Meijer, E. W. and Reynolds, J. R. (1999) Enhanced Contrast Ratios and Rapid Switching in Electrochromics Based on Poly(3,4-propylenedioxythiophene) Derivatives. *Advanced Materials.* 11**.** 1379-1382.

Xu, J. K., Nie, G. M., Zhang, S. S., Han, X. J., Hou, J. and Pu, S. Z. (2005) Electrochemical Copolymerization of Indole and 3,4-Ethylenedioxythiophene. *Journal of Materials Science.* 40**.** 2867-2873.

Xu, Y., Wang, J., Sun, W. and Wang, S. (2006) Capacitance Properties of Poly(3,4-ethylenedioxythiophene)/Polypyrrole Composites. *Journal of Power Sources.* 159**.** 370-373.

Yang, J. Y., Lipkin, K. and Martin, D. C. (2007) Electrochemical Fabrication of Conducting Polymer Poly(3,4-ethylenedioxythiophene) (PEDOT) Nanofibrils on Microfabricated Neural Prosthetic Devices. *Journal of Biomaterials Science-Polymer Edition.* 18**.** 1075-1089.

Zhang, S. S., Hou, J., Zhang, R., Xu, J. K., Nie, G. M. and Pu, S. Z. (2006) Electrochemical Polymerization of 3,4-Ethylenedioxythiophene in Aqueous Solution Containing *N*-Dodecyl-β-D-Maltoside. *European Polymer Journal.* 42**.** 149-160.

CHAPTER 3

ELECTROCHEMICAL SENSORS

3.1 Chemical Sensor

According to the International Union of Pure and Applied Chemistry (IUPAC), a chemical sensor is "a device that transforms chemical information, ranging from the concentration of a specific sample component to total composition analysis, into a useful analytical signal" (Hulanicki *et al.*, 1991). This definition emphasises two important aspects in chemical sensing *i.e.* molecular recognition and signal transduction. Chemical sensors can be divided into different classes depending on different transducing processes namely optical sensors, electrochemical sensors, electrical sensors, mass sensitive sensors, magnetic sensors, thermometric sensors and other sensors which include the determination of chemical composition. However, electrochemical sensors are by far the most established sensor. Electrochemical sensor involves measuring potential (potentiometric sensors) or current (amperometric sensors). The former sensor class includes the well-established ion-selective electrodes (ISEs). This field has rapidly grown in just a few decades due to relatively low cost, portability and fast read-out signal. The fundamental in potentiometric measurement is the potential (E) arising between two electrodes in approximately zero current flow conditions. This simple concept makes the practical electroanalytical method very useful for the application in clinical and environmental quality control. Today, there are more than 60 different ions have been detected using the principle of ISE (Bakker *et al.*, 1997).

3.1.1 Sensing Components in Ion-selective Membrane

Ion-selective-electrodes (ISEs) can be divided into three main groups, namely glass membrane, crystalline membrane (solid membrane) and polymeric membrane (liquid membrane). The most common glass membrane electrode is the glass pH electrode. This electrode incorporates both glass and reference electrode in one body. A crystalline membrane is commonly used for environmental monitoring of heavy metal ions such as copper, cadmium and silver. Both glass membrane and crystalline membrane have good selectivity but only a few ions can be measured using the approach.

A polymeric membrane is normally used to separate a filling solution containing a solution of the target ion and the test solution. It is commonly known as ion-selective membrane (ISM). This polymeric membrane consists of four components, in which the nature and the amount of each component have a great effect on the characteristics of the chemical sensors. The four basic membrane components are:

- Polymeric matrix
- Ionophore (membrane – active recognition)
- Plasticizer (membrane solvent)
- Lipophilic additive salt (Ionic additives)

One of the main advantages of a polymeric membrane is its high selectivity achieved by incorporating molecular recognition (an ion carrier). However, a polymeric membrane needs to be stable in order to be effective. Typically, the component of sensing membrane consists of 33% (w/w) polyvinyl chloride (PVC) as polymeric matrix, 66% plasticizer for homogenzing the matrix and 1% ionophore (Bakker *et al.*, 1997, Moody *et al.*, 1970). The first membranes using neutral-carrier were prepared using silicon rubber (Pick *et al.*, 1973) or PVC (Pick *et al.*, 1973) without the addition of lipophilic ionic sites. Later it was realised that these ISEs only exhibited a Nernstian response due to the presence of ionic impurities (Horvai *et al.*, 1986, Lindner *et al.*, 1988, Vandenberg *et al.*, 1987) and other membrane components (Bühlmann *et al.*, 1995). It has been shown that

membranes without ionic sites do not give any response to the target ion (Bühlmann *et al.*, 1995, Buhlmann *et al.*, 1995).

Shatkay (1967) was the first to use a polymer as a homogenous membrane matrix for an ion-selective membrane and PVC is a common material used as the polymer matrix. PVC is used as a matrix that gives the membrane mechanical strength and structural integrity but is not intended to be an active component in the membrane. Polyurethane (PU) is also used as a polymer matrix due to enhanced biocompatibility and its adhesive property (Roncali, 1997), however they tend to result in higher detection limits (Nam and Cha, 2000).

The ionophore is an electron-rich complexing compound that can bind to a specific ion. It can be an ion exchanger (charged) or a neutral macrocyclic compound that has cavities to surround the target ions. The ionophore is the most important component in any polymeric membrane, as it is responsible for the selectivity and sensitivity of the sensor which depends on the binding between the ionophore and the target ion. The selectivity of an ISE towards other ions originates from the difference in binding strength between the ionophore and various ions. A good ionophore must complex the ion of interest with higher affinity than interfering ions and the complexation must be reversible. The ions will be transferred through an organic membrane by carrier translocation. A number of naturally occurring ionophores have been used as ISE membrane components such as valinomycin, crown ether, nonactin, ionomycin, nigericin and monensin. Since some of the natural ionophores have limited selectivity, many synthetic ionophores have also been synthesised (Kuras and Gutmaniene, 2000).

A plasticizer is an important component in an ISE membrane. It is added to increase the plasticity *i.e.* turning the hard brittle plastic into a soft flexible elastomer by reducing the glass transition temperature (T_g) of the PVC to below room temperature. It should be inert and not form complexes with ions. The plasticizer also plays a role in dissolving the ionophore and lipophilic ionic additives in order to provide a homogenous and miscible system with the polymer matrix. For practical use as ISE membrane,

leaching of the plasticizer should be avoided, otherwise it would affect the electrode performance over time. Leaching of the plasticizer from the membrane will increase the loss of ionophore and lipophilic additives. Common plasticizers used include adipates, phthalates, sebacates and phenyl ethers (Bakker *et al.*, 1997).

Lipophilic additive salts also known as ionic additives are ion exchangers. It is well established that the addition of a known quantity of lipophilic additive has greatly improved the electrode response time, stability, reproducibility and selectivity. It has also been shown that membranes without ionic sites do not respond to the concentration changes of the ion of interest (Shi *et al.*, 2002). Therefore, it is a necessary for any membrane to have ion exchange sites in order to provide permselectivity. Initially, the main objective of adding a tetraphenyl borate salt to the membrane of a cation-selective electrode was to reduce the anionic interference observed in the presence of lipophilic anions like thiocyanate (Morf *et al.*, 1974). Lipophilic additives also serve to lower the electrical resistance of the membrane, which is especially important for microelectrodes (Budai and Molnar, 2001). The most common lipophilic salt additives used in ISEs are tetraphenyl borate salts for cation-selective electrodes and tetraalkyl ammonium salts for anion-selective electrodes.

3.1.2 Potentiometric Measurements Using Ion-selective Electrodes

Potentiometric measurements are made using a potentiometer to determine the difference in potential between a working electrode and a reference electrode (EMF measurement). In potentiometric measurements, two electrodes need to be used as the absolute potential of an individual half-cell cannot be determined. The two electrodes are:

- an ion-selective electrode with membrane
- an external reference electrode

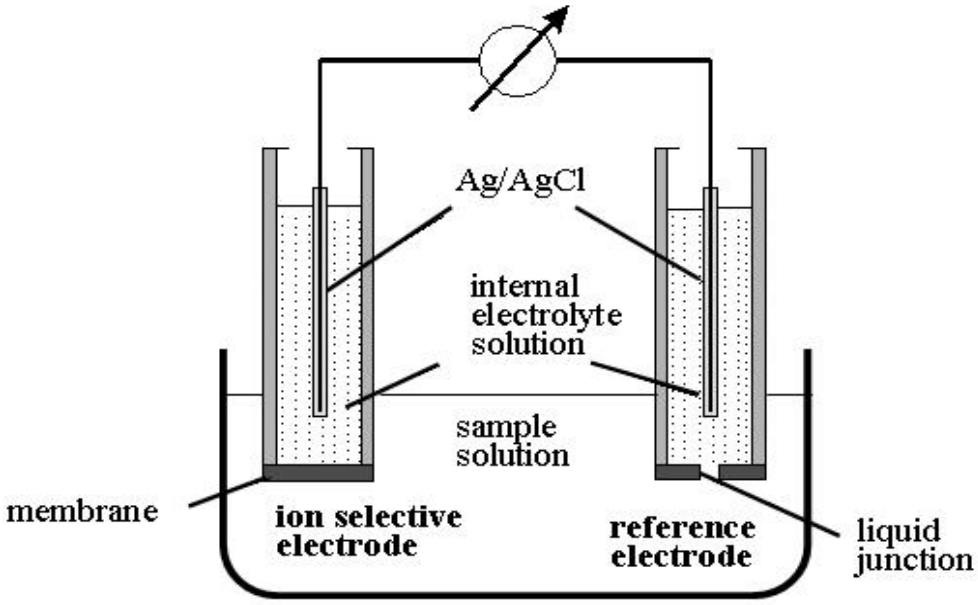

Figure 3.1: Schematic representation of a typical potentiometric cell. (http://www.nico2000.net/datasheets/How%20ISEs%20Work.htm)

Ion-selective electrodes (ISEs) are electrodes that respond selectively to the activity (not concentration) of a particular ion sensed by the selective membrane. The conventional ISE consists of a Teflon tube filled with inner filling solution. The electrical contact is made via internal reference electrode (usually Ag/AgCl). The external reference electrode should be stable and has a fixed potential such as a Ag/AgCl or saturated calomel electrode. The electrochemical cell of the ISE measurement can be represented as:

external reference electrode	test solution	membrane	inner solution	internal reference electrode

Ag | AgCl | KCl (sat' d) || test solution | membrane | inner solution | AgCl | Ag

E_1 E_2 E_J E_M E_3 E_4

The potential of a membrane is generated when both electrodes are in contact with the sample solution. The primary ion is transferred from the sample solution to the membrane phase and a potential difference is generated by selective ion exchange at both interfaces. The measurement is made at zero current condition. In this condition, the transfer of primary ion from the solution to the membrane is equal to the transfer of ions from the membrane to the solution. The measured voltage is a difference of potentials and not possible to measure the absolute potentials. The voltage across the whole cell is the sum of different potential generated at all solid-solid, solid-liquid and liquid-liquid interfaces.

$$\text{EMF} = E_1 + E_2 + E_3 + E_4 + E_\text{J} + E_\text{M} \quad \textbf{(3.1)}$$

In an ideal condition, potentials of E_1 through E_5 are constant. Therefore, the electromotive force (EMF) across the galvanic cell can be expressed as (Bakker *et al.*, 1997):

$$EMF = E_\text{constant} + E_J + E_M \quad \textbf{(3.2)}$$

E_M is the membrane potential which includes the phase boundary potentials (E_PB) at both aqueous sample|membrane interfaces and the diffusion potential within the membrane (E_D). E_J is the liquid junction potential created at the porous frit, practically used instead of the salt bridge (||) for which $E_\text{J} = 0$. It is important to note that this liquid junction potential that prohibits the true assessment of single ion activities with ion-selective electrodes (Sigel *et al.*, 1991). E_J originates from a separation of charge created on the interface due to the different mobilities of ions migrating at different rates. For ions of similar mobility E_J can be very small and it can be neglected. For an ISE, the E_D is zero if no ion concentration gradients occur. Then, the EMF is only dependent on the variation of the phase boundary potential at sample solution|membrane interface (E_PB) (Bakker *et al.*, 1997):

$$\text{EMF} = E_\text{constant} + E_\text{PB} \quad \textbf{(3.3)}$$

3.1.3 Characteristic of ISE

3.1.3.1 Sensitivity

In an ideal condition, the potential difference between internal filling solution and sample solution should be a linear function of the logarithm of the ion activity. In this case, the EMF can be described by the Nernst equation:

$$E = E^0 \pm \frac{RT}{nF} \log a \qquad \textbf{(3.4)}$$

where:

E experimentally observed potential

E^0 standard potential

R gas constant

T temperature (K)

n number of electron

F Faraday constant (96, 485 C mol^{-1})

a activity of primary ion

Based on the Nernst equation, the potential observed is proportional to the logarithm of the activity of the primary ion. The term RT/nF is the slope of the linear range of the calibration curve (**Figure 3.2**). The sensitivity of an ISE is based on this slope. The theoretical value of the slope according to the Nernst equation is 59.16 mV/dec (25 °C) for a monovalent ion or 59.16/2 = 29.58 mV/dec for a divalent ion. However, any slope in the range of 50 – 60 mV/dec (monovalent) can be regarded as near ideal. The slope will change when there is a mixture of primary and interfering ions and increase if the interfering ions are of a different charge, according to Nicolsky-Eisenman equation (equation 3.5). In addition, based on Nerst equation, the slope will change with temperature at the rate of 3.4% per 10 °C.

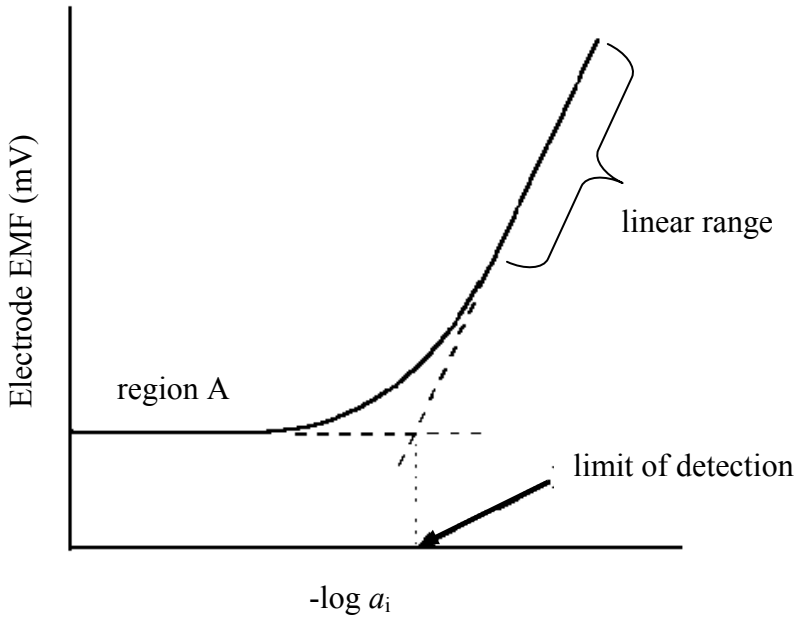

Figure 3.2: Typical calibration curve of an ion-selective electrode.

3.1.3.2 Selectivity

Selectivity is one of the important characteristics of ISE. It is defined as the degree of ability to discriminate the primary ion in the solution in the presence of other ions. Ideally, an ISE will only respond to primary ion not to the other ions in a sample solution. However, in a real situation interfering ions compete with the primary ion and can be extracted into the membrane. This phenomenon causes deviation from the Nernstian response. The Nernst equation must then be modified to take into account the selectivity-weighted activities for both ions and this equation is called the Nicolsky-Eisenman equation:

$$E = E^0 \pm \frac{2.303RT}{nF} \log\left[a_i + \Sigma K_{ij}^{pot} \left(a_j\right)^{z_i/z_j} \right] \qquad \textbf{(3.5)}$$

where:

E the experimentally observed potential

E^0 standard potential (constant)

R gas constant

T temperature (K)

a_i activity of primary ion

a_j activity of interfering ion

K_{ij}^{pot} selectivity coefficient

z_i charge number: an integer with sign and magnitude corresponding to the charge of primary ion

z_j charge number: an integer with sign and magnitude corresponding to the charge of interfering ion

The selectivity coefficients are most commonly expressed as the logarithm of K_{ij}^{pot}. Negative values indicate a preference for the primary ion relative to the interfering ion. On the other hand, positive values indicate a preference for the interfering ion. The K_{ij}^{pot} values can be determined by:

- *Separate solution method (SSM)*

The EMF of measuring primary ion and interfering ion are both determined in pure single electrolyte solution, one containing the ion A at the activity a_A (with no B), the other one containing the ion B at the same activity $a_B = a_A$ (with no A). If the measured values are E_1 and E_2, the selectivity coefficient is calculated as:

$$\log K_{A,B}^{pot} = \frac{E_2 - E_1}{2.303RT / z_A F} + \left(1 - \frac{z_A}{z_B}\right)\log a_A \qquad \textbf{(3.6)}$$

This method is simple but the data obtained are often not representative for real conditions of sample solution.

- *Fixed interference method (FIM)*

The EMF of a cell is measured in a solution with a fixed activity of the interfering ion whilst varying the activity of primary ion. The selectivity coefficient is calculated from:

$$K_{ij}^{pot} = \frac{a_i}{a_j^{z_i / z_j}} \qquad \textbf{(3.7)}$$

Both z_i and z_j have the same sign. The a_i value is determined by the intersection of the extrapolated linear response of the plot of EMF values *vs* the logarithm of the activity of the primary ion. This method reflects the experimental conditions more accurately and is recommended by IUPAC (Umezawa *et al.*, 2000).

- *Matched potential method (MPM)*

In this method, primary ion and interfering ion are added to the same reference background solution separately in different amounts until the potential observed is the same. This method does not depend on the Nicolsky-Eisenman equation and the selectivity coefficient is defined as the activity ratio of primary and interfering ions that gives the same potential change under identical conditions. A known activity (a_A') of the primary ion solution is added into a reference solution that contains a fixed activity (a_A) of primary ions, and the corresponding potential is recorded. A solution of an interfering ion is then added to the reference solution until the same potential change is obtained. The change in potential produced at the constant background of the primary ion must be the same in both cases.

$$k_{IJ}^{\mathrm{MPM}} = \frac{(a_{\mathrm{A}}{}' - a_{\mathrm{A}})}{a_{\mathrm{B}}} \qquad \textbf{(3.8)}$$

A lowercase *k* is used to distinguish from the Nicolsky coefficient (Bakker, 1997) as they are not comparable in most cases depending on the experimental condition (Macca, 1996).

3.1.3.3 Limit of Detection (LOD)

According to IUPAC (Buck and Lindner, 1994), the limit of detection (LOD) is defined as the concentration for which, under the specified conditions, the cell EMF, *E,* deviates from the average EMF in region A by a multiple of the standard error of a single measurement of the EMF in this region as depicted in **Figure 3.2**. The multiple of the standard error depends on a statistical significance level selected (2 for 95% or 3 for 99%). This detection limit can often be reduced with the modification of the internal filling solutions by adding a chelating agent, an ion exchange resin or replaced by a solid contact (Bakker and Pretsch, 2005, Bobacka, 2006, Pretsch, 2007).

3.1.3.4 Response time

Another important characteristic of an ISE is response time. It is particularly important for batch and flow systems. However, this characteristic is largely underrated since many authors do not even report response time or the definition is adjusted according to convenience (Macca, 2004). The confusion about the definition of response time is due to the fact that the IUPAC definition has changed several times (Macca, 2004). The currently accepted definition is the time which elapses between the instant when an ion-selective electrode and a reference electrode are brought into contact with a sample solution (or at which the activity of the ion of interest in a solution is changed) and the first instant at which the EMF/time slope ($\Delta E/\Delta t$) becomes equal to a limiting value selected on the basis of the experimental conditions (Buck and Lindner, 1994).

The following section will explain some studies related to PEDOT as solid contact in preparation of an ASSISE.

3.2 PEDOT-based Material as A Solid Contact

ASSISEs are usually fabricated in two steps *i.e.* deposition of the conducting polymer transducer on solid electronic conductor and coating by ISM, most often plasticized PVC (Bobacka, 2006). PEDOT has shown to be one of the most interesting conducting polymers as solid contacts to produce ASSISE (Bobacka, 1999, Bobacka *et al.*, 2001b, Bobacka *et al.*, 2004, Ocypa *et al.*, 2006).

Bobacka *et. al* (1999) have studied the influence of the capacitance of PEDOT as a solid contact on the potential stability of the electrodes. A high redox capacitance of the ion-to-electron transducer was found to stabilise the electrode potential (Bobacka, 1999). PEDOT doped with poly(styrene sulfonate) (PSS) has been successfully used to obtain ISEs sensitive to potassium (Bobacka, 1999, Vázquez *et al.*, 2002), calcium (Michalska and Maksymiuk, 2004), aromatic cations (Bobacka *et al.*, 2002) and silver (Bobacka *et al.*, 2001a, Bobacka *et al.*, 2004). Bobacka *et al.* (2002) have used PEDOT/PSS as solid contact for complexation of aromatic cation (*N*-methylpyridinium) by tetraphenylborate that acted as charge carrier in the plasticized PVC membrane. Vázquez *et al.* (2002) have shown that the potential recorded for potassium-selective electrodes based on PEDOT as solid contact is less sensitive to O_2 and CO_2 (solution pH changes) compared to PPy.

A PEDOT/PSS suspension, a water-based compound that is commercially available from Bayer AG (known as Baytron P) is very suitable for practical applications. This suspension contains a non-stoichiometric polyelectrolyte complex of PEDOT and PSS, with an excess of PSS that stabilises the colloidal particle of the polymer (Ghosh and Inganäs, 1999). A solution-casting technique was used to deposit PEDOT/PSS suspension on screen-printed gold substrates as described by Vázquez *et al.* (2004b). The PEDOT/PSS film was crosslinked by a multivalent cation (Mg^{2+}, Ca^{2+}, $Fe^{2+/3+}$ and $Ru(NH_3)_6^{2+/3+}$) to form a hydrogel in order to decrease the water solubility of the PEDOT/PSS before application of the plasticized PVC K^+-selective membrane. The incorporation of $Ru(NH_3)_6^{2+/3+}$ redox couple into the transducer phase produced sensors with the most stable potentials and also increased the total bulk redox capacitance of the

polymer film (Vázquez *et al.*, 2004b). The potentiometric measurement showed that PEDOT/PSS crosslinked with $Ru(NH_3)_6^{2+/3+}$ was less sensitive to CO_2 (pH solution changes) than the bare Au substrate (Vázquez *et al.*, 2004b).

The K^+-selective electrode obtained by solution casting of PEDOT/PSS (Vázquez *et al.*, 2004a, Vázquez *et al.*, 2004b) showed a linear response from 10^{-5} to 10^{-1} M KCl. Casting PEDOT/PSS solution was also found to be a more advantageous method to deposit the conducting polymer compared to electropolymerised PEDOT for mass production due to its simplicity and fast fabrication (Vázquez *et al.*, 2004a). Flow cells with small-volume for all-solid-state K^+-selective electrode using PEDOT/PSS as solid internal contact was described by Vázquez *et al.* (2004a). This approach would be a feasible method for the clinical analysis application (Vázquez *et al.*, 2004a).

A new type of ion-selective electrodes, the so-called all-plastic electrodes, have been developed by Michalska and Maksymiuk (2004) by solution-casting of PEDOT/PSS (Baytron P) on insulating plastic substrate. The PEDOT/PSS served both as electronic contact and ion-to-electron transducer. However, the obtained layer structure can still peel off from the support resulting in loss of electrical contact. It was found that modification of conducting polymer suspension by adding more PSS ions induced the effective binding of K^+ in the transducer layer, thus improving the linear response range and selectivity (Michalska and Maksymiuk, 2004). Cu^{2+}-selective electrode with super-Nernstian response was obtained for Cu^{2+} activity below 10^{-4} M using a similar approach (Michalska *et al.*, 2005). This observation was due to the prevention of leakage of primary ion from the membrane. Recently, Xu *et al.* (2010) have developed a disposable blood potassium sensor based on PEDOT/PSS. The response time of the sensor was 15 s when less than 15 μL of sample was applied (Xu *et al.*, 2010).

Ocypa *et al.* (2006) has reported a Cu^{2+} chemical sensor based on PEDOT film doped with hexacyanoferrate anion, PEDOT(HCF). It was found that Cu^{2+} can spontaneously accumulate in the PEDOT(HCF) layer under the open circuit condition. This spontaneous incorporation of analyte has resulted in significant improvement of

selectivity (up to four orders of magnitude) or lower detection limit of potentiometric response. Michalska *et al.* (2003) studied the direct use of a PEDOT film as an ion-sensing membrane rather than as a transducer layer. The PEDOT(Cl) film was not found to be a promising material for long-life potentiometric sensor as the polymer film became brittle and poorly adhesive on glassy carbon after prolonged conditioning. Recently, PEDOT doped with negatively charged multi-walled carbon nanotubes (MWCNTs) use as a solid contact for a K^+-selective electrode was demonstrated by Mousavi *et al.* (2009). PEDOT(CNT)/K^+-ISM on screen-printed carbon electrode modified with carboxyl functionalized MWCNT (SPCE-MWCNT) showed better long-term potential stability than PEDOT(CNT)/K^+-ISM on glassy carbon. Results obtained from cyclic voltammetric and electrochemical impedance spectroscopic studies revealed a high redox capacitance of PEDOT(CNT), which is favorable for an ion-to-electron transducer in ASSISE (Mousavi *et al.*, 2009).

Paczosa-Bator *et al.* (2006) described the influence of surface topography and morphology of PEDOT doped with ATP film on potentiometric response. More smooth and less rough films result in better potentiometric characteristics. Ag^+-ion selective electrode using spherical hydrocarbons (cyclophanes) as π-coordinating ionophores was reported by Bobacka *et al.* (2001a). The selectivity coeffients of the ISEs to Ag^+ were found to depend on both the symmetry and formal ring size of the cyclophanes. The cyclophanes that do not contain any heteroatoms can be highly selective to 'soft' cations like Ag^+, based on cation-π interactions between Ag^+ and benzene rings (Bobacka *et al.*, 2001a).

3.3 Ion Amperometry of Ion-selective Electrode

Ion amperometry is a measurement of ion transfer from an aqueous to an organic phase induced by applying potential. Many researchers consider this electroanalytical technique to be interesting due to the capability to make measurements of redox inactive species at the interface between two immiscible solutions. The measured current is proportional to the sample concentration and can be mediated by ionophore presence in the organic phase. The mechanism of ion selective extraction can be simply written in two steps:

$$M^z\,(s) \rightleftharpoons M^z(m) \tag{3.9}$$

$$M^z\,(m) + L\,(m) \rightleftharpoons ML^z(m) \tag{3.10}$$

where:

M^z	target ion with the charge number z
L	neutral ionophore
s	sample solution
m	membrane phase

The equilibrium potential difference $\Delta_s^m\phi$ at the solution|membrane interface can be written as:

$$\Delta_s^m\phi = \phi(m) - \phi(s) = \Delta_s^m\phi_M^0 + \frac{RT}{zF}\ln\frac{a_m(s)}{a_m(m)} \tag{3.11}$$

The standard ion transfer potential $\Delta_s^m\phi_M^0$ is related to the difference of the standard chemical potential μ^0 of the ion in the sample solution and membrane *i.e.* standard molar Gibbs free energy of the ion transfer from solution to membrane $\Delta G_{tr,M}^{0,s\to m}$:

$$\Delta_{\mathrm{s}}^{\mathrm{m}}\phi_{\mathrm{M}}^{0} = -\frac{\mu^{0}(\mathrm{m}) - \mu^{0}(\mathrm{s})}{ZF} = -\frac{\Delta G_{\mathrm{tr,M}}^{0,\mathrm{s}\rightarrow\mathrm{m}}}{zF} \qquad \textbf{(3.12)}$$

For ISEs, most of the work is mainly focused on potentiometric measurements. However, for the same type of ion-selective membrane, amperometric measurements can also be performed using the concept of ion amperometry (Horváth *et al.*, 1990). It is also found that the amperometric working range for the determination of ions extends to considerably lower concentrations than in potentiometry (Horváth *et al.*, 1990). The application of the ion amperometry concept in this study will be explained in **Chapter 7**.

3.4 Electrochemical Chiral Sensors

3.4.1 Chirality

Stereoisomers are compounds made up of the same atoms bonded by the same sequence of bonds but differing in the way their atoms are arranged in space. There are two kinds of stereoisomers *i.e.* enantiomers and diastereomers. Enantiomers are pairs of molecules that are non-superimposable mirror images of each other. The presence of enantiomers is known as chirality and the molecules are called chiral molecules. In contrast, achiral molecules are molecules that are identical to their mirror image. Many chiral compounds contain an asymmetric carbon *i.e.* carbon atom bonded with four different groups such as 2-bromobutane (**Figure 3.3**). However, if a molecule has a plane of symmetry, it is not a chiral molecule even though it has asymmetric carbons (**Figure 3.4**) but chiral molecules can possess other symmetry elements such as rotational symmetry. Thus, a few aspects need to be considered to identify whether a molecule is chiral or achiral.

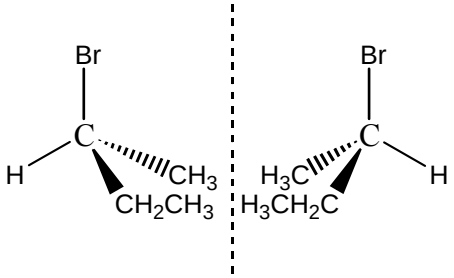

Figure 3.3: Enantiomers of 2-bromobutane.

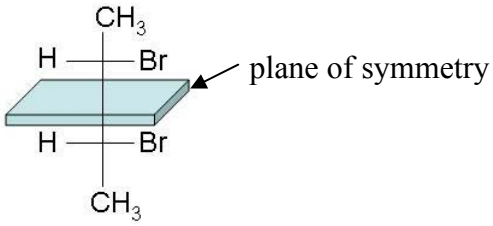

Figure 3.4: Plane of symmetry of 2,3-bromobutane.

Enantiomers have identical chemical and physical properties such as boiling point, melting point and solubility. However, enantiomers interact differently with plane-polarised light. An enantiomer of a chiral molecule rotates plane-polarised light in one direction, while the other enantiomer rotates the light in the opposite direction. This phenomenon is called optical activity and was first observed by Louis Pasteur (Bruice, 2004). A mixture consisting of an equimolar mixture of two enantiomers is called a racemate and is optically inactive. Diastereomers are all stereoisomers that are not enantiomers, e.g. (*Z*)- and (*E*)-but-2-ene.

3.4.2 Chiral PEDOT

The induction of chirality in conducting polymers may occur via several routes, such as covalent attachment of chiral substituents to the monomer as a side chain and incorporation of chiral dopant anions. The first chiral conducting polymers prepared via the electropolymerisation of pyrrole monomer bearing optically active substituents was reported by Elsenbaumer *et al.* (1985). Since that time, many optically active CPs have

been prepared for polypyrrole, polyaniline and polythiophene (Kane-Maguire and Wallace, 2010). However, the induction of chirality in derivatives of polythiophene *i.e.* PEDOT has not been studied to the same extent as polypyrrole and polyaniline.

Chiral PEDOT was reported for the first time by Caras-Quintero and Bäuerle (2004) via introduction of two substituents at the ethylene bridge, when two chiral centers are formed. However, the chiral properties of the resulting polymer were not investigated. Recently, a new chiral PEDOT derivative was synthesised from oxidative polycondensation of EDOT and (–)-myrtenal (Kawashima and Goto, 2011). The chiral substituent induces helical conformation of the main chain to exhibit chiroptical activity. A blue shift of the circular dichroism (CD) spectra upon doping with iodine of the resultant oligomer suggests the change in electronic structure and tuning of chiroptical activity.

The use of chiral anions incorporated into conducting polymer can vary from relatively small species to bulky biological compounds. This approach has been extensively used by Goto and Akagi to prepare optically active chiral PEDOT utilising chiral liquid crystals as dopant anions (Goto, 2009, Goto and Akagi, 2004, Goto and Akagi, 2006). Electrochemical polymerisation of EDOT in aqueous solution of chiral nematic liquid crystal (N*-LC) hydroxypropyl cellulose (HPC) formed PEDOT/HPC with strong bisignate CD, which is associated to the PEDOT π-π* absorption band (Goto and Akagi, 2006). The addition of a small amount of *n*-hexylcyanobiphenyl during the electropolymerisation of EDOT can also induce the formation of helical structure (Goto and Akagi, 2004). The method used in these studies has opened up a new technique for the preparation of chiral polymer as the polymerisation mechanism using N*-LC differs from chiral polymerisation using chiral catalyst or polymerisation of a monomer bearing chiral substituents.

3.4.3 Chiral Sensors Based on Conducting Polymer

It is well known that biological systems tend to favour one enantiomer of a chiral molecule over the other. This is due to different stereochemistry *i.e.* enantiomers have different spatial arrangements and different binding characteristics to chiral species. This interesting feature has initiated the development of various chiral sensors (Trojanowicz and Kaniewska, 2009) but it is relatively novel in electrochemical sensing.

Chiral discrimination of enantiomers of camphosulfonic acid (CSA) using different polypyrroles grafted with chiral side chains was investigated by Pleus and Schwientek (1998). The enantioselective properties were investigated using cyclic voltammetry in the presence of enantiomers of CSA and potentiodynamic polymerisation using the same chiral electrolytes. Electropolymerisation was easily achieved in acetonitrile containing (*S*)-CSA and inhibited using (*R*)-CSA. From the literature, it is found that this concept of discrimination of enantiomers using chiral conducting polymers is very little reported. However, there are some studies reported regarding enantioselective potentiometric sensors (Kaniewska *et al.*, 2008, Xu *et al.*, 2009) but this approach is beyond of the scope of the studies reported in this thesis. To the best of our knowledge, there are no chiral sensors based on PEDOT has been developed to study the discrimination of enantiomers. Thus, in this thesis, the chiral discrimination of enantiomers using PEDOT doped with chiral molecules as chiral selectors will be discussed in **Chapter 8.**

References

Bakker, E. (1997) Selectivity of Liquid Membrane Ion-Selective Electrodes. *Electroanalysis.* 9**.** 7-12.

Bakker, E., Buhlmann, P. and Pretsch, E. (1997) Carrier-Based Ion-Selective Electrodes and Bulk Optodes. 1. General Characteristics. *Chemical Reviews.* 97**.** 3083-3132.

Bakker, E. and Pretsch, E. (2005) Potentiometric Sensors For Trace-Level Analysis. *Trac-Trends in Analytical Chemistry.* 24**.** 199-207.

Bobacka, J. (1999) Potential Stability of All-Solid-State Ion-Selective Electrodes Using Conducting Polymers As Ion-to-Electron Transducers. *Analytical Chemistry.* 71**.** 4932-4937.

Bobacka, J. (2006) Conducting Polymer-Based Solid-State Ion-Selective Electrodes. *Electroanalysis.* 18**.** 7-18.

Bobacka, J., Alaviuhkola, T., Hietapelto, V., Koskinen, H., Lewenstam, A., Lamsa, M., Pursiainen, J. and Ivaska, A. (2002) Solid-Contact Ion-Selective Electrodes For Aromatic Cations Based on π-Coordinating Soft Carriers. *Talanta.* 58**.** 341-349.

Bobacka, J., Lahtinen, T., Nordman, J., Haggstrom, S., Rissanen, K., Lewenstam, A. and Ivaska, A. (2001a) All-Solid-State Ag^{+}-ISE Based on [2,2.2]*p,p,p*-Cyclophane. *Electroanalysis.* 13**.** 723-726.

Bobacka, J., Lewenstam, A. and Ivaska, A. (2001b) Equilibrium Potential of Potentiometric Ion Sensors Under Steady-State Current By Using Current-Reversal Chronopotentiometry. *Journal of Electroanalytical Chemistry.* 509**.** 27-30.

Bobacka, J., Väänänen, V., Lewenstam, A. and Ivaska, A. (2004) Influence of Anionic Additive on Hg^{2+} Interference on Ag^{+}-ISEs Based on 2.2.2 p,p,p-Cyclophane as Neutral Carrier. *Talanta.* 63**.** 135-138.

Bruice, P. Y. (2004) *Organic Chemistry.* (Fourth Ed ed.). Prentice Hall.

Buck, R. P. and Lindner, E. (1994) Recommendations for Nomenclature of Ion-Selective Electrodes (IUPAC Recommendations 1994). *Pure and Applied Chemistry.* 66**.** 2527-2536.

Budai, D. and Molnar, Z. (2001) Novel Carbon Fiber Microeletrodes for Extracellular Electrophysiology. *Acta Biologica Szegediensis.* 45**.** 65-73.

Bühlmann, P., Yajima, S., Tohda, K., Umezawa, K., Nishizawa, S. and Umezawa, Y. (1995) Studies on The Phase Boundaries and The Significance of Ionic Sites of Liquid Membrane Ion-Selective Electrodes. *Electroanalysis.* 7**.** 811-816.

Buhlmann, P., Yajima, S., Tohda, K. and Umezawa, Y. (1995) EMF response of neutral-carrier based ion-sensitive field effect transistors with membranes free of ionic sites *Electrochimica Acta.* 40**.** 3021-3027.

Caras-Quintero, D. and Bäuerle, P. (2004) Synthesis of The First Enantiomerically Pure and Chiral, Disubstituted 3,4-Ethylenedioxythiophenes (EDOTs) and Corresponding Stereo- and Regioregular PEDOTs. *Chemical Communications.* 926-927.

Elsenbaumer, R. L., Eckhardt, H., Iqbal, Z., Toth, J. and Baughman, R. H. (1985) Chiral Metals: Synthesis and Properties of a New Class of Conducting Polymers *Molecular Crystals and Liquid Crystals.* 118**.** 111-116.

Ghosh, S. and Inganäs, O. (1999) Self-Assembly of a Conducting Polymer Nanostructure by Physical Crosslinking: Applications to Conducting Blends and Modified Electrodes. *Synthetic Metals.* 101**.** 413-416.

Goto, H. (2009) Vortex Fibril Structure and Chiroptical Electrochromic Effect of Optically Active Poly(3,4-Ethylenedioxythiophene) (PEDOT*) Prepared by Chiral Transcription Electrochemical Polymerisation in Cholesteric Liquid Crystal. *Journal of Materials Chemistry.* 19**.** 4914-4921.

Goto, H. and Akagi, K. (2004) Preparation of Poly (3,4-Ethylenedioxythiophene) in a Chiral Nematic Liquid-Crystal Field. *Macromolecular Rapid Communications.* 25**.** 1482-1486.

Goto, H. and Akagi, K. (2006) Optically Active Electrochromism of Poly(3,4-Ethylenedioxythiophene) Synthesized by Electrochemical Polymerization in Lyotropic Liquid Crystal of Hydroxypropyl Cellulose/Water: Active Control of Optical Activity. *Chemistry of Materials.* 18**.** 255-262.

Horvai, G., Graf, E., Toth, K., Pungor, E. and Buck, R. P. (1986) Plasticized Poly(vinyl chloride) Properties and Characteristics of Valinomycin Electrodes. 1. High-Frequency Resistances and Dielectric Properties. *Analytical Chemistry.* 58**.** 2735-2740.

Horváth, V., Horvai, G. and Pungor, E. (1990) Amperometric Measurements with Ion-Selective Electrode Membranes in a Flow System. *Microchimica Acta.* 100**.** 217-224.

Hulanicki, A., Glab, S. and Ingman, F. (1991) Chemical Sensors Definitions and Classification. *Pure and Applied Chemistry.* 63**.** 1247-1250.

Kane-Maguire, L. A. P. and Wallace, G. G. (2010) Chiral Conducting Polymers. *Chemical Society Reviews.* 39**.** 2545-2576.

Kaniewska, M., Sikora, T., Kataky, R. and Trojanowicz, M. (2008) Enantioselectivity of Potentiometric Sensors with Application of Different Mechanisms of Chiral Discrimination. *Journal of Biochemical and Biophysical Methods.* 70**.** 1261-1267.

Kawashima, H. and Goto, H. (2011) Synthesis and Properties of a Chiroptically Active Oligomer from 3,4-Ethylenedioxythiophene and (–)-Myrtenal. *Materials.* 4**.** 1013-1022.

Kuras, A. and Gutmaniene, N. (2000) Technique for Producing a Carbon-Fibre Microelectrode with the Fine Recording Tip. *Journal of Neuroscience Methods.* 96**.** 143-146.

Lindner, E., Graf, E., Niegreisz, Z., Toth, K., Pungor, E. and Buck, R. P. (1988) Responses of Site-Controlled, Plasticized Membrane Electrodes. *Analytical Chemistry.* 60**.** 295-301.

Macca, C. (1996) Determination of Potentiometric Selectivity. *Analytica Chimica Acta.* 321**.** 1-10.

Macca, C. (2004) Response Time of Ion-Selective Electrodes: Current Usage versus IUPAC Recommendations. *Analytica Chimica Acta.* 512**.** 183-190.

Michalska, A., Galuszkiewicz, A., Ogonowska, M., Ocypa, M. and Maksymiuk, K. (2003) PEDOT Films: Multifunctional Membranes for Electrochemical Ion Sensing. *Journal of Solid State Electrochemistry* 381-389.

Michalska, A. and Maksymiuk, K. (2004) All-Plastic, Disposable, Low Detection Limit Ion-Selective Electrodes. *Analytica Chimica Acta.* 523**.** 97-105.

Michalska, A., Ocypa, M. and Maksymiuk, K. (2005) Highly Selective All-Plastic, Disposable, Cu^{2+}-Selective Electrodes. *Electroanalysis.* 17**.** 327-333.

Moody, G. J., Oke, R. B. and Thomas, J. D. R. (1970) A Calcium-Sensitive Electrode Based on a Liquid Ion Exchanger in a Poly(vinyl chloride) Matrix. *Analyst.* 95**.** 910-918.

Morf, W. E., Ammann, D. and Simon, W. (1974) Elimination of the Anion Interference in Neutral Carrier Cation-Selective Membrane Electrodes. *Chimia.* 28**.** 65-67.

Mousavi, Z., Bobacka, J., Lewenstam, A. and Ivaska, A. (2009) Poly(3,4-Ethylenedioxythiophene) (PEDOT) Doped with Carbon Nanotubes as Ion-to-Electron Transducer in Polymer Membrane-Based Potassium Ion-Selective Electrodes. *Journal of Electroanalytical Chemistry.* 633**.** 246-252.

Nam, H. and Cha, G. S. (2000) IN YANG, V. C. & NGO, T. (Eds.) *Biosensors and Their Applications.* Kluwer Academic/Plenum.

Ocypa, M., Michalska, A. and Maksymiuk, K. (2006) Accumulation of Cu(II) Cations in Poly(3,4-ethylenedioxythiophene) Films Doped by Hexacyanoferrate Anions and Its Application in Cu^{2+}-Selective Electrodes with PVC Based Membranes. *Electrochimica Acta.* 51**.** 2298-2305.

Paczosa-Bator, B., Peltonen, J., Bobacka, J. and Lewenstam, A. (2006) Influence of Morphology and Topography on Potentiometric Response of Magnesium and Calcium Sensitive PEDOT Films Doped with Adenosine Triphosphate (ATP). *Analytica Chimica Acta.* 555**.** 118-127.

Pick, J., Pungor, E., Vasak, M. and Simon, W. (1973) Potassium- Selective Silicone-Rubber Membrane Electrode Based on a Neutral Carrier. *Analytica Chimica Acta.* 64**.** 477-480.

Pleus, S. and Schwientek, M. (1998) Enantioselective Electrodes: Synthesis and Use of Polypyrroles Prepared from Chiral Pyrrole Derivatives. *Synthetic Metals.* 95**.** 233-238.

Pretsch, E. (2007) The New Wave of Ion-Selective Electrodes. *TrAC Trends in Analytical Chemistry.* 26**.** 46-51.

Roncali, J. (1997) Synthetic Principles for Bandgap Control in Linear pi-Conjugated Systems. *Chemical Reviews.* 97**.** 173-205.

Shatkay, A. (1967) Ion Specific Membranes as Electrodes in Determination of Activity of Calcium. *Analytical Chemistry.* 39**.** 1056-1065.

Shi, G. Q., Xu, J. K. and Fu, M. X. (2002) Raman Spectroscopic and Electrochemical Studies on the Doping Level Changes of Polythiophene Films During Their Electrochemical Growth Processes. *Journal of Physical Chemistry B.* 106**.** 288-292.

Sigel, H., Zuberbuhler, A. D. and Yamauchi, O. (1991) Comments on Potentiometric pH Titrations and The Relationship between pH-meter Reading and Hydrogen Ion Concentration. *Analytica Chimica Acta.* 255**.** 63-72.

Trojanowicz, M. and Kaniewska, M. (2009) Electrochemical Chiral Sensors and Biosensors. *Electroanalysis.* 21**.** 229-238.

Umezawa, Y., Buhlmann, P., Umezawa, K., Tohda, K. and Amemiya, S. (2000) Potentiometric Selectivity Coefficients of Ion-Selective Electrodes Part I. Inorganic Cations - (Technical report). *Pure and Applied Chemistry.* 72**.** 1851-2082.

Vandenberg, A., Vanderwal, P. D., Skowronskaptasinska, M., Sudholter, E. J. R. and Reinhoudt, D. N. (1987) Nature of Anionic Sites in Plasticized Poly(vinyl chloride) Membranes. *Analytical Chemistry.* 59**.** 2827-2829.

Vázquez, M., Bobacka, J., Ivaska, A. and Lewenstam, A. (2002) Influence of Oxygen and Carbon Dioxide on the Electrochemical Stability of Poly(3,4-ethylenedioxythiophene) Used as Ion-to-Electron Transducer in All-Solid-State Ion-Selective Electrodes. *Sensors and Actuators B-Chemical.* 82**.** 7-13.

Vázquez, M., Bobacka, J., Ivaska, A. and Lewenstam, A. (2004a) Small-Volume Radial Flow Cell for All-Solid-State Ion-Selective Electrodes. *Talanta.* 62**.** 57-63.

Vázquez, M., Danielsson, P., Bobacka, J., Lewenstam, A. and Ivaska, A. (2004b) Solution-Cast Films of Poly(3,4-ethylenedioxythiophene) as Ion-to-Electron Transducers in All-Solid-State Ion-Selective Electrodes. *Sensors and Actuators B-Chemical.* 97**.** 182-189.

Xu, H., Yang, X. X., Wang, Y., Zheng, J. B., Luo, Z. Y. and Li, G. (2010) Disposable Blood Potassium Sensors Based on Screen-Printed Thick Film Electrodes. *Measurement Science & Technology.* 21**.** 055802.

Xu, L., Yang, Y., Wang, Y. and Gao, J. (2009) Chiral Salen Mn(III) Complex-Based Enantioselective Potentiometric Sensor for l-Mandelic Acid. *Analytica Chimica Acta.* 653**.** 217-221.

CHAPTER 4

INTRODUCTION TO EXPERIMENTAL TECHNIQUES AND FUNDAMENTAL PRINCIPLES OF ELECTROCHEMISTRY

4.1 Introduction

In this chapter, general techniques used in this project and fundamental concepts of electrochemistry are generally described. The detailed procedures of experiments are explained in the experimental part of the corresponding chapter.

4.2 Scanning Electron Microscopy (SEM)

The scanning electron microscope (SEM) is a powerful microscope that uses electrons rather than light in imaging an object. It is a non-destructive analysis. The images of conducting polymers are taken by scanning the sample with a high intensity beam of electrons. In this study, the surface morphology analyses were carried out using Philip XL30 environmental SEM and Hitachi SU70. The electrons interact with atoms at or near the surface of the sample and the images are obtained. The magnification of SEM can reach up to 250 000 or more, which is about 250 times greater than the conventional light microscope. A high resolution can be obtained by using electron microscopes as it uses electrons and not photons (light rays) for visualization and much smaller values of wavelength can be employed. The resolution in microscopy is the capability to distinguish two point objects of about equal intensity. The image of an infinitely small scattering object as formed by an objective lens is not itself infinitely small (due to the diffraction effects of the lens). Therefore, an Airy pattern, which consists of a central bright disk and progressively weaker rings, is observed. When two bright points are separated by a small distance d, they may be resolved if the peaks of their Airy pattern are separated by the following distance:

$$r_{\text{Airy}} = 0.6\frac{\lambda}{\text{NA}_{\text{object}}} \quad \textbf{(4.1)}$$

where r_{Airy} is the radius of the first dark ring in Airy pattern, which may also be considered the resolution and NA is numerical aperture. Because the object is luminous, it is not necessary to include the NA of the condenser lens and this condition is known as Rayleigh criterion.

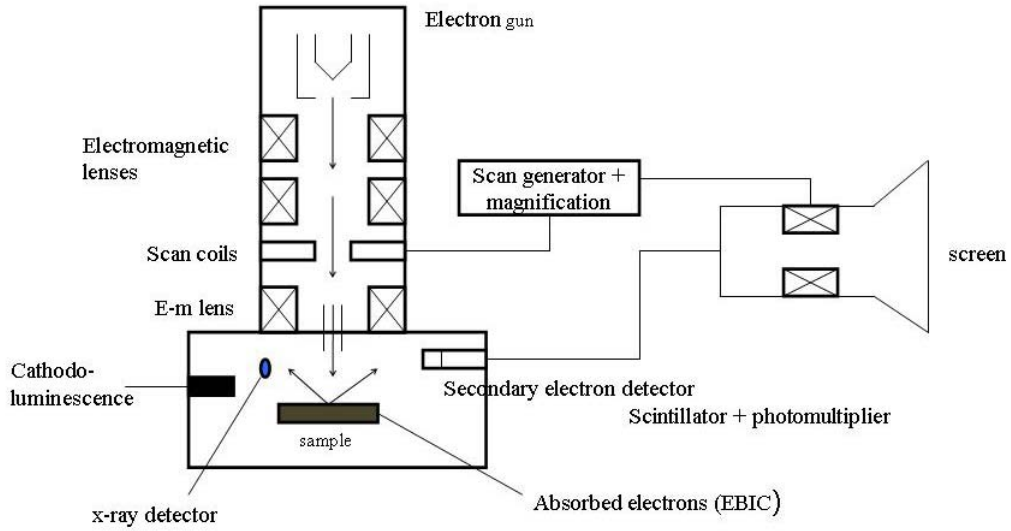

Figure 4.1: Schematic diagram of SEM.

4.3 Atomic Force Microscopy (AFM)

Atomic force microscopy (AFM) is a very high resolution technique of scanning probe microscopy. The AFM consists of a cantilever with a sharp tip at its end. The tip is brought into close proximity to a sample surface. The force between the tip and the sample leads to a deflection of the cantilever. Typically, the deflection is measured using a laser spot reflected from the top of the cantilever. A schematic diagram of AFM is shown in **Figure 4.2**. AFM has some advantages over an SEM. AFM can function in ambient air or solvent without the need of a vacuum like SEM does. In addition, AFM

can plot 3-dimensional images but SEM can only provide 2-dimensional images without coating. However the drawback of AFM is the area it can scan is just micrometer sized compared to SEM which can scan up to millimeter scale. Another advantage of AFM is that it can image the non-conducting surfaces without further coating. As a result, it can be used for imaging untreated solid samples (e.g. polymers) and can be extended to biological systems such as crystals of amino acids and organic monolayers.

The AFM measurements were made on conducting polymers prepared on ITO coated glass. All measurements were carried out using AFM nanoscope IV by applying tapping mode to the samples to minimise surface forces and enhance contrast.

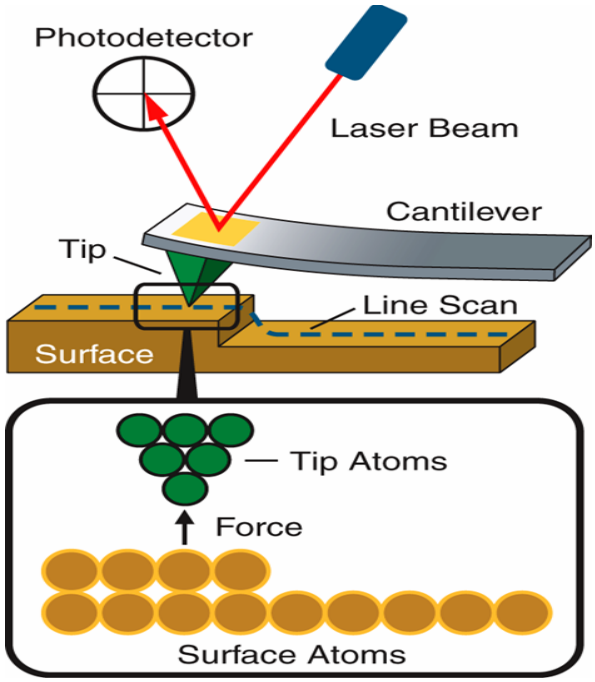

Figure 4.2: Atomic force microscope.
(http://www.home.agilent.com/agilent/editorial.jspx?cc=DE&lc=ger&ckey=1774141&nid=-33986.0.02&id=1774141)

4.4 Raman Spectroscopy

Raman spectroscopy **(Figure 4.3**) is based on inelastic scattering of monochromatic light by matter. The light is usually a laser source. Inelastic means that the frequency of photons in monochromatic light changes upon interaction with a sample. The sample is illuminated with monochromatic light and scattered light is examined by spectrometer.

In Raman spectroscopy, the energy levels of molecules are explored by examining the frequencies present in the radiation scattered by molecules. During a scattering event, (1) an electron is excited from the ground to an excited (often virtual) state by absorbing a photon, (2) stimulated emission of a photon induced by a second photon occurs, as the excited state transforms back to a specific vibrational level in the ground state. About 1 in 10^7 of the incident photons collide with molecules, give up some their energy, and emerge with a lower frequency (Atkins, 1998). These photons produce what are referred to as Stokes lines in the spectrum of the scattered radiation. A small fraction of the scattered fraction photons gains energy in striking a molecule in the sample and emerges with a higher frequency; these photons produce what are referred to as anti-Stokes lines in the spectrum of the scattered radiation. If the scattered photons have the same frequency as the incident photons, this is called Rayleigh scattering. There are a number of types of Raman spectroscopy such as resonance Raman, stimulated Raman, surface-enhance Raman, tip-enhance Raman and polarised Raman. The measurement is straightforward and no sample preparation is required.

Raman and infrared spectroscopy are complementary techniques. Infrared absorption requires that a vibrational mode of the molecule have a change in dipole moment or charge distribution associated with it. In contrast, scattering involves a momentary distortion of the electrons distributed around a bond in a molecule, followed by reemission of the radiation as the bond returns to its normal state. In its distorted form, the molecule is temporarily polarized; that is, it develops momentarily an induced dipole that disappears upon relaxation and reemission. The Raman activity of a given vibrational

mode may differ markedly from its infrared activity. An important advantage of Raman spectra over infrared lies in the fact that water does not cause interference therefore Raman spectra can be obtained from aqueous solutions. In addition, glass or quartz cells can be employed, thus avoiding the inconvenience of working with sodium chloride or other atmospherically unstable window materials. In this work, resonance Raman is used in order to obtain information about the vibrations of molecules in conducting polymers.

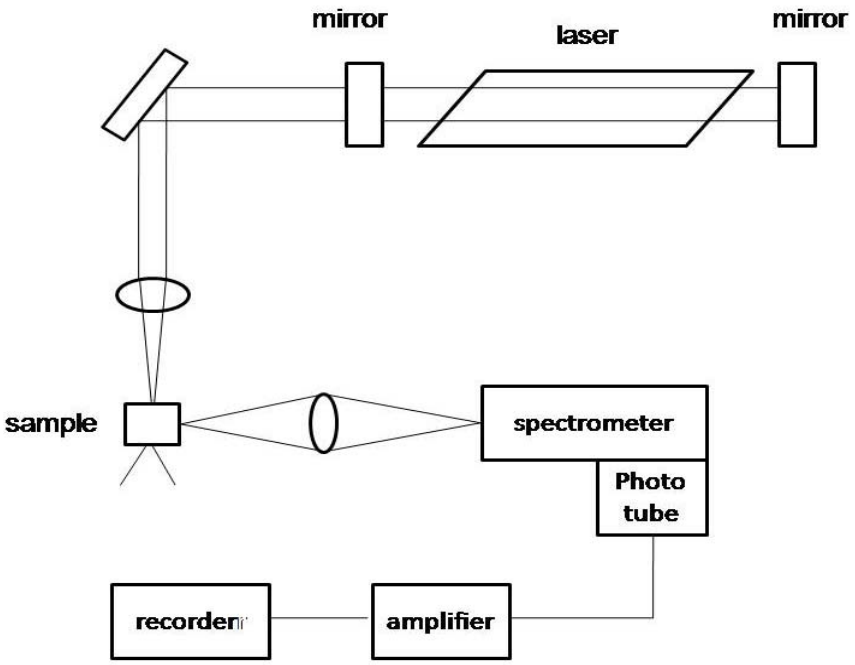

Figure 4.3: Schematic diagram of a Raman spectrometer.

Raman spectroscopy (Jobin Yvon Horiba LabRAM spectrometer) was used to record Raman spectra of the conducting polymer deposited on electrodes. Resonance Raman was used and the excitation wavelength was 633 nm in order to obtain the vibrational spectra of the conducting polymer films. The Raman scattering measurements were performed in ambient atmosphere and at room temperature. The sample was simply placed on the sample holder followed by taking a signal. At least three spectra were taken at different regions of each sample to ensure that the spectra really are typical of the sample.

4.5 Contact Angle Measurement

Contact angle measurement is a technique used to evaluate the surface tension of a solid by wetting the surface with liquid. The term 'wetting' refers to phenomena when a liquid is brought to have contact with a solid surface. The surface tension is related to the hydrophilicity/hydrophobicity and wettability of the surface. It is determined by interaction across the interfaces *i.e.* solid, liquid and vapour as shown in **Figure 4.4**. This interaction can be quantified by contact angle (θ), which is the angle subtended by a tangent to the liquid drop at the point on the triple-phase contact line. This phenomenon can be described by Young's equation (**Equation (4.2)**), where θ is the equilibrium contact angle and the surface tension of the solid-liquid, solid-vapour and liquid-vapour interfaces are represented as γ_{sl}, γ_{sv} and γ_{lv}, respectively.

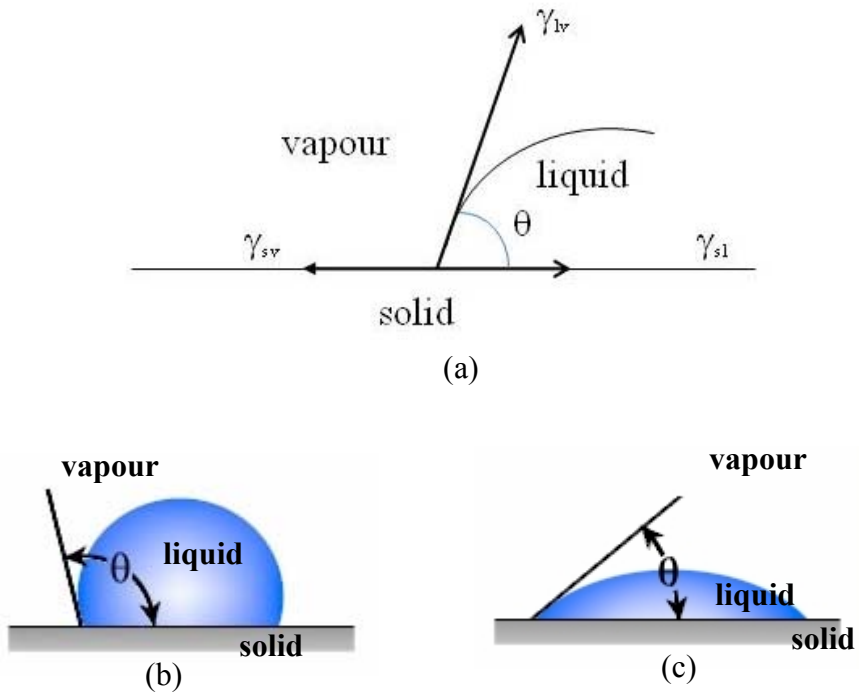

Figure 4.4: (a) Schematic diagram of the contact angle formed between a liquid and a solid in surrounding vapour phase. Contact angle (θ) of (b) hydrophobic drop and (c) hydrophilic drop**.**

$$\gamma_{sv} = \gamma_{sl} + \gamma_{lv}\cos\theta \qquad \textbf{(4.2)}$$

Typically, wettability measurements are measured using a sessile (stationary) drop. When a drop of liquid is placed on a solid surface, it forms a droplet that has a characteristic angle. The change in the contact angle is generally governed by the surface chemistry (chemical composition) and the surface morphology of the film (Cassie and Baxter, 1944, He *et al.*, 2003, Wenzel, 1936).

On a homogenous solid surface, the contact angle is independent of volume *i.e.* volume when ignoring gravity effects (Johnson, 1959). Young's equation (**Equation (4.2)**) is based on ideal surfaces which are chemically homogenous, atomically smooth, rigid and not prone to chemical interaction with the liquid or vapour phase (Good, 1992). In this case, a single unique contact angle exists. However, for a non-ideal solid surface that does not have perfect smoothness, rigidity, or chemical homogeneity, it might have more than one or a range of contact angles and is said to have contact angle hysteresis. In such case, a single static contact angle is not sufficient to report. The advancing contact angle (θ_a) is the maximum stable angle and the receding contact angle (θ_r) is the minimum stable angle. Hysteresis ($\Delta\theta$) is defined as the difference between these two contact angles (**Equation (4.3)**). If θ_a and θ_r are not intentionally measured, the angle determined will lie somewhere between the two extremes (Good, 1992). Contact angle hysteresis is due to existence of many different thermodynamically stable contact angles on a non-ideal solid. These varying thermodynamically stable contact angles are known as metastable state.

$$\Delta\theta = \theta_a - \theta_r \qquad \textbf{(4.3)}$$

One of the main reasons of the existence of contact angle hysteresis is surface roughness (de Gennes, 1985). This effect is strong on a porous material as described by Wenzel (1936) and Cassie (1944) (**Figure 4.5**).

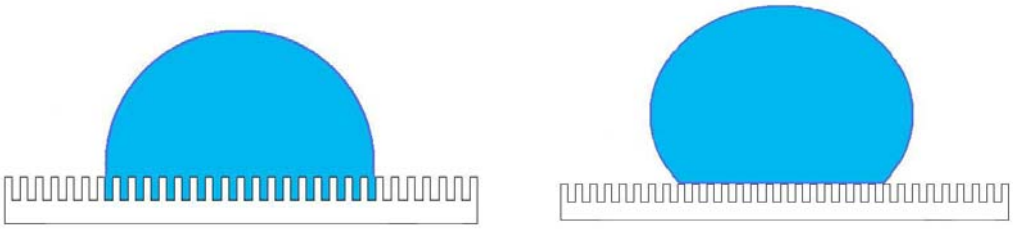

Figure 4.5: (a) Wenzel's model: the liquid drop follows the surface asperities and (b) Cassie-Baxter's model: the liquid rests on top of the surface asperities.

In Wenzel's model (1936), the droplet fills up the rough surface to form completely wetted contact with the surface (**Figure 4.5a**). The droplet follows the surface roughness; hence the contact angle and the hysteresis increase with roughness. The contact angle on a rough surface for this model can be described by Wenzel's equation (**Equation (4.4)**). If a surface is in Wenzel state, the contact angle hysteresis will be very large: trying to remove a liquid makes it contact itself. This is due to fraction left in textures, which leading to a low receding contact angle (Callies and Quere, 2005). A value as low as 40° was reported (Wenzel, 1936), making this state hydrophilic-like in the receding stage.

$$\cos\theta^* = r\cos\theta \qquad \textbf{(4.4)}$$

where,

θ^* apparent contact angle of the liquid on the rough surface

r surface roughness (defined as the ratio of real surface area over the projected surface area normal to the substrate

θ Young's contact angle (described in **Equation (4.3)**)

On the other hand, in Cassie-Baxter's model (1944), the liquid only contacts with the top of the asperities with air trapped in the hollows and grooves of the rough surface on the submicron-scale as illustrated in **Figure 4.5b**. In this state, the droplet will easily roll off a surface with extremely low adhesion. For an ideal hydrophobic surface, the hysteresis is quite small as the contact angle drops with the number of heterogeneities on the surface responsible for pinning is reduced (Callies and Quere, 2005).

In order to examine the hydrophilicity and wettability properties, the conducting polymers were synthesised on GC and ITO coated glass electrodes. The contact angle of a water droplet on the surface of polymer surface was measured using FTÅ 200. The measurements were conducted by dropping 10 μl of water onto the conducting polymer surface and the advancing and receding contact angles measured by adding or removing 5 μl, respectively. The measurements were recorded after the water droplet had reached apparent equilibrium *i.e.* a relatively constant shape.

4.6 Introduction of Electrochemistry

Electrochemistry is the branch of chemistry concerned with the interrelation of electrical and chemical effects. In other words, electrochemistry involves chemical reactions that involve electrical currents and potentials. It deals with the study of chemical changes caused by the passage of an electric current and the production of electrical energy by chemical reactions. Electrochemistry is not merely physical chemistry, nor even chemistry, but it covers the field of science from biology through chemistry to physics and material science.

The fundamental process in electrochemistry is the transfer of electrons (amperometry/voltammetry) or ions (potentiometry). In potentiometric measurements, only two electrodes are typically involved *i.e.* working and reference electrodes. The potential is measured relative to this reference electrode and the current is zero.

In amperometry, a three electrode system is used instead of two electrodes. The chemical reactions take place in a solution at the interface of electrode and electrolyte, subsequently electron transfer occurs between the working electrode and the redox species in a solution (analyte); it is heterogeneous process. The process is called a redox reaction, which involves reduction and oxidation processes. Reduction and oxidation processes are process of accepting and donating electrons, respectively. These both processes must be coupled and occur simultaneously as one species is oxidised and another reduced to ensure solution neutrality. However, typically these reactions are spatially separated, occurring at working and counter electrodes respectively.

Electrochemistry has an enormous application including environmental monitoring, industrial quality control, battery industries, development of chemical sensors and biomedical analysis. In future, electrochemical sensors will be more selective, rugged and smaller and also will be used in many processes (e.g. medical monitoring and environmental analysis). In the following subtopic, the basic principles of electrochemistry are explained briefly.

4.7 Three-electrode System

In a three-electrode system, the potentiostat applies the voltage between the working electrode and the reference electrode and current only passes between the working electrode and the counter electrode. As a result, the observed voltammogram provides a direct measurement of redox phenomena occurring only at the working electrode. The current of the working electrode is recorded as a function of its potential measured against the reference electrode, as the voltage is applied between them and the reference electrode potential is constant. **Figure 4.6** and **Figure 4.7** display the three electrode circuit and the arrangement of them, respectively. In some experiments, inert gas such as nitrogen or helium needs to be introduced in the system in order to make the environment inert (oxygen is removed).

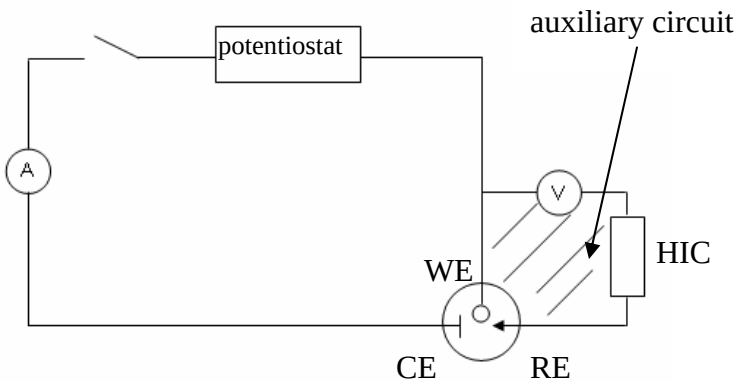

WE : working electrode
RE : reference electrode
CE : counter electrode
HIC : high impedance circuit

Figure 4.6: Three electrode circuit**.**

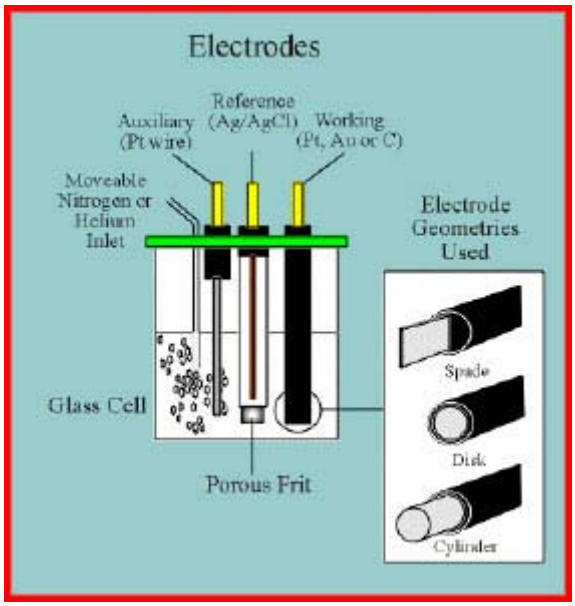

Figure 4.7: Three electrode system.
(http://www.chem.ucla.edu/~bacher/CHEM174/equipment/CV1.html)

When an analyte is oxidised at the working electrode, a current passes electrons through the external electric circuitry to the counter electrode. This current then flows from the counter electrode to the working electrode, where reduction of an electroactive species in the solution occurs. The current resulting from redox reactions at the working and counter electrode is called faradaic current. There are two factors which contribute to the rate of the electrochemical reaction:

- electron transfer: the rate of the overall electron transfer process at the electrode surface, and
- mass transport: the rate at which the reactants and products (electroactive species) are transported to and from the surface of the working electrode.

4.8 Supporting Electrolyte

A supporting electrolyte is a salt added in excess to the analyte solution. Most commonly, it is an alkali metal salt that does not react at the working electrode at the potential being used but has ionic conductivity. The supporting electrolyte can also be an acid, base, buffer solution or complexant. The ions exhibit a discharge potential far from that of the reduction or oxidation of the substance (analyte) being analysed. The salts suppress the migration effect, confine the interfacial region as close as possible to the electrode and minimise solution resistance. The supporting electrolyte and its concentration should be chosen, so that the transport numbers of the electroactive species are practically zero (Brett and Brett, 1993).

4.9 Electrodes

Commonly there are three electrodes in electrochemistry experiments *i.e.* working electrode (WE), reference electrode (RE) and counter electrode (CE). Every electrode plays a vital role and brief explanations are given below.

4.9.1 Working Electrode

Working electrode (WE) is an electrode of interest on which electrochemistry processes are studied. Oxidation and reduction processes occur at this electrode. In other words, the analytical process occurs at this electrode. The WE is made from a chemically

inert conductor such as gold, platinum, carbon or mercury. The surface area of this electrode is typically just a few mm^2 to limit the current flow.

Figure 4.8: Working electrodes (http://www.bioanalytical.com/products/ec/sve.php).

4.9.2 Reference Electrode

A reference electrode (RE) is an electrode for which the electrode potential is known and constant. This electrode potential has to be stable (with time and temperature) and independent of the properties of the solution because it is used to measure/control the potential of the working electrode by the application of a voltage between them. This means that the electrode must be unaffected by the passage of the small amounts of current required in making potentiometric measurements. The high stability of the electrode potential is usually reached by employing a redox system with constant (buffered or saturated) concentrations of each of the participants of the redox reaction. There are three common reference electrodes used *i.e.* saturated hydrogen electrode (Xu *et al.*), silver-silver chloride (Ag/AgCl) and saturated calomel electrode (SCE). **Figure 4.9** shows the relative potentials of the different reference electrodes used.

Ag/AgCl electrode functions as a redox electrode and the reaction is between the silver metal (Ag) and its salt, silver chloride (AgCl). Nernst equation shows that the dependence of the potential of the Ag/AgCl electrode is on the activity of chloride ions (**Equation 4.6**). The electrode potential against SHE is +0.222 V when 3.5 M Cl^- is present.

Half cell for SCE: $AgCl(s) + e^- \rightleftharpoons Ag(s) + Cl^-$ **(4.5)**

$$E = E° - \frac{RT}{F} \ln a_{Cl^-} \quad \textbf{(4.6)}$$

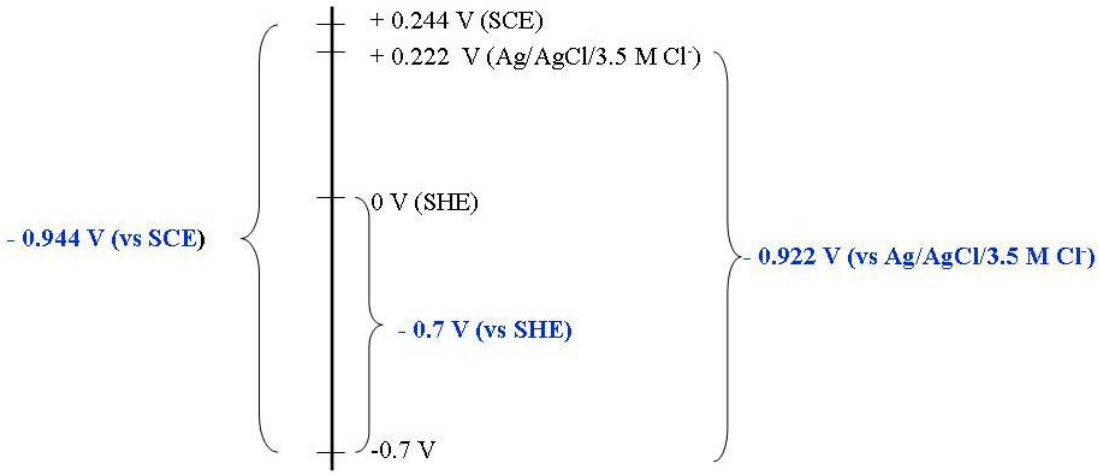

Figure 4.9: Schematic representation of electrode potentials of different reference electrodes.

4.9.3 Counter Electrode

The counter electrode (CE) is also known as the auxiliary electrode. It is used to complete the circuit (**Figure 4.6**) carrying the current flowing through the cell. The CE is of opposite polarity to the WE and typically has a larger surface area than the WE to ensure that the rate of redox reaction at the WE determines the current. The commonly used counter electrodes are platinum plate, platinum coil and a short length of platinum wire.

Figure 4.10: Counter electrode
(http://www.bio-logic.info/potentiostat/electrodes.html#Counter_electrodes).

The following sections (**Section 4.10 – Section 4.11**) describe the phenomena involved in solution and at the interfacial surface.

4.10 Mass Transport

The ultimate goal of voltammetric analyses (refer **Section 4.12**) is quantitative determination. It is imperative to obtain some degree of correlation between the peak (or wave) height and the unknown concentration in the solution. The phenomena involved during the movement of ions in solution are convection, migration and diffusion. These processes are depicted in **Figure 4.11**.

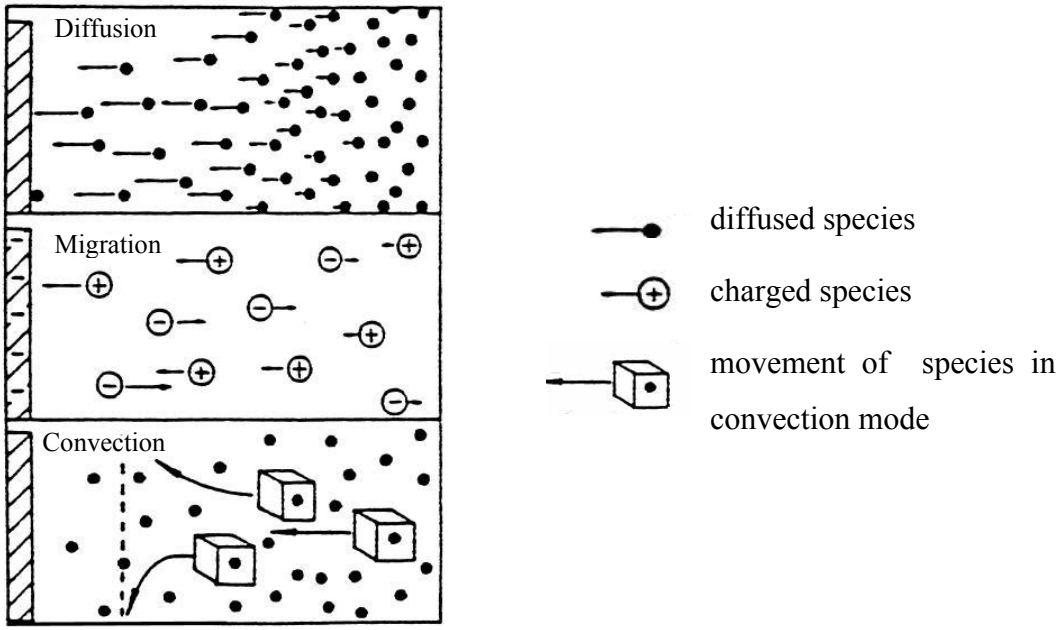

Figure 4.11: Diffusion, migration and convection processes (Maloy, 1983).

4.11 Mechanism of Electrode Reactions

Figure 4.12 displays a schematic diagram of the electron transfer mechanism. In this diagram, only oxidation or reduction processes are considered without chemical transformation.

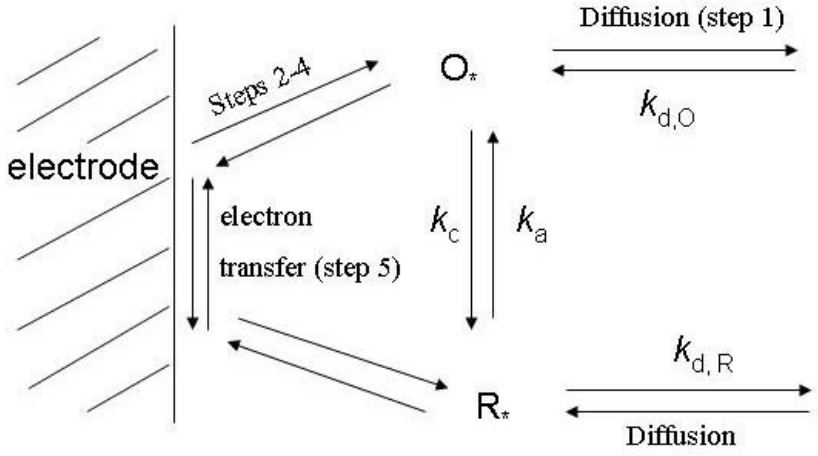

Figure 4.12: Schematic diagram of electron transfer at the electrode.

The mechanism follows the steps as below (Brett and Brett, 1993, Vetter, 1967):

- Step 1 - Diffusion of the species to where the reaction occurs
- Step 2 - Rearrangement of the ionic atmosphere (10^{-8} s)
- Step 3 - Reorientation of the solvent dipoles (10^{-11}s)
- Step 4 - Alterations in the distances between the central ion and the ligands (10^{-14} s)
- Step 5 - Electron transfer (10^{-16}s)
- Step 6 - Relaxation in the inverse sense

The details of techniques used in electroanalysis, particularly voltammetric techniques to investigate these steps are explained in the following sections.

4.12 Voltammetric Techniques

There are a number of electroanalytical techniques such as potentiometry, electrogravimetry, coulometry and voltammetry. Voltammetry is a technique where the applied potential is controlled (normally using a potentiostat) and the current flowing in an electrochemical cell is measured. This method employs conditions that polarise the working electrode. Polarisation is departure of the electrode potential (or cell potential) from the equilibrium value to cause passage of a faradaic current. In order to enhance the polarisation, the working electrodes in voltammetry are relatively small, with surface area of a few square millimeters at the most and in some applications, only a few square micrometers. Polarisation can be achieved by applying potential to an electrode to a more positive value (anodic polarisation) or to a more negative value (cathodic polarisation) than the equilibrium value. Voltammetry is widely used by analytical, inorganic and biological chemists for fundamental studies of:

- oxidation and reduction processes in various media
- adsorption processes on surfaces, and
- electron transfer mechanisms at chemically modified electrode surfaces.

4.12.1 Potential Sweep Techniques

4.12.1.1 Cyclic Voltammetry

Cyclic voltammetry (CV) is an important and widely used electroanalytical method for obtaining qualitative information about electrochemical reactions. It is a common and often the first technique used to gain preliminary information about electrochemical reactions. The CV provides information on the thermodynamics of redox processes, the kinetic of heterogeneous electron transfer reactions, mass transfer processes and on coupled chemical reactions or adsorption processes. From a practical point of view, this technique has no quantitative application in some cases but is a powerful tool to investigate the reversibility of redox systems.

In cyclic voltammetry, the potential of a working electrode is changed linearly with time starting from a potential where no redox reaction of analyte occurs, E_1 (**Figure 4.13**). After the potential has swept the region in which one or more chemical reactions take place (E_1 to E_2), the direction of linear sweep is reversed (E_2 to E_1) sweeping at the same rate. As a result, a triangular potential waveform is formed (**Figure 4.13**). A CV experiment may use one full cycle or partial cycle, or several cycles. The obtained result is displayed in terms of current as a function of potential and is known as a cyclic voltammogram (**Figure 4.14**). It is the electrochemical equivalent of a spectrum in spectroscopy techniques. It is important to note that there are a number of different axis conventions. In order to avoid complication, here, the International Union of Pure and Applied Chemistry (IUPAC) convention will be used throughout. In IUPAC convection, positive potentials are plotted in the positive *x*-axis direction and anodic current (due to oxidations) are positive.

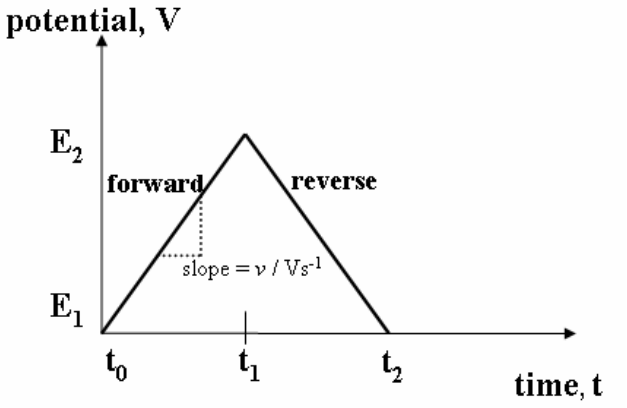

Figure 4.13: Cyclic voltammetry potential waveform.

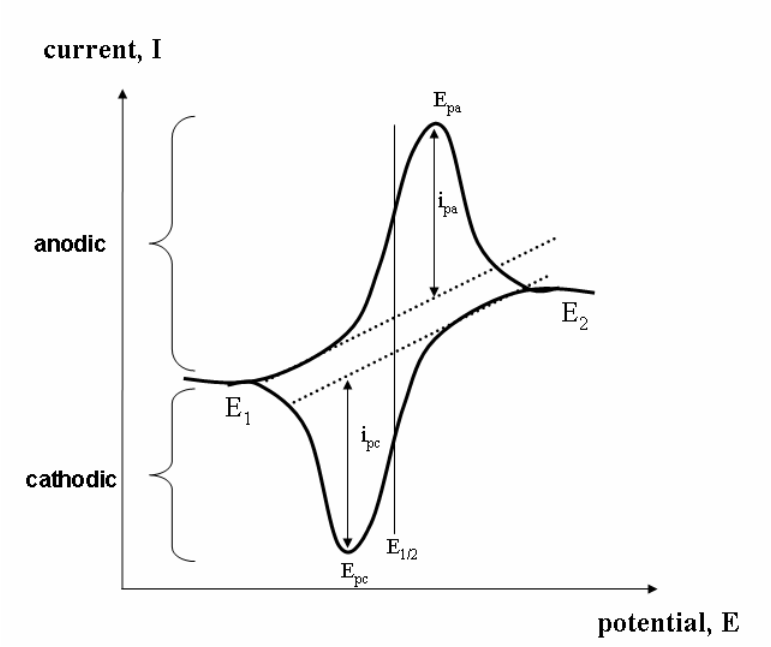

Figure 4.14: A typical cyclic voltammogram.

CV is very a simple and direct method for measuring formal redox reaction potential in the simplest case when the reaction is electrochemically reversible (the redox reactions are fast). A CV is characterised by several important parameters *i.e.* anodic peak potential (E_{pa}), cathodic peak potential (E_{pc}), anodic peak current (i_{pa}), cathodic peak current (i_{pc}) and half peak potential ($E_{p/2}$) and half wave potential ($E_{1/2}$).

The definition of $E_{1/2}$ has been borrowed from classical polarography based on the **Equation (4.7)** below:

$$E_{1/2} = E^{0'} + \left(\frac{RT}{nF}\right)\ln\left(\frac{D_R}{D_o}\right)^{\frac{1}{2}} \qquad \textbf{(4.7)}$$

where:

$E^{0'}$ the formal potential of the redox couple pertaining to the ionic strength of the solution used (V)

Ionic strength $I = \frac{1}{2}\Sigma c_i z_i^2$, c_i =concentration of the ion *i* (mol dm^{-3}), z_i = charge of ion *i*

R universal gas constant (8.314 J K^{-1} mol^{-1})

T temperature (K)

F Faraday constant (96, 485 C mol^{-1})

D_R diffusion coefficient of oxidised form (cm^2 s^{-1})

D_o diffusion coefficient of reduced form (cm^2 s^{-1})

n number of electrons in the half redox reaction

Since $D_o \sim D_R$, $E_{1/2}$ is usually within a few mV of $E^{0'}$. For the half peak potential, $E_{p/2}$ (where the current is half of the peak current), the value of $E_{1/2}$ can be determined by:

$$E_{p/2} = E_{1/2} \pm \frac{28}{n} \text{ mV} \qquad \textbf{(4.8)}$$

It can be summarised that for a reversible process, these information can be obtained from voltammogram:

- Peak currents (I_{pa} and I_{pc}) are proportional to square root of scan rate ($v^{1/2}$).
- Value of E_{pa} and E_{pc} are independent of scan rate.
- The difference between the anodic and cathodic peak current potentials is 59/*n* mV and does not depend on the nature of electrodes or on the scan (or sweep)

rate, where n is the number of electrons involved in the half-reaction. $\Delta E_p = \left| E_{pa} - E_{pc} \right| = 59/n$ mV

- Anodic peak current (I_{pa}) is approximately equal to cathodic peak current (I_{pc}) in absolute value but opposite in sign ($I_{pa} \equiv I_{pc}$).
- Formal potential ($E^{0'}$) is centered between E_{pa} and E_{pc} *i.e.* $E^{0'} = E_{1/2} = \left(\frac{E_{pa} + E_{pc}}{2} \right)$

Electrochemical irreversibility is when slow electron transfer kinetics result in ΔE_p exceeding the reversible value. While an electron transfer reaction may appear reversible at a low sweep rate, increasing the sweep rate may lead to increasing values of ΔE_p, a sure sign of reversibility (unless *iR* drop is present). Hence, to detect slow electron transfer kinetics, ΔE_p is measured for different sweep rates. Quantitative information is obtained from Randles-Sevcik equation, which at 25°C is

$$i_p = (2.69 \times 10^5)\, n^{\frac{3}{2}} A D^{\frac{1}{2}} v^{\frac{1}{2}} C \qquad \textbf{(4.9)}$$

where:

i_p peak current (A)
n number of electrons involved in redox reaction
A electrode area (cm^2)
D diffusion coeffient ($cm^2\ s^{-1}$)
v scan rate (Vs^{-1})
C bulk concentration ($mol\ cm^{-3}$)

4.12.2 Step and Pulse Techniques

The purpose of carrying out step and pulse voltammetric experiments is generally to reduce the capacitive current as much as possible. The difference between the various pulse voltammetric techniques is the excitation waveform and the current sampling region.

4.12.2.1 Step Voltammetric Technique

There are two types of step voltammetric techniques:

- potential is applied (controlled) to the WE and the current is measured.
- current is applied (controlled) to the WE and potential is measured.

4.12.2.1.1 Chronoamperometry

The basis of this controlled potential technique is the measurement of the current response to an applied potential step. Chronoamperometry (CA) involves stepping the potential of the WE from an initial potential, E_1 at which (generally) no faradaic reaction occurs, to a potential E_2 at which the mass transfer limited faradaic reaction occurs and surface concentration at the electrode becomes zero (**Figure 4.15a**). The current corresponding to the mass transport limited current has been calculated for simple systems $R \rightarrow O + ne^-$, where initially only O or R species are present (Brett and Brett, 1993). For a planar electrode, it is expressed by the Cottrell equation:

$$i(t) = \frac{nFACD^{1/2}}{\pi^{1/2} t^{1/2}} = kt^{-1/2} \qquad \textbf{(4.10)}$$

where:

n number of electrons involved in redox reaction

F Faraday constant (96, 485 C mol^{-1})

A area of (planar) electrode (cm^2)

C bulk concentration (mol/cm^3)

D diffusion coefficient (cm^2/s)

t time (s)

The resulting current is plotted against time as shown schematically in (**Figure 4.15b**), which is called a chronoamperogram. When the potential is changed (E_1 to E_2), the double layer first has to be charged, giving rise to a capacitive current, I_c. **Figure 4.16** shows the evolution of capacitive and faradaic current. According to Cottrell equation,

the I_f is proportional to the area of the electrode. Using a good quality of potentiostat, I_c decays to zero in less than 50 μs, thus it can be neglected for longer times (Brett and Brett, 1993). Both I_f and I_c in **Figure 4.16** have similar shape to **Figure 4.15b** i.e there is the largest current at t = 0, and they decay but the I_c decays much more sharply than I_f.

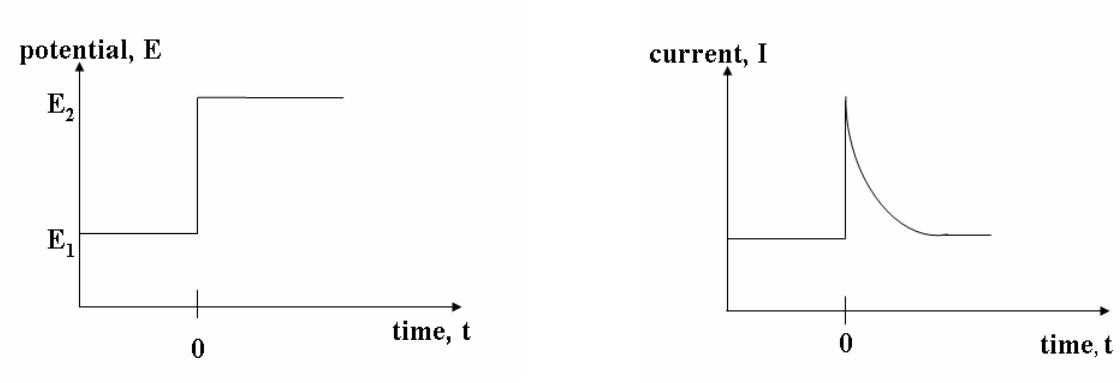

(a) (b)

Figure 4.15: Chronoamperometry: (a) potential as a function of time profile (b) current as a function of time.

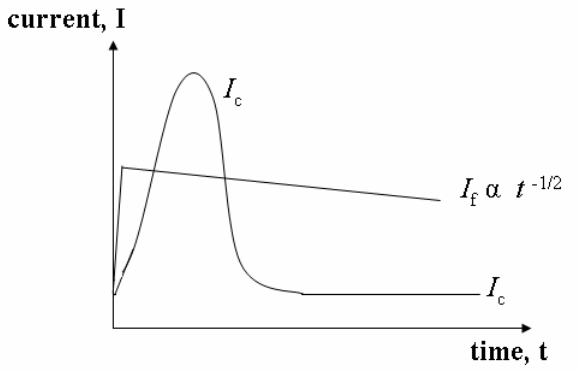

Figure 4.16: Evolution of current (capacitive current, I_c and faradaic current, I_f) with time following the application of a potential step.

The profile of concentration during the step potential experiments is illustrated in **Figure 4.17**. As the experiments continue, the analyte concentration depletion extends diffuses further from the electrode, therefore the concentration drops further into solution.

.

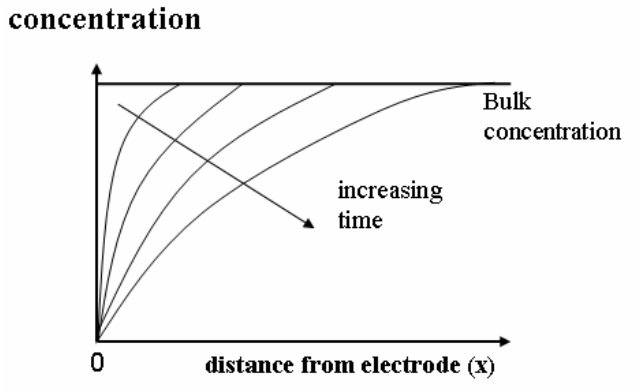

Figure 4.17: Variation of concentration during potential step.

4.12.2.1.2 Chronopotentiometry

Chronopotentiometry (CP) is a controlled current technique, in which the current is applied between the working and auxiliary electrode and the potential of working electrode is measured with respect to the reference electrode. A typical current excitation signal and potential response is depicted in **Figure 4.18**. The principle of this technique is that a redox reaction must occur at the surface of working electrode in order to support the applied current.

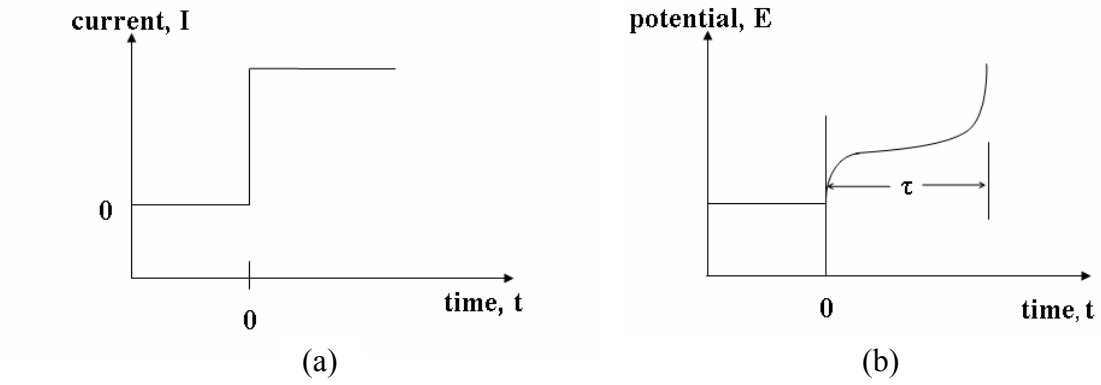

Figure 4.18: Chronopotentiometry: (a) typical potential as a function of time profile (b) current as a function of time.

4.12.2.2 Pulse Voltammetry Techniques

Pulse voltammetric techniques were introduced by Barker and Jenkin in 1952. By using these techniques, the detection limits for analyte can be as low as 10^{-8} M. The techniques are all based on a sampled potential step (chronoamperometry) technique. The differences between each pulse voltammetric techniques are the excitation waveform and the current sampling used. Here, two techniques commonly used will be explained.

4.12.2.2.1 Differential Pulse Voltammetry (DPV)

Figure 4.19 displays the potential waveform of pulses applied, superimposed on a staircase during the DPV scan. The pulse duration is around 5 – 100 ms whereas the period of the staircase waveform is at least 10 times longer (0.5 – 5 s). For the potential, typically the pulse height is about 50 mV and the step height of the staircase is about 10 mV or less. When the pulse voltage is applied, both the charging (capacitive current) and faradaic currents suddenly increase. But the charging current decreases rapidly and near the end of the pulse, only the faradaic component remains.

In this method as shown in **Figure 4.19**, two current measurements are made alternately, one at I_1 just prior to the pulse and one at I_2 just before the end of the pulse. The difference in current per pulse ΔI is recorded as a function of linearly increasing voltage and a differential curve (bell-shaped) with a peak is obtained as schematically shown in **Figure 4.20**. The voltammograms have a relatively flat baseline. Obviously the name of this method is derived from its reliance on this differential current measurement. The height of the peak is directly proportional to the concentration of electroactive species in the electrochemical cell as expressed by **Equation (4.11)**. It means that the shape of the response function and the height of the peak can be treated quantitatively in a straightforward manner. For reversible reaction, the peak potential, E_p is approximately equal to the standard potential for the half reaction ($E_{1/2}$).

$$i_p = \frac{nFAD^{1/2}C}{\pi^{1/2}t^{1/2}}\left(\frac{1-\sigma}{1+\sigma}\right) \qquad \sigma = \exp\left(\frac{nF\Delta E}{2RT}\right) \tag{4.11}$$

With increasing irreversibility, E_p moves away from $E_{1/2}$ (reversible system), at the same time as peak width increases and its height diminishes. Quantitative treatment for reversible systems demonstrated that, with only R (positive sign) or only O (negative sign) initially present (**Equation (4.12)**). The ΔE is the pulse amplitude (Brett and Brett, 1993).

$$E_p = E_{1/2} \pm \frac{\Delta E}{2} \qquad \textbf{(4.12)}$$

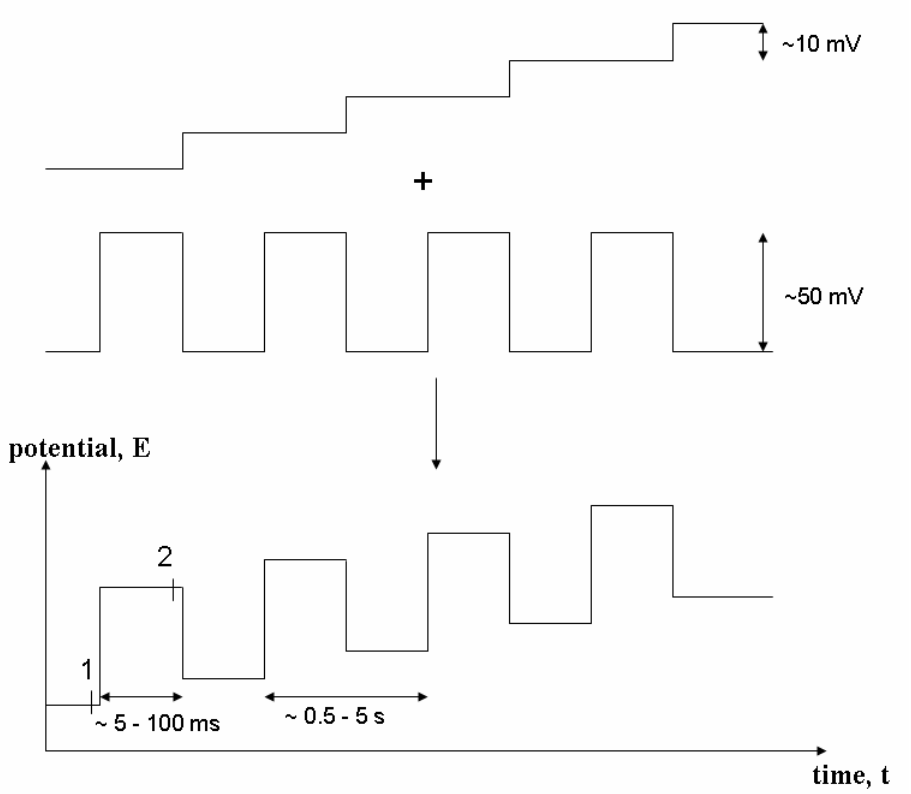

Figure 4.19: Schematic waveform of pulses superimposed on a staircase for differential pulse voltammetry.

By using this technique the contribution of non faradaic currents (capacitive current) is significantly reduced by subtracting the current ($\Delta I = I_2$-I_1). As the current is

sampled twice, a peak is obtained with a near total suppression of the capacitive current. Another advantage of this method is the detection limit lies in the range of ppb (10^{-7} to 10^{-8} M). The better detection limits can be attributed to the enhancement of the faradaic current with respect to the non faradaic charging current. DPV is very useful technique for analytical determination, for example metal ion quantification in a sample.

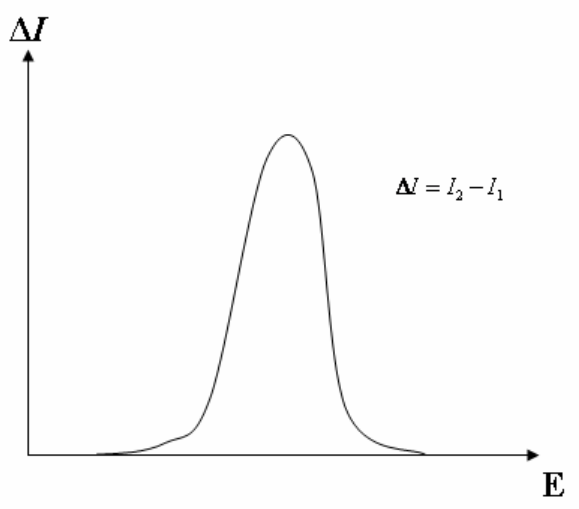

Figure 4.20: Schematic I-E profile resulting from DPV scan.

4.12.2.2.2 Square Wave Voltammetry (SWV)

In square wave voltammetry, the excitation is obtained by superimposing the pulse waveform on the staircase signal, as shown in **Figure 4.21**. The length of the staircase and the period of the pulses (t) are identical, usually about 5 ms. The potential step of the staircase ΔE_s is typically 10 mV. Operating under this condition, which correspond to a pulse frequency of 200 Hz, a 1 V scan requires 0.5 s. The waveform is similar to DPV, in which the preelectrolysis period and the pulse are of equal duration, and the pulse is opposite from the scan direction. However, the interpretation of results is facilitated by considering the waveform as consisting of a staircase scan, each tread of which is superimposed by a symmetrical double pulse, one in the forward direction and

one in the reverse (**Figure 4.21**). Over many cycles, the waveform is a bipolar square wave superimposed on the staircase.

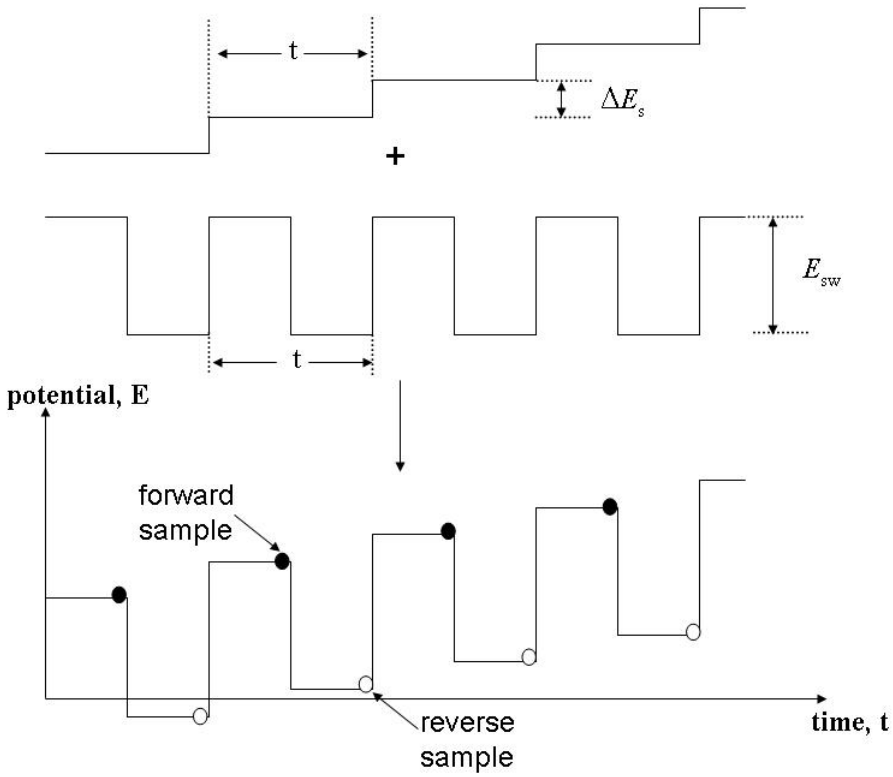

Figure 4.21: Schematic waveform of pulses superimposed on a staircase for SWV**.**

For a reversible reduction reaction, the size of the pulse is great enough that oxidation of the product formed on the forward pulse occurs during the reverse pulse. Thus, as shown on **Figure 4.22**, the forward pulse produces a cathodic current I_1 whereas the reverse pulse gives anodic current I_2. The current is sampled twice *i.e.* during the last part of the direct pulse and during the last part of reverse. The difference between measurements is plotted versus the base staircase potential with complete removal of the capacitive current. It means that SWV is a large amplitude differential technique. The resulting peak-shaped voltammogram is symmetrical about the half-wave potential and the peak current is proportional to the concentration.

Due to the speed of measurement, it is possible and practical to increase the precision of analyses by signal averaging results from several voltammetric scans. The detection limit for SWV is 10^{-7} to 10^{-8}. It seems that this technique will gain considerable use for the analysis of inorganic and organic species. The performance is as good as that of DPV but with some improvements concerning the sensitivity and the spurious signals (capacitive current) suppression. Excellent sensitivity accrues from the fact that the net current is larger than either the forward or reverse component, since it is the difference between them. The sensitivity is higher than that of differential pulse polarography, in which the reverse current is not used. The sensitivity of this technique can be increased by enhancing the amplitude of the square wave or the frequency. The limit of the enhancing is strictly related to the kinetics aspects of the redox systems, it has to be slower than the velocity of the scanning potential. SWV also has been used in detectors for liquid chromatography (Dobberpuhl and Johnson, 1995, Lacourse, 1993). Compared to the other electroanalytical techniques, SWV combines the background suppression and the sensitivity of DPV.

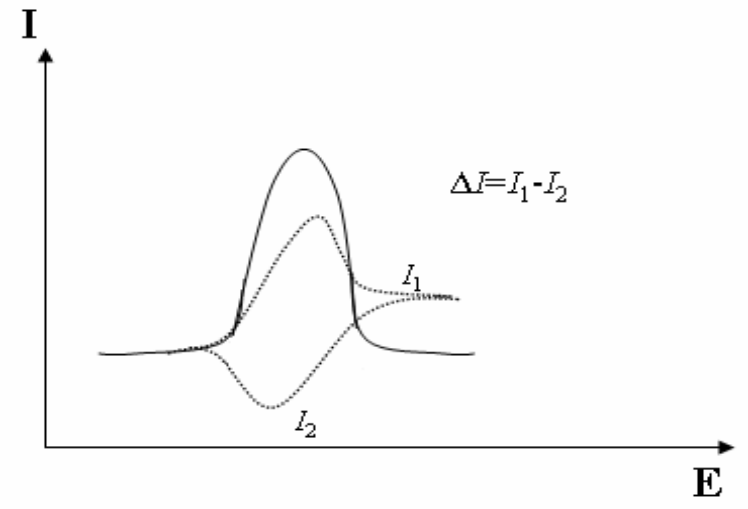

Figure 4.22: Schematic voltammetric profiles of the current measured during the forward and reverse pulses and resultant difference, **Δ***I*, plotted against the staircase potentials E**.**

4.13 Electrochemical Impedance Spectroscopy (EIS)

Electrochemical impedance spectroscopy (EIS) is an efficient electrochemical technique for studying a variety of chemical, electrochemical and surface reactions. This technique is used due to the ability of the method to give information on both the bulk and interfacial properties of the polymer coated electrodes. EIS is the process of measuring impedance (complex resistance) response over a wide range of frequencies. The reason EIS provides so much information is due the response of the system changes with frequency. Thus, a broad range of information can be obtained in a single measurement.

The impedance is described by an analogous equation to Ohm's law ($R = E/I$), where R is the resistance (Ohms), E is dc potential (V) and I is the current (A) in direct current (dc). This relationship is only valid for ideal resistor that does not exist in reality. Impedance is a measure the ability of a circuit element to resist the flow of electrical current that can be represented:

$$E = I.Z \tag{4.13}$$

Impedance measurements are made by applying a small AC potential of known frequency (ω) with small amplitude (E_o) to a system and measuring the current and phase difference ϕ of the concomitant electrical current that develops across it.

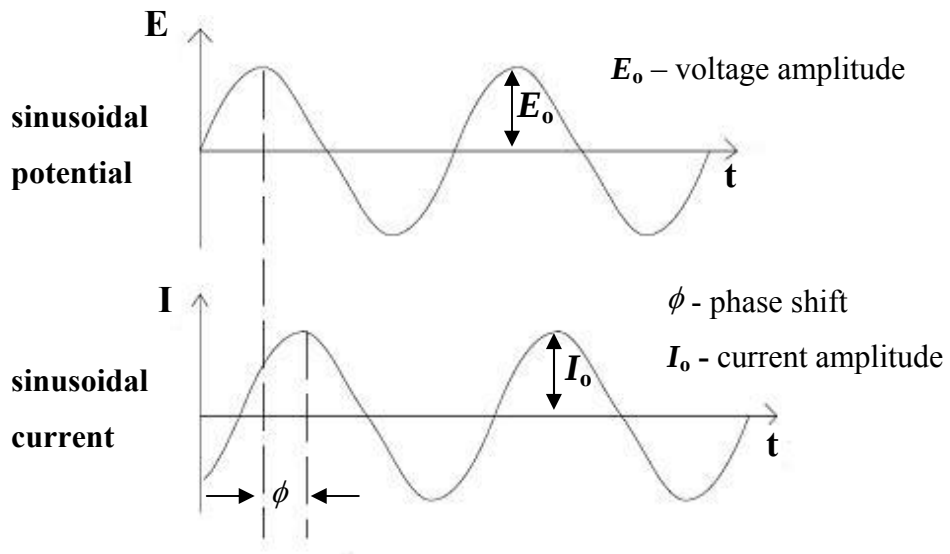

Figure 4.23: Phasor diagram of sinusoidal potential and current.

The excitation voltage (or potential with respect to the reference electrode) can be expressed as

$$E_t = E_o \sin(\omega t) \tag{4.14}$$

where

E_t potential at time t (V)
E_o potential amplitude (V)
ω radial frequency (rad/s)
t time (s)

The radial frequency ω (radians/second) can be expressed as

$$\omega = 2\pi f \tag{4.15}$$

f is frequency (Hz)

The response of sinusoidal current (I_t) has a phase shift (ϕ) and different amplitude (I_o):

$$I_t = I_o \sin(\omega t + \phi) \tag{4.16}$$

where

I_t current at time t (A)

I_o current amplitude (A)

ϕ phase shift (rad)

ϕ is the phase difference between the sinusoidal voltage and sinusoidal current (**Figure 4.23**). ϕ = 0 for purely resistive behaviour. The consideration of phase shift makes the impedance a more general concept than resistance. Impedance can be calculated as with Ohm's Law:

$$Z = \frac{E_t}{I_t} = \frac{E_o \sin(\omega t)}{I_o \sin(\omega t + \phi)} = Z_o \frac{\sin(\omega t)}{\sin(\omega t + \phi)} \tag{4.17}$$

The impedance can be expressed as a vector, in which the magnitude and the direction of the vector is given by the components Z' and Z'' (complex number) along the axes:

$$Z = Z' + jZ'' \tag{4.18}$$

Z' and Z'' are the real and imaginary part of the impedance vector, respectively. j is a imaginary number defined as $j = \sqrt{-1}$. Mathematicians use symbol i for the imaginary number but electrochemists use symbol j since i is used for a symbol of current.

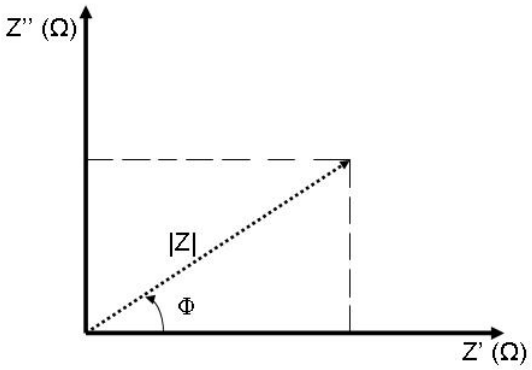

Figure 4.24: The impedance *Z* plotted as a planar vector using rectangular and polar coordinates.

The two coordinates are defined as:

$$Z' = |Z| \cos(\phi) \tag{4.19}$$

$$Z'' = |Z| \sin(\phi) \tag{4.20}$$

The phase angle (**Equation (4.21)**) and the modulus (**Equation (4.22)**) are expressed as:

$$\phi = \tan^{-1} \frac{Z'}{Z''} \tag{4.21}$$

$$|Z| = \sqrt{(Z')^2 + (Z'')^2} \tag{4.22}$$

The impedance value varies depending on the frequencies and can be plotted as a function of frequency. This makes the technique a spectroscopic method. Since the impedance values are complex numbers, they can be represented in two different manners *i.e.* Nyquist and Bode plots. The Nyquist plot (**Figure 4.25a**) shows the data as real (Z') *vs* imaginary (Z'') while the Bode plot (**Figure 4.25b**) shows the amplitude and phase values over the range of frequencies. In Nyquist plot, each point gives the

characteristics of the complex impedance at given frequency. However, this plot does not give the frequency value, which is the main disadvantage of the plot

The interface of electrode|electrolyte can be modelled as an equivalent circuit (**Figure 4.26**). The simplest circuit for a faradaic reaction is called the Randles circuit (**Figure 4.26(b)**) which consists of solution resistance (R_s) connected in series with a double-layer capacitor (C_{dl}) in parallel with a charge transfer resistor (R_{ct}) and a Warburg element (Z_w). Z_w results from the diffusion of redox species from the bulk electrolyte to the electrode interface. In a polymer film, the finite film thickness can result in a phase angle to shift from 45° to 90° corresponding to a shift from Warburg-like response for frequencies higher than the characteristic diffusion frequency to a capacitive-like one (CPE) at lower frequencies (Bobacka *et al.*, 2000, Hass *et al.*, 2005) when the film is completely reduced or oxidised. The equivalent circuit can be complicated depending on the nature of the electrochemical process and the interface involved. The equivalent circuit can be identifed from either plot.

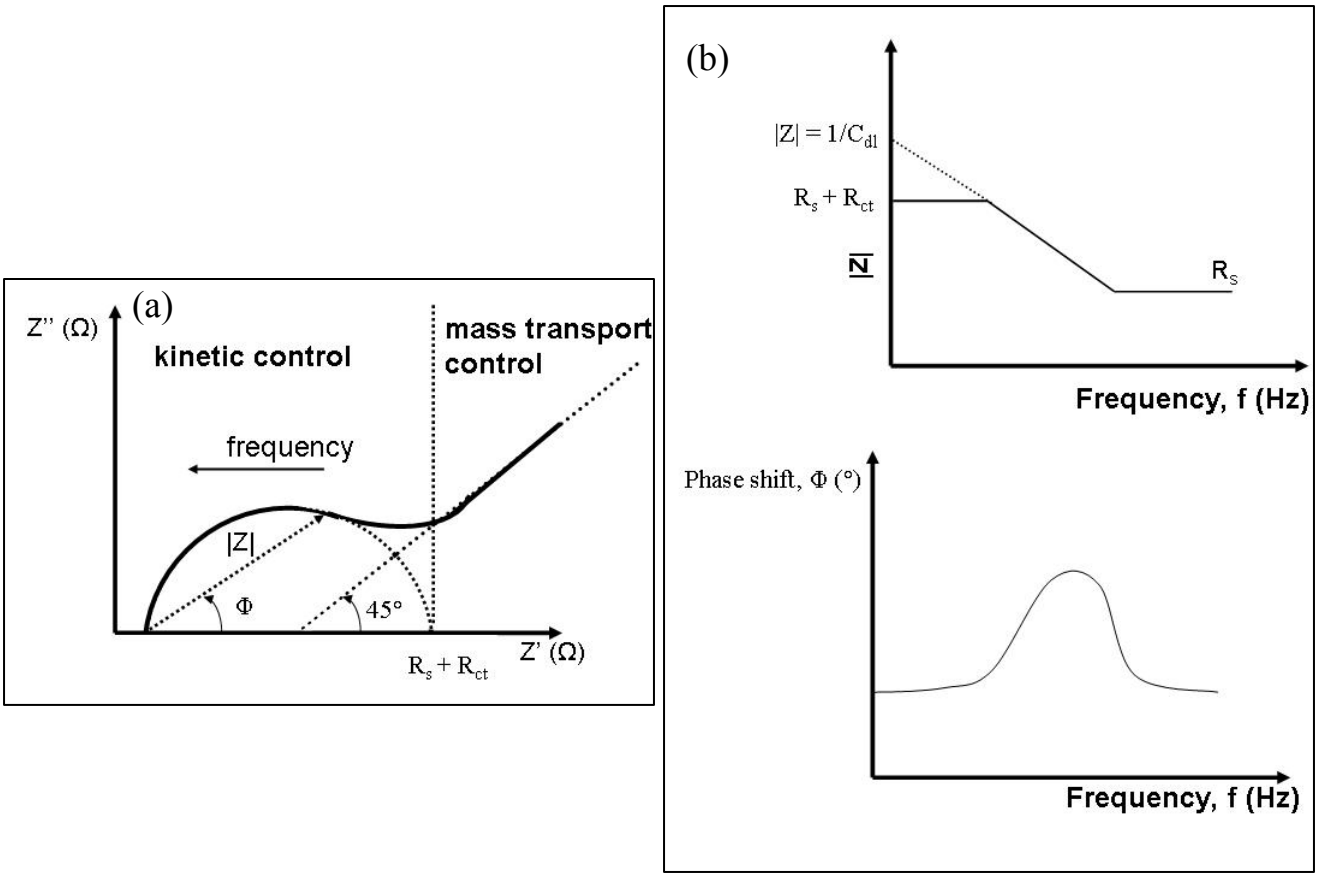

Figure 4.25: (a) Nyquist plot and (b) Bode plot.

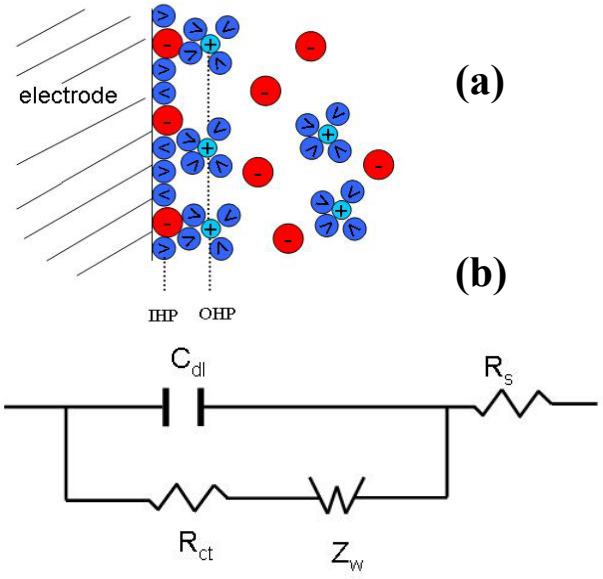

Figure 4.26: (a) Electrode|solution interface and (b) Randles circuit.

References

Atkins, P. W. (1998) *Physical Chemistry.* Oxford Melbourne Tokyo, OUP Oxford.

Bobacka, J., Lewenstam, A. and Ivaska, A. (2000) Electrochemical impedance spectroscopy of oxidized poly(3,4-ethylenedioxythiophene) film electrodes in aqueous solutions. *Journal of Electroanalytical Chemistry.* 489**.** 17-27.

Brett, C. M. A. and Brett, A. M. O. (1993) *Electrochemistry Pricinple, Method, and Applications.* New York, Oxford University Press Inc.

Callies, M. and Quere, D. (2005) On water repellency. *Soft Matter.* 1**.** 55-61.

Cassie, A. B. D. and Baxter, S. (1944) Wettability of porous surfaces. *Transactions of the Faraday Society.* 40**.** 546-550.

De Gennes, P. G. (1985) Wetting: statics and dynamics. *Reviews of Modern Physics.* 57**.** 827.

Dobberpuhl, D. A. and Johnson, D. C. (1995) Pulsed electrochemical detection of alkanoamines separated by multimodal high-performance liquid-chromatography. *Journal of Chromatography A.* 694**.** 391-398.

Good, R. J. (1992) Contact angle, wetting, and adhesion: A critical review. *Journal of Adhesion Science and Technology.* 6**.** 1269-1302.

Hass, R., Garcia-Canadas, J. and Garcia-Belmonte, G. (2005) Electrochemical Impedance Analysis of The Redox Switching Hysteresis of ppoly(3,4-ethylenedioxythiophene) Flms. *Journal of Electroanalytical Chemistry.* 577**.** 99-105.

He, B., Patankar, N. A. and Lee, J. (2003) Multiple equilibrium droplet shapes and design criterion for rough hydrophobic surfaces. *Langmuir.* 19**.** 4999-5003.

Lacourse, W. R. (1993) Pulsed electrochemical detection at noble-metal electrodes in high-performance liquid-chromatography. *Analusis.* 21**.** 181-195.

Maloy, J. T. (1983) Factors affecting the shape of current-potential curves. *Journal of Chemical Education.* 60**.** 285-289.

Vetter, K. J. (1967) Electrochemical kinetics. *Academic Press, New York.*

Wenzel, R. N. (1936) Resistance of solid surfaces to wetting by water. *Industrial and Engineering Chemistry.* 28**.** 988-994.

Xu, Y., Wang, Y., Liang, J., Huang, Y., Ma, Y., Wan, X. and Chen, Y. (2009) A hybrid material of graphene and poly (3,4-ethyldioxythiophene) with high conductivity, flexibility, and transparency. *Nano Research.* 2**.** 343-348.

CHAPTER 5

INVESTIGATION OF PHYSICAL PROPERTIES OF PEDOT AND DERIVATIVES

5.1 Introduction

The discovery of conducting polymers has attracted much interest among scientists. Polythiophene (PTh) is attractive compared to other conducting polymers due to its environmental stability (Roncali, 1992). The addition of substituents to the thiophene ring can change the physical and chemical properties of thiophene. Among the conducting polymers, those based on poly(3,4-ethylenedioxythiophene) (PEDOT) have been of interest as these conducting polymers are the most chemically stable to date (Groenendaal *et al.*, 2000). Additionally, PEDOT has a low oxidation potential and high stability in its oxidised form. The presence of oxygen atoms adjacent to the position 3 and 4 of thiophene moiety (**Figure 5.1**) and the formation of 3,4-cycloalkylthiophene lowers the oxidation potential, and makes the oxidised form more stable with less steric distortion compared to other 3,4-disubstituted polythiophenes (Roncali *et al.*, 2005). The substitution at these positions also prevents the existence of α-β' and β-β' coupling during the polymerisation resulting in a highly well defined polymer structure (Groenendaal *et al.*, 2000).

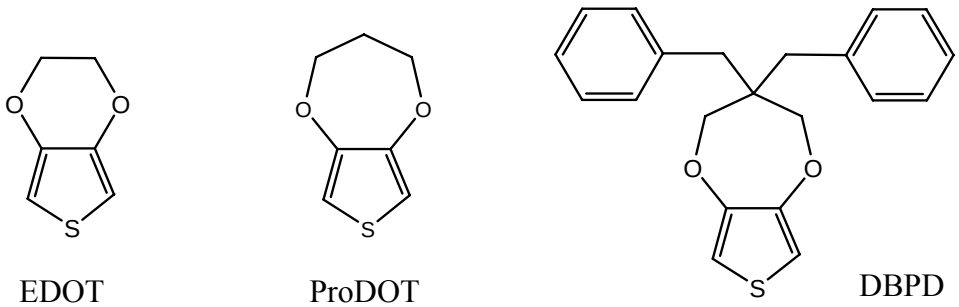

EDOT ProDOT DBPD

Figure 5.1: Structure of EDOT, ProDOT and DBPD.

Several studies on PEDOT polymers have been carried out to understand the electrical and optical properties of PEDOT, however information available on the physical properties such as surface studies, hydrophobicity and charge capacity is limited. In a previous report, Kieboom and coworkers (1997) observed that smooth surface of PEDOT on a macroscopic scale was independent of the nature of the counter ions (PF_6^-, BF_4^- or triflate) used. However, microscopic studies revealed that PEDOT/PF_6 shows fibrillar structure whereas the PEDOT/BF_4 and PEDOT/triflate exhibit a more granular structure under higher magnification (Aleshin *et al.*, 1998, Kiebooms *et al.*, 1997).

A comparison of the surface morphology of PEDOT, polyaniline (PAn), PTh and polypyrrole (PPy) has been made by Berman and Hanks (2000). From their observations, the PEDOT film was the most problematic to study. PEDOT/BF_4 grew both as a film and a fine precipitate (with CH_2Cl_2 as solvent). This finding may be due to the additional solubility imparted by the ethylenedioxy moiety. The cations can rapidly deposit on the electrode surface and form oligomeric radical cations which are able to diffuse away from the electrode surface. Finally, these radicals can partially precipitate as a flocculating powder. Additionally, the PEDOT films swell dramatically during the coating process due to the greater compatibility of the polymer with the organic solvent.

The choice of solvent and electrolyte is also very important in electropolymerisation since polymerisation reaction proceeds via radical cation intermediates (Genies *et al.*, 1983). Both solvent and electrolyte should be stable at the oxidation potential of the monomer. It becomes noticeable that reaction will be sensitive to nucleophilicity in the environment near the electrode. Use of an aprotic solvent is preferable as they are poor nucleophiles resulting in acetonitrile (ACN) being commonly used. Furthermore, ACN has wide potential window (Bard and Faulker, 2001) and relatively high permittivity (ε_r = 35.95), which allow a good dissociation of the electrolyte and thus a good ionic conductivity. However, a wide variety of other aprotic solvents such as benzonitrile and propylene carbonate with weak nucleophile character have also been used.

In this study, three compounds from the 3,4-alkylenedioxythiophene family *i.e.* PEDOT, poly(3,4-propylenedioxythiophene) (PProDOT) and poly(3,3-dibenzyl-3,4-propylenedioxythiophene) (PDBPD) prepared in acetonetrile (ACN) were studied. The properties of PEDOT films prepared in aqueous solutions were also investigated. However, the main focus of this study is to comparatively investigate the characteristics of the polymer films.

5.2 Experimental

5.2.1 Chemicals and Reagents

3,4-Ethylenedioxythiophene (EDOT), 3,4-propylenedioxythiophene (ProDOT), 3,3-dibenzyl-3,4-propylenedioxythiophene (DBPD) monomers were kindly provided by Prof. Anil Kumar from the Indian Institute of Technology, Bombay. These monomers have high purity (> 99.5%) as reported by Kumar's group (Krishnamoorthy *et al.*, 2001, Kumar *et al.*, 1998). Potassium chloride (KCl) and lithium perchlorate ($LiClO_4$) were obtained from Sigma, UK. ACN was purchased from Fisher, UK. All chemicals were used as received without any purification.

5.2.2 Cleaning of Working Electrodes

Glassy carbon (GC) electrodes (Bioanalytical System Inc.) and indium tin oxide coated glass (ITO) electrodes (Pilkington, UK) were used as the working electrode for the preparation of conducting polymers. The diameter of the GC electrode was 3 mm. All the working electrodes were cleaned before the polymerisation process.

The GC working electrodes was cleaned by polishing with 0.05 μm alumina slurry on an alumina polishing pad (microcloth pad) in circular motion followed by thorough rinsing with deionised water. The electrode was then cleaned ultrasonically in deionised water for a few minutes to remove any residual alumina. ITO electrodes were

cleaned ultrasonically using isopropyl alcohol and followed by distilled water for 30 min. Prior to each experiment, the ITO electrodes were rinsed with ethanol.

5.2.3 Preparation of Conducting Polymers

5.2.3.1 Preparation of Conducting Polymer in Non Aqueous Solution

All polymerisations were made using a multichannel potentiostat model VMP (Perkin-Elmer Instruments). EDOT, ProDOT and DBPD were electropolymerised in ACN with 10 mM monomer and 0.1 M $LiClO_4$ in the solution. In this condition, the ClO_4^- will be doped into the film during the synthesis. The choice of 10 mM is based on the previous publications (Bobacka *et al.*, 2000, Mousavi *et al.*, 2008, Yang *et al.*, 2007). Platinum foil (1 cm^2) and Ag wire were used as the counter electrode and pseudo-reference electrode, respectively. All experiments were carried out at room temperature.

5.2.3.2 Preparation of PEDOT in Aqueous Solution

For the electropolymerisation of EDOT in aqueous solution, 0.01 M EDOT in 0.1 M KCl was used. The solution was stirred vigorously in order to disperse the EDOT monomer evenly in the solution. Experiments were also conducted using 0.1 M $LiClO_4$ as a supporting electrolyte. The electropolymerisation was carried out using a cell with three-electrode system. Platinum foil (1 cm^2) and Ag/AgCl (3.5 M KCl) were used as counter and reference electrodes, respectively. The potential was scanned for 20 cycles at 50 mVs^{-1} from -0.2 V to 1.3 V or -1 V to 1.3 V.

5.2.4 Polymer Characterisation

5.2.4.1 Environmental Scanning Electron Microscopy (ESEM) and Field Emission Scanning Electron Microscopy (FE-SEM)

An environmental scanning electron microscope (ESEM) and field emission scanning electron miscrope (FE-SEM) were used to examine the structure of the conducting polymers using a Philips XL30 SEM (Philips/FEI) and Hitachi SU70 (Hitachi High Technologies), respectively. For conducting polymers deposited on conventional electrodes, the images were taken by placing the electrode at a tilt position (**Figure 5.2**) in order to get clearer images of the polymer films. The typical accelerating voltage of ESEM and SEM was 5.0 kV.

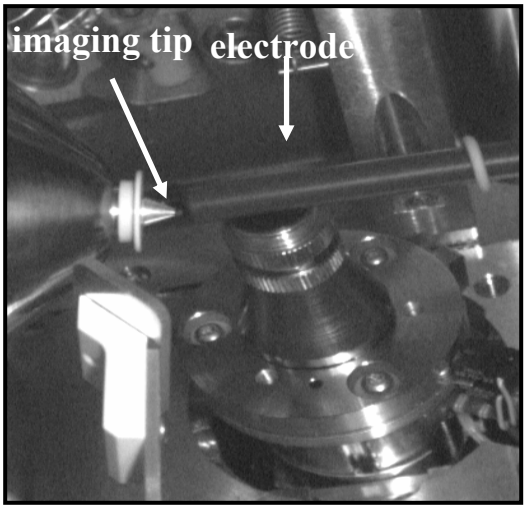

Figure 5.2: Tilt position of electrode for ESEM imaging.

5.2.4.2 Atomic Force Microscopy (AFM)

Surface morphology and roughness of the polymer surface were determined by AFM (Nanoscope IV, Digital Instruments, Inc., Santa Barbara, California, USA). The measurements were carried out at room temperature using tapping mode. The average roughness, R_a was calculated using Nanoscope software. R_a is defined as the arithmetic average deviation from the centre line *i.e.* the distance between the highest and the lowest point of the surface irregularities.

5.2.4.3 Contact Angle Measurement

Contact angle measurements were made using FTÅ 200 apparatus (First Ten Angstroms, Inc.) consisting of a goniometer with a drop of fixed volume. The advancing contact angle was measured by dropping 10 μL of water droplet on the solid surface. A given fixed volume (5 μL) was then added to the droplet already on the solid surface by lowering the needle slowly towards it. For receding contact angle measurements, the same procedure was carried out but a fixed volume of water (5 μL) was withdrawn. In order to obtain more precise data, several measurements have been carried out and the average of contact angles from the images was used to represent the wetting properties of the sample. The contact angles were measured a few seconds after application of the drop, when the water droplet had reached stability. All measurements were made at room temperature.

5.2.4.4 Raman Spectroscopy

A Horiba Jobin Yvon LabRAM spectrometer (HORIBA Jobin Yvon Inc., USA) was used to record Raman spectra of conducting polymers. The excitation wavelength was 633 nm and the all measurements were carried out at room temperature and ambient pressure. For each sample, at least three spectra were taken at different regions of each sample to ensure that the spectra were representative of the sample as a whole.

5.3 Results and Discussion

5.3.1 Oxidation Potential of EDOT and Its Derivatives

Before deposition of a polymer by electrochemical techniques, the potential windows of the GC electrode in background solutions were investigated. The potential windows of glassy carbon in ACN and aqueous solutions are tabulated in **Table 5.1**. The GC electrode has a wide potential window in $LiClO_4$/ACN solution ranging from -3.7 to 2.95 V (*vs* Ag wire), whereas in $LiClO_4$/aqueous solution the potential window was -2 to 1.98 V (*vs* Ag/AgCl). In the case of KCl/aqueous, the potential window was -1.8 to 1.3 V *vs* Ag/AgCl. These results indicate that all the systems are suitable for the oxidation of PEDOT and its derivatives as shown by the Diaz mechanism (Genies *et al.*, 1983, Sadki *et al.*, 2000) as shown in **Figure 5.3.** This mechanism is analogous to the oxidative polymerisation of pyrrole.

Table 5.1: Potential window of glassy carbon electrode.

Solution	Potential window
$LiClO_4$/aqueous	-2.0 V to 1.98 V *vs* Ag/AgCl
KCl/aqueous	-1.8 V to 1.3 V *vs* Ag/AgCl
$LiClO_4$/ACN	-3.7 V to 2.95 V *vs* Ag wire

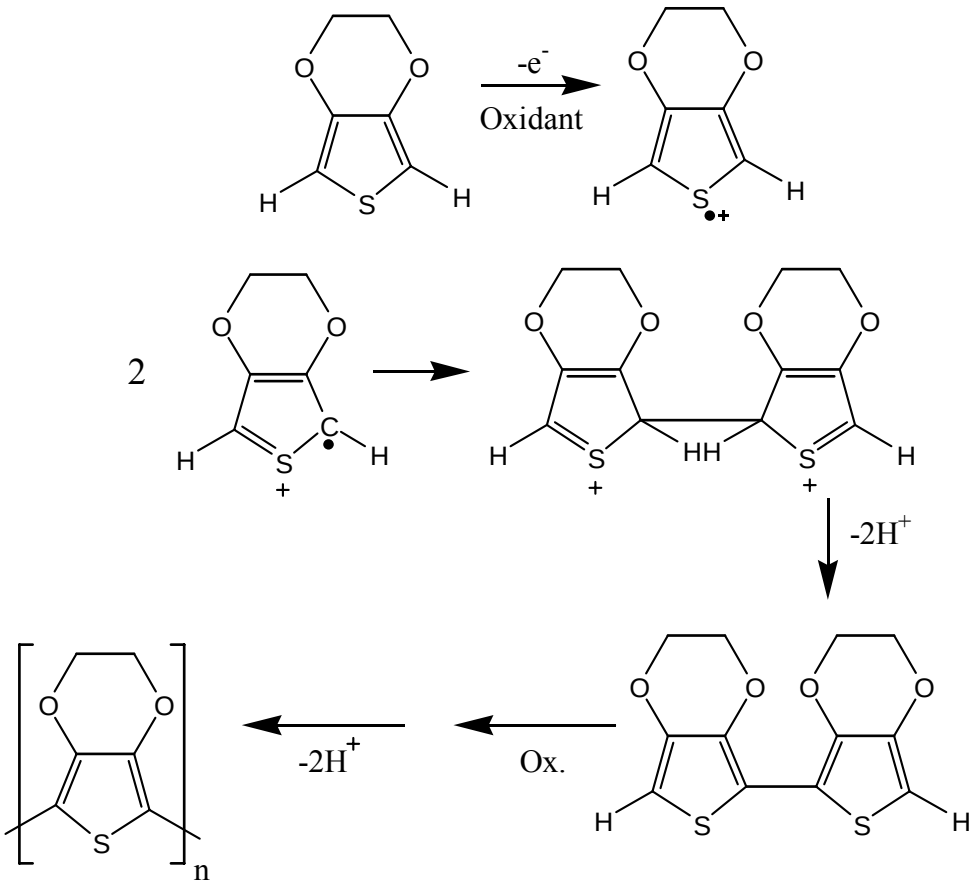

Figure 5.3: The Diaz mechanism of electropolymerisation of EDOT (Genies *et al.*, 1983).

Figure 5.4 shows the first cycle of current-voltage curves obtained during the potentiodynamic synthesis of PEDOT, PProDOT and PDBPD. EDOT, ProDOT and DBPD monomers have onset oxidation potentials of 1.10, 1.14 and 1.37 V, respectively. These oxidation potentials were obtained from the onset potential of forward scan. The trace crossing on the reverse scan in **Figure 5.4b** is typical first cycle for electrodeposition of conducting polymers. This feature is due to the initiation of the nucleation process of the polymer film which is analogous to the theory of metal deposition (Downard and Pletcher, 1986).

In all cases, the anodic current of reverse scan (at potential > 1.0 V) was higher than the forward scan except for DBPD at potentials beyond 1.38 V (**Figure 5.4a**). It was found that the onset potential of the reverse scan (anodic current) was shifted to 0.93 V

(EDOT), 0.99 V (ProDOT) and 1.15 V (DBPD). This behaviour is attributed to the initial product formed (*i.e.* dimers, oligomers and bipolarons) on the electrode surface which are much easier to oxidise than the monomer itself due to conjugation (Diaz *et al.*, 1981). In the dimeric structure, the extra delocalisation in the π-systems over the two rings lowers the energy difference, making it more easily oxidised. Similar results were also observed by other authors (Kumar *et al.*, 1998, Seshadri *et al.*, 2003). In this case, there is no thermodynamic effect could be observed under the condition of the experiments. The inset of **Figure 5.4** reveals the presence of peaks (-1.0 to -0.25 V) indicating that the polymers start growing at the reverse scan. It should be noted that the background electrolyte is electrochemically silent in the whole potential range applied.

In the case of DBPD, the first attempt to electropolymerise the monomer was carried out using the same potential (-1.0 to 1.3 V) as applied to the EDOT and ProDOT. It was found that there was no significant increase in current indicating the DBPD monomer is not being oxidised (**Figure 5.5**). Since the oxidation of the monomer is a vital process, which is the first step in electropolymerisation (Sadki *et al.*, 2000), the potential was extended to 1.5 V in order to oxidise the monomer (**Figure 5.4**). It was reported (Gratzl *et al.*, 1990, Krische and Zagorska, 1989) that high potential > 1.55 V *vs* $Ag/AgNO_3$ (1.36 V *vs* SHE) would irreversibly damage the conjugated system as a result of overoxidation. However, in our case, based on the applied potential (-1 to 1.5 V *vs* Ag wire pseudo reference electrode), the overoxidation process was not observed.

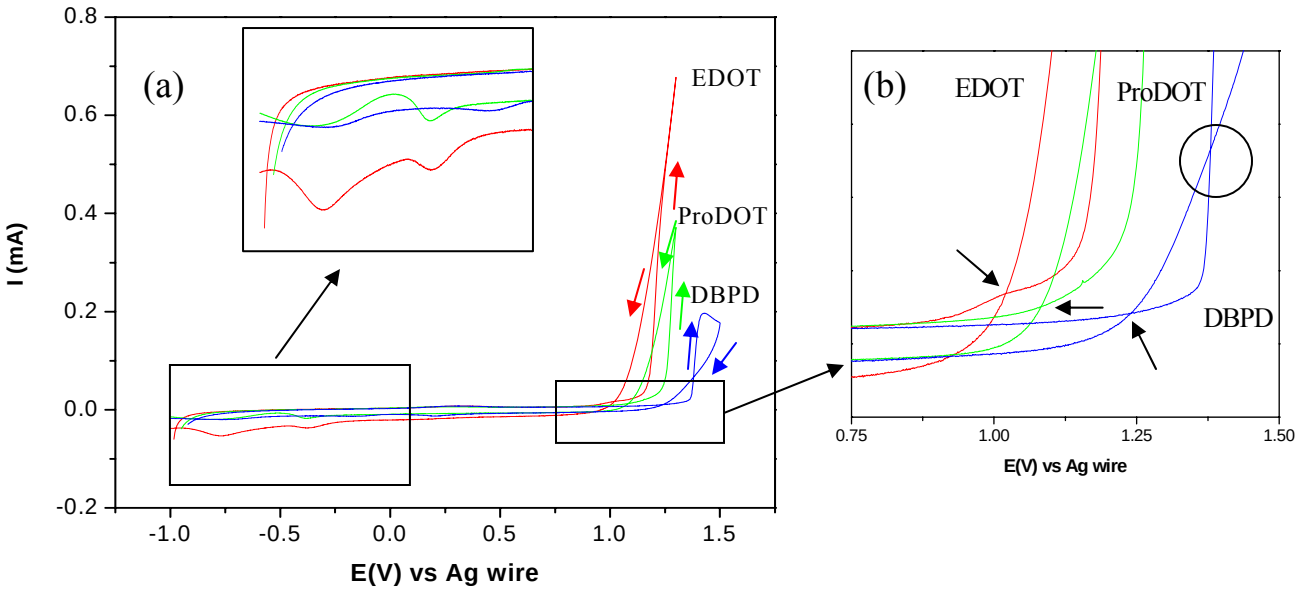

Figure 5.4: First voltammetric cycles during the electropolymerisation of polymers on a glassy carbon electrode in a solution containing 10 mM monomer + 0.1 M $LiClO_4$/ACN. Scan rate = 50 mVs^{-1}.

Table 5.2: Oxidation potential of monomer.

Monomer	**Onset oxidation potential (V) *vs* Ag wire**
EDOT	1.10
ProDOT	1.14
DBPD	1.37

The oxidation potential of DBPD (1.37 V) is higher compared to EDOT (1.10 V) and ProDOT (1.14 V) (**Figure 5.4**) due to the existence of two phenyl groups with electron withdrawing effect. However, the addition of one alkyl group ($-CH_2$) to the EDOT structure (forming ProDOT) did not have a significant effect on the oxidation potential compared to EDOT. Electropolymerisation of DPBD shows an unusual crossover pattern in their CV curve as indicated by the circle in **Figure 5.4b**. In this case, the diffusion of reactive species (monomer, radical cation, dication, etc) to the vicinity of

electrode surface becomes crucial (Chang *et al.*, 2005) as the amount of DPBD is limited due to the slower movement of bulky molecules.

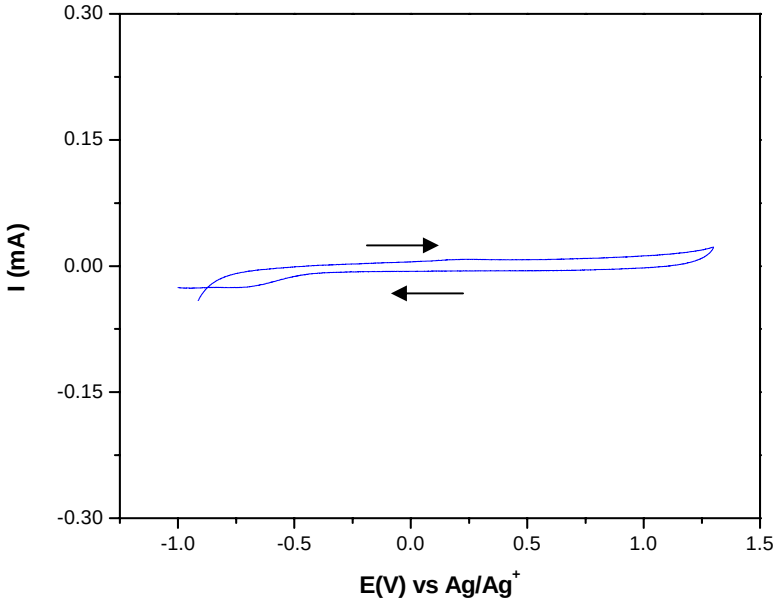

Figure 5.5: First voltammetric cycle during the electropolymerisation of DBPD on a glassy carbon electrode between -1.0 and 1.3 V. Scan rate = 50 mVs^{-1}.

5.3.2 Electropolymerisation of EDOT, ProDOT and DBPD on GC Electrodes

EDOT, ProDOT and DBPD monomers were used to prepare the polymers in ACN on the glassy carbon electrodes. These electrodes hereafter will be called GC/PEDOT/$LiClO_4$(ACN), GC/PProDOT/$LiClO_4$(ACN) and GC/PDBPD/$LiClO_4$(ACN), respectively. Electropolymerisation of all conducting polymers was carried out at the same concentration (10 mM monomer) for 20 scans. PEDOT is commonly synthesised in non-aqueous solution (organic media) (Han *et al.*, 2006, Park *et al.*, 2006, Wang and Wong, 2006), in contrast to other polymers such as PAn which are commonly synthesised in aqueous media. After the polymerisation, a blue black solid was seen deposited on the surface of each electrode.

In the oxidative polymerisation of EDOT using cyclic voltammetry, an irreversible oxidation was observed at +1.10 V (**Figure 5.6**). In the subsequent cycles, the

current of monomer oxidation increased and the redox peaks of the polymer started growing around +0.17 and -0.2 V. These results are in agreement with previous publication (Varis *et al.*, 2007, Zhang *et al.*, 2006). In general, CVs of GC/PProDOT/$LiClO_4$(ACN) (**Figure 5.8**) were similar to GC/PEDOT/$LiClO_4$(ACN). It was observed that GC/PEDOT/$LiClO_4$(ACN) and GC/PProDOT/$LiClO_4$(ACN) had two reduction peaks which is similar to that observed by Bendikov and Harmon (2005).

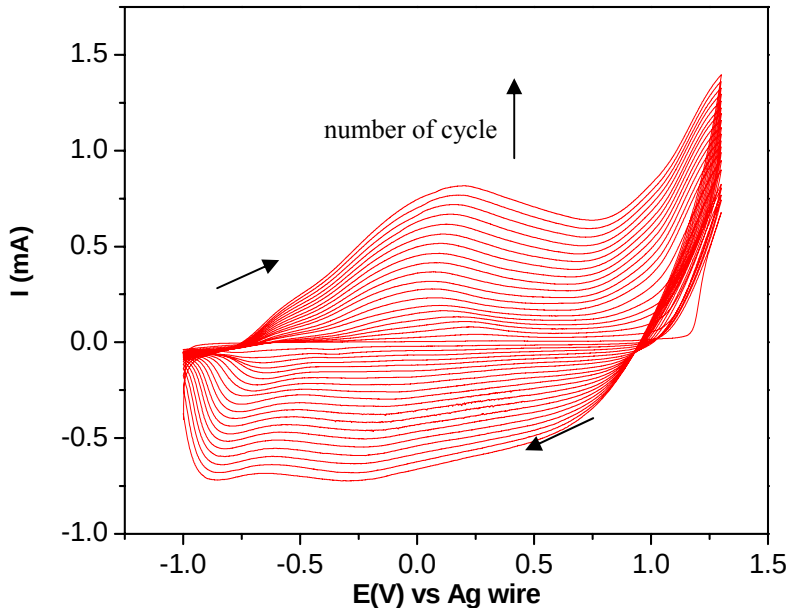

Figure 5.6: Potentiodynamic electropolymerisation of 0.01 M EDOT in 0.1 M $LiClO_4$/acetonitrile on GC electrode at 50 mVs^{-1}.

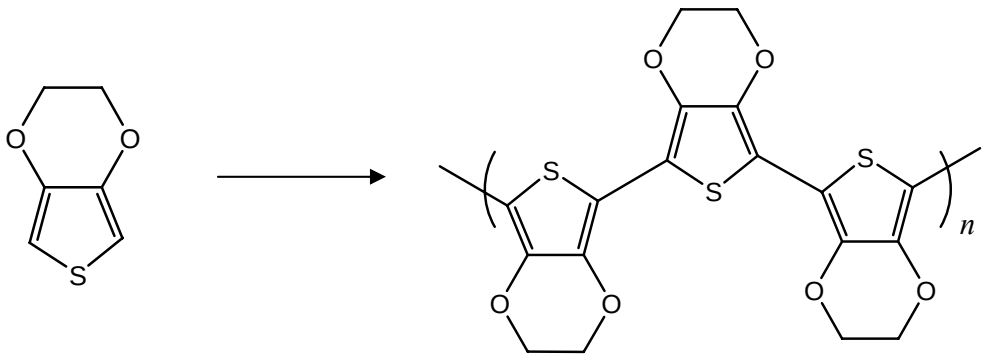

Figure 5.7: Polymerisation of EDOT (*n* = number of polymerisation).

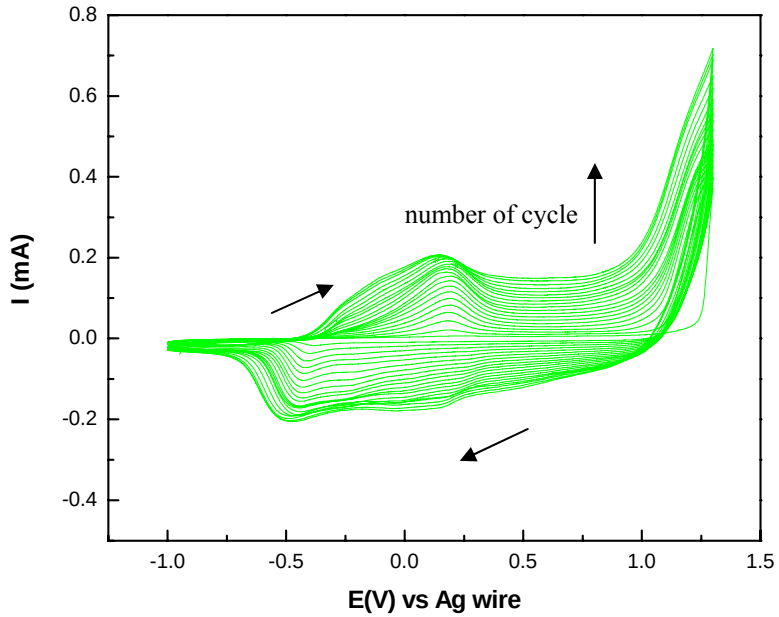

Figure 5.8: Potentiodynamic electropolymerisation of 0.01 M ProDOT in 0.1 M $LiClO_4$/acetonitrile on GC electrode at 50 mVs^{-1}.

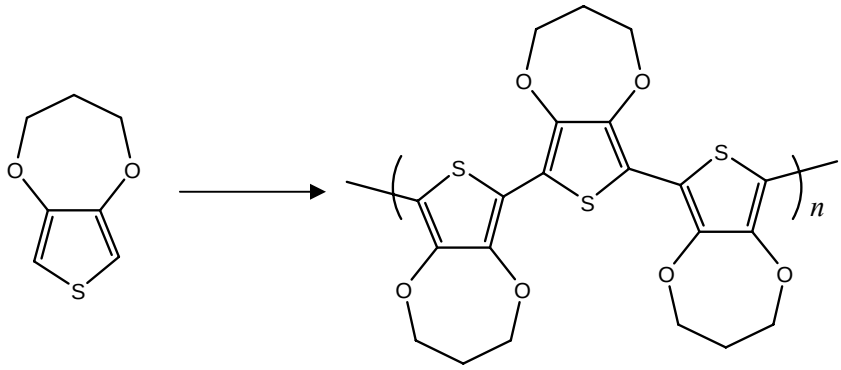

Figure 5.9: Polymerisation of ProDOT (*n* = number of polymerisation).

Electrochemically synthesised PDBPD was obtained from a solution of 10 mM DBPD and 0.1 M $LiClO_4$ in ACN, by cycling the potential between -1.0 and 1.5 V. The typical CVs are illustrated in **Figure 5.10**. Between the 2nd and 9th cycle, the current of the monomer oxidation increased and the current started to decline from the 10th cycle to the 20th cycle. The existence of new well-defined redox peaks (0.2 - 0.75 V) indicated that the polymer is redox active. It was noticeable that the redox peaks were sharper that GC/PEDOT/$LiClO_4$(ACN) and GC/PProDOT/$LiClO_4$(ACN). This is probably enhanced

by π-π* stacking which may be due to the extended conjugation of phenyl groups (inset **Figure 5.10**). π-π interactions are caused by intermolecular overlapping of *p* orbitals in the conjugated system. The E_{pa} of the polymer for the 3rd cycle was at ca. 0.25 V and it shifted to more anodic potential in subsequent cycles. The E_{pa} for the 20th cycle was at 0.7 V. This large shift in the redox peaks and the decrease in current after 17th cycle may be attributed to the increase in the resistance of polymeric film as the film becomes thicker during the polymer growth.

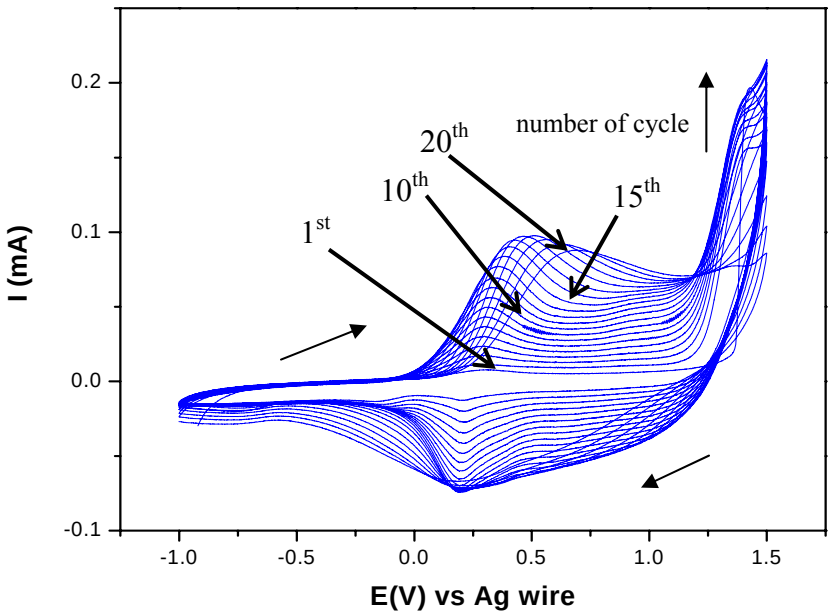

Figure 5.10: Potentiodynamic electropolymerisation of 0.01 M DBPD in 0.1 M $LiClO_4$/acetonitrile on GC electrode at 50 mVs^{-1}.

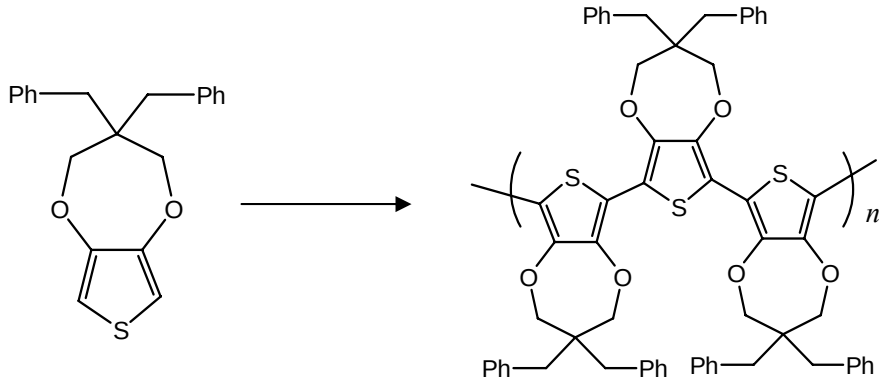

Figure 5.11: Polymerisation of DBPD (*n* = number of polymerisation, Ph = phenyl).

5.3.3 Electropolymerisation of EDOT, ProDOT and DBPD on ITO Electrodes

The CVs corresponding to the potentiodynamic electropolymerisation of EDOT, ProDOT and DBPD on ITO electrodes from a solution containing 10 mM monomer and 0.1 M $LiClO_4$ as supporting electrolyte in ACN are shown in **Figure 5.12** - **Figure 5.14**. Hereafter these electrodes will be called ITO/PEDOT/$LiClO_4$(ACN), ITO/PProDOT/$LiClO_4$(ACN) and ITO/PDBPD/$LiClO_4$(ACN), respectively. The CV obtained with ITO/PEDOT/$LiClO_4$(ACN) showed broad peaks in the range -0.9 to +0.8 V. In contrast, well defined redox peaks were observed in the case of ITO/PProDOT/$LiClO_4$(ACN) and ITO/PDBPD/$LiClO_4$(ACN). The only difference was the ITO/PDBPD/$LiClO_4$(ACN) showed a sharper redox peak, than those observed with PEDOT and ITO/PProDOT/$LiClO_4$(ACN), even after 20 scans. It was also noted that the shape of the CV of film growth on the two substrates (GC and ITO electrodes) was distinct and they were therefore expected to demonstrate differences in physical properties.

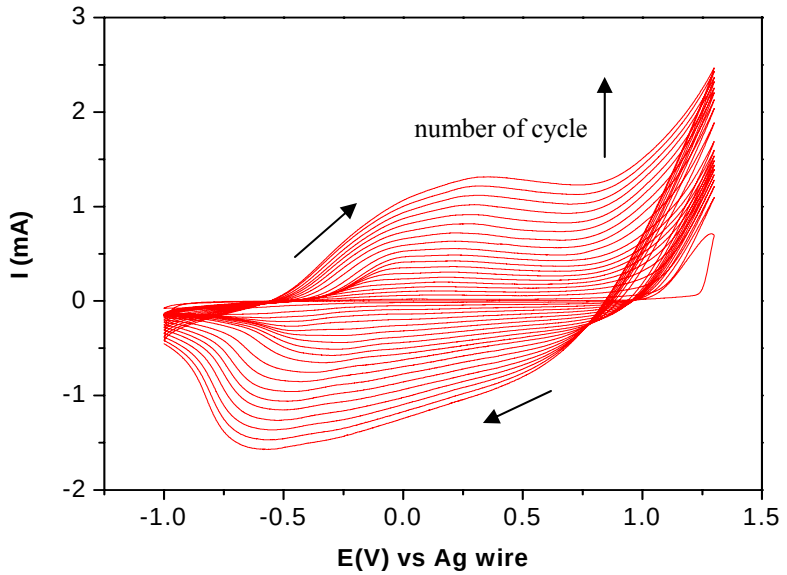

Figure 5.12: Potentiodynamic electropolymerisation of 0.01 M EDOT + 0.1 M $LiClO_4$ in acetonitrile on ITO electrode at 50 mVs^{-1}.

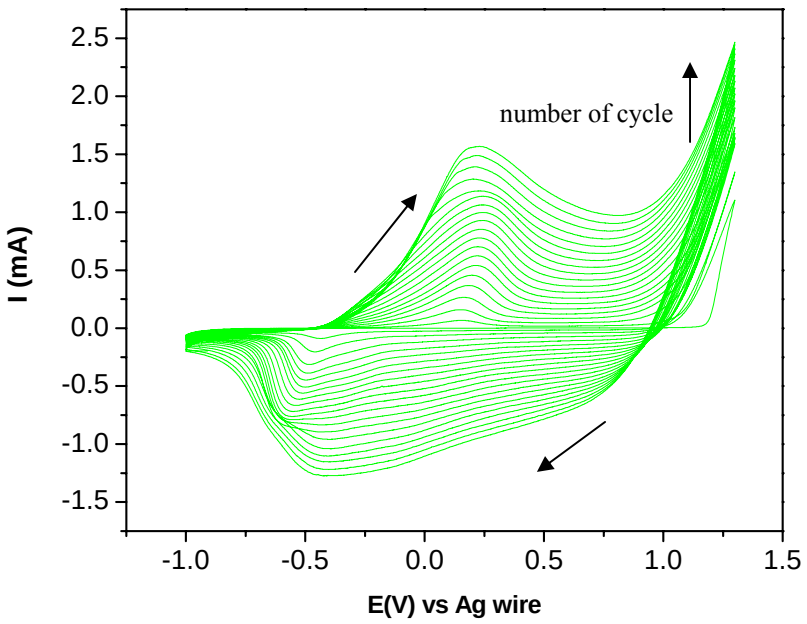

Figure 5.13: Potentiodynamic electropolymerisation of 0.01 M ProDOT + 0.1 M $LiClO_4$ in acetonitrile on ITO electrode at 50 mVs^{-1}.

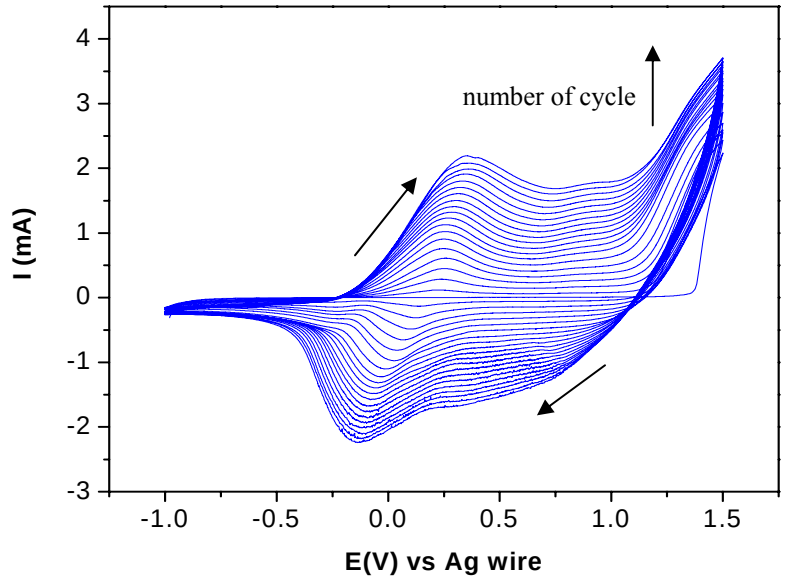

Figure 5.14: Potentiodynamic electropolymerisation of 0.01 M DBPD + 0.1 M $LiClO_4$ in acetonitrile on ITO electrode at 50 mVs^{-1}.

5.3.4 Electropolymerisation of EDOT in Aqueous Solution

Since EDOT exists as a liquid and is partially soluble in water at room temperature (1994), electropolymerisations of EDOT in aqueous solutions (KCl and $LiClO_4$) were also carried out. The oxidative polymerisations of 0.01 M EDOT in 0.1 M KCl on GC and ITO electrodes are shown in **Figure 5.15** and **Figure 5.16**, respectively. These electrodes are denoted as GC/PEDOT/KCl(Aq) and ITO/PEDOT/KCl(Aq).

The potential was swept between -0.2 V to 1.3 V for 20 cycles at a scan rate of 50 mVs^{-1}. The current increased drastically when the applied potential was larger than 0.9 V, implying the formation of radical cations (Roncali *et al.*, 2005). One obvious well-defined oxidation peak was observed at around 1.2 V for the first cycle (**Figure 5.15**). As the number of cycle increases, this onset anodic current significantly lowered especially between the first and second cycles. Nien *et al*. (2006) inferred that the high potential range may result from decomposition of water in the electrolyte and cause the partial degradation of the PEDOT film. However this phenomenon was not observed in the case of ITO/PEDOT/KCl(Aq) (**Figure 5.16**).

It should be noted that after several cycles (**Figure 5.15** and **Figure 5.16**), new broad oxidation and reduction peaks were observed, which indicates the formation of PEDOT (**Figure 5.7**) on the electrode *i.e.* the EDOT radical cations start to electropolymerise onto the GC and ITO electrodes. These redox peaks are attributed to the doping/dedoping processes of PEDOT film. The current is probably due to the transport of both electronic and ionic charges (polaron +e and anion –e) (El Moustafid *et al.*, 2003). It was reported that the anions play a significant role in the process of oxidation and electropolymerisation of EDOT by compensating the positive charge inside the PEDOT film. The current of these peaks increased as well, implying that the amount of PEDOT was increasing.

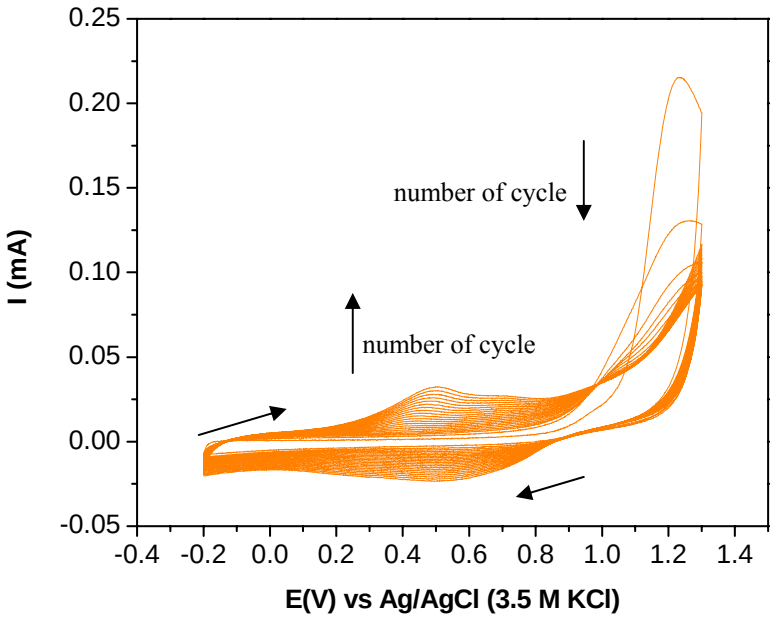

Figure 5.15: Potentiodynamic electropolymerisation of 0.01 M EDOT + 0.1 M KCl in aqueous solution on GC electrode at 50 mVs^{-1}.

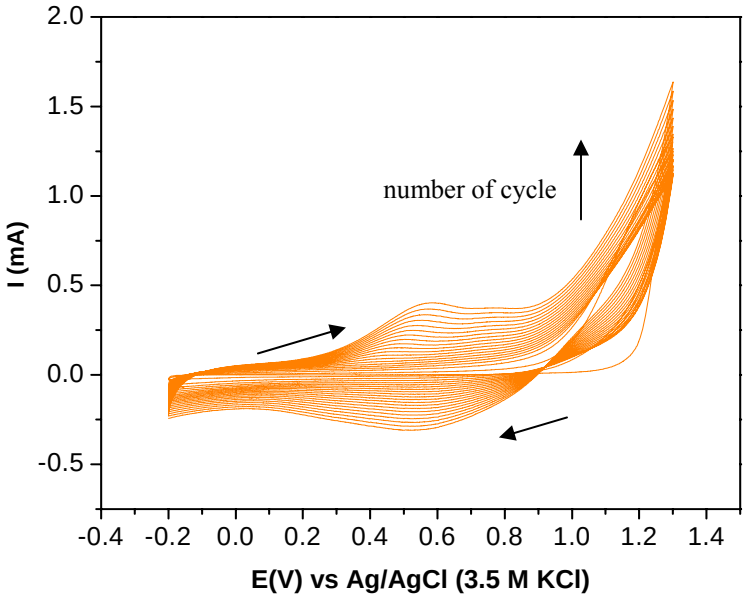

Figure 5.16: Potentiodynamic electropolymerisation of 0.01 M EDOT + 0.1 M KCl in aqueous solution on ITO electrode at 50 mVs^{-1}.

Polymers have been prepared by electrochemically oxidising or reducing their monomers under appropriate experimental conditions as long as their monomeric molecules can be oxidised or reduced within the background potential of an electrolyte solvent system used for the synthesis experiments. In this work, electropolymerisation of EDOT in an aqueous solution containing $LiClO_4$ supporting electrolyte on GC and ITO electrodes were also performed. Typical CVs of PEDOT electrodeposited in $LiClO_4$ aqueous solution on GC and ITO electrodes are shown in **Figure 5.17** and **Figure 5.18**, respectively. The shapes of CVs differ significantly from the PEDOT synthesised in KCl (**Figure 5.15** and **Figure 5.16**). In the potential range of -0.2 to 1.3 V (similar potential in the case of PEDOT in KCl), only oxidation peak of EDOT was present. There was no new peak observed after several cycles (**Figure 5.17**). In contrast, if the range of potential scanning is extended to -1 V (**Figure 5.17** and **Figure 5.18**), a new redox couple peak was observed associated with oxidative doping and reductive dedoping of the polymer. This indicates that redox process of PEDOT doped with ClO_4^- prepared in aqueous solution occurs between -1 and +0.75 V (**Figure 5.17**). Based on this result, the best potential range is between -1 to 1.3 V in order to see redox activity of PEDOT in $LiClO_4$ aqueous solution.

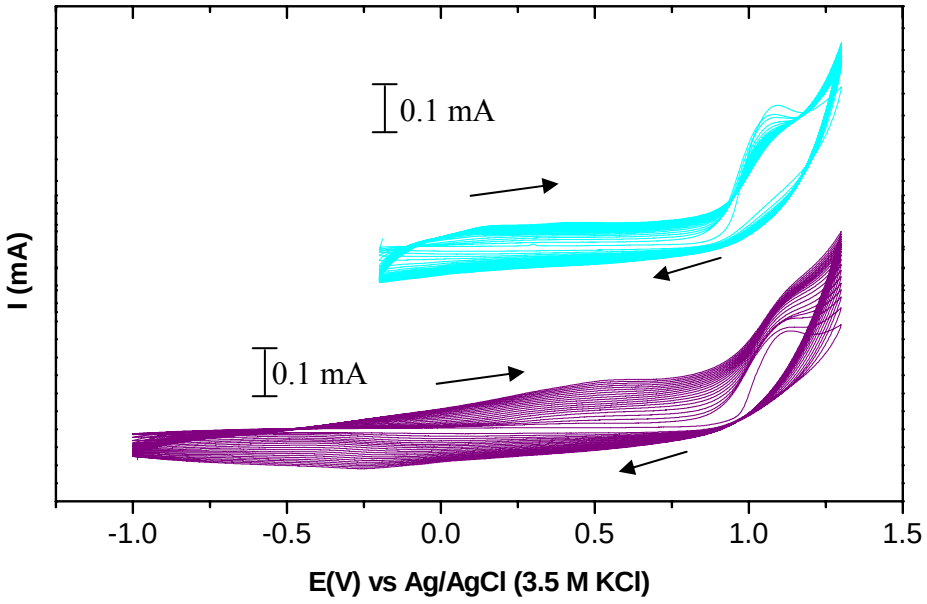

Figure 5.17: Potentiodynamic electropolymerisation of 0.01 M EDOT + 0.1 M $LiClO_4$ in aqueous solution on GC electrode at 50 mVs^{-1}.

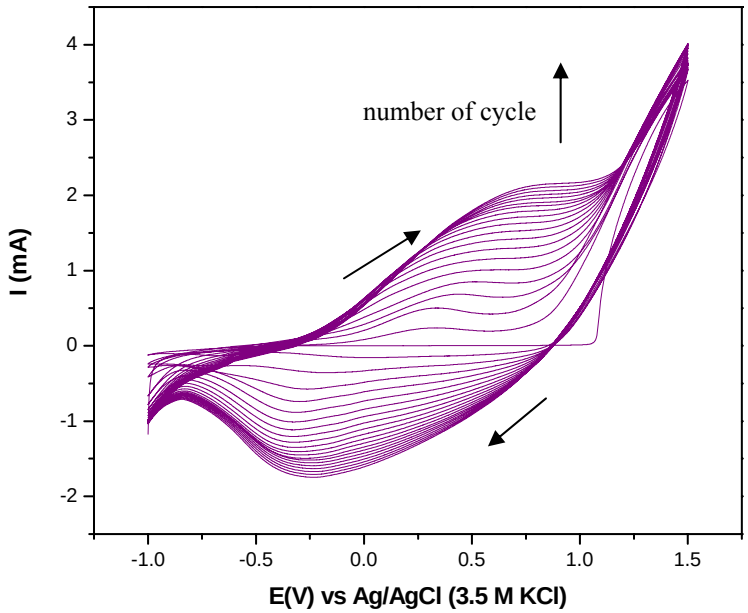

Figure 5.18: Potentiodynamic electropolymerisation of 0.01 M EDOT + 0.1 M $LiClO_4$ in aqueous solution on ITO electrodes at 50 mVs^{-1}.

5.3.5 Polymerisation Charge and Thickness of Polymer Films

The CV of each electropolymerisation was further analysed to obtain changes in the total polymerisation charge during each cycle of electropolymerisation by integrating the current vs time plot. As illustrated in **Figure 5.19**, the polymerisation charge (Q_{pol}) of GC/PEDOT/$LiClO_4$(ACN) and ITO/PEDOT/$LiClO_4$(ACN) increased steadily with time. GC/PProDOT/$LiClO_4$(ACN) and ITO/PProDOT/$LiClO_4$(ACN) show the same behaviour (**Figure 5.20**) with total polymerisation charge of 75.7 and 36.5 mC/cm^2, respectively. GC/PDBPD/$LiClO_4$(ACN) and ITO/PDBPD/$LiClO_4$(ACN) revealed a different pattern in which the anodic charge increased gradually until the 13^{th} cycle before decreasing (**Figure 5.21**). In both cases (PEDOT and PProDOT), the polymerisation charges were higher for GC than ITO electrodes, however in the case of PDPBD the anodic charge was almost similar for both electrodes. For PEDOT prepared in aqueous solution (**Figure 5.22** and **Figure 5.23**), films formed with $LiClO_4$ showed much higher and increasing anodic charge than KCl, indicating formation of a good film as confirmed by SEM images (**Section 5.3.6**).

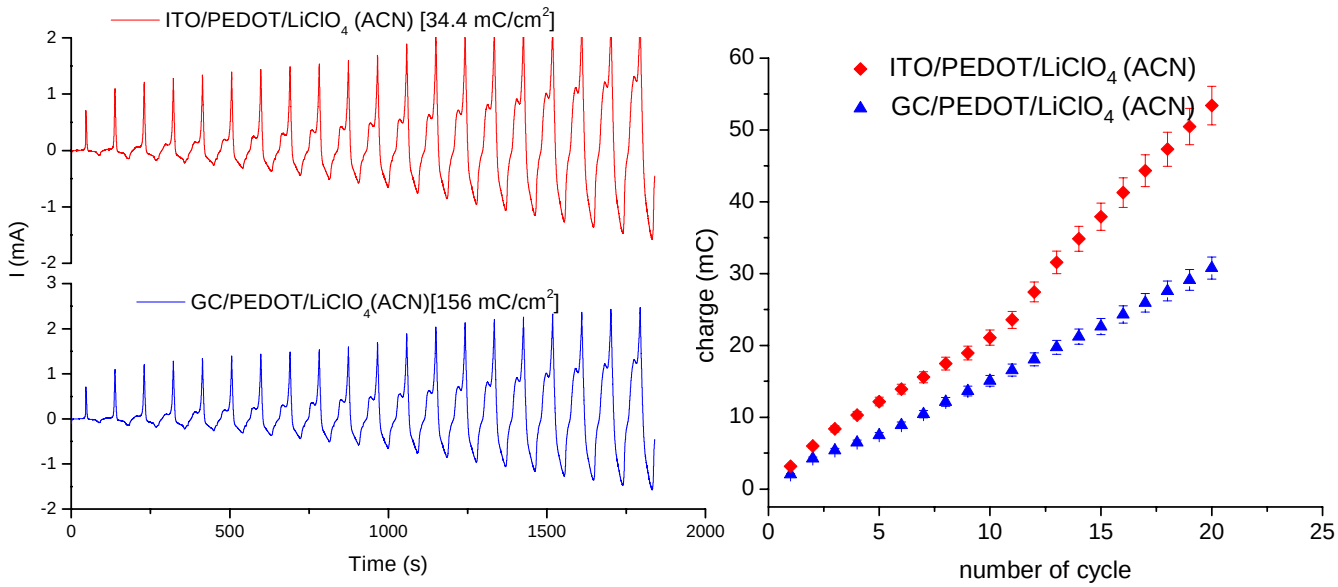

Figure 5.19: Kinetics of potentiodynamic electropolymerisation of PEDOT deposited on GC and ITO electrodes in acetonitrile. Values in parantheses refer to the total polymerisation charge.

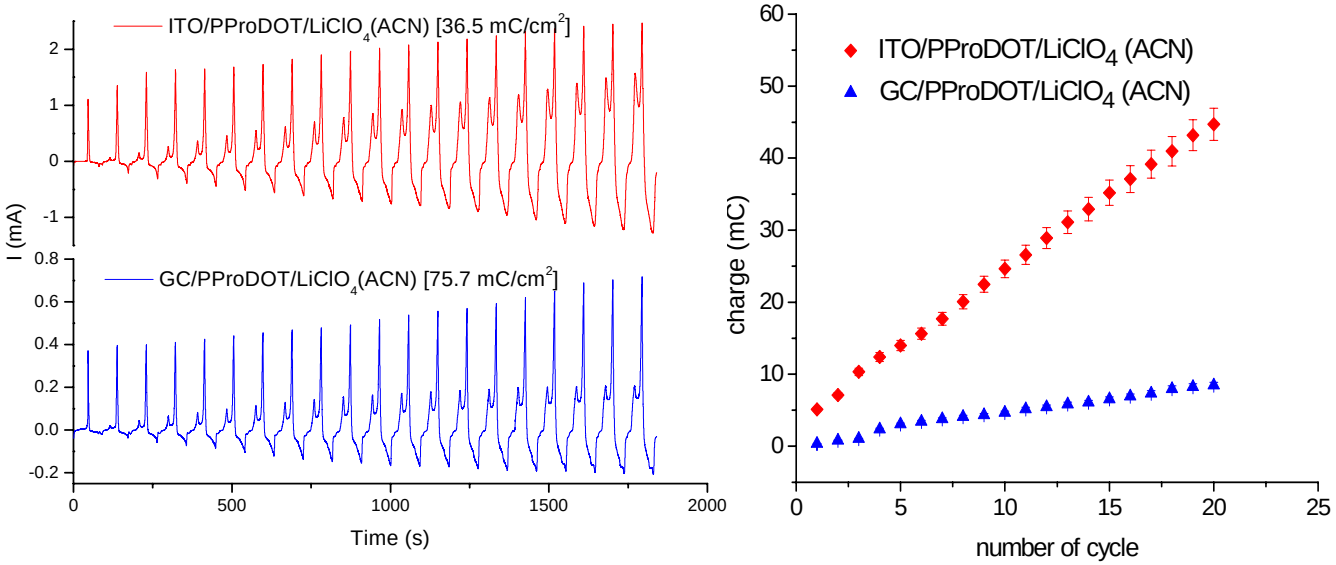

Figure 5.20: Kinetics of potentiodynamic electropolymerisation of PProDOT deposited on GC and ITO electrodes in acetonitrile. Values in parantheses refer to the total polymerisation charge.

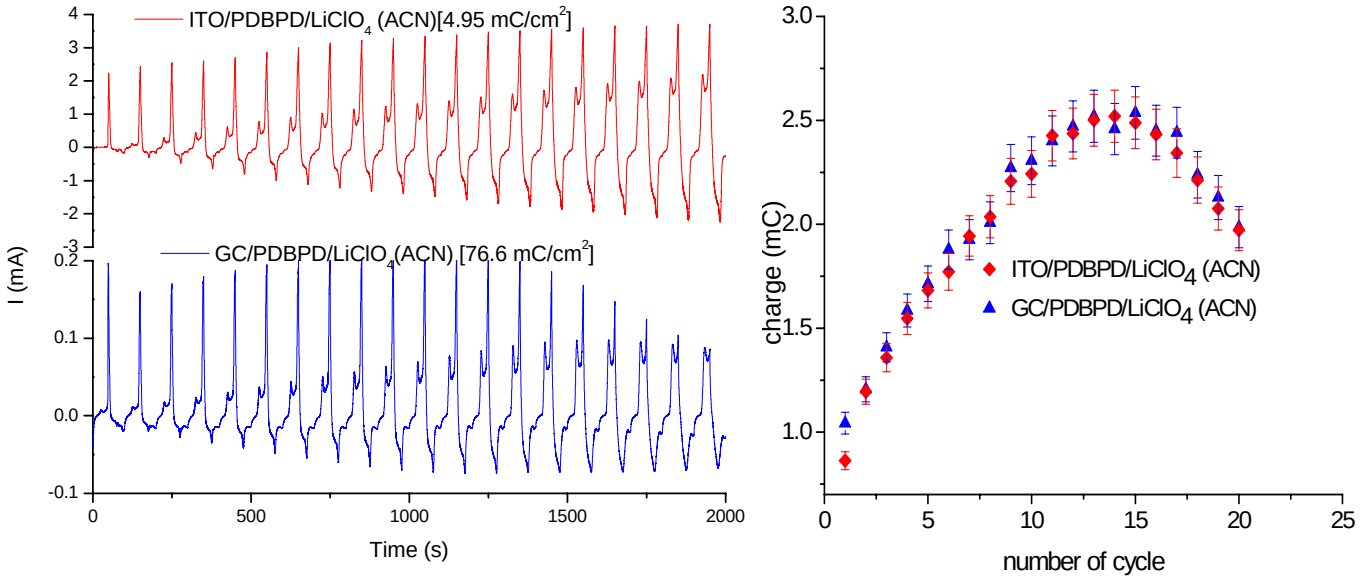

Figure 5.21: Kinetics of potentiodynamic electropolymerisation of PDBPD deposited on GC and ITO electrodes in acetonitrile. Values in parantheses refer to the total polymerisation charge.

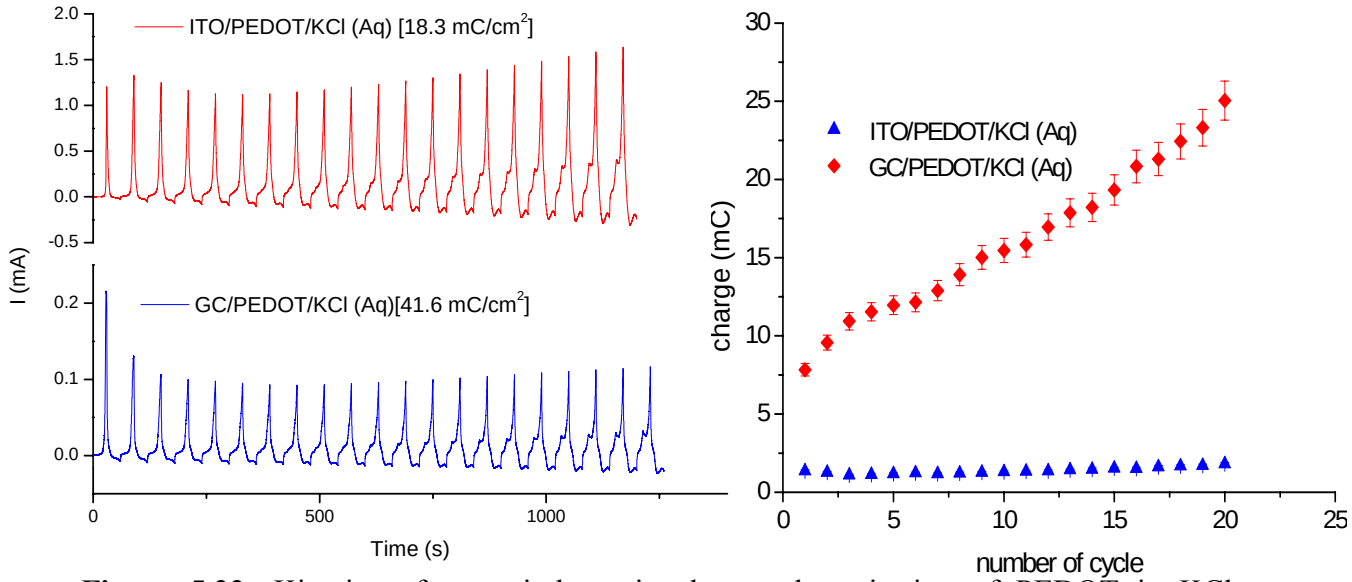

Figure 5.22: Kinetics of potentiodynamic electropolymerisation of PEDOT in KCl deposited on GC and ITO electrodes in aqueous solution. Values in parantheses refer to the total polymerisation charge.

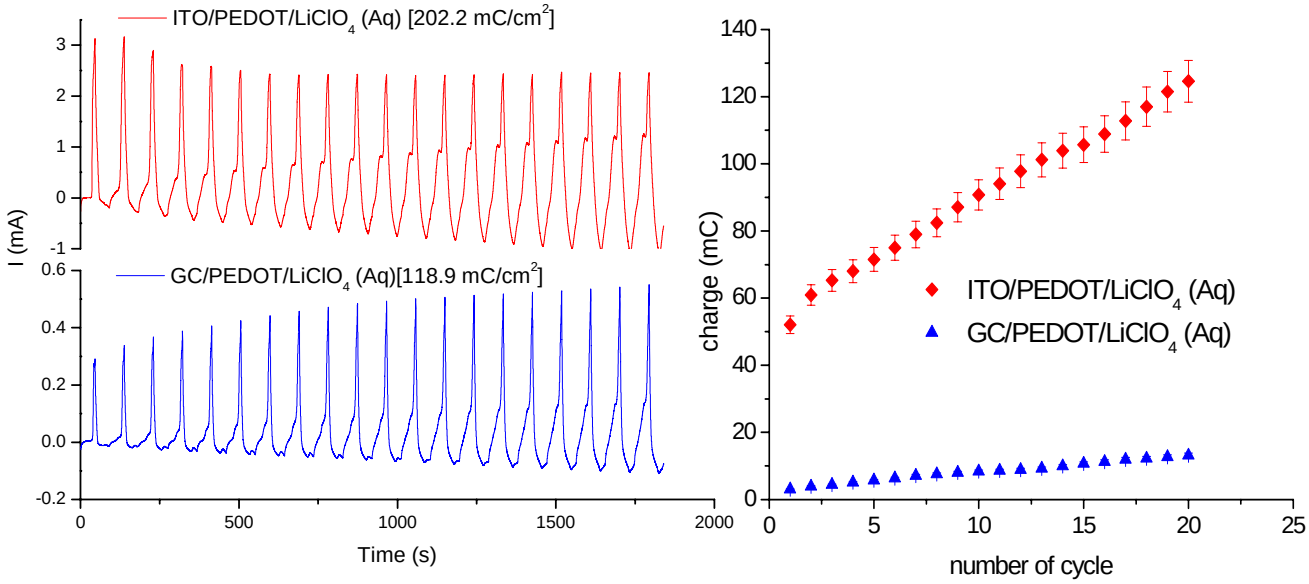

Figure 5.23: Kinetics of potentiodynamic electropolymerisation of PEDOT in $LiClO_4$ deposited on GC and ITO electrodes in aqueous solution. Values in parantheses refer to the total polymerisation charge.

Table 5.3: Polymerisation charge and film thickness.

Electrode	Polymerisation charge, Q_{pol} (mC)	Film thickness (µm)
GC/PEDOT/$LiClO_4$ (ACN)	156.0 ± 8.5	29.40 ± 0.78
ITO/PEDOT/$LiClO_4$ (ACN)	34.4 ± 1.5	47.53 ± 1.4
GC/PProDOT/$LiClO_4$ (ACN)	75.7 ± 2.1	9.94 ± 0.20
ITO/PProDOT/$LiClO_4$ (ACN)	36.5 ± 1.2	51.08 ± 2.64
GC/PDBPD/$LiClO_4$ (ACN)	76.6 ± 0.4	8.78 ± 0.08
ITO/PDBPD/$LiClO_4$ (ACN)	4.95 ± 0.4	8.66 ± 0.08
GC/PEDOT/KCl (Aq)	41.6 ± 0.2	2.55 ± 0.01
ITO/PEDOT/KCl (Aq)	18.3 ± 4.9	29.69 ± 0.45
GC/PEDOT/$LiClO_4$ (Aq)	118.9 ± 3.0	15.50 ± 0.28
ITO/PEDOT/$LiClO_4$ (Aq)	202.2 ± 21.2	167.61 ± 1.95

In previous publications, Bobacka and coworkers (2000) obtained films of thickness 0.1-1.5 μm by assuming 2.25 electrons/monomer (Bobacka *et al.*, 2000) and the film density of 1 g cm^{-3} (Bobacka *et al.*, 2000). The film thickness is correlated to the electrical charge using Faraday's law and assuming 100% current efficiency: t= qM/ρAzF, where t is the film thickness, q is the electrical charge associated with film formation, M is the molar mass of the polymer, F is the Faraday constant, A is the area of the working surface, ρ is the density of the polymer and z is the number of electrons involved. Two electrons are required to polymerise the monomer and the value of 0.25 was obtained from the doping level (γ); $\frac{2+\gamma}{\gamma} = \frac{Q_{pol}}{Q_{redox}}$ (Haegel *et al.*, 2001), Q_{pol} is the total charge used for polymer deposition and Q_{redox} is determined by integrating the redox peak. In this study the electropolymerisation process led to reproducible solvated films of micron thickness (**Table 5.3**). In previous reports, Michalska and co-workers (Michalska *et al.*, 2003) obtained films of micron thickness using similar procedures. These films are particularly useful for ion-to-electron signal transduction particularly in electrochemical sensing applications.

5.3.6 Morphology and Structural Studies

5.3.6.1 Conducting Polymers Prepared on Glassy Carbon Electrodes

Surface morphologies of polymers were investigated by environmental scanning electron microscope (ESEM) and field emission scanning electron microscopy (FESEM). Generally, the preparation conditions *i.e.* the type of dopant ions and solvent have a significant impact on nature of the films. ESEM micrographs of GC/PEDOT/$LiClO_4$(ACN), GC/PProDOT/$LiClO_4$(ACN) and GC/PDBPD/$LiClO_4$(ACN) are shown in **Figure 5.24**. GC/PEDOT/$LiClO_4$(ACN) (**Figure 5.24a**) showed a rough surface morphology whereas GC/PProDOT/$LiClO_4$(ACN) (**Figure 5.24b**) revealed porous structure. This porous structure gives the opportunity to the ions in the electrolyte to get access to the interior of the film. This behaviour will be explained in **Chapter 6**. In the case of GC/PDBPD/$LiClO_4$(ACN) (**Figure 5.24c**), it showed a more compact

structure compared to GC/PProDOT/$LiClO_4$(ACN). This feature may be due to the bulky structure of the DBPD monomer.

The morphology of PEDOT prepared in aqueous solution containing $LiClO_4$ (GC/PEDOT/$LiClO_4$(Aq)) showed a granular structure as displayed in **Figure 5.25a**. On the other hand, GC/PEDOT/KCl(Aq) (**Figure 5.25b**) revealed a poorly defined film containing a mixed structure of film and fibril-like structure. This feature may be due to low solubility and low dispersity of EDOT in this medium. Many recesses on the surface were also observed.

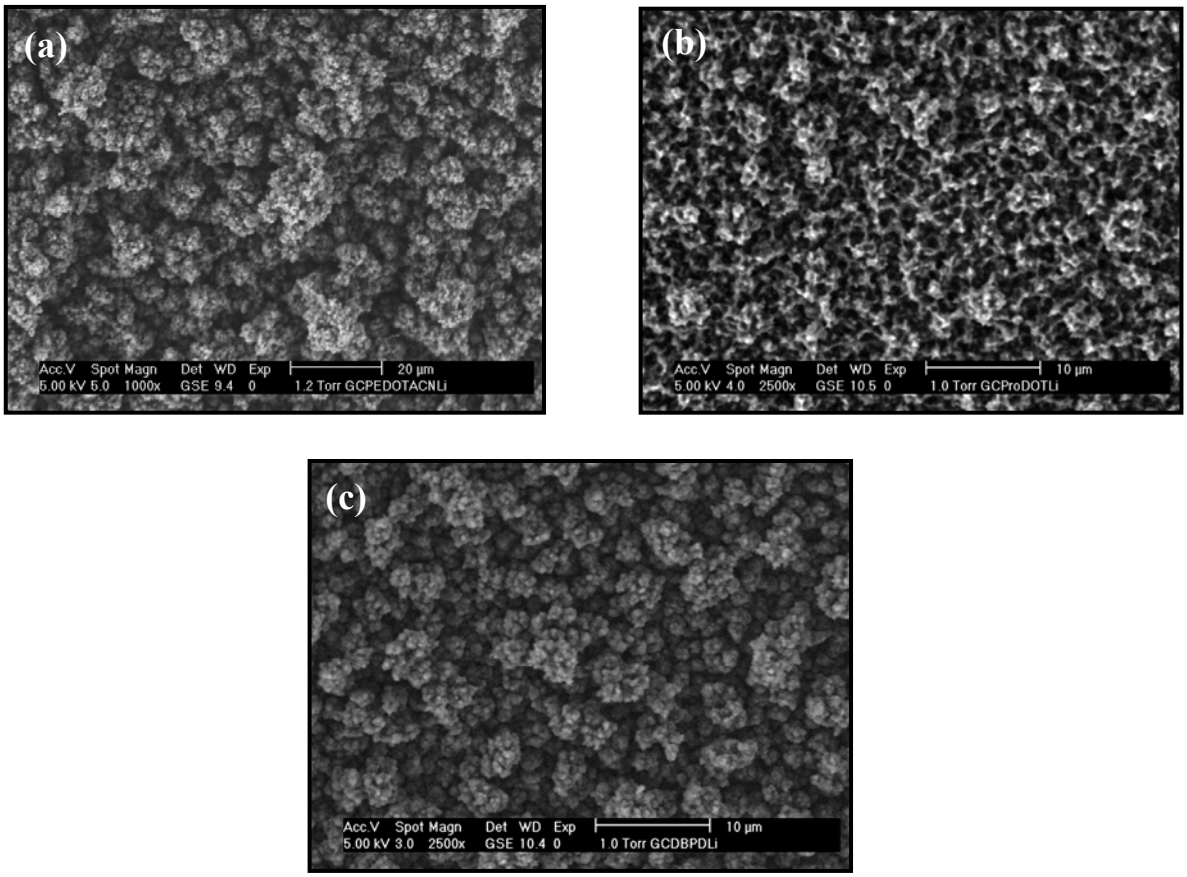

Figure 5.24: ESEM micrographs of (a) PEDOT (b) PProDOT and (c) PDBPD synthesised on glassy carbon in acetonitrile containing $LiClO_4$.

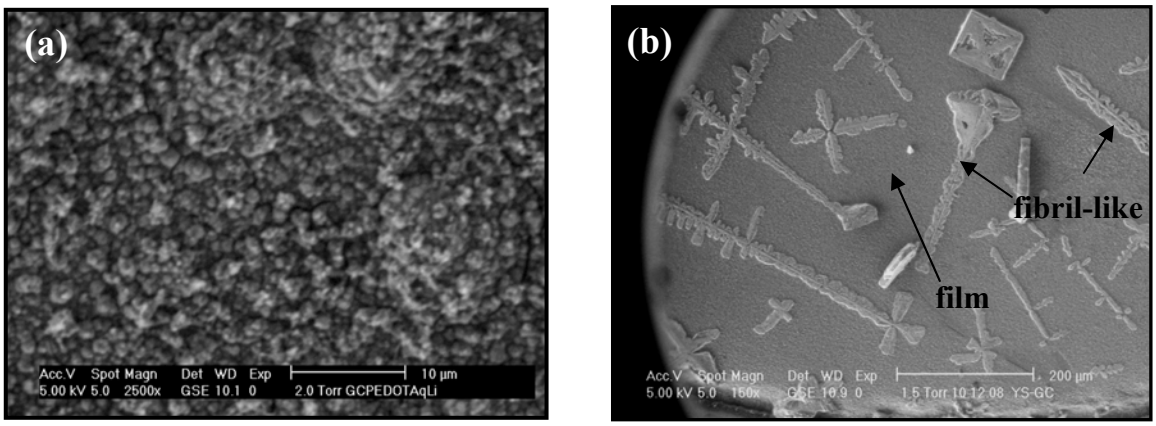

Figure 5.25: ESEM micrographs of PEDOT prepared on glassy carbon in aqueous solution containing 0.1 M: (a) $LiClO_4$ and (b) KCl.

5.3.6.2 Conducting Polymers Prepared on ITO Electrodes

Conducting polymers deposited on ITO electrodes showed similar morphologies to those synthesised on GC electrode. The flat shape of ITO electrode makes it possible to further analyse the morphologies using field emission SEM (FE-SEM).

Figure 5.26a illustrates that ITO/PEDOT/$LiClO_4$(ACN) had large agglomerated particles. On the other hand, ITO/PProDOT/$LiClO_4$(ACN) showed smooth film implying formation of good conducting polymer (**Figure 5.26b**). High magnification SEM image (inset **Figure 5.26b**) revealed a fine porous structure, which is similar to the PProDOT prepared on a GC electrode. As can be seen in **Figure 5.26c**, ITO/PDBPD/$LiClO_4$(ACN) grew both as a film and a fine particle precipitate (inset image). According to Bergman and Hanks (2000), besides condensing on the electrode surface, oligomeric radical cations can diffuse away from electrode surface and partially precipitate as a flocculating powder.

In the case of PEDOT prepared in aqueous solution, a poor quality film was observed when KCl (**Figure 5.27b**) was used as a supporting electrolyte, whereas granular particles were obtained in $LiClO_4$ solution (**Figure 5.27a**). This is due to the fact that perchlorate ion is five times more lipophilic than the chloride ion. This helps the

EDOT to be more soluble in aqueous $LiClO_4$ solution (Gemene *et al.*, 2007). Additionally, according to Asami *et al*. (2006), the Li^+ ions in $LiClO_4$ contributed to the formation of an electric bilayer inside the droplet of EDOT monomer in order to form PEDOT.

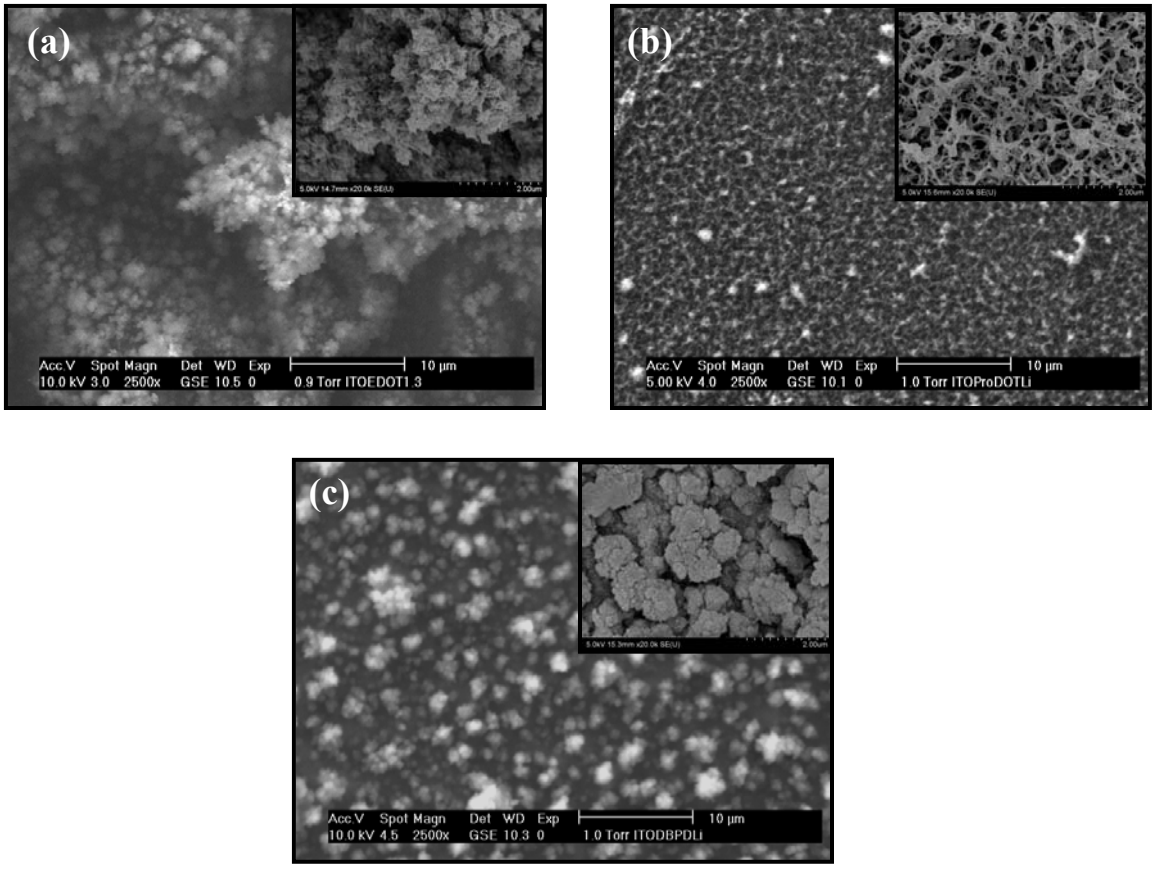

Figure 5.26: ESEM micrographs of (a) PEDOT (b) PProDOT and (c) PDBPD prepared on ITO electrodes in ACN containing 0.1 M $LiClO_4$. Inset: FE-SEM micrographs (magnification 20k ×).

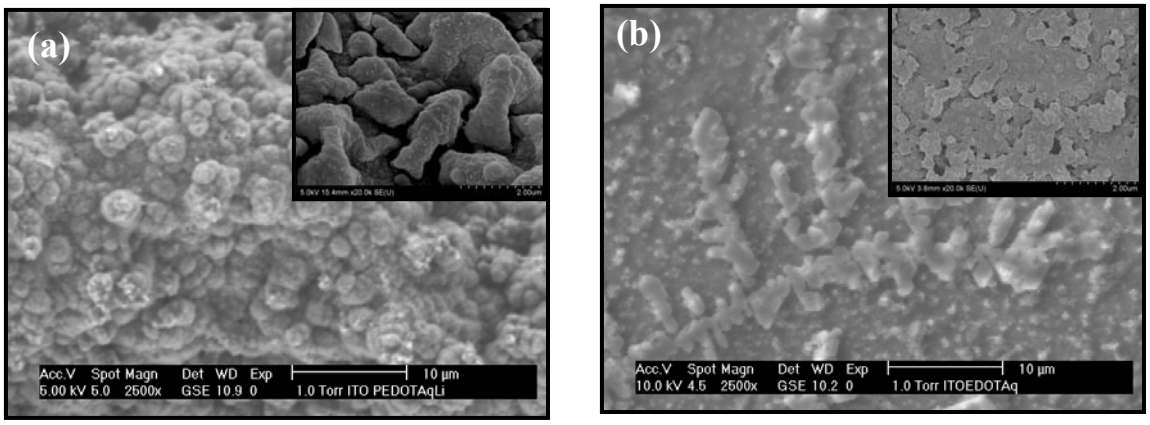

Figure 5.27: ESEM micrographs of PEDOT prepared on ITO electrodes in aqueous solution containing 0.1 M (a) $LiClO_4$ and (b) KCl.

5.3.7 Atomic Force Microscopy

Atomic force microscope (AFM) was used to study more details of the surface morphology of the polymer films coated on the electrode surface. The surface roughness and morphology of film electrodeposited on ITO electrodes was examined using tapping mode and the roughness factor was estimated. The AFM images of the bare ITO electrode (**Figure 5.28**), showed roughness factors (RMS value) of 5 ± 1 nm indicating a smooth surface. This value is consistent with the value obtained by Yano *et al.*(2009) (RMS = 0.7 - 11 nm). For ITO/PEDOT/$LiClO_4$(ACN), the surface becomes rough with an RMS value of 55 nm (**Figure 5.28**). This observation is in good agreement with the ESEM image displayed in **Figure 5.26a.**

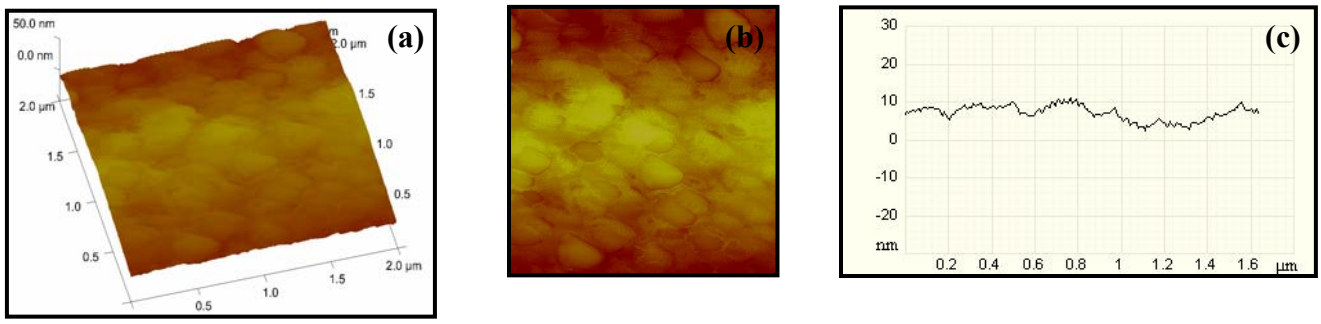

Figure 5.28: AFM image of bare ITO electrode: (a) 3D image (b) 2D image and (c) typical surface roughness profile (RMS: 5 ± 1 nm).

ITO/PProDOT/$LiClO_4$(ACN) and ITO/PDBPD/$LiClO_4$(ACN) (**Figure 5.29b** and **c**) indicated RMS roughness values of 201 nm and 631 nm, respectively. Thus, the order of roughness is PEDOT > PProDOT > PDBPD. These results are in accordance with ESEM images (**Section 5.3.6.2**) and are consistent with those presented in contact angle measurements (**Section 5.3.8**).

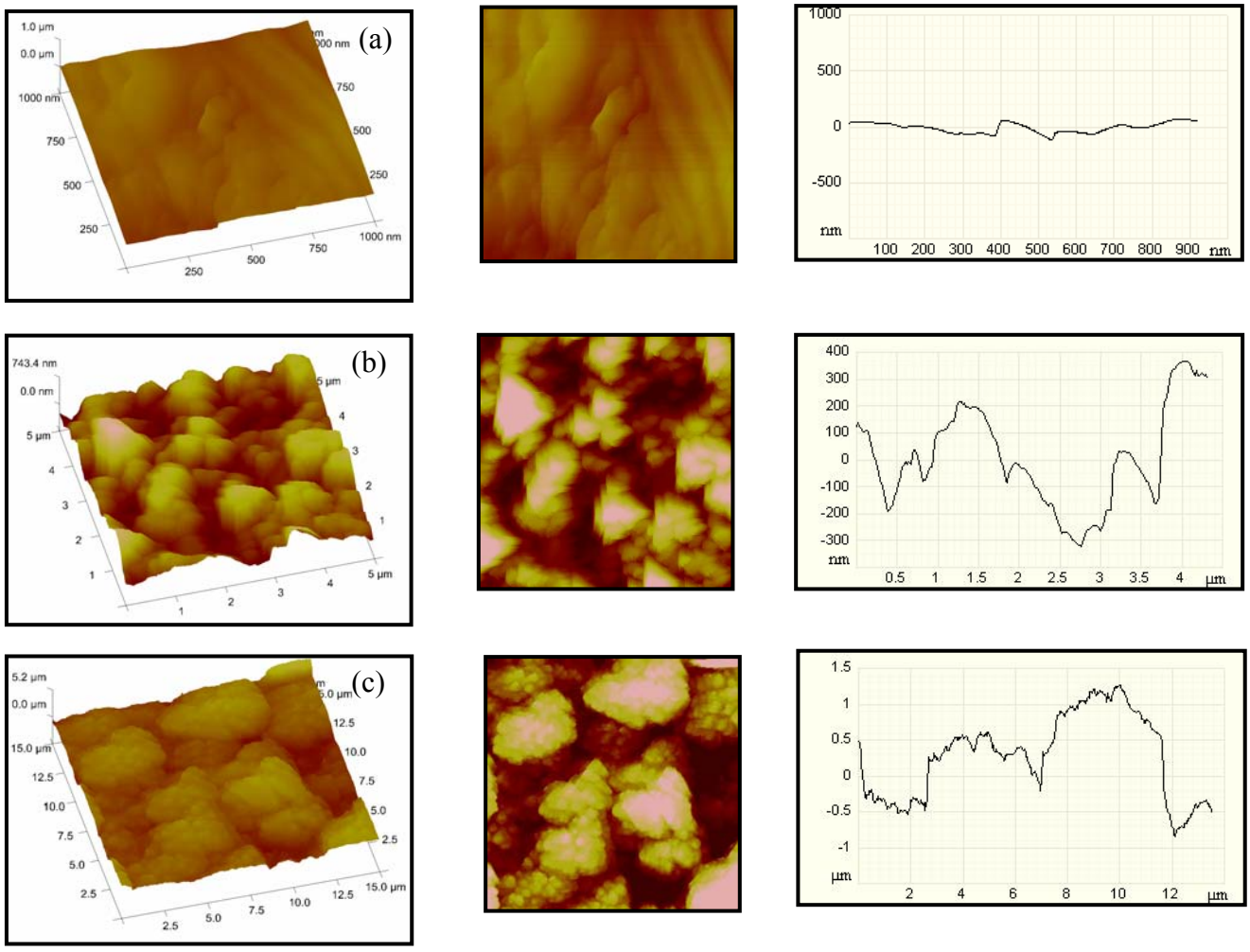

Figure 5.29: AFM images of (a) PEDOT (RMS: 50 ± 6 nm) (b) PProDOT (RMS: 196 ± 13 nm) (c) PDBPD (RMS: 626 ± 49 nm) prepared in 0.1 M monomer + 0.1 M $LiClO_4$ containing ACN. 3-dimensional (left) topographic topview (middle) and typical roughness profile (right).

The effect of different supporting electrolytes on the surface roughness of PEDOT was also examined. It was found that $LiClO_4$ gave smoother surface roughness than PEDOT prepared in KCl (**Figure 5.30**). The results above have shown that different monomers with slightly different structures gave strong influence on the morphology and surface roughness of the polymer films.

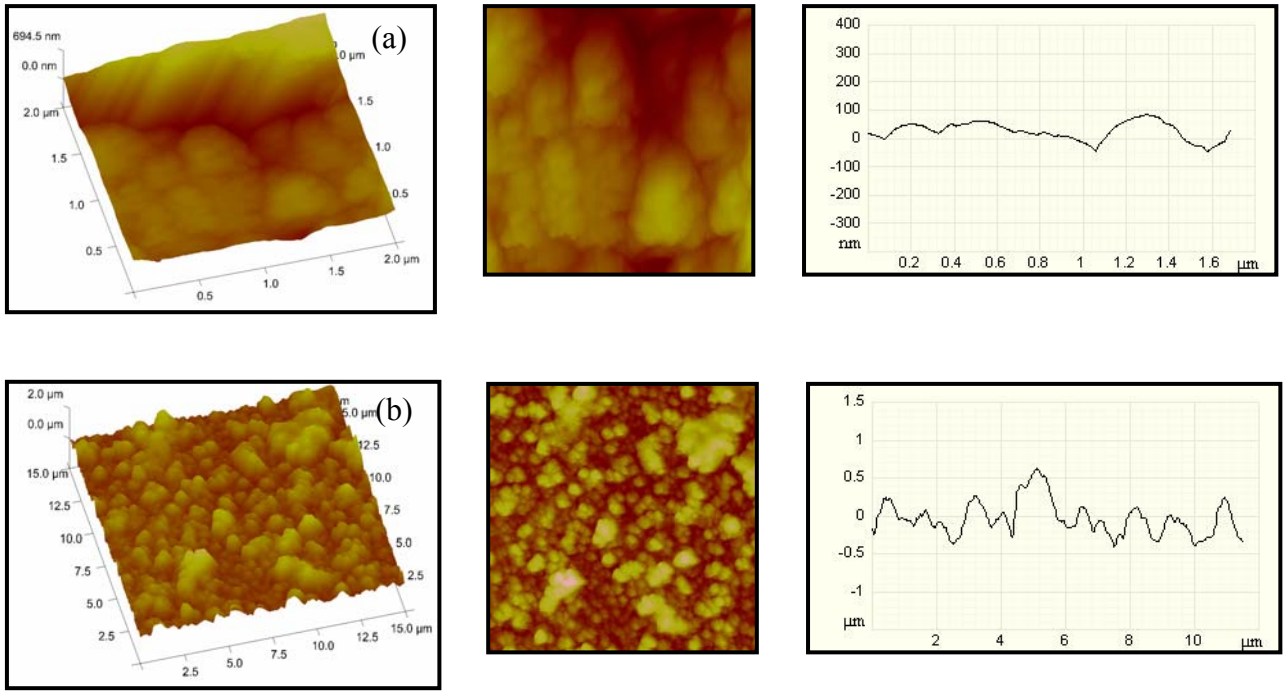

Figure 5.30: AFM images of PEDOT prepared in aqueous solution containing 0.1 M: (a) $LiClO_4$ (RMS: 103 ± 30 nm) (b) KCl (RMS: 235 ± 7 nm). 3-dimensional (left) topographic topview (middle), typical roughness profile (right).

Table 5.4: Surface roughness of PEDOT and derivative coated ITO electrodes.

Sample	Surface roughness (nm)*
Bare ITO electrode	5 ± 1
PEDOT/$LiClO_4$ (ACN)	50 ± 6
PProDOT/$LiClO_4$ (ACN)	196 ± 13
PDBPD/$LiClO_4$ (ACN)	626 ± 49
PEDOT/KCl (Aq)	235 ± 30
PEDOT/$LiClO_4$ (Aq)	103 ± 7

*Average of 3 measurements at each sample and at least two samples for each material.

5.3.8 Contact Angle Measurements of Polymer Films

5.3.8.1 Polymer Films Deposited on GC Electrodes

Contact angle measurements were utilised to study the hydrophilic/hydrophobic and wettability properties of different conducting polymers. At the interface between the liquid and solid phases, interactions involving electrostatic, van der Waals interactions, dipole-dipole interactions and hydrogen bonding greatly affect the wettability of the films. Teasdale and Wallace (1995) investigated the effect of contact angle measurements based on a range of polymer polarities. They found that poly(3-carbethoxy-4-methylpyrrole) and poly(3-carboxy-4-methylpyrrole) had lower contact angles compared to polypyrrole due to the increase of hydrogen bonding between the polymer and water.

In order to obtain the dynamic wetting properties of the polymer films, the advancing (θ_a) and receding (θ_r) contact angles were measured and the contact angle hysteresis ($\Delta\theta = \theta_a - \theta_r$) were calculated. Information on contact angle hysteresis by determining the advancing and receding contact angles enables to one to discern whether the surface is in a Wenzel's or Casssie-Baxter's state, allowing insight into the surface morphology and adhesion properties of a material (Callies and Quere, 2005). Contact angles are given as mean average ± standard deviation. Initially, the advancing and

receding contact angles of bare GC electrode were measured and found to be 78.68 ± 0.33° and 59.12 ± 0.19°, respectively (**Figure 5.31a** and **b**).

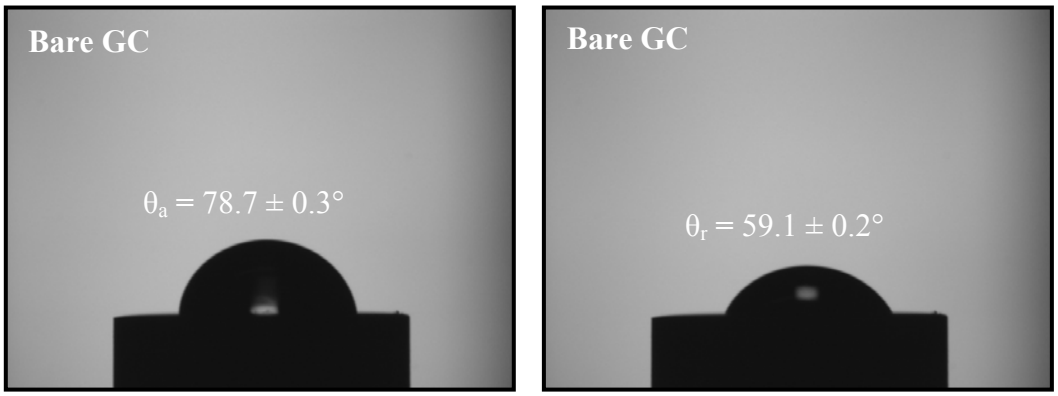

Figure 5.31: Images of advancing (θ_a) and receding (θ_r) contact angle of bare GC.

Figure 5.32 and **Figure 5.33** show the images of advancing and receding water contact angles of GC/PEDOT/$LiClO_4$(ACN), GC/PProDOT/$LiClO_4$(ACN) and GC/PDBPD/$LiClO_4$(ACN) and the data is summarised in **Figure 5.34**. The result showed that the contact angle increased in the order PEDOT < PProDOT < PDBPD. This suggests that the films formed by PDBPD were the least wettable surface. The change in the contact angle is governed by the surface chemistry and surface morphology of the polymer film (Cassie and Baxter, 1944, He *et al.*, 2003, Wenzel, 1936). This result also indicates that the presence of the additional functional group on the side chain of PEDOT increases the contact angle. This phenomenon is more pronounced when dibenzyl moiety is present in the structure of PDBPD. Additionally, the difference in morphology of the polymer films has also affected the contact angle (**Section 5.3.6.1**).

It can be seen that the most distinctive feature was shown by GC/PDBPD/$LiClO_4$(ACN) (**Figure 5.34**). This polymer film exhibited very small hysteresis (1.33° ± 0.9) indicating that the water droplet was in Cassie-Baxter's state (1944) *i.e.* the droplet rests on the asperities with air trapped in the hollows. It was found that the droplet was easily rolled off on the GC/PDBPD/$LiClO_4$(ACN) surface with extremely low adhesion. This can be described as a hydrophobic surface.

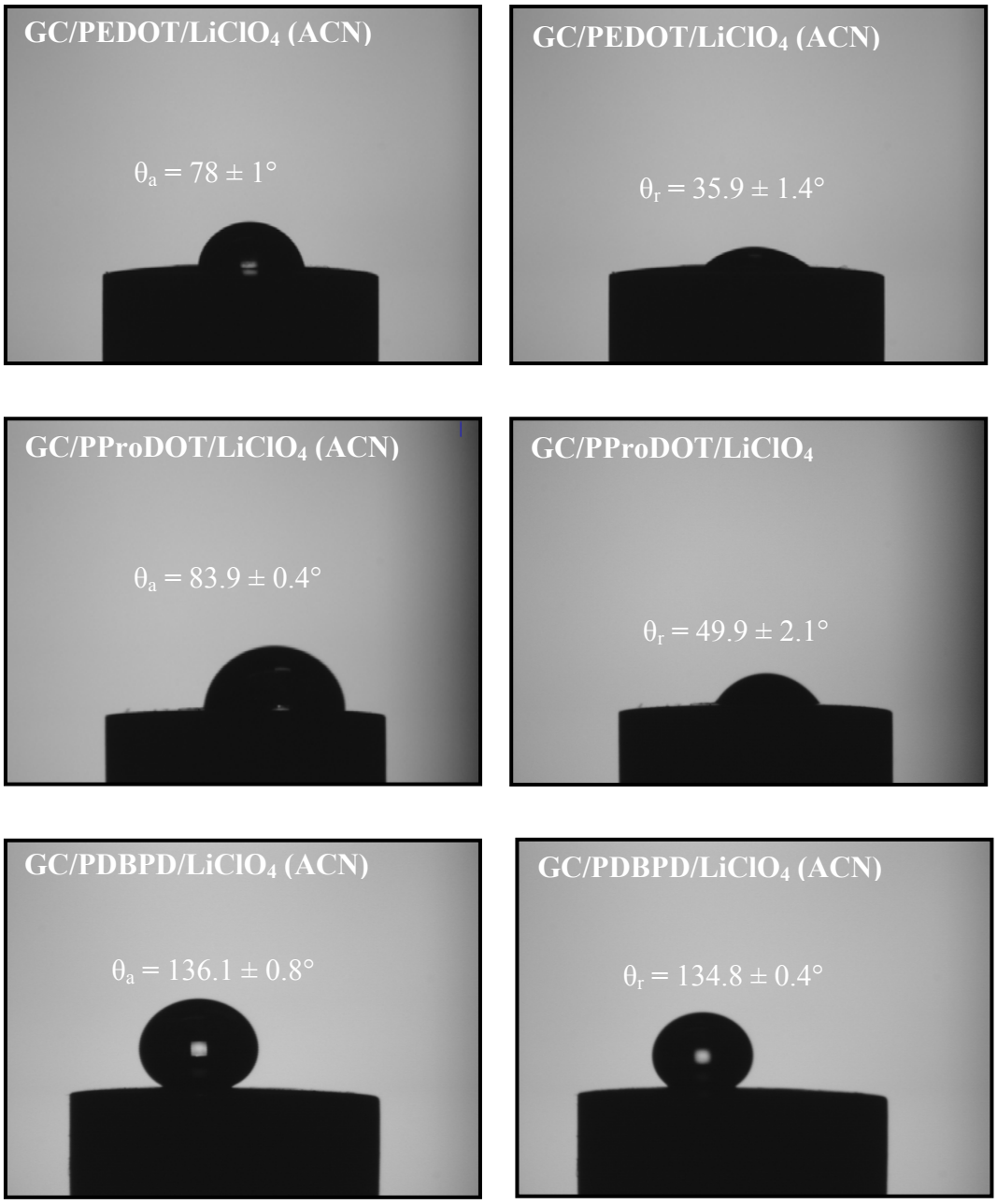

Figure 5.32: Images of advancing (θ_a) and receding (θ_r) contact angles of PEDOT, PProDOT and PDBPD deposited on GC prepared in ACN containing $LiClO_4$.

The contact angles of PEDOT prepared in aqueous solution are displayed in **Figure 5.33**. It was observed that the contact angle hysteresis of GC/PEDOT/$LiClO_4$(Aq)

was similar to that prepared in ACN (**Figure 5.34b** and **f**). In contrast, GC/PEDOT/KCl(Aq) showed smaller hysteresis. This result gives an indication that the doping ion has a greater effect on the contact angle than the medium of electropolymerisation. Work conducted by Liu *et al.* (Liu *et al.*, 1994) also found that the surface energies of polyaniline varied greatly depending on the choice of counter anion.

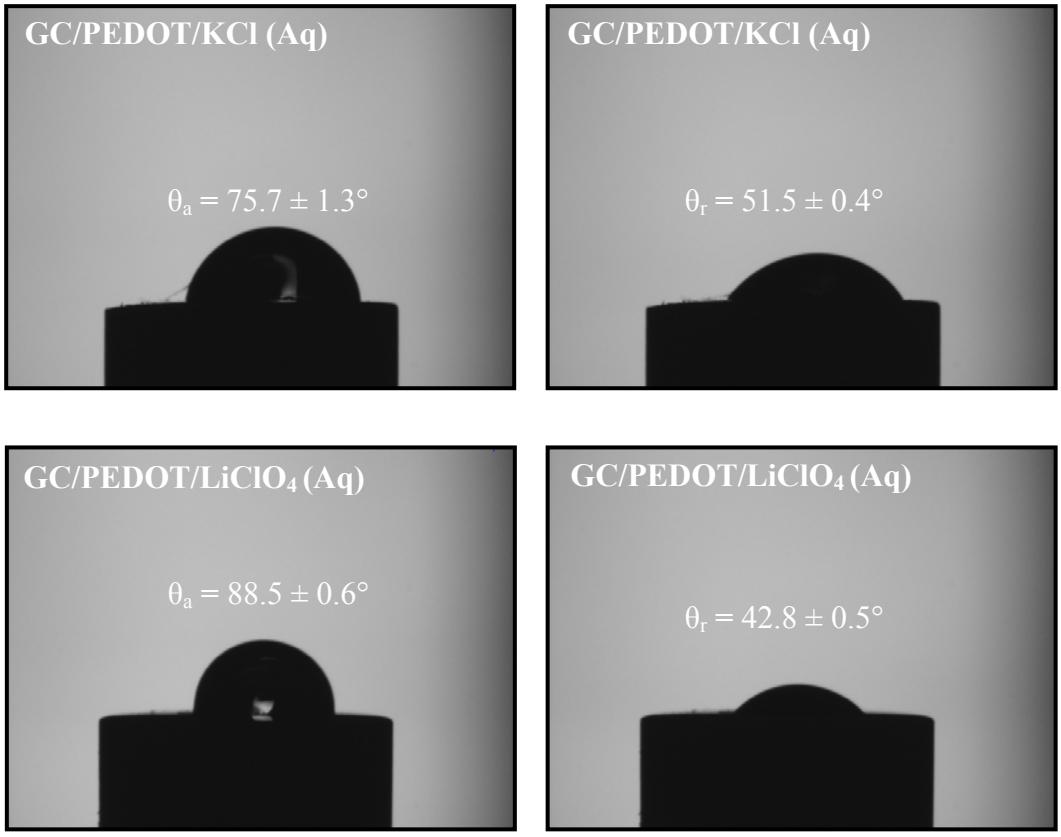

Figure 5.33: Images of advancing (θ_a) and receding (θ_r) contact angles of PEDOT deposited on GC prepared in aqueous solution containing KCl or $LiClO_4$.

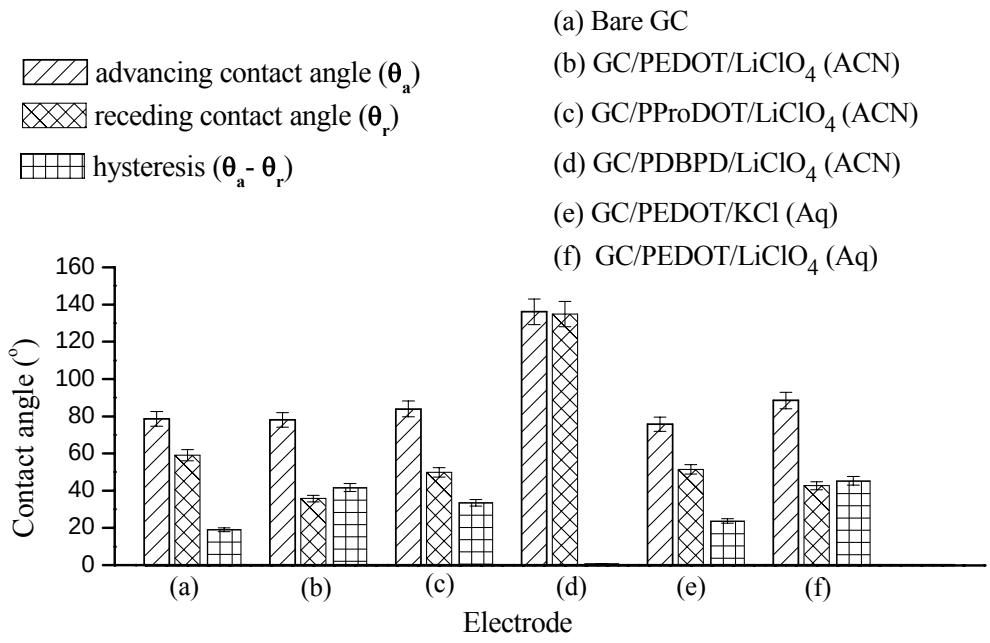

Figure 5.34: Advancing (θ_a) and receding (θ_r) contact angles of conducting polymers deposited on GC electrodes.

5.3.8.2 Polymer Films Deposited on ITO Electrodes

The contact angle measurements of polymer films deposited on ITO electrodes were also analysed. It was found that the contact angles of ITO/PEDOT/$LiClO_4$(ACN), and ITO/PProDOT/$LiClO_4$(ACN) (**Figure 5.36**) were lower than contact angles of bare ITO electrode (**Figure 5.35**) indicating that upon deposition of PEDOT and PProDOT on ITO electrodes, the surface became more wettable than bare ITO electrode (**Figure 5.36**). In contrast, PDPBD exhibited high contact angles and higher contact angle hysteresis (**Figure 5.38**) probably attributable to the physical heterogeneity of the rougher surface of the polymer films. These results are in good agreement with AFM measurements, with rougher surface showing higher contact angle. These results can be explained by Wenzel's model (Wenzel, 1936), which describes a droplet in contact with the asperities rather that resting upon it (Cassie-Baxter's model (Cassie and Baxter, 1944)). In this model, the contact angle hysteresis increases as the surface roughness increases due to the enlargement of contact interface area. Therefore, the increase in contact angle hysteresis

could be understood as a result of increase in surface roughness. These polymer films particularly PDBPD is quite new and has the potential for constructing hydrophobic conducting surfaces. The results on these polymer films obtained indicated that the substrate used for deposition of polymer films affected the contact angle significantly in comparison to GC electrodes.

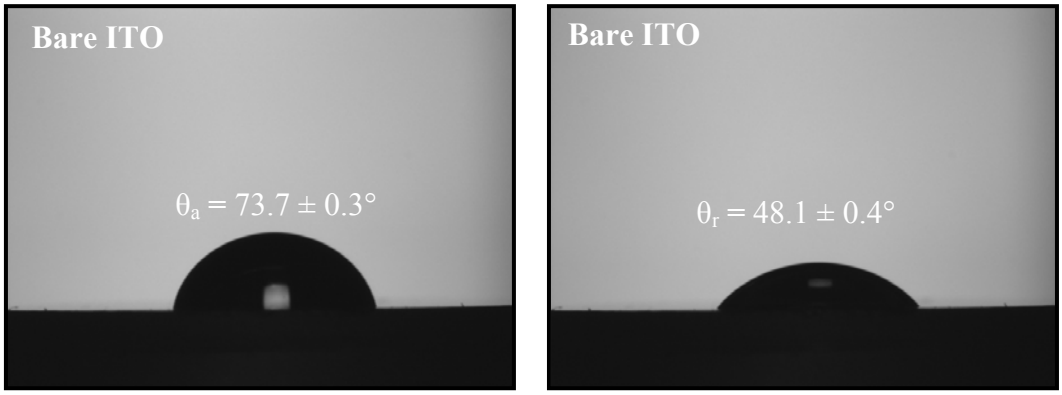

Figure 5.35: Images of advancing (θ_a) and receding (θ_r) contact angle of bare ITO glass**.**

PEDOT was also further investigated with that prepared in aqueous solution containing either $LiClO_4$ or KCl as a supporting electrolyte (**Figure 5.37**). It was shown that PEDOT prepared in aqueous medium containing KCl had almost similar wettability properties as synthesised in organic media ($LiClO_4$ in ACN). However, PEDOT prepared in aqueous $LiClO_4$ demonstrates a superhydrophilic surface as the water droplet spread instantaneously and permeated into the polymer film and gave 0° of contact angle.

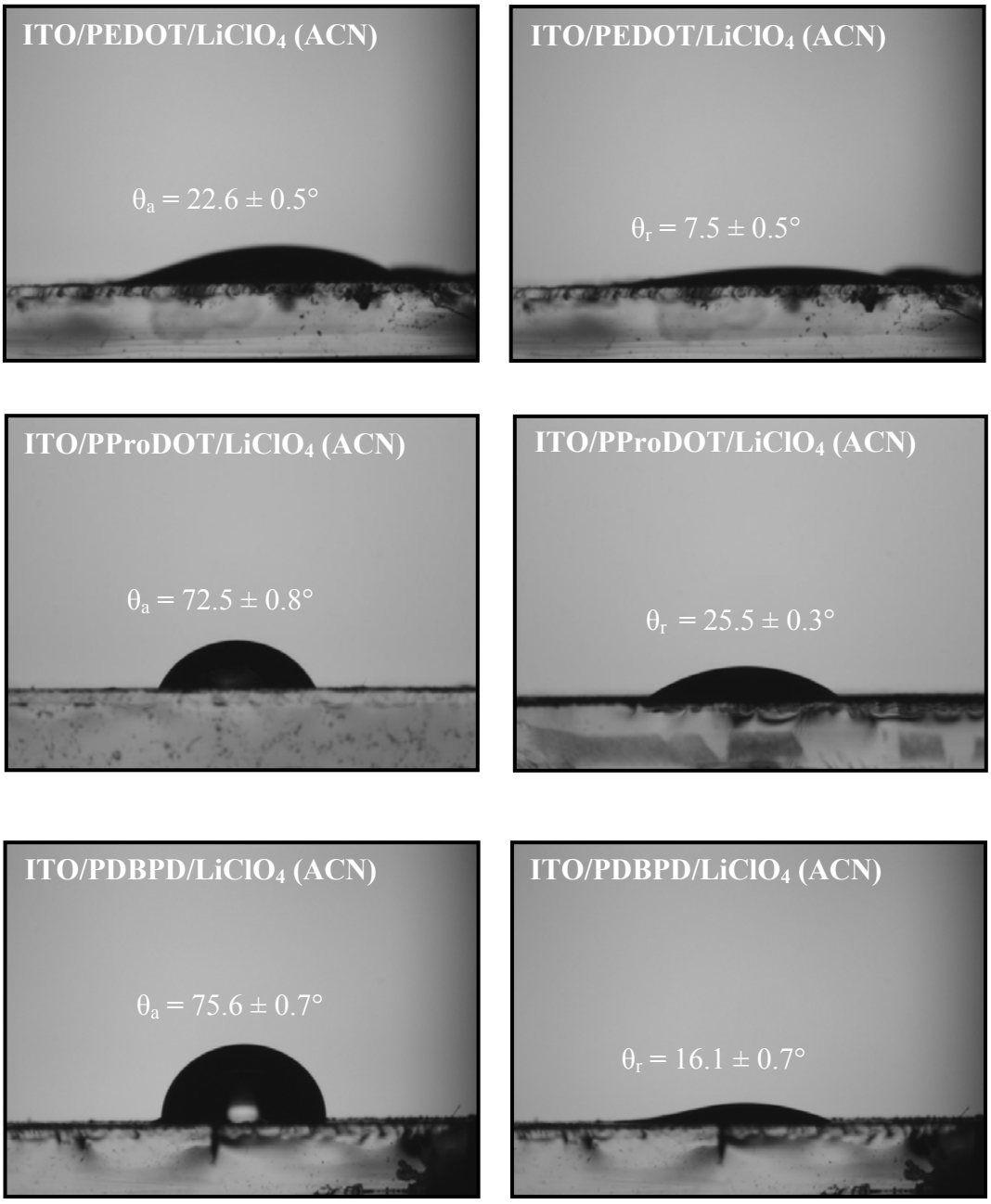

Figure 5.36: Images of advancing (θ_a) and receding (θ_r) contact angles of PEDOT, PProDOT and PDBPD deposited on ITO electrodes prepared in ACN containing $LiClO_4$.

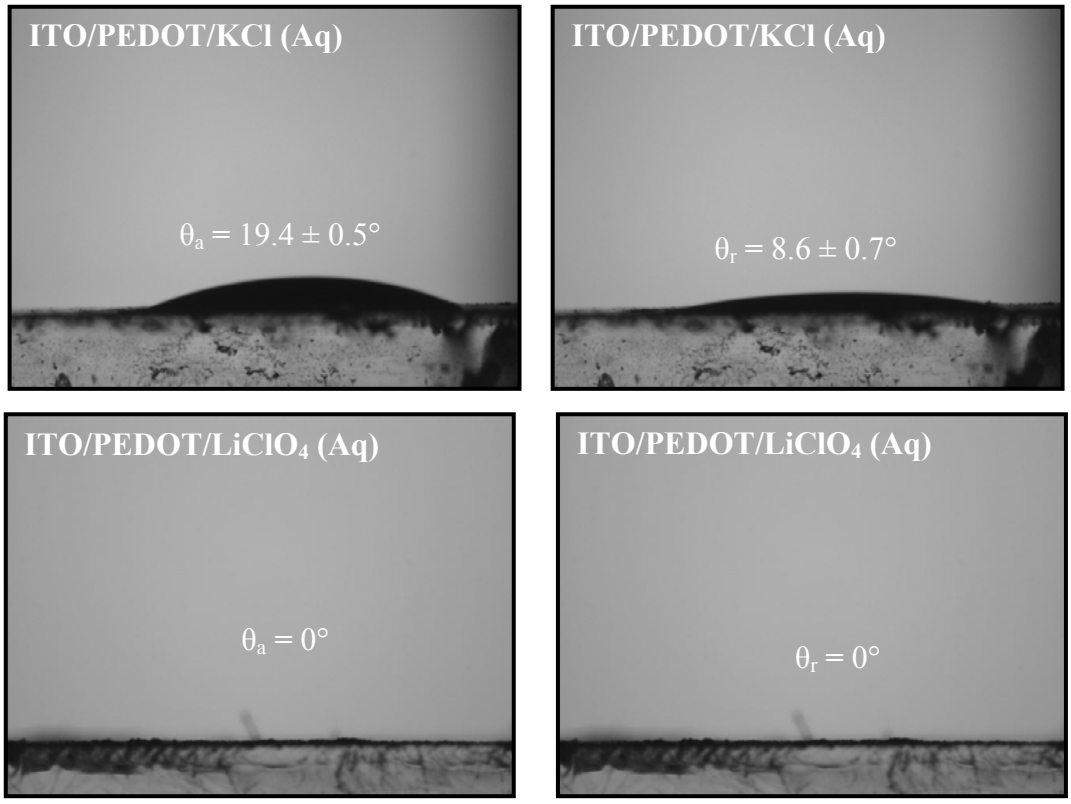

Figure 5.37: Images of advancing (θ_a) and receding (θ_r) contact angles of PEDOT deposited on ITO electrodes prepared in aqueous solution containing KCl or $LiClO_4$.

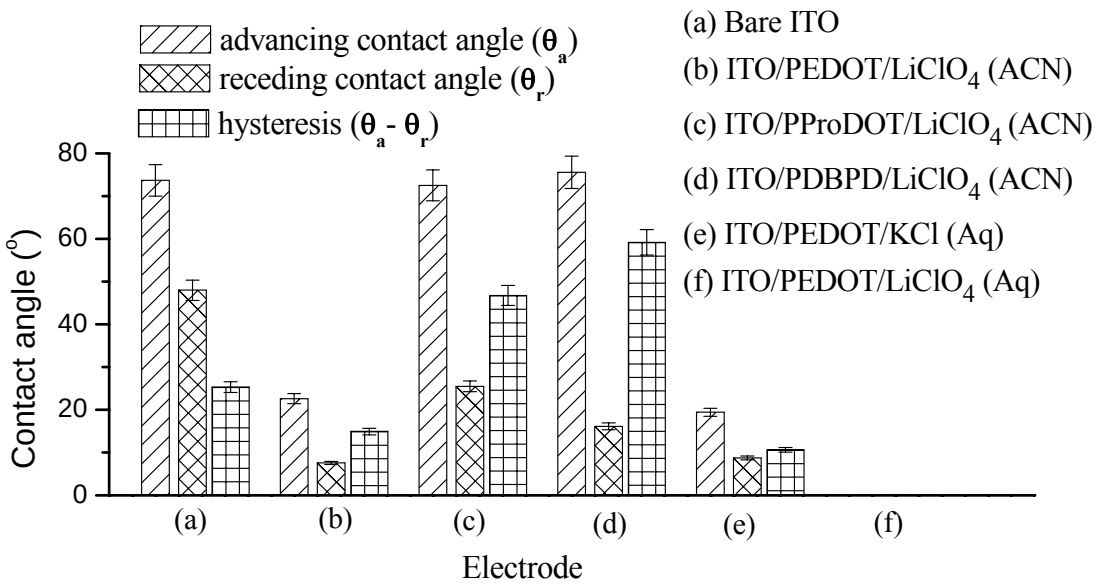

Figure 5.38: Advancing (θ_a) and receding (θ_r) contact angles of conducting polymers deposited on ITO electrodes.

5.3.9 Raman Spectroscopy

Raman spectroscopy measurements with an excitation wavelength of 633 nm were made on conducting polymer films deposited on ITO electrodes at different region of polymer surfaces. The results indicate that the nature of the polymer is similar over the whole surface of the ITO electrodes.

The peak assignments for PEDOT, PProDOT and PDBPD prepared in ACN and PEDOT prepared in aqueous solutions (**Table 5.5**) indicate that for the PProDOT and PDBPD prepared in ACN, the spectral traces are almost identical to PEDOT. However, it was noticeable that the symmetric $C_\alpha = C_\beta$ band was split into two for PProDOT and PDBPD unlike the PEDOT prepared in ACN. However, only one peak which is associated to oxyethylene ring deformation was observed for PDBPD.

As displayed in **Figure 5.39,** PProDOT spectrum shows a peak at 1509 cm^{-1} resulting from asymmetric $C_\alpha = C_\beta$ stretching and the most intense peak at 1407 cm^{-1} is due to the symmetric $C_\alpha = C_\beta$ stretching mode (Louarn *et al.*, 1991). A band at 1373 cm^{-1} is associated with the C_β-C_β stretching vibration, whereas two bands at 925 cm^{-1} and 520 cm^{-1} are due to the oxyethylene ring deformation (Garreau *et al.*, 1999). C-O-C deformation and C-S-C deformations are assigned at 1139 cm^{-1} and 785 cm^{-1}, respectively (Chiu *et al.*, 2006). The absence of C_α-H or C_β-H bending at around 1045 cm^{-1} like thiophene (Chen *et al.*, 2003) indicates a highly conjugated system in the structure of polymers.

For PEDOT prepared in aqueous solutions, the most intense peak was located around 1430 cm^{-1} and was broadened. In all cases, the Raman spectra for conducting polymers electrodeposited on GC electrode have also been carried out and showed no difference. This indicates that the GC electrode did not affect the chemical nature of the polymers.

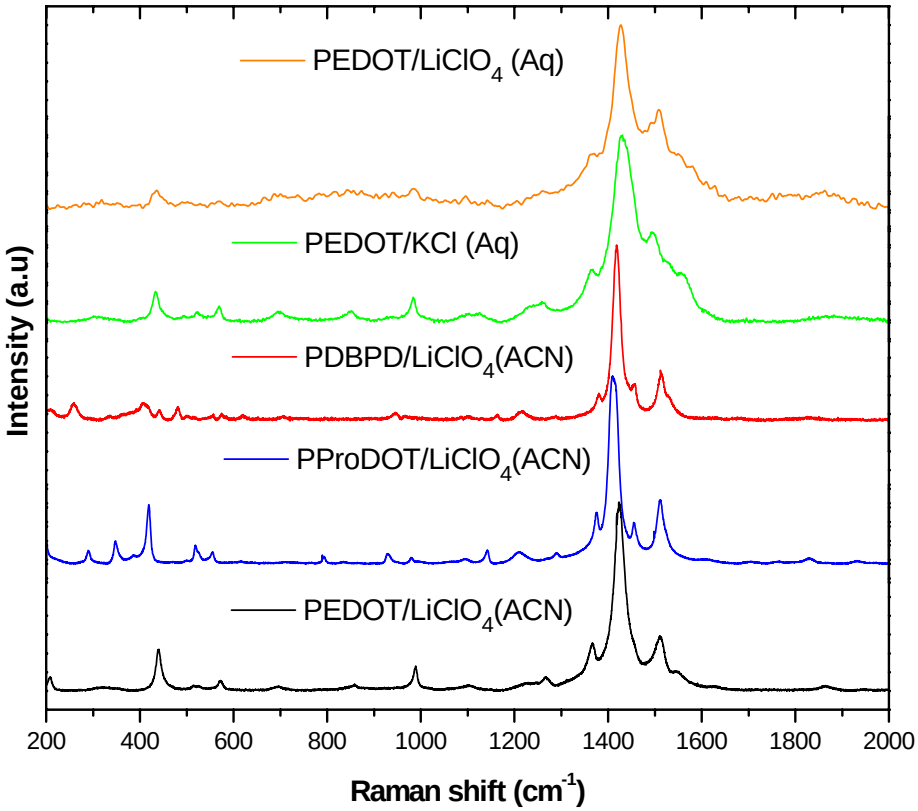

Figure 5.39: Raman spectra of: (a) PEDOT, (b) PProDOT, (c) PDBD prepared in 0.1 M $LiClO_4$/acetonitrile; (d) PEDOT prepared in 0.1 M KCl (Aq) and (e) PEDOT prepared in 0.1 M $LiClO_4$ (Aq).

Table 5.5: Peak vibrational wavenumbers (cm^{-1}) of PEDOT, PProDOT and PDBPD films.

Polymer prepared in ACN (cm^{-1})			Polymer prepared in aqueous (cm^{-1})		Assigment of the band (Garreau *et al.*, 1999, Louarn *et al.*, 1996)
PEDOT	PProDOT	PDBPD	PEDOT/KCl	PEDOT/$LiClO_4$	
1513	1509	1512	1502	1512	asymmetric $C_\alpha = C_\beta$ stretching
1425	1407, 1433	1417, 1439	1436	1430	symmetric $C_\alpha = C_\beta$ stretching
1369	1373	1377	1385	1388	C_β-C_β stretching
1270	1199	1204	1266	1265	C_α-$C_{\alpha'}$ inter ring bond
1121	1139	1167	1129	1143	distorted C-O-C deformation
990	925	942	987	987	oxyethylene/ oxypropylene ring deformation
708	785	719	708	720	symmetric C-S-C deformation
576	520	-	572	515	oxyethylene/ oxypropylene ring deformation

5.3.10 Conclusions

The results showed that electrochemical oxidation of EDOT and its derivatives on electrodes yielded conducting polymer film modified electrodes. There is not much difference of morphology between polymer films coated on GC and ITO electrodes. Electropolymerisation of EDOT in aqueous medium has resulted in poor films especially using KCl as an electrolyte. In contrast, electropolymerisation of EDOT in $LiClO_4$ aqueous solution showed better morphology due to the fact that $LiClO_4$ is more lipophilic than KCl, which aids the solubility of EDOT. It was found that PDBPD possessed the most compact morphology, rough and less wettable than those of other conducting polymers. This new hydrophobic PDBPD is particularly interesting and has the potential for constructing hydrophobic conducting surfaces. In order to have a better understanding of the properties of the conducting polymer, some other characterisation techniques such as cyclic voltammetry (CV) and electrochemical impedance spectroscopy (EIS) will be further explained in **Chapter 6**.

References

(1994) Provisional Product Information Sheet, Trial Product A14060, Bayer AG, Nov 1994.

Aleshin, A. N., Kiebooms, R. and Heeger, A. J. (1998) Metallic conductivity of highly doped poly(3,4-ethylenedioxythiophene). *Synthetic Metals.* 369-370.

Asami, R., Fuchigami, T. and Atobe, M. (2006) Development of a novel environmentally friendly electropolymerization of water-insoluble monomers in aqueous electrolytes using acoustic emulsification. *Langmuir.* 22**.** 10258-10263.

Bard, A. J. and Faulker, L. R. (2001) *Electrochemistry methods, fundamentals and applications.* (2nd ed.). New York, John Wiley & Sons.

Bendikov, T. A. and Harmon, T. C. (2005) Long-lived solid state perchlorate ion selective sensor based on doped poly(3,4-ethylenedioxythiophene) (PEDOT) films. *Analytica Chimica Acta.* 551**.** 30-36.

Bergman, B. and Hanks, T. W. (2000) Spectroscopic, microscopic, and surface analysis of alkanethiol- and fluoroalkanethiol-modified conducting polymer thin films. *Macromolecules.* 33**.** 8035-8042.

Bobacka, J., Lewenstam, A. and Ivaska, A. (2000) Electrochemical impedance spectroscopy of oxidized poly(3,4-ethylenedioxythiophene) film electrodes in aqueous solutions. *Journal of Electroanalytical Chemistry.* 489**.** 17-27.

Callies, M. and Quere, D. (2005) On water repellency. *Soft Matter.* 1**.** 55-61.

Cassie, A. B. D. and Baxter, S. (1944) Wettability of porous surfaces. *Transactions of the Faraday Society.* 40**.** 546-550.

Chang, C. C., Her, L. J. and Hong, J. L. (2005) Copolymer from electropolymerization of thiophene and 3,4-ethylenedioxythiophene and its use as cathode for lithium ion battery. *Electrochimica Acta.* 50**.** 4461-4468.

Chen, F., Shi, G. Q., Zhang, J. X. and Fu, M. X. (2003) Raman spectroscopic studies on the structural changes of electrosynthesized polythiophene films during the heating and cooling processes. *Thin Solid Films.* 424**.** 283-290.

Chiu, W. W., Travas-Sejdic, J., Cooney, R. P. and Bowmaker, G. A. (2006) Studies of dopant effects in poly(3,4-ethylenedioxythiophene) using Raman spectroscopy. *Journal of Raman Spectroscopy.* 37**.** 1354-1361.

Diaz, A. F., Crowley, J., Bargon, J., Gardini, G. P. and Torrance, J. B. (1981) Electrooxidation of aromatic oligomers and conducting polymers. *Journal of Electroanalytical Chemistry.* 121**.** 355-361.

Downard, A. J. and Pletcher, D. (1986) A study of the conditions for the electrodeposition of polythiophen in acetonitrile. *Journal of Electroanalytical Chemistry.* 206**.** 147-152.

El Moustafid, T., Gregory, R. V., Brenneman, K. R. and Lessner, P. M. (2003) Electrochemical deposition and characterization of poly(3,4-ethylenedioxythiophene) from aqueous solutions. *Synthetic Metals.* 135-136**.** 435-436.

Garreau, S., Louarn, G., Buisson, J. P., Froyer, G. and Lefrant, S. (1999) In situ spectroelectrochemical Raman studies of poly(3,4-ethylenedioxythiophene) (PEDT). *Macromolecules.* 32**.** 6807-6812.

Gemene, K. L., Shvarev, A. and Bakker, E. (2007) Selectivity enhancement of anion-responsive electrodes by pulsed chronopotentiometry. *Analytica Chimica Acta.* 583**.** 190-196.

Genies, E. M., Bidan, G. and Diaz, A. F. (1983) Spectroelectrochemical study of polypyrrole films. *Journal of Electroanalytical Chemistry.* 149**.** 101-113.

Gratzl, M., Hsu, D. F., Riley, A. M. and Janata, J. (1990) Electrochemically deposited polythiophene. 1. Ohmic drop compensation and the polythiophene paradox. *Journal of Physical Chemistry.* 94**.** 5973-5981.

Groenendaal, B. L., Jonas, F., Freitag, D., Pielartzik, H. and Reynolds, J. R. (2000) Poly(3,4-ethylenedioxythiophene) and its derivatives: Past, present, and future. *Advanced Materials.* 12**.** 481-494.

Haegel, F.-H., Schlüpen, J., Schultze, J. W., Winkels, S. and Stromberg, C. (2001) Anodic polymerization of thiophene derivatives from microemulsions and liquid crystals. *Electrochimica Acta.* 46**.** 3973-3984.

Han, D. H., Kim, J. W. and Park, S. M. (2006) Electrochemistry of conductive polymers 38. Electrodeposited poly(3,4-ethylenedioxy-thiophene) studied by current sensing atomic force microscopy. *Journal of Physical Chemistry B.* 110**.** 14874-14880.

He, B., Patankar, N. A. and Lee, J. (2003) Multiple equilibrium droplet shapes and design criterion for rough hydrophobic surfaces. *Langmuir.* 19**.** 4999-5003.

Kiebooms, R., Aleshin, A., Hutchison, K. and Wudl, F. (1997) Thermal and electromagnetic behavior of doped poly(3,4-ethylenedioxythiophene) films. *Journal of Physical Chemistry B.* 101**.** 11037-11039.

Krische, B. and Zagorska, M. (1989) The polythiophene paradox. *Synthetic Metals.* 28**.** C263-C268.

Krishnamoorthy, K., Ambade, A. V., Kanungo, M., Contractor, A. Q. and Kumar, A. (2001) Rational design of an electrochromic polymer with high contrast in the visible region: dibenzyl substituted poly(3,4-propylenedioxythiophene). *Journal of Materials Chemistry.* 11**.** 2909-2911.

Kumar, A., Welsh, D. M., Morvant, M. C., Piroux, F., Abboud, K. A. and Reynolds, J. R. (1998) Conducting poly(3,4-alkylenedioxythiophene) derivatives as fast electrochromics with high-contrast ratios. *Chemistry of Materials.* 10**.** 896-902.

Liu, M. J., Tzou, K. and Gregory, R. V. (1994) Influence of the doping conditions on the surface energies of conducting polymers. *Synthetic Metals.* 63**.** 67-71.

Louarn, G., Mevellec, J. Y., Buisson, J. P. and Lefrant, S. (1991) Experimental and theoretical study of vibrational properties of polythiophene, polymethylthiophene and polyoctylthiophene. *Journal de Chimie Physique.* 987-995.

Louarn, G., Trznadel, M., Buisson, J. P., Laska, J., Pron, A., Lapkowski, M. and Lefrant, S. (1996) Raman spectroscopic studies of regioregular poly(3-alkylthiophenes). *Journal of Physical Chemistry.* 100**.** 12532-12539.

Michalska, A., Galuszkiewicz, A., Ogonowska, M., Ocypa, M. and Maksymiuk, K. (2003) PEDOT films: multifunctional membranes for electrochemical ion sensing. *Journal of Solid State Electrochemistry* 381-389.

Mousavi, Z., Alaviuhkola, T., Bobacka, J., Latonen, R. M., Pursiainen, J. and Ivaska, A. (2008) Electrochemical characterization of poly (3,4-ethylenedioxythiophene) (PEDOT) doped with sulfonated thiophenes. *Electrochimica Acta.* 53**.** 3755-3762.

Nien, P. C., Tung, T. S. and Ho, K. C. (2006) Amperometric glucose biosensor based on entrapment of glucose oxidase in a poly(3,4-ethylenedioxythiophene) film. *Electroanalysis.* 18**.** 1408-1415.

Park, J., Kim, J. and Son, Y. (2006) Conducting polymer micro-tubules hosting electroactive species without guest modification. *Synthetic Metals.* 156**.** 714-720.

Roncali, J. (1992) Conjugated poly(thiophenes): Synthesis, functionalization, and applications. *Chemical Reviews.* 92**.** 711-738.

Roncali, J., Blanchard, P. and Frere, P. (2005) 3,4-Ethylenedioxythiophene (EDOT) as a versatile building block for advanced functional p-conjugated systems. *Journal of Materials Chemistry.* 15**.** 1589-1610.

Sadki, S., Schottland, P., Brodie, N. and Sabouraud, G. (2000) The mechanisms of pyrrole electropolymerization. *Chemical Society Reviews.* 29**.** 283-293.

Seshadri, V., Wu, L. and Sotzing, G. A. (2003) Conjugated polymers via electrochemical polymerization of thieno[3,4-b]thiophene (T34bT) and 3,4-ethylenedioxythiophene (EDOT). *Langmuir.* 19**.** 9479-9485.

Teasdale, P. R. and Wallace, G. G. (1995) In situ characterization of conducting polymers by measuring dynamic contact angles with Wilhelmy's plate technique. *Reactive Polymers.* 24**.** 157-164.

Varis, S., Ak, M., Akhmedov, I. M., Tanyeli, C. and Toppare, L. (2007) A novel multielectrochromic copolymer based on 1-(4-nitrophenyl)-2,5-di(2-thienyl)-1H-pyrrole and EDOT. *Journal of Electroanalytical Chemistry.* 603**.** 8-14.

Wang, X. J. and Wong, K. Y. (2006) Effects of a base coating used for electropolyrnerization of poly(3,4-ethylenedioxythiophene) on indium tin oxide electrode. *Thin Solid Films.* 515**.** 1573-1578.

Wenzel, R. N. (1936) Resistance of solid surfaces to wetting by water. *Industrial and Engineering Chemistry.* 28**.** 988-994.

Yang, J. Y., Lipkin, K. and Martin, D. C. (2007) Electrochemical fabrication of conducting polymer poly(3,4-ethylenedioxythiophene) (PEDOT) nanofibrils on microfabricated neural prosthetic devices. *Journal of Biomaterials Science-Polymer Edition.* 18**.** 1075-1089.

Yano, H., Kouro, D., Sasaki, N. and Muramatsu, S.-I. (2009) Improvement of polymer/fullerene solar cells by controlling geometry of the ITO substrate surface. *Solar Energy Materials and Solar Cells.* 93**.** 976-979.

Zhang, S. S., Hou, J., Zhang, R., Xu, J. K., Nie, G. M. and Pu, S. Z. (2006) Electrochemical polymerization of 3,4-ethylenedioxythiophene in aqueous solution containing *N*-dodecyl-β-D-maltoside. *European Polymer Journal.* 42**.** 149-160.

CHAPTER 6

ELECTROCHEMICAL PROPERTIES OF PEDOT, PPRODOT AND PDBPD COATED ELECTRODES

6.1 Introduction

Studies on understanding the properties of faradaic and interfacial charge transfer mechanism in conducting polymers has increased due to the potential applications as supercapacitors, electrochemical sensors, light emitting diodes and antistatic coatings (Groenendaal *et al.*, 2000, Kirchmeyer and Reuter, 2005). Different charge transfer phenomena can be observed for different interfaces which involve electron transfer at the metal|polymer interface and ion transfer at the polymer|solution interface. In the presence of electroactive species in a solution, electron transfer can occur at the polymer|solution interface (Bull *et al.*, 1982). In the bulk of polymer film, electron and ion transport take place. Therefore, for various applications, the kinetics and mechanism of these phenomena need to be fully understood. The physical characteristics and properties of conducting polymers that have been described in **Chapter 5** would affect these phenomena.

Cyclic voltammetry (CV) is used to get general ideas of charge transfer, redox behaviour and kinetics. In addition, electrochemical impedance spectroscopy (EIS) technique is used as a powerful method to study the charge transfer and capacitance of conducting polymer coated electrodes. Various equivalent circuits of PEDOT have been described in literature (Deepa *et al.*, 2009, Richardson-Burns *et al.*, 2007, Sundfors *et al.*, 2002). Differences in physical properties (roughness/smoothness and uniformity) of polymer films obtained, which is due to the various experimental conditions applied, such as medium, types of electrodes, composition of electrolyte and electrochemical techniques used, strongly affect the impedance measurements. Therefore,

it is not surprising that the impedance data obtained for PEDOT is not easily fitted to the impedance data reported in literature. Bobacka *et al*. (2000) have studied the electrochemical properties of PEDOT by EIS in a solution containing no electroactive species. The PEDOT was prepared in aqueous solutions with different supporting electrolytes (KCl, NaCl and NaPSS) and it was found that the PEDOT film contains an excess of supporting electrolyte, which facilitates ion diffusion in the film. Further investigations (Sundfors *et al.*, 2002) using a solution containing a redox couple ($Fe(CN)_6^{3-/4-}$) revealed that electron transfer takes place in parallel with ion transfer at the polymer|solution interface. The circuit resembled the Randles circuit where the traditional double layer capacitance is replaced by the bulk redox capacitance and the associated transport impedance of the PEDOT. Deepa and co-workers (2009) showed that PEDOT functionalised 1-fluoro-2-nitro-4-azidobenzene behaved as a cation and anion exchanger whereas the non-functionalised PEDOT film acted only as an anion exchanger. This functionalised PEDOT showed lower charge transfer resistance for oxidation and reduction due to the surface roughness and the unusual particle morphology of the film.

Disagreement in the current literature on the impedance response of PEDOT derivatives prompted us to investigate this important phenomenon. In this work, CV and EIS were used to study the ion transport, charge transfer and capacitance of PEDOT and its derivatives.

6.2 Experimental

6.2.1 Chemicals and Reagents

Potassium chloride (KCl) and lithium perchlorate ($LiClO_4$) were obtained from Sigma. Potassium ferricyanide, $K_3Fe(CN)_6$ and potassium ferrocyanide $K_4Fe(CN)_6$ were purchased from Aldrich, UK. Acetonitrile (ACN) was obtained from Fisher, UK. All chemicals were used as received without any further purification.

6.2.2 Preparation of Conducting Polymer Modified Electrodes

The preparation of conducting polymer films was similar to that described in **Chapter 5**. Both aqueous (0.1 M $LiClO_4$, 0.1 M KCl) and non-aqueous (0.1 M $LiClO_4$) in ACN electrolytes were used. Briefly, the conducting polymers were prepared in a solution containing 10 mM monomer dissolved in ACN (or aqueous) solution. 0.1 M $LiClO_4$ or 0.1 M KCl was used as a supporting electrolyte. A glassy carbon (GC) (Bioanalytical System Inc.) or ITO electrode (Pilkington, UK) was used as a working electrode.

For polymerisation in aqueous media, platinum foil and Ag/AgCl (3.5 M KCl) were used as a counter and reference electrode, respectively. Ag/AgCl was replaced with a Ag wire for electropolymerisation in non-aqueous media. The polymer films were prepared using cyclic voltammetry for 20 scans.

6.2.3 Cyclic Voltammetry Measurements

A multichannel potentiostat model VMP (Perkin-Elmer Instruments) was used for cyclic voltammetric measurements. All measurements were performed with one compartment three-electrode cell *i.e.* polymer film coated GC electrode (or ITO electrode) as a working electrode, a platinum plate as a counter electrode and an Ag/AgCl (3.5 M KCl) as a reference electrode. All potentials were measured with respect to this reference electrode. For CV measurements in monomer free solution, 0.1 M $LiClO_4$ in ACN, 0.1 M KCl or 0.1 M $LiClO_4$ in aqueous solution was used. For measurements in non-aqueous solution, a Ag wire was used instead of Ag/AgCl (3.5 M KCl). CV measurements were also performed in a solution containing 10 mM $K_3Fe(CN)_6$ as a redox probe dissolved in 1 M KCl. All measurements were carried out at room temperature and the cell was housed in a Faraday cage to prevent stray fields causing interfering currents.

6.2.4 Electrochemical Impedance Spectroscopy Measurements

Electrochemical impedance spectroscopy (EIS) measurements were performed with a Solartron 1260 Impedance/Gain-Phase Analyzer. A solution consists of equimolar 5 mM $Fe(CN)_6^{3-/4-}$ with 1 M KCl supporting electrolyte in one compartment of three-electrode electrochemical cell. The solution was purged with high purity Ar for 10 minutes prior to electrochemical experiments. A platinum foil and an Ag/AgCl (3.5 M KCl) were used as a counter and reference electrode, respectively. The GC (or ITO) electrode coated with conducting polymer was used as the working electrode. The amplitude of the applied sine wave potential was 10 mV with a frequency range of 100 kHz to 1 Hz (51 data points) was applied. The direct current (dc) potential was varied from -0.2 to +0.6 V, centred on the formal potential of the redox pair of the $Fe(CN)_6^{3-/4-}$ obtained from the bare GC and ITO electrodes. The data obtained from EIS measurements were analysed with commercially available software Zplot/Zview (Version 3.1c, Scribner Associates, Inc.). All experiments were performed at room temperature in a Faraday cage to eliminate external interference.

6.3 Results and Discussion

6.3.1 Ion Transport

Freshly prepared polymer film coated GC and ITO electrodes were used to investigate the electrochemical properties in a monomer free supporting electrolyte solution. The polymer films were rinsed with electrolyte solution before the measurements to remove the unreacted monomer after the potentiodynamic polymerisation for 20 scans.

Figure 6.1 and **Figure 6.2** show the cyclic voltammograms (CVs) of PEDOT, PProDOT and PDBPD coated GC and ITO electrodes in acetonitrile containing 0.1 M $LiClO_4$ (monomer free solution), respectively. These polymer films were prepared in a

non-aqueous solution (ACN), which was carried out at a sweep rate of 50 mVs^{-1} between voltage limits of -1 V to 1.3 V over 20 scans. In most cases, the CV was cycled between +1 V and -1 V. GC/PEDOT/$LiClO_4$(ACN) showed one broad oxidation peak centred at +0.3 V and a reduction peak at around -0.5 V (**Figure 6.1a**). In contrast, GC/PProDOT(ACN) showed a broad reduction peak and a well defined oxidation peak at +0.39 V (**Figure 6.1b**). The anodic peak corresponds to the oxidation of polymer film and the insertion of anion (ClO_4^-) as a charge compensator (Melato *et al.*, 2008). This process is known as a doping and the transport of ClO_4^- occurs at polymer film|solution interface.

In the case of GC/PDBPD(ACN) (**Figure 6.1c**), the CV showed much lower currents, in the microampere region compared to GC/PEDOT(ACN) and GC/PProDOT(ACN. The magnified CV (inset **Figure 6.1**) revealed the oxidation peak (+0.23 V) was more intense than the reduction peak (-1 V). The same phenomenon was observed for PProDOT. It seems that the exclusion of counter anion from the polymer film is more difficult than the insertion which might be due to the quinoid configuration (**Figure 6.3b**) rather than benzoid configuration (**Figure 6.3a**) that some of the PProDOT and PDBPD chains exhibit in the reduced state (Zykwinska *et al.*, 2003). These results are in good agreement with the Raman spectra obtained (**Chapter 5**), in which there was a red-shift for $C_\alpha = C_\beta$ symmetric stretching vibration for PProDOT (1407 cm^{-1}) and PDBPD (1417 cm^{-1}) in comparison to PEDOT (1425 cm^{-1}) (Dai *et al.*, 2009). The red-shift is due to the change of the $C_\alpha = C_\beta$ in benzoid structure to $C_\alpha - C_\beta$ in quinoid structure (**Figure 6.3**). It is clearly seen that the capacitance current for PDBPD is much lower compared to PEDOT and PProDOT (**Figure 6.1**). This characteristic will be further studied by electrochemical impedance spectroscopy (**Section 6.3.4.4**).

CVs of polymer films modified ITO electrodes (**Figure 6.2**) in monomer free solution also revealed observable oxidation and reduction peaks. These peaks are associated to the doping and dedoping processes.

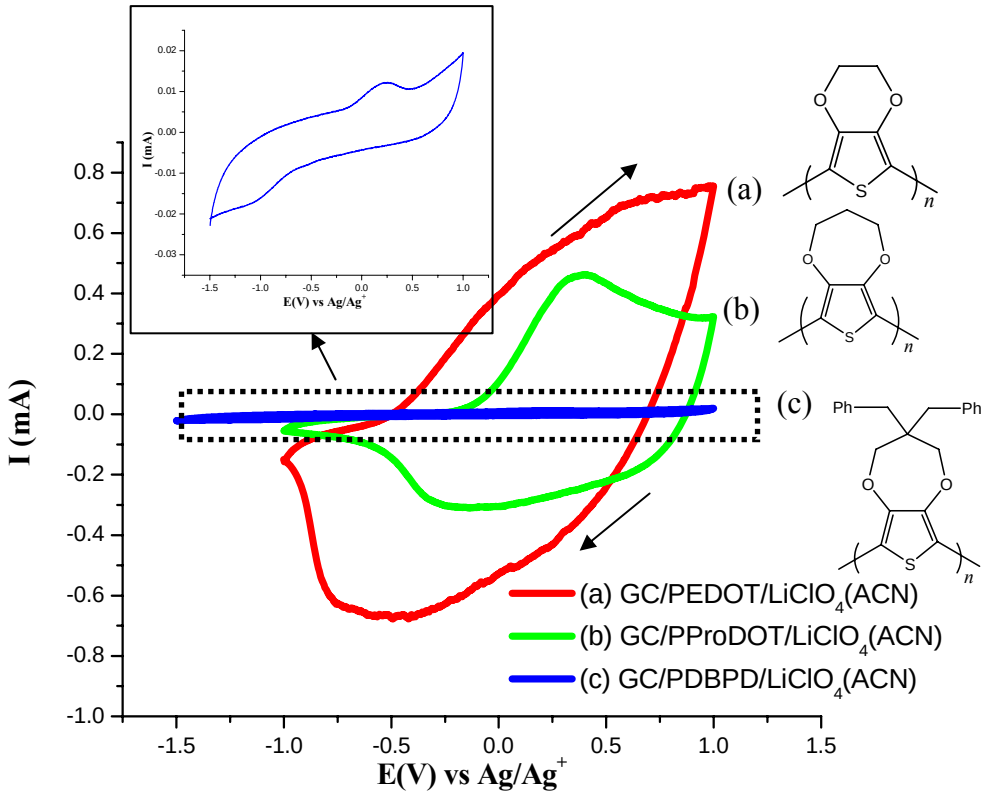

Figure 6.1: CVs of (a) GC/PEDOT/$LiClO_4$(ACN) (b) GC/PProDOT/$LiClO_4$(ACN) and (c) GC/PDBPD/$LiClO_4$(ACN) in ACN containing 0.1 M $LiClO_4$ at 100 mVs^{-1}. Inset: magnification of CV of GC/PDBPD/$LiClO_4$ (ACN).

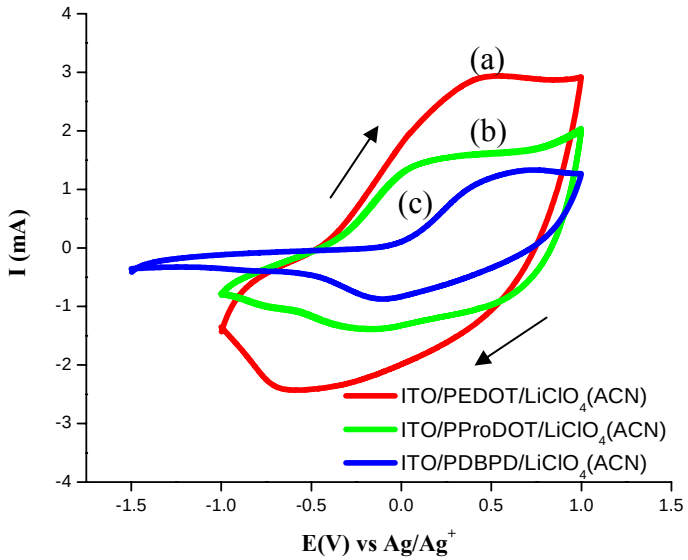

Figure 6.2: CVs of (a) ITO/PEDOT/$LiClO_4$(ACN) (b) ITO/PProDOT/$LiClO_4$(ACN) and (c) ITO/PDBPD/$LiClO_4$(ACN) in ACN containing 0.1 M $LiClO_4$ at 100 mVs^{-1}.

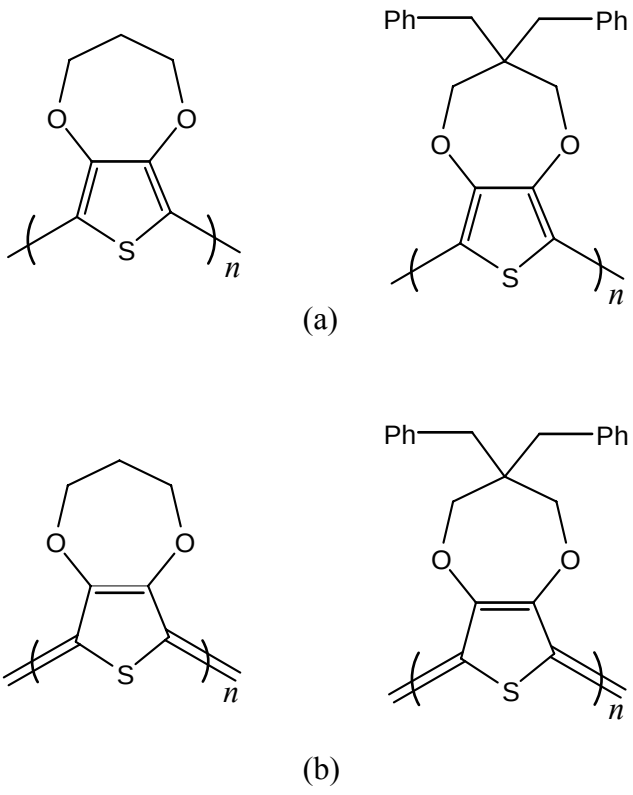

Figure 6.3: (a) Benzoid and (b) quinoid structures of PProDOT and PDBPD.

Figure 6.4 shows the CVs of PEDOT coated GC and ITO electrodes in monomer free solution *i.e.* 0.1 M KCl and 0.1 M $LiClO_4$ for polymer films prepared in KCl and $LiClO_4$ aqueous solutions, respectively. The doping peaks of PEDOT/KCl coated GC (**Figure 6.4a**) and ITO electrodes (**Figure 6.4b**) were observed at the same potential around +0.17 V. The sharp doping peak with GC/PEDOT/KCl(Aq) indicates a facile process. The dedoping potential peak of GC/PEDOT/KCl(Aq) was observed at around +0.5 V, however the dedoping peak of ITO/PEDOT/KCl(Aq) was quite difficult to locate precisely, due to the width of the peak. It is noticeable that PEDOT coated GC electrodes prepared in aqueous solutions (**Figure 6.4a**) had two dedoping peaks indicating the dedoping process may be occurring in two steps, possibly two kinetic steps are involved in the release of the counterions (Zykwinska *et al.*, 2003).

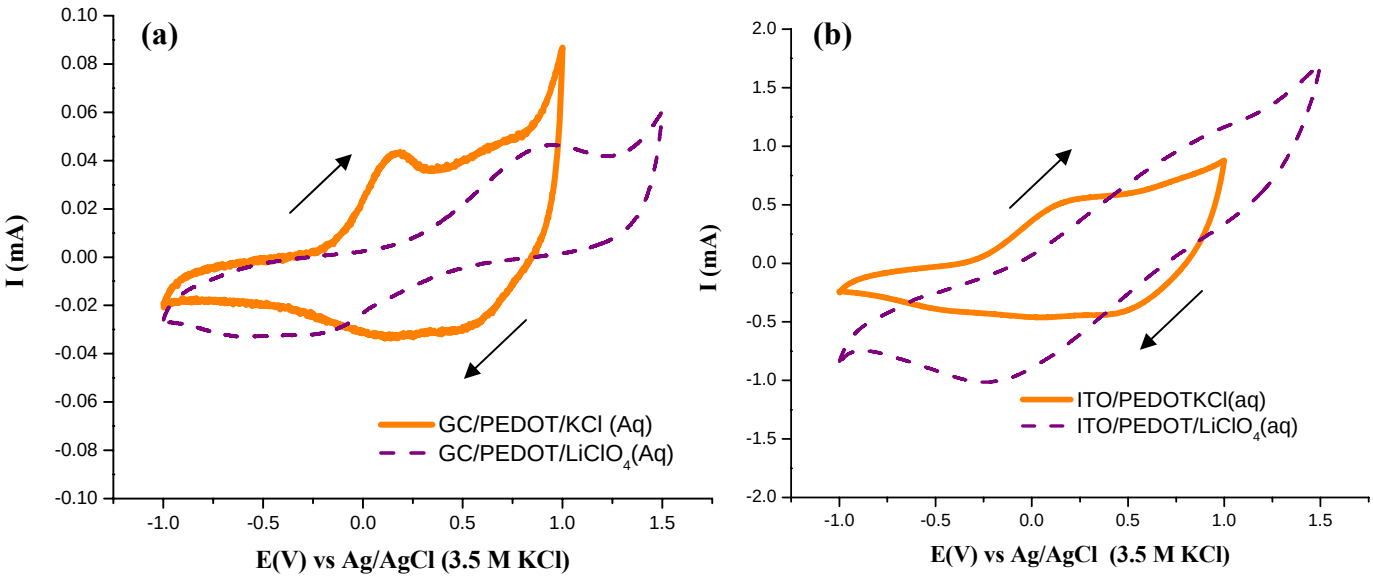

Figure 6.4: CVs of PEDOT coated (a) GC electrode and (b) ITO electrode in 0.1 M KCl (or 0.1 M $LiClO_4$) at 100 mVs^{-1}.

6.3.2 Cyclic Voltammogram of Bare Electrodes

The CV analyses were also conducted using 10 mM potassium ferricyanide as a redox probe and 1 M KCl as the background electrolyte. The measurements were conducted at room temperature.

Figure 6.5 displays the CV of the background solution containing 1 M KCl. There was no significant peak current, indicating that there was no electron transfer at the interface of the electrode. The small amount of current was due to the capacitive current as a result of the existence of a double layer. As can be seen in **Figure 6.6**, there were two well defined peaks *i.e.* anodic and cathodic peaks. The observable oxidation and reduction peaks were due to the redox couple process of $Fe(CN)_6^{3-}/Fe(CN)_6^{4-}$.

$$Fe(CN)_6^{3-} + e^- \rightleftharpoons Fe(CN)_6^{4-} \qquad \textbf{(6.1)}$$

It was observed that the anodic and cathodic peak currents for bare GC were proportional to the square root of scan rate (**Figure 6.6b**), which is in agreement with Randles-Sevcik equation. In addition, the anodic and cathodic peak potentials were independent of the scan rates, which suggesting that the redox reaction was reversible and the electrochemical reaction was diffusion-controlled *i.e.* the overall rate of the reaction was controlled by the rate of diffusion of the electroactive species to/from the electrode rather than the rate of the reaction, even at high scan rate. However, the peak separation between E_{pa} and E_{pc} *i.e.* ΔE_p was 75 mV, which is higher than the theoretical value, 59 mV. This finding is consistent as reported in literature (ΔE_p = 71 mV) (Lu *et al.*, 2008), which could be due to the adsorption of ferricyanide on carbon surfaces (Chen *et al.*, 1995, Cline *et al.*, 1994).

Background CV of bare ITO electrode in 1 M KCl showed only capacitive current, which is similar to the bare GC electrode. The CVs of bare ITO electrode in 10 mM $K_3Fe(CN)_6$ in 1 M KCl as seen in **Figure 6.7a** showed the separation of anodic and cathodic peak (ΔE_p) was 180 mV at scan rate of 50 mVs^{-1}. This value is similar to the value obtained from literature (ΔE_p = 170 mV) (Ahuja *et al.*, 2010) and the ΔE_p values increased with increasing scan rates, indicating slower kinetic rates of electron transfer. This could be due to the uncompensated resistance (*iR* drop) and resistance of the ITO which affects the apparent reversibility. The plot of current *vs* square root of scan rate still revealed a linear correlation (**Figure 6.7**).

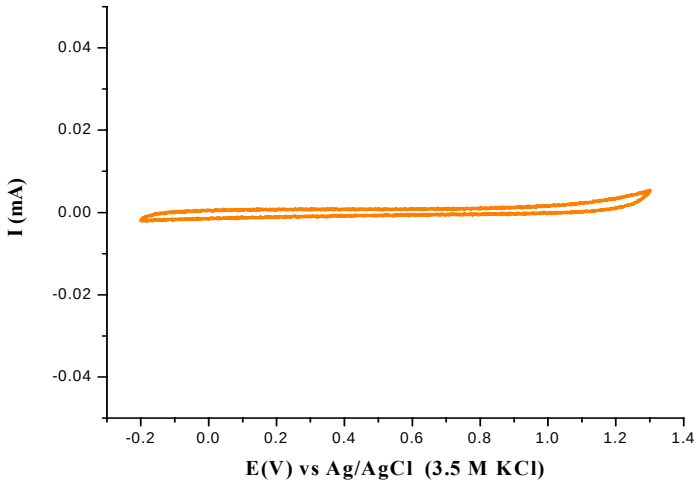

Figure 6.5: Background CV of GC electrode in 1 M KCl at 50 mVs^{-1}.

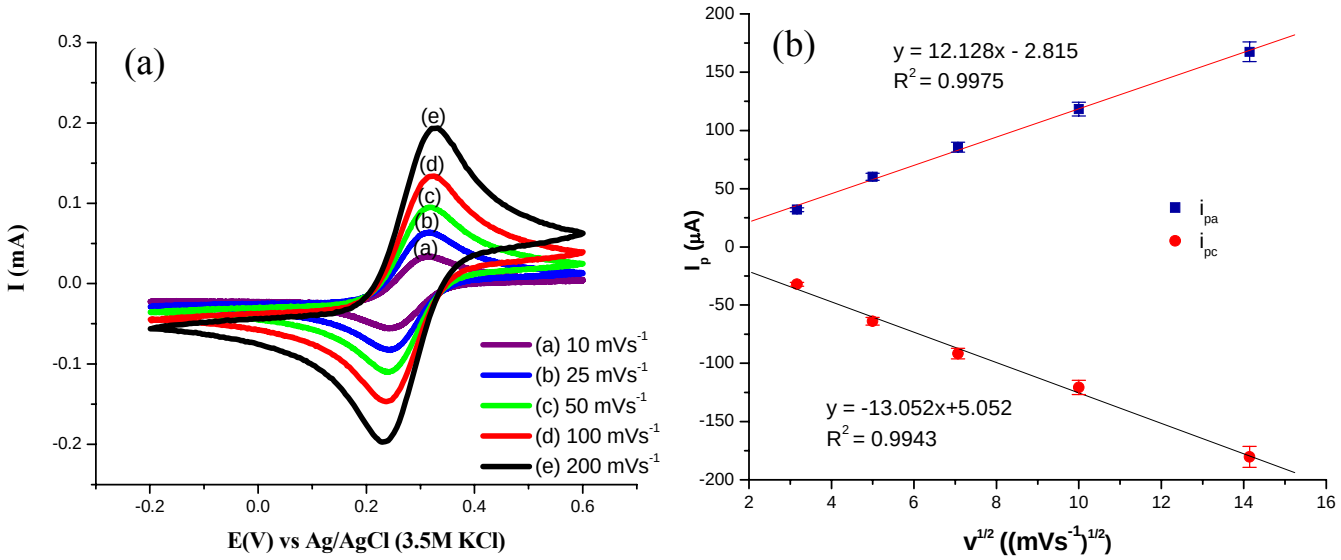

Figure 6.6: (a) CVs of bare GC electrode in 10 mM $K_3Fe(CN)_6$ + 1 M KCl and (b) peak current *vs* square root of scan rate.

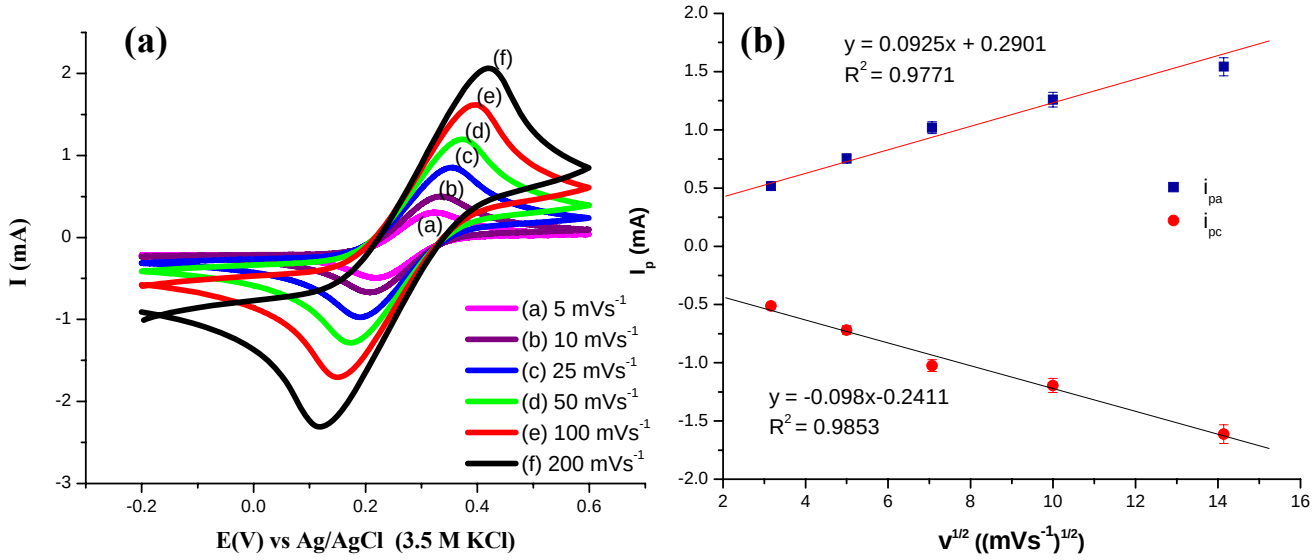

Figure 6.7: (a) CVs of bare ITO electrode in 10 mM $K_3Fe(CN)_6$ + 1 M KCl and (b) peak current *vs* square root of scan rate.

6.3.3 Cyclic Voltammetry Measurements of Polymer Films Coated Electrodes

6.3.3.1 Cyclic Voltammograms of PEDOT, PProDOT and PDBPD Films Prepared in Acetonitrile

In order to investigate the electron transfer behaviour, the CVs response were studied by monitoring the redox couple of $K_3Fe(CN)_6$. The overlaid CVs of PEDOT, PProDOT and PDBPD films coated GC electrode are presented in **Figure 6.8**.

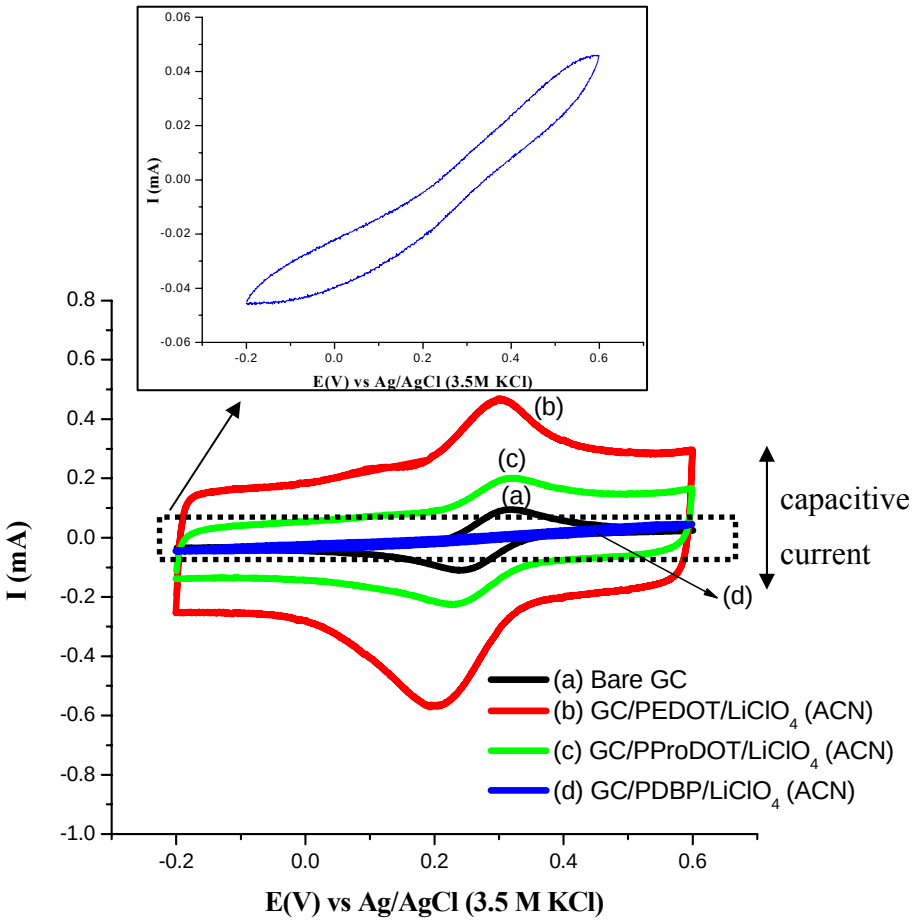

Figure 6.8: CVs of polymer film coated GC electrodes (prepared in acetonitrile) at 50 mVs^{-1} in 10 mM $K_3Fe(CN)_6$ + 1 M KCl. Inset: magnification of CV of GC/PDBPD/$LiClO_4$(ACN).

PEDOT and PProDOT coated GC electrodes showed a well-defined reversible peak (**Figure 6.8**). The redox peak is due to the redox active species $Fe(CN)^{3-/4-}$. CV was performed at different scan rates (**Figure 6.9a** and **c**) and the results showed that peak currents (anodic and cathodic) of both samples were proportional to the square root of scan rate, indicating the reaction was diffusion controlled (**Figure 6.9b** and **d**). This observation has shown that the GC electrodes were not fully covered by the PEDOT and PProDOT films. The SEM images as reported in **Chapter 5** also revealed that GC/PEDOT/$LiClO_4$(ACN) and GC/PProDOT/$LiClO_4$(ACN) had granular and porous structure, respectively. These morphologies allow the ferricyanide to directly contact with the GC electrode surface. It is noticeable that PEDOT coated GC had huge capacitive current compared to the other polymer films (**Figure 6.8**). This behaviour will be explained in details in **Section 6.3.4.4**.

The inset in **Figure 6.8** shows the magnification of the CV of GC/PDBPD/$LiClO_4$(ACN). The CV revealed the redox reaction was suppressed. This result implies that the GC electrode was fully covered by PDBPD film as seen in SEM image in **Chapter 5**. PDBPD films had compact structure compared to the PEDOT and PProDOT coated GC electrodes. This morphology has blocked the movement of the redox active ions in the electrolyte to the electrode surface.

Further, CV measurements for GC/PDBPD/$LiClO_4$(ACN) at low scan rates were carried out in order to detect the presence of pinholes. Sigmoidal-shaped CVs as can be seen in **Figure 6.10** were observed (5 and 10 mVs^{-1}), indicating the presence of pinholes in between solid polymer deposited on the electrode which allow the redox active species to penetrate through it (**Figure 6.11**). The sigmoidal-shaped CVs observed are analogous to the microelectrode behavior. In CV measurements, as the redox reaction takes place at the potential applied, the diffusion will grow at the vicinity of electrode surface. For a macroelectrode, the mass transport is characteristic of linear diffusion (**Figure 6.12a**) and it gives Nernstian CV behaviour. In a microelectrode, a sigmoidal-shaped CV is obtained due to the radial diffusion (**Figure 6.12b**). This observation will be further confirmed by electrochemical impedance spectroscopy measurement (**Section 6.3.4.2**).

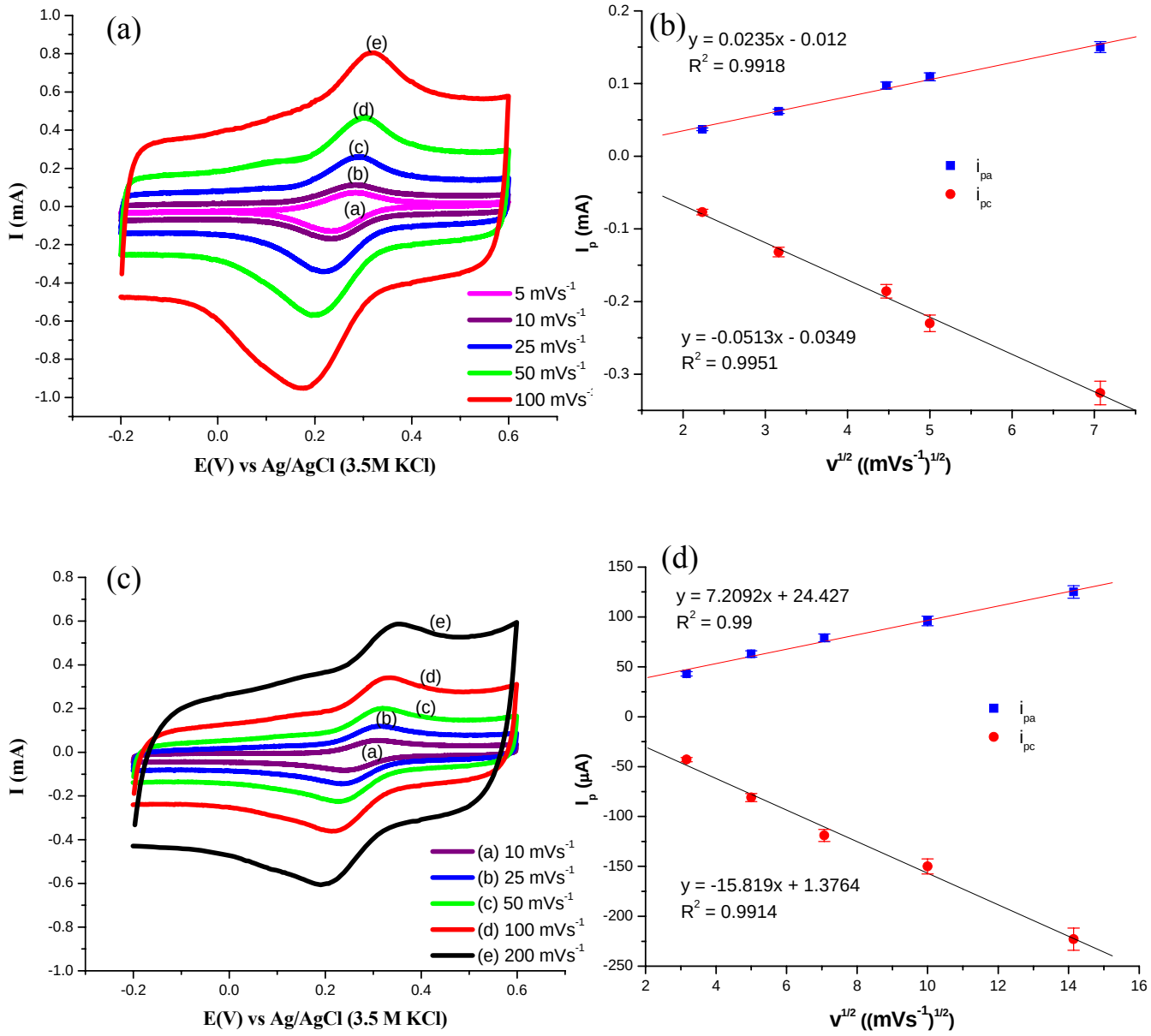

Figure 6.9: CVs of (a) GC/PEDOT/$LiClO_4$(ACN) and (c) GC/PProDOT/$LiClO_4$(ACN) in 10 mM $K_3Fe(CN)_6$ + 1 M KCl at various scan rates; (b) and (d): plot of anodic and cathodic peak currents *vs* square root of scan rate.

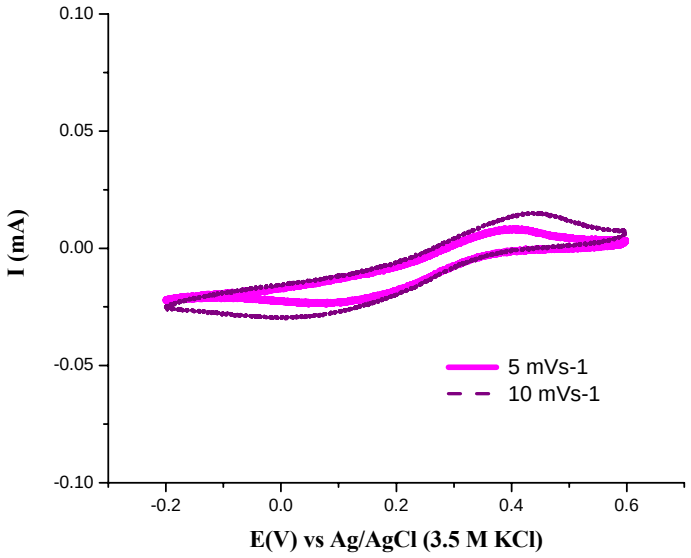

Figure 6.10: CVs of GC/PDBPD/$LiClO_4$(ACN) at slow scan rates.

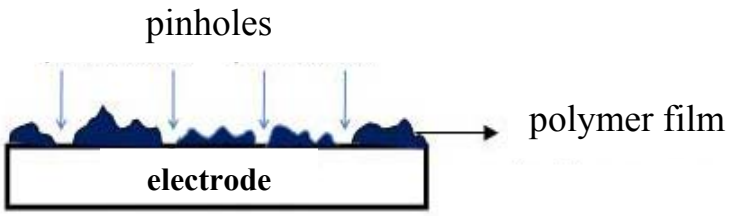

Figure 6.11: Pinholes in between deposited polymer on the electrode surface.

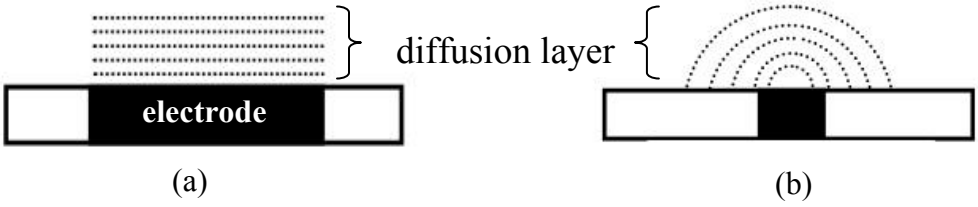

Figure 6.12: Illustration of (a) linear and (b) radial diffusion.

The CVs of PEDOT, PProDOT and PDBPD coated on ITO electrodes are illustrated in **Figure 6.13**. PEDOT and PProDOT showed that the redox reaction was not suppressed and the capacitive current increased compared to bare GC electrode. It was noted that the potential of oxidation and reduction shifted to more positive and more negative values, respectively in comparison to bare ITO electrode (**Figure 6.13**).

In the case of PDBPD film coated ITO electrode (**Figure 6.13d**), the capacitive current suppressed and the peak separation increased (ΔE_p= 400 mV) compared to bare ITO (ΔE_p= 180 mV), indicating slow kinetics. This phenomenon was more pronounced at slower scan rates (**Figure 6.15**). It was also observed that the reactions for PEDOT, PProDOT and PDBPD coated on ITO electrodes were diffusion controlled as indicated by a linear correlation between peak currents and the square root of scan rate (**Figure 6.14b**, **d** and **Figure 6.15b**).

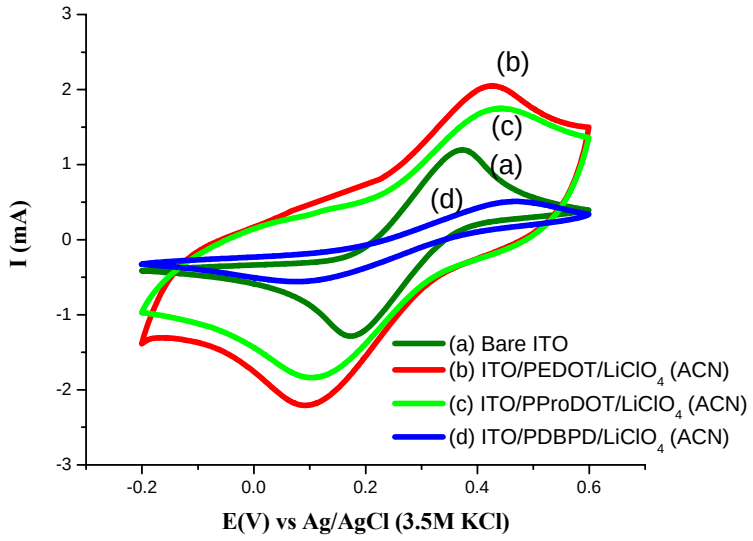

Figure 6.13: CVs of polymer film coated ITO electrodes (prepared in acetonitrile) at 50 mVs^{-1} in 10 mM $K_3Fe(CN)_6$ + 1 M KCl. Scan rate = 50 mVs^{-1}.

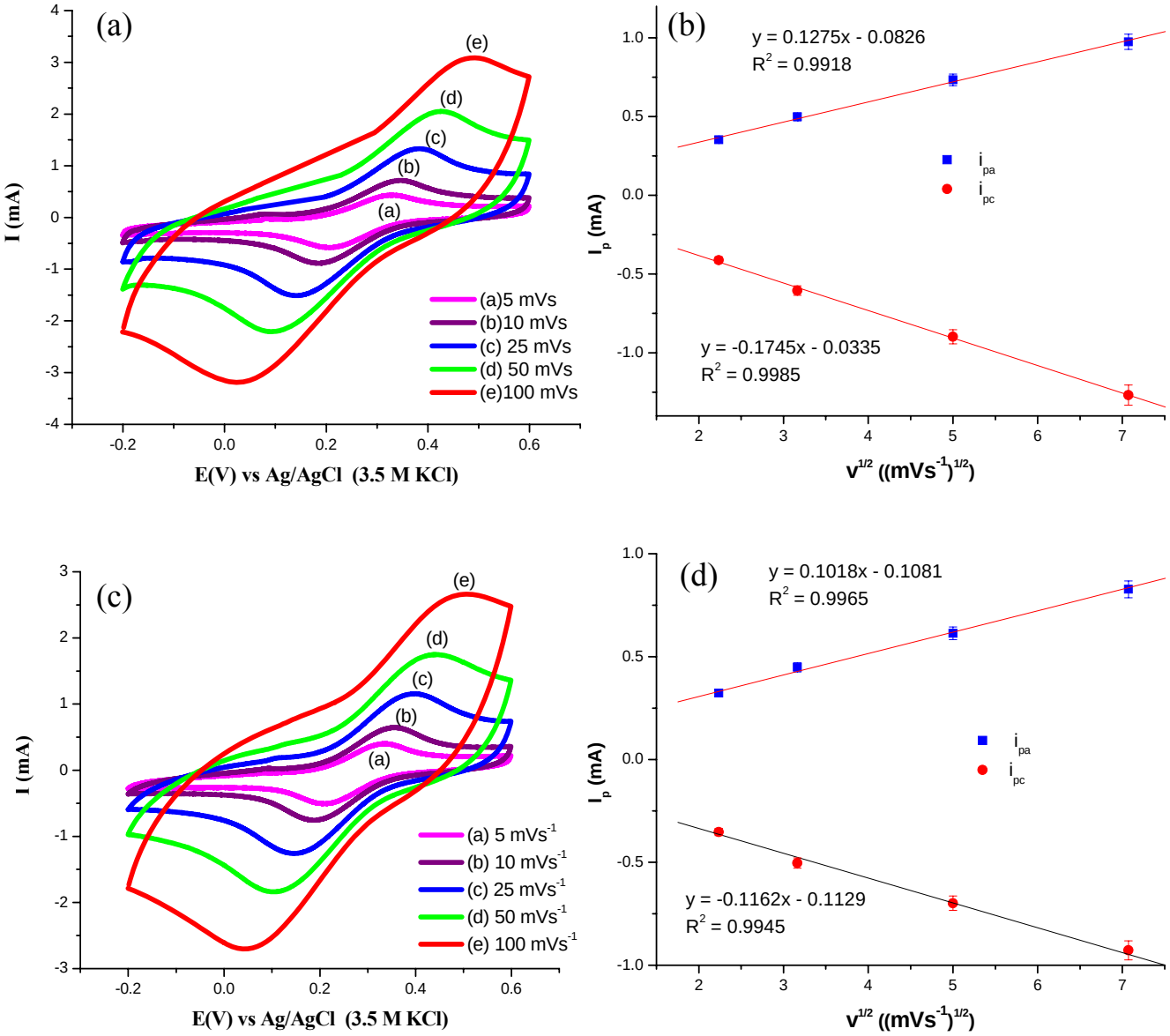

Figure 6.14: CVs of (a) ITO/PEDOT/$LiClO_4$(ACN) and (c) ITO/PProDOT/$LiClO_4$(ACN) in 10 mM $K_3Fe(CN)_6$ + 1 M KCl at various scan rates. (b) and (d): plot of anodic and cathodic peak currents *vs* square root of scan rate.

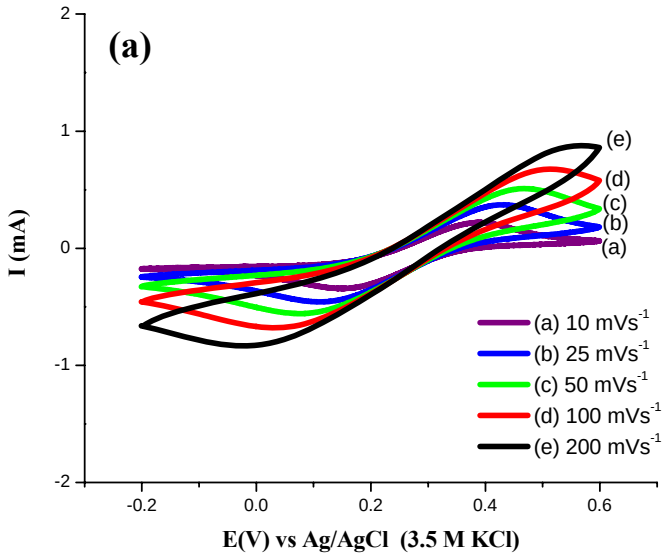

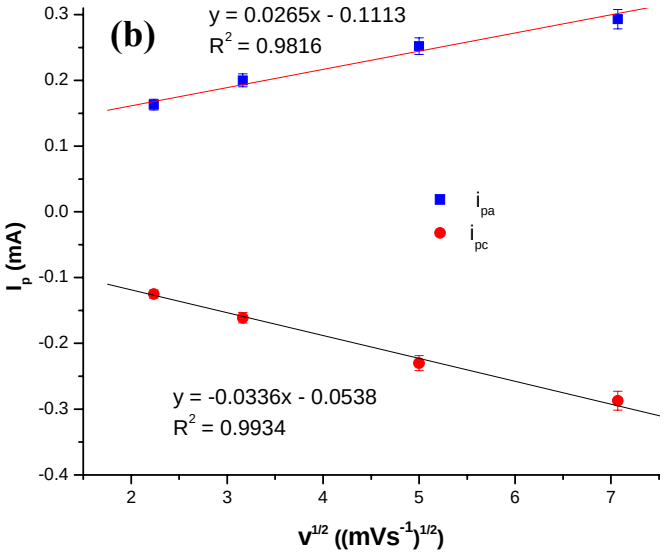

Figure 6.15: (a) CVs of ITO/PDBPD/$LiClO_4$(ACN) in 10 mM $K_3Fe(CN)_6$ + 1 M KCl and (b) peak current *vs* square root of scan rate.

6.3.3.2 Cyclic Voltammograms of PEDOT Prepared in Aqueous Solution

The anodic and cathodic peak potentials for CV of GC/PEDOT/KCl(Aq) (**Figure 6.16b**) in ferricyanide solution were more separated (ΔE_p = 171 mV) compared to the bare GC electrode (75 mV). In addition, the peak separation increases with increasing scan rate (**Figure 6.17a**) and the peak currents were not directly proportional to the square root of scan rate (**Figure 6.17b**), indicating that the reaction was quasi reversible and controlled by a charge transfer step rather than by the diffusion step. On the other hand, the GC/PEDOT/$LiClO_4$(Aq) showed reversible peaks (**Figure 6.17c**). The current responses were directly proportional to the square root of the scan rate (**Figure 6.17d**), indicating that there are some holes on the surface of the electrode that permitted the redox active ion to get access and subsequently allow the electron to transfer. The CVs also revealed that the capacitive currents for GC/PEDOT/KCl(Aq) and GC/PEDOT/$LiClO_4$(Aq) were higher than bare GC. This characteristic will further discussed in **Section 6.3.4.4**.

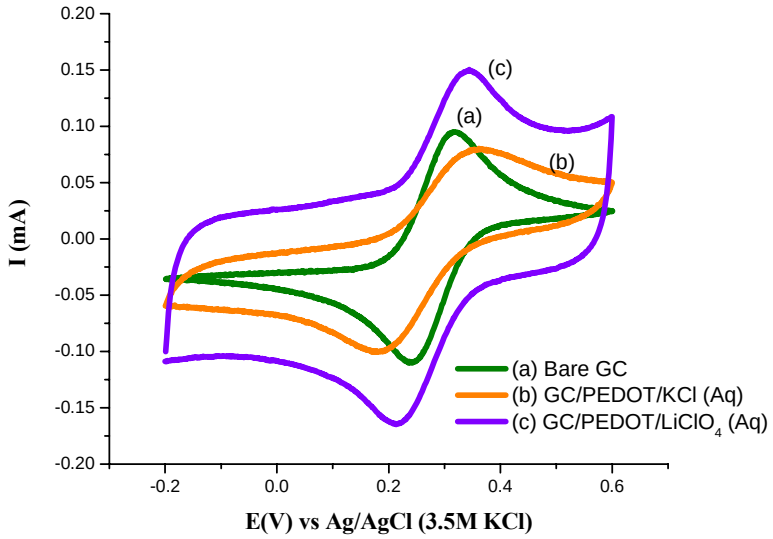

Figure 6.16: CVs of PEDOT coated GC electrode (prepared in aqueous solution) at 50 mVs^{-1} in 10 mM $K_3Fe(CN)_6$ + 1 M KCl.

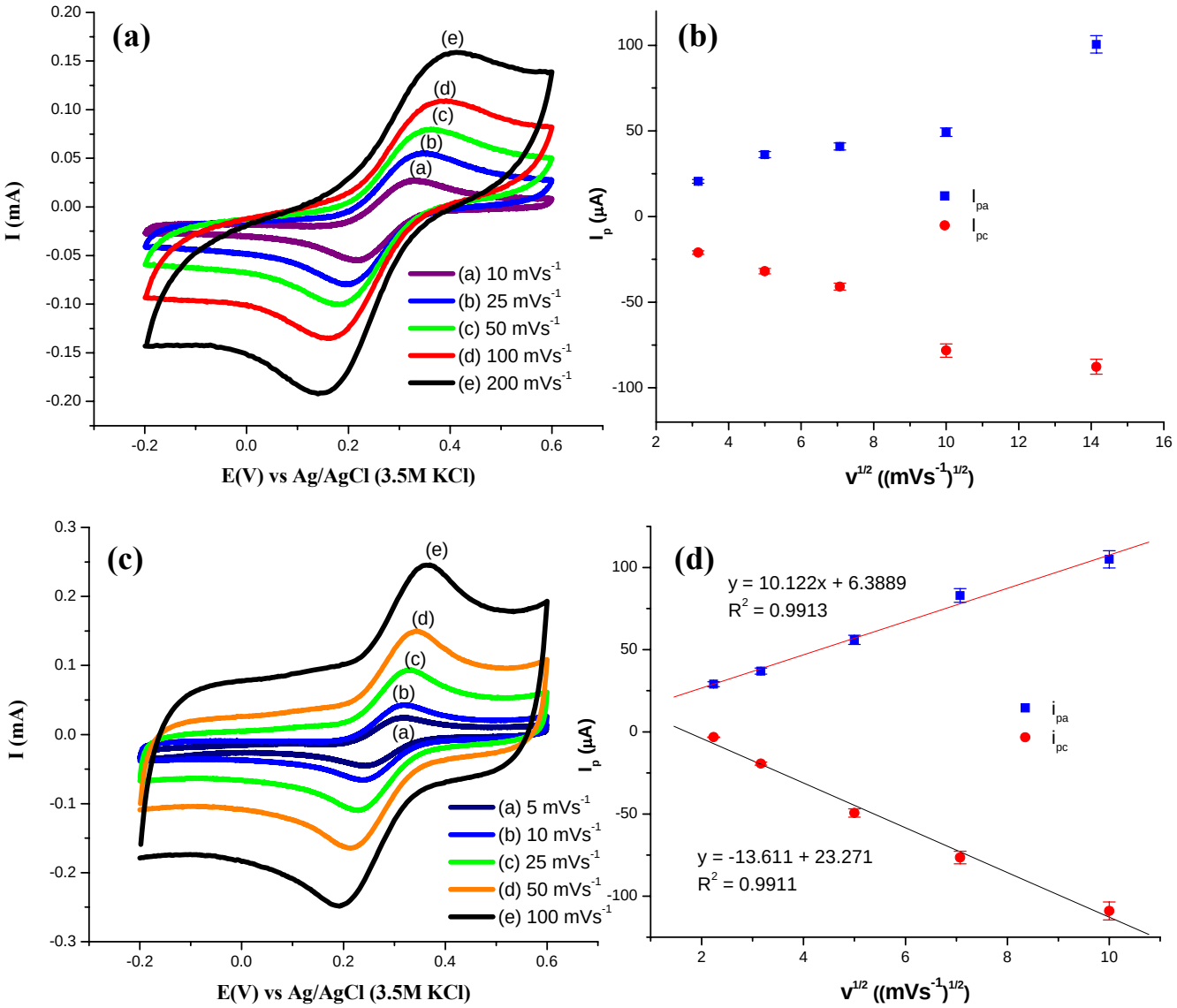

Figure 6.17: CVs of (a) GC/PEDOT/KCl(Aq) and (c) GC/PEDOT/$LiClO_4$(Aq) in 10 mM $K_3Fe(CN)_6$ + 1 M KCl at various scan rates; (b) and (d): plot of anodic and cathodic peak currents *vs* square root of scan rate.

CVs behaviour of PEDOT coated ITO electrodes prepared in aqueous solutions were carried out as a comparison. It was found that the redox responses of ITO/PEDOT/$LiClO_4$(Aq) (**Figure 6.18c**) and ITO/PEDOT/KCl(Aq) were not suppressed (**Figure 6.18b**). It was observed that the anodic and cathodic peaks for ITO/PEDOT/KCl(Aq) were more separated and more pronounced with increasing scan rates (**Figure 6.19**), indicating slow kinetic. However, the peaks currents were linearly correlated with the square root of scan rate (**Figure 6.19b**). In the case of ITO/PEDOT/$LiClO_4$(Aq), the peak currents were not directly proportional to the square root of scan rate (**Figure 6.20b**).

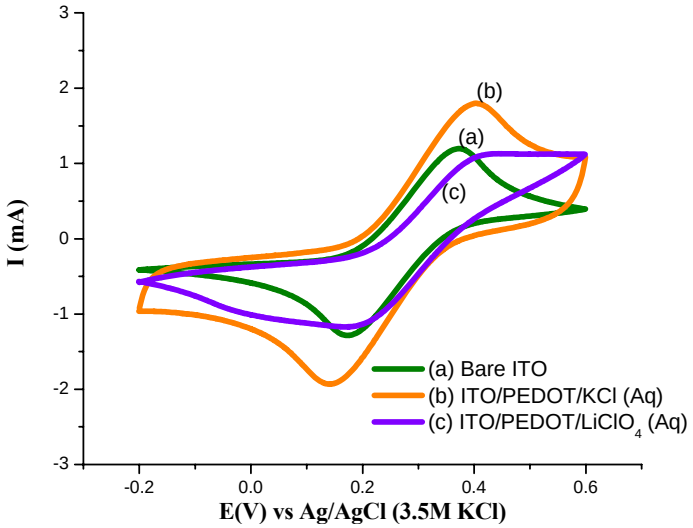

Figure 6.18: CVs of PEDOT coated ITO electrode (prepared in aqueous solution) at 50 mVs^{-1} in 10 mM $K_3Fe(CN)_6$ + 1 M KCl.

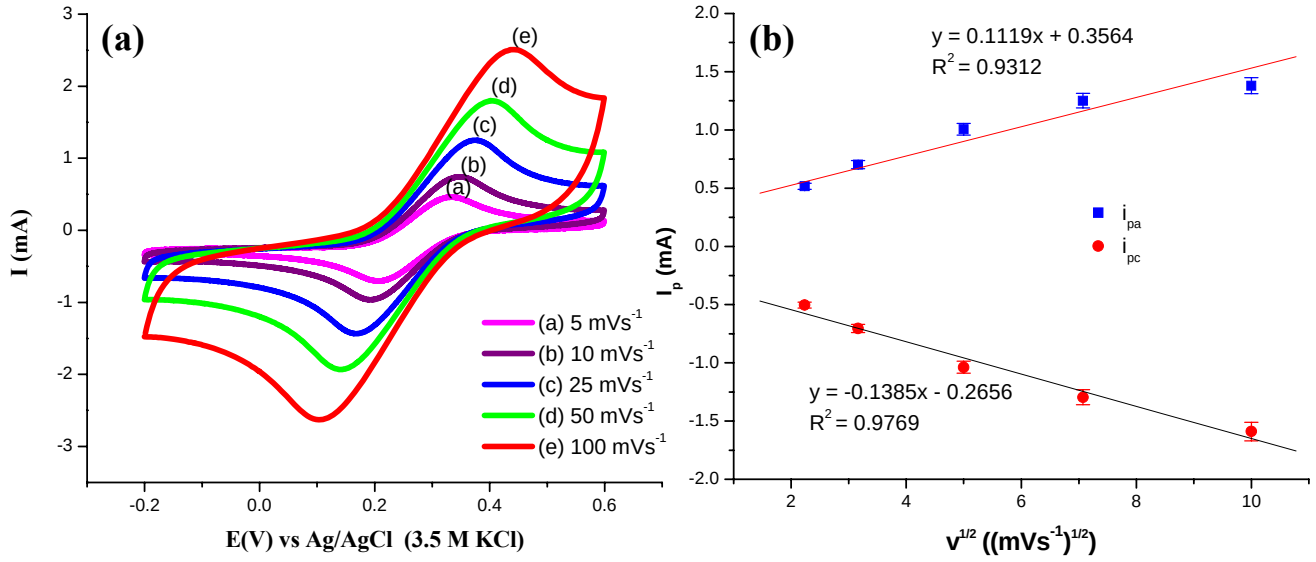

Figure 6.19: (a) CVs and (b) plot of anodic and cathodic peak currents *vs* square root of scan rate of ITO/PEDOT/KCl(Aq).

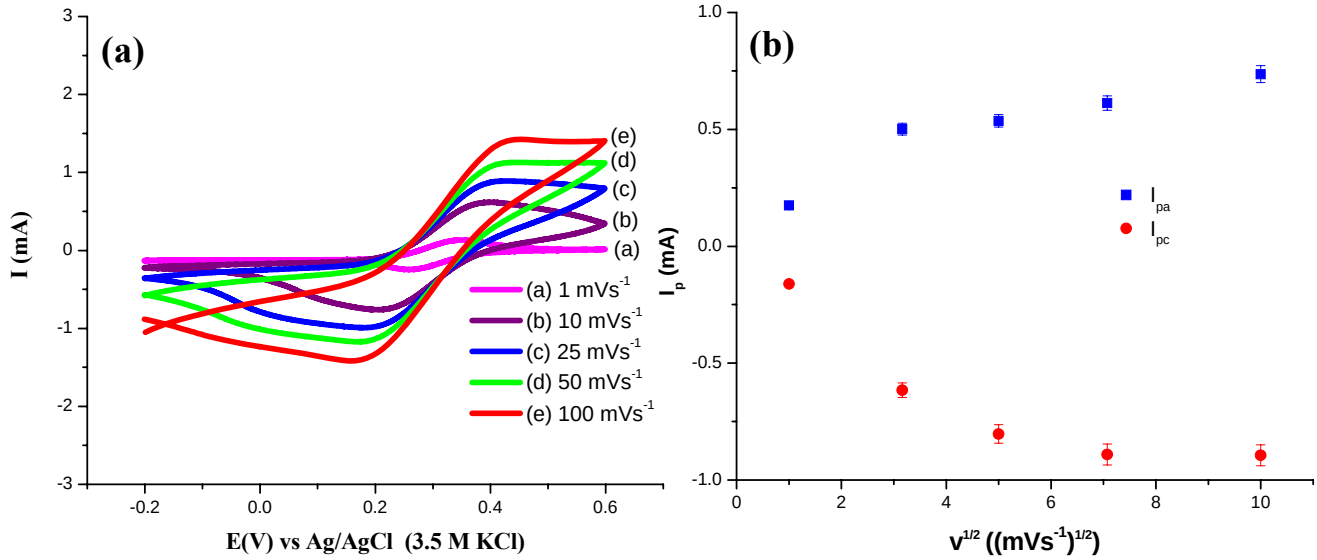

Figure 6.20: (a) CVs and (b) plot of anodic and cathodic peak currents *vs* square root of scan rate of ITO/PEDOT/$LiClO_4$(Aq).

6.3.4 Electrochemical Impedance Spectroscopy (EIS) Studies

EIS has been proved to be a powerful tool for investigating electrode process (Cao, 1990a, Cao, 1990b). In this work, EIS was used to characterise the interfacial properties of conducting polymer modified electrodes that can be correlated with the CV measurements. The measurements are based on the response of electrochemical cell to a small amplitude alternating potential.

A typical Faradaic impedance spectrum presented as a Nyquist plot (Z'' *vs* Z') consists of a semicircular domain at high frequencies, and the diameter of the semicircle corresponds to the interfacial charge transfer resistance (R_{ct}). The complex impedance can be presented as Z' and Z'' components that originate mainly from the resistance and capacitance of the cell, respectively.

The EIS response is often interpreted in terms of an equivalent circuit. Typically, the components in electronic equivalent circuits are modelled based on electrochemical process taking place at the electrode|electrolyte interface that correspond to the impedance spectra.

In this work, EIS measurements were conducted in equimolar concentration, 5 mM of $Fe(CN)_6^{3-/4-}$ in 1 M KCl. The measurements were performed with a Solartron 1260 Impedance/Gain-Phase Analyser consisting of a potentiostat PAR model 283 potentiostat connected to a personal computer. An ac voltage of 10 mV in amplitude with a frequency range from 1 Hz to 10^5 Hz was superimposed on the dc potential and applied to the studied electrodes. This approach is used to perturb the cell by an alternating signal (sinusoidal) of small amplitude and observe the behaviour in which the system follows the perturbation at the steady state. The dc potential was always set up at the formal potential of $Fe(CN)_6^{3-/4-}$ (+0.27 V for GC and +0.31 V for ITO electrode). The formal potentials, E^o were estimated as the mid-point of oxidation and reduction peak potentials. These values were obtained from CV measurements of bare GC and ITO electrodes in equimolar solution. Experimental data of the electrochemical impedance

plot were analyzed using commercially available software Zplot/Zview (Version 3.1c, Scribner Associates, Inc.).

6.3.4.1 EIS Measurements of Bare Electrodes

Figure 6.21 shows the Nyquist plot of bare GC and ITO electrodes. Both bare electrodes illustrate the impedance spectra that follow the theoretical shape which consist of a semicircle at the high frequency region indicating the presence of a charge-transfer limited process followed by a linear behavior at the low frequency corresponding to the diffusion of the species to the electrode surface. The experimental data and fitting were plotted as dotted line and solid line, respectively. It was clearly seen that the diameter of the semicircle of bare GC (**Figure 6.21a**) was larger than the bare ITO (**Figure 6.21b**), indicating high resistance of GC electrode (**Section 6.3.4.4**).

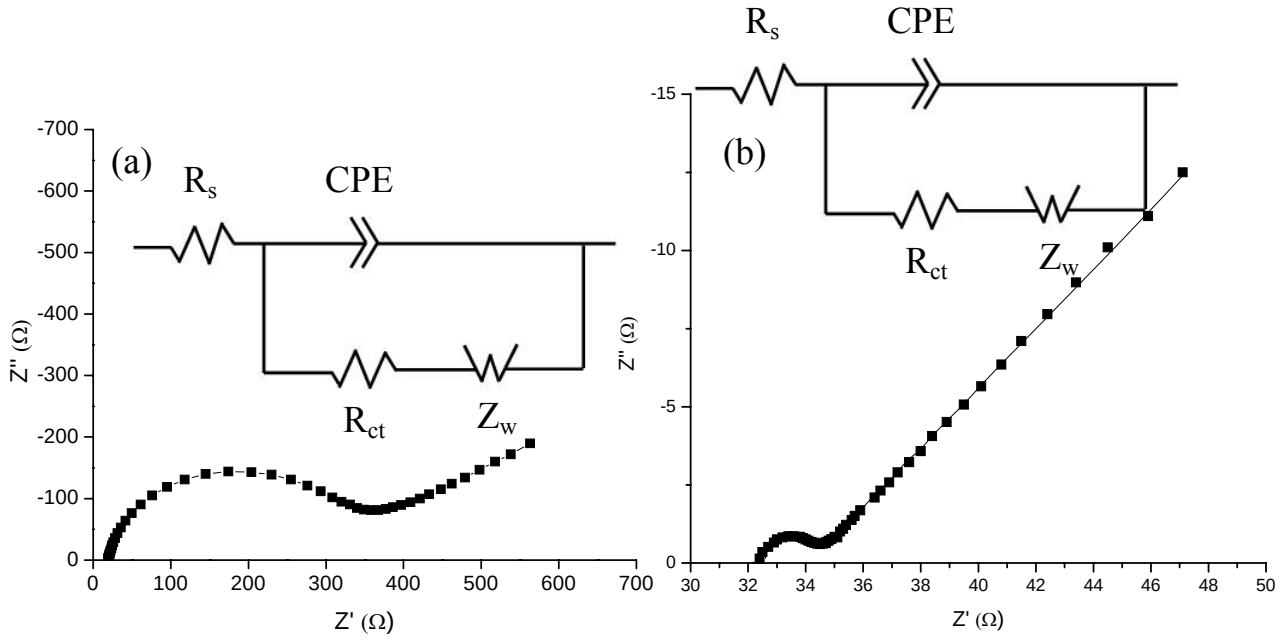

Figure 6.21: Nyquist plot of (a) bare GC and (b) ITO electrodes in the presence of equimolar 5 mM $Fe(CN)_6^{3-/4-}$. Inset : equivalent circuit used for fitting.

6.3.4.2 EIS Measurements of Polymer Films Prepared in ACN

Figure 6.22 - **Figure 6.24** display the Nyquist plots of PEDOT, PProDOT and PDBPD coated GC and ITO electrodes. PEDOT coated GC and ITO electrodes (**Figure 6.22**) showed a semicircle at high frequency region indicating the redox reaction was kinetically controlled and the GC and ITO electrodes were not fully covered by PEDOT films. This observation is in good agreement with the CV measurements as explained in **Section 6.3.3.1** (**Figure 6.8** and **Figure 6.13**). A straight line (45°) was observed at low frequency region presenting the facile nature of the redox reaction, meaning the diffusion was semi-infinite and was mass transfer controlled.

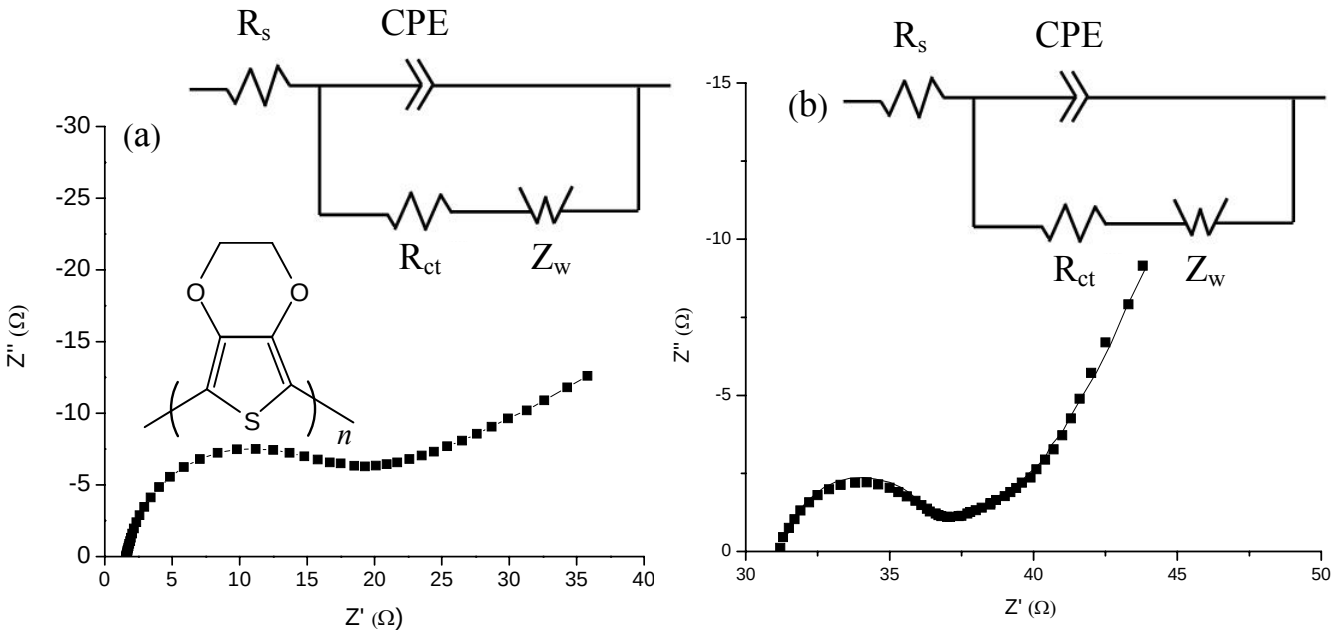

Figure 6.22: Nyquist plot of (a) GC/PEDOT/$LiClO_4$(ACN) and (b) ITO/PEDOT/$LiClO_4$(ACN) in 5 mM $Fe(CN)_6^{3-/4-}$ with 1 M KCl supporting electrolyte. Inset: equivalent circuit used for fitting.

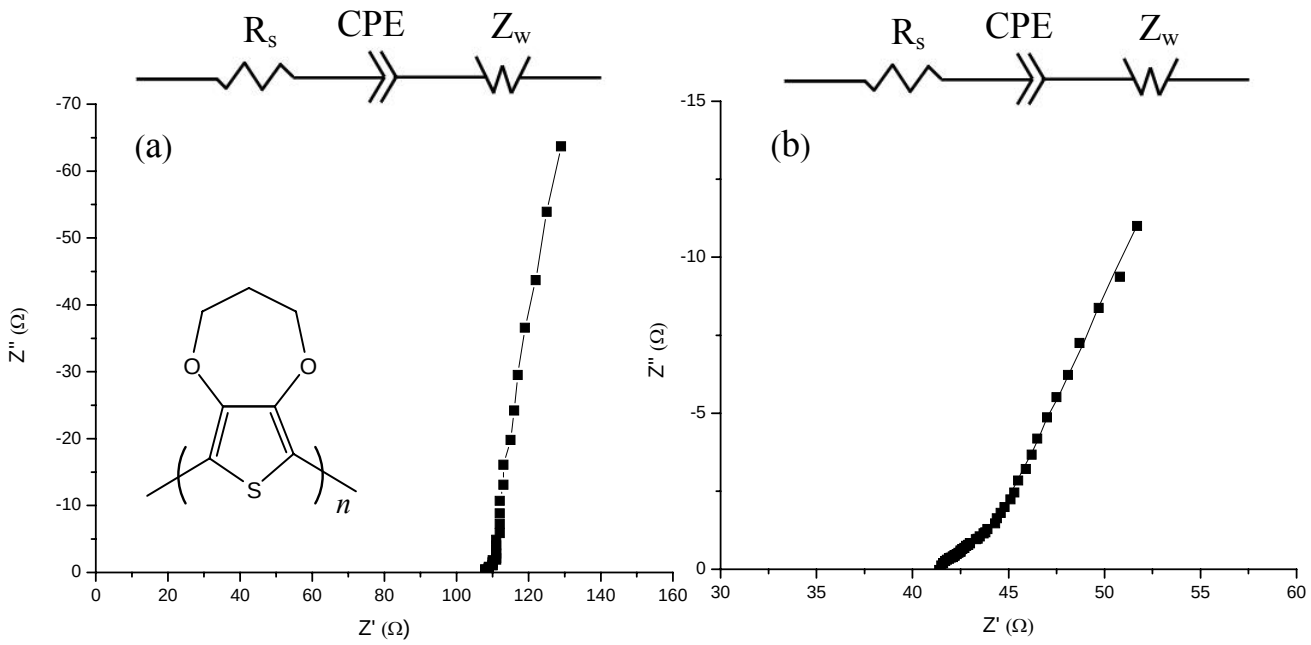

Figure 6.23: Nyquist plot of (a) GC/PProDOT/$LiClO_4$(ACN) and (b) ITO/PProDOT/$LiClO_4$(ACN) in 5 mM $Fe(CN)_6^{3-/4-}$ with 1 M KCl supporting electrolyte. Inset: equivalent circuit used for fitting.

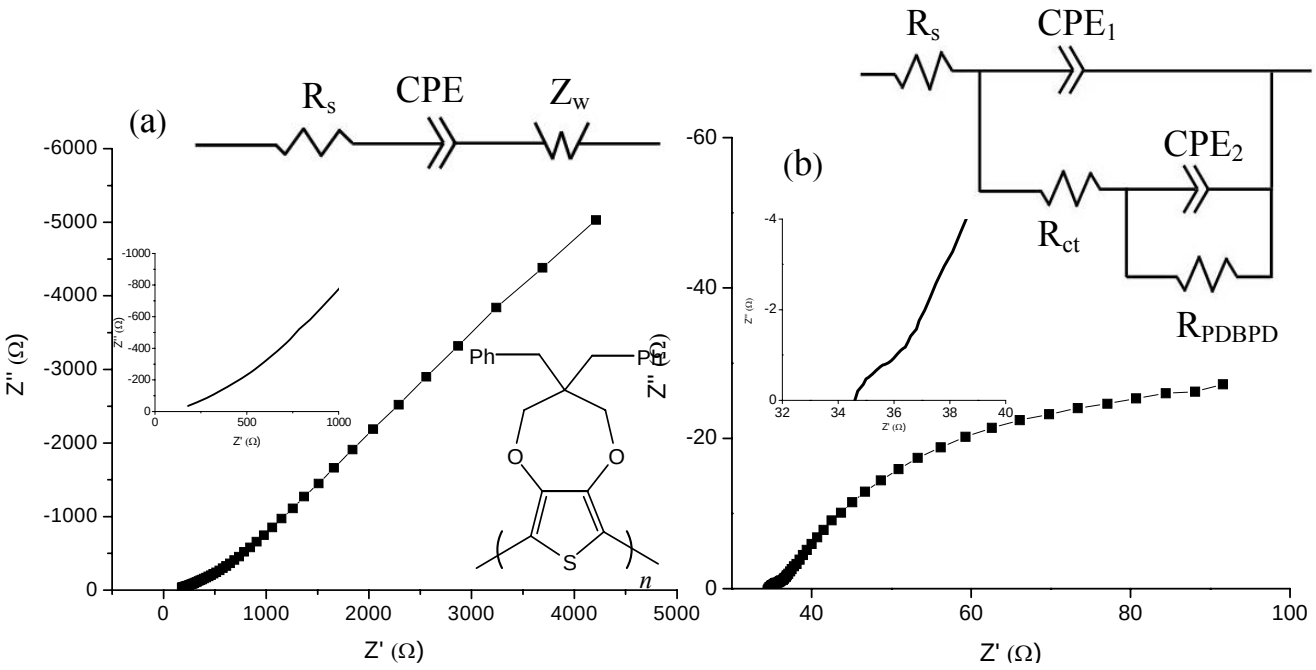

Figure 6.24: Nyquist plot of (a) GC/PDBPD/$LiClO_4$(ACN) and (b) ITO/PDBPD/$LiClO_4$(ACN) in 5 mM $Fe(CN)_6^{3-/4-}$ with 1 M KCl supporting electrolyte. Inset: equivalent circuit used for fitting.

In the case of PProDOT film (**Figure 6.23a** and **b**), only straight line was observed without the presence of semicircle, indicating the facile interfacial ion and electron transfer (Bobacka, 1999). The straight line for GC/PProDOT/$LiClO_4$(ACN) (**Figure 6.23a**) was close to 90°, indicating the properties of the polymer tend to pure capacitor but the capacitance value was lower than PEDOT (**Section 6.3.4.4**). However, in the case of ITO/PProDOT/$LiClO_4$(ACN) (**Figure 6.23b**), the straight line at the low frequency region was distorted.

The EIS spectrum of GC/PDBPD/$LiClO_4$(ACN) (**Figure 6.24a**) exhibits straight line with 45° *i.e.* semi-infinite diffusion. It was also noted that no semicircle presence at high frequency region (inset **Figure 6.24a**) and the capacitance of PDBPD was lower than PProDOT (**Section 6.3.4.4**). This could be attributable to the hydrophobic properties of PDBPD film (θ_a = 136.11°, θ_r = 134.78°, as reported **Chapter 5**). This means that the molecule in the solution had no full contact on the surface of PDBPD film during the EIS measurement (**Figure 6.25**). Even though PProDOT showed hydrophobic properties (θ_a = 83.89°, θ_r = 49.92°), this phenomenon was not observed due to the porous structure of PProDOT (**Chapter 5**).

In the case of PDBPD coated ITO electrode (**Figure 6.24b**), two semicircles were observed *i.e.* large and small (inset **Figure 6.24b**) semicircles at low and high frequency region, respectively. This observation indicates two charge transport processes with different time constants. This is probably due to the nature of the ITO substrates which does not support ordered π–π stacking, and therefore result in a compact, thick and hydrophobic film with different regimes of electron transport. In this case, there is no Warburg element as evidenced by the absence of diffusion length that can result in a phase angle to shift from 45° (diffusive) to 90° (capacitive) regimes. This observation indicates the redox reaction is complete charge transfer control and in accordance with the CV measurement (**Figure 6.13**).

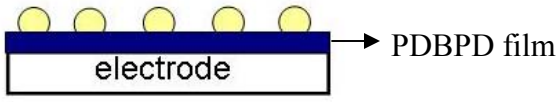

Figure 6.25: Illustration of molecule droplets on the PDBPD film.

6.3.4.3 EIS Measurements of PEDOT Films Prepared in Aqueous Solutions

Nyquist plots of all PEDOT prepared in aqueous solutions (KCl or $LiClO_4$) showed similar pattern as bare electrodes (ITO and GC electrodes) *i.e.* a semicircle at high frequency region and a straight line (45°) at low frequency region. This observation shows the facile nature of the redox reaction at the interfacial region (**Figure 6.26** and **Figure 6.27**). The only difference feature observed was the diameter of semicircle, indicating the different values of the charge transfer resistance for each sample which will be explained in **Section 6.3.4.4**.

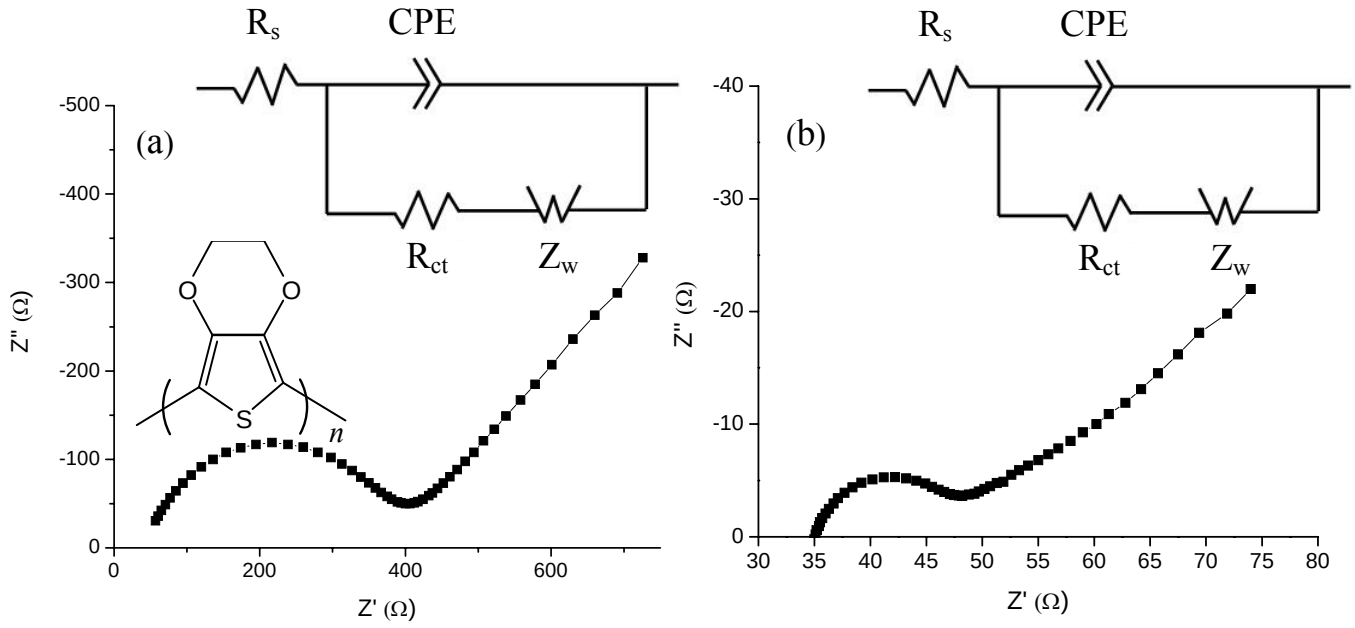

Figure 6.26: Nyquist plot of (a) GC/PEDOT/KCl(Aq) and (b) ITO/PEDOT/ KCl(Aq) in 5 mM $Fe(CN)_6^{3-/4-}$ with 1 M KCl supporting electrolyte . Inset: equivalent circuit used for fitting.

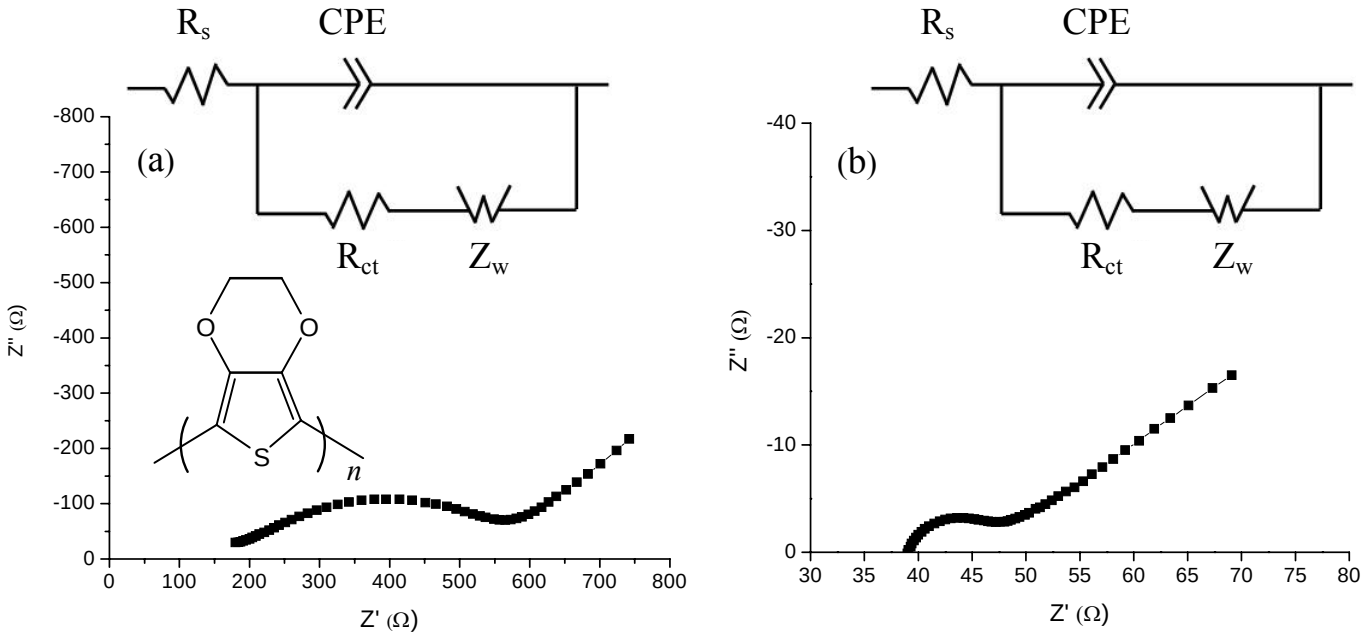

Figure 6.27: Nyquist plot of (a) GC/PEDOT/$LiClO_4$(Aq) and (b) ITO/PEDOT/$LiClO_4$(Aq) in 5 mM $Fe(CN)_6^{3-/4-}$ with 1 M KCl supporting electrolyte. Inset: equivalent circuit used for fitting.

6.3.4.4 Equivalent Circuits, Resistance and Capacitance

In a typical EIS, electrochemical reactions occur at the electrode|electrolyte interface can be modelled by extracting components of the electronic equivalent circuit that correspond to the experimental impedance spectra. Inset of **Figure 6.21** displays the equivalent electrical circuit used for fitting the data obtained from bare GC and ITO electrodes. The electronic components include the resistance of solution (R_s), a constant phase element (CPE) corresponding to the double layer capacitance, charge transfer resistance (R_{ct}) associated with the oxidation/reduction of $Fe(CN)_6^{3-/4-}$ and Warburg impedance (Z_w) resulting from the diffusion of ions from the bulk electrolyte to the electrode interface.

In most cases, the equivalent circuit of modified Randles' model was used, in which the double layer capacitance (C_{dl}) was replaced by frequency dependent CPE in

order to take into account the frequency dispersion behaviour due to the roughness and inhomogenity of the electrode surface (Oliveira-Brett *et al.*, 2002). This model was found to have good fitting for the EIS experimental data.

Generally, the R_s and Z_w are not affected by the chemical process occurring at the electrode interface since these two components represent the bulk properties of electrolyte and diffusion of the charge in a solution. In contrast, CPE and R_{ct} depend on the characteristics at the electrode|electrolyte interface. Theoretically, the value of R_s is independent of any modification on the electrode surface. However, practically, the R_s may differ due to the properties of the surface of modified electrode as observed in this work. This could be due to the diffusion of ions in the different morphology of polymer films as observed in the SEM images. As can be seen in **Table 6.1**, all polymer films coated GC and ITO electrodes showed higher R_s compared to bare electrodes except PEDOT/$LiClO_4$(ACN). In the case of polymer film coated ITO electrodes, the R_s values did not vary significantly. However, it was noticeable that for each sample, the R_s value remained the same for different E_{dc} applied. The error values in **Table 6.1** were obtained from data fitting.

Table 6.1: Resistance of solution from EIS data.

	Solution resistance, R_s	
	GC (Ω/cm^2)	**ITO (Ω/cm^2)**
Bare	279.86 ± 0.03	16.29± 0.21
PEDOT/$LiClO_4$(ACN)	23.29 ± 0.01	15.68± 0.09
PProDOT/$LiClO_4$(ACN)	1544.29 ± 2.31	20.65± 0.41
PDBPD/$LiClO_4$(ACN)	1501.43 ± 0.91	17.23± 0.11
PEDOT/KCl(Aq)	598.86 ± 1.15	17.54± 0.08
PEDOT/$LiClO_4$(Aq)	2300.00 ± 3.98	19.54± 0.04

Equivalent circuits of PEDOT prepared in ACN (inset **Figure 6.22**) and aqueous solutions (inset **Figure 6.26** and **Figure 6.27**) of different counter ions ($LiClO_4$ and KCl) showed similar circuit as bare electrodes regardless of electrodes used (GC or ITO electrode). On the other hand, equivalent circuits for GC/PProDOT/$LiClO_4$(ACN),

ITO/PProDOT/$LiClO_4$(ACN) and GC/PDBPD/$LiClO_4$(ACN) consist of R_s, CPE and Z_w placed in series without the R_{ct} component due to the absence of semicircle (inset **Figure 6.23** and **Figure 6.24a**). In the case of ITO/PDBPD/$LiClO_4$(ACN), the equivalent circuit as shown in inset of **Figure 6.24b** consists of two RC circuit in order to fit the EIS data to the two semicircles.

The equivalent circuits for fitting the EIS data were used to extract the value of R_{ct} and the data are tabulated in **Table 6.2**. The resistance of charge transfer of bare GC and ITO electrodes were 4235.71 ± 1.86 Ω/cm^2 and 0.79 ± 0.09 Ω/cm^2, respectively. The R_{ct} value for bare GC was higher than reported in literature (R_{ct} (bare GC) = 3962.95 Ω/cm^2 (Yang *et al.*, 2007a). In contrast, bare ITO has a lower R_{ct} value in comparison to literature (R_{ct} (bare ITO) = 3.40 kΩ/cm^2 (Ahuja *et al.*, 2010)). The GC electrode (0.07 cm^2) has smaller area than ITO electrode (2 cm^2), which accounts for its higher R_{ct} value and the value of R_{ct} (**Table 6.2**) as proportion of R_s value (**Table 6.1**) is smaller for ITO i.e there is probably a larger electronic resistance per unit area for ITO, which would be consistent with a larger iR drop (**Figure 6.7**). The capacitance values were obtained from the bode plot ($C = 1/|Z|$) and found that bare GC and ITO electrodes had capacitance of 1.21 μF and 19.26 μF, respectively. These results showed that ITO electrode had higher value of capacitance compared to GC electrode.

Table 6.2: Resistance and capacitance of polymer coated electrodes.

	Charge transfer resistance, R_{ct} (Ω/cm^2)		**Capacitance, C (μF)**	
	GC	**ITO**	**GC**	**ITO**
Bare	4235.71 ± 1.86	0.79 ± 0.09	1.21 ± 0.01	19.26 ± 0.39
PEDOT/$LiClO_4$(ACN)	176.43 ± 0.79	2.37 ± 0.16	23.94 ± 0.16	22.35 ± 0.33
PProDOT/$LiClO_4$(ACN)	-	-	6.96 ± 0.01	18.93 ± 0.25
PDBPD/$LiClO_4$(ACN)	-	47.98 ± 2.15	0.15 ± 0.01	9.77 ± 0.13
PEDOT/KCl(Aq)	4290.00 ± 0.74	3.15 ± 0.04	1.26 ± 0.01	12.96 ± 0.20
PEDOT/$LiClO_4$(Aq)	6605.71 ± 8.28	3.52 ± 0.23	1.29 ± 0.01	14.09 ± 0.19

Upon deposition of PEDOT on GC electrode (prepared in ACN), it was observed that diameter of the semicircle decreased, indicating the R_{ct} decreased significantly, which was 24-order of magnitude lower than that of the bare GC electrode. However, this phenomenon was not observed in the case of PEDOT coated ITO electrode. This result implies that PEDOT enhance or facilitate the charge transfer on the GC electrode but not in the case of ITO electrode.

PEDOT prepared in aqueous solutions ($LiClO_4$ or KCl) for both GC and ITO electrodes showed higher R_{ct} as compared to the bare electrodes. These results are in good agreement with the CV measurements (**Figure 6.13** and **Figure 6.16**), in which the separation of peak was higher than bare GC (ΔE_p = 75 mV) and bare ITO electrode (ΔE_p = 180 mV) electrodes.

It was observed that ITO/PDBPD/$LiClO_4$(ACN) displayed extremely high R_{ct} compared to the other polymer film coated ITO electrodes. The reasons for this phenomenon were mainly the compact structure and the hydrophobicity properties of PDBPD (as reported in **Chapter 5**).

Generally, the capacitance values of polymer film coated GC electrodes are higher compared to polymer film coated ITO electrodes (**Table 6.2**). Comparison was made for the same electrode used and it was found that PEDOT prepared in ACN was highly capacitive compared to PProDOT and PDBPD prepared under the same experimental condition (10 mM monomer, 20 scans). This result is in accordance with the CV measurements (**Figure 6.8** and **Figure 6.13**) and indicates the PEDOT is suitable to be used as solid contact in all-solid-state ion-selective electrodes (Bobacka, 1999) and fuel cell applications (Groenendaal *et al.*, 2000). On the other hand, PDBPD showed the lowest capacitance, hence it is not suitable for battery applications but is possibly good for sensing devices.

To study the effect of nature of solvent and counter anion on the capacitance, the impedance of PEDOT prepared in 0.1 M $LiClO_4$ (or 0.1 M KCl) in aqueous solution was

measured and the value of capacitance was calculated. As can be seen in **Table 6.2**, the capacitance is strongly dependent on the medium but weakly dependent on the supporting electrolyte used to prepare the polymer films.

6.3.4.5 Kinetics of Electron Transfer

EIS measurement can be used to evaluate the effect of polymer films on the kinetics of redox reaction at a GC electrode. The kinetics of electron transfer at the interface of polymer film|solution can be analysed using Butler-Volmer equation (Bard and Faulker, 2001). The exchange current (i_o) is given as:

$$\begin{aligned} i_o &= nFAk_o C_{Ox} \exp\left[-\alpha nF(E_{dc} - E^o/(RT)\right] \\ &= nFAk_o C_{Red} \exp\left[(1-\alpha)nF(E_{dc} - E^o)/(RT)\right] \end{aligned} \quad \textbf{(6.2)}$$

where:

n	number of electrons involved in the electrode reaction
F	Faraday constant (96, 485 C mol^{-1})
A	area of electrode (cm^2)
k_o	rate constant (cm s^{-1})
C_{ox}	bulk concentration of oxidised species (M)
C_{Red}	bulk concentration of reduced species (M)
α	symmetry factor (transfer coefficient)
E_{dc}	equilibrium dc potential (V)
E^o	formal potential of redox couple (V)
R	universal gas constant (8.3142 J K^{-1} mol^{-1})
T	temperature (K)

In the EIS measurements, the conditions used were $E_{dc} = E^o$ and $C_{ox} = C_{Red} = C$**.** As a result, **Equation (6.2)** can be simplified as (Bard and Faulker, 2001):

$$i_o = nFAk_o C \quad \textbf{(6.3)}$$

The resistance of charge transfer (R_{ct}) is defined as (Bard and Faulker, 2001):

$$R_{ct} = \frac{RT}{nFi_o} \tag{6.4}$$

Combination of **Equation (6.3)** and **(6.4)** gives

$$k_o = \frac{RT}{n^2F^2R_{ct}AC} \tag{6.5}$$

Equation (6.5) is used to calculate the rate constant (k_o) and the R_{ct} value is obtained by fitting the EIS data to the equivalent circuit. k_o value for bare GC (k_o = 0.00257 cm s^{-1}) is in agreement with the result reported in literature (k_o = 0.0028 cm s^{-1}) (Heiduschka and Dittrich, 1992) for ferri/ferrocyanide. As can be seen in **Table 6.3**, k_o value for GC/PEDOT/$LiClO_4$(ACN) was significantly high since the resistance of charge transfer is low. This value is higher compared to the value of PEDOT doped with PSS coated on Pt (k_o = 0.0038 – 0.0232 cm s^{-1}) (Sundfors *et al.*, 2002). The values k_o of PProDOT and PDBPD coated GC electrodes could not be estimated but are high as indicated by the absence of semicircle (no R_{ct}) as seen in **Figure 6.23a** and **Figure 6.24a**, indicating the electron transfer is very facile.

Table 6.3: Rate constant (k_o) of polymer film coated GC electrodes calculated from Equation 6.5.

Sample	**k_o (10^{-3} cm s^{-1})**
Bare GC	2.57 ± 0.02
GC/PEDOT/$LiClO_4$(ACN)	61.58 ± 3.70
GC/PProDOT/$LiClO_4$(ACN)	-
GC/PDBPD/$LiClO_4$(ACN)	-
GC/PEDOT/KCl(Aq)	2.21 ± 0.01
GC/PEDOT/$LiClO_4$(Aq)	1.64 ± 0.03

6.4 Conclusions

The results presented in this work showed that doping and dedoping processes occur when polymer film was oxidised and reduced at high and low potential, respectively. CV measurements in a solution containing redox probe revealed that the electrodes were not fully covered by polymer films except PDBPD film, indicating the existence of pinholes. Since PEDOT showed large capacitive current, it has the potential to be used as solid contact in all-solid-state ion-selective electrode and fuel cell applications that require charge storage, whereas PDBPD could be good for sensing due to its low capacitance. As indicated by Bobacka *et al*. (1999), high capacitance is required for the potential stability of all-solid-state ion-selective electrodes. In addition, PEDOT has shown dense and smoother morphology compared to PProDOT and PDBPD (Chapter 5). As a result, PEDOT has been chosen to be used as a solid contact for potentiometric studies that will be explained in Chapter 7.

It was found that the R_{ct} values of polymer film coated ITO electrodes were lower compared to polymer film coated GC electrodes. The capacitance of PEDOT coated electrodes are strongly dependent on the medium but not the counter ion used. The heterogeneous rate constant (k_o) showed that the electron transfer between $Fe(CN)_6^{3-/4-}$ and GC/PEDOT/$LiClO_4$(ACN) was facile, idicating a conducting polymer.

References

Ahuja, T., Rajesh, Kumar, D., Tanwar, V. K., Sharma, V., Singh, N. and Biradar, A. M. (2010) An Amperometric Uric Acid Biosensor Based on Bis[sulfosuccinimidyl] suberate Crosslinker/3-aminopropyltriethoxysilane Surface Modified ITO Glass Electrode. *Thin Solid Films.* 519**.** 1128-1134.

Bard, A. J. and Faulker, L. R. (2001) *Electrochemistry Methods, Fundamentals and Applications.* (2nd ed.). New York, John Wiley & Sons.

Bobacka, J. (1999) Potential Stability of All-Solid-State Ion-Selective Electrodes Using Conducting Polymers As Ion-to-Electron Transducers. *Analytical Chemistry.* 71**.** 4932-4937.

Bobacka, J., Lewenstam, A. and Ivaska, A. (2000) Electrochemical Impedance Spectroscopy of Oxidized Poly(3,4-Ethylenedioxythiophene) Film Electrodes in Aqueous Solutions. *Journal of Electroanalytical Chemistry.* 489**.** 17-27.

Bull, R. A., Fan, F. R. F. and Bard, A. J. (1982) Polymer-Film on Electrodes. 7. Electrochemical-Behavior at Polypyrrole-Coated Platinum and Tantalum Electrodes. *Journal of the Electrochemical Society.* 129**.** 1009-1015.

Cao, C. N. (1990a) On The Impedance Plane Displays for Irreversible Electrode Ractions Based on The Stability Conditions of The Steady-State. II, Two State Variables Besides Electrode Potential *Electrochimica Acta.* 35**.** 837-844.

Cao, C. N. (1990b) On The Impedance Plane Displays for Irreversible Electrode Reactions Based on The Stability Conditions of The Steady-State. I, One State Variable Besides Electrode Potential. *Electrochimica Acta.* 35**.** 831-836.

Chen, P. H., Fryling, M. A. and Mccreery, R. L. (1995) Electron Transfer Kinetics at Modified Carbon. Electrode Surfaces: The Role of Specific Surface Sites. *Analytical Chemistry.* 67**.** 3115-3122.

Cline, K. K., Mcdermott, M. T. and Mccreery, R. L. (1994) Anomalously Slow Electron Transfer at Ordered Graphite Electrodes: Influence of Electronic Factors and Reactive Sites. *The Journal of Physical Chemistry.* 98**.** 5314-5319.

Dai, T., Qing, X., Lu, Y. and Xia, Y. (2009) Conducting Hydrogels with Enhanced Mechanical Strength. *Polymer.* 50**.** 5236-5241.

Deepa, M., Bhandari, S. and Kant, R. (2009) A Comparison of Charge Transport Behavior in Functionalized and Non-Functionalized Poly 3,4-(ethylenedioxythiophene) Films. *Electrochimica Acta.* 54**.** 1292-1303.

Groenendaal, B. L., Jonas, F., Freitag, D., Pielartzik, H. and Reynolds, J. R. (2000) Poly(3,4-Ethylenedioxythiophene) and Its Derivatives: Past, Present, and Future. *Advanced Materials.* 12**.** 481-494.

Heiduschka, P. and Dittrich, J. (1992) Impedance Spectroscopy and Cyclic Voltammetry at Bare and Polymer Coated Glassy Carbon Electrodes *Electrochimica Acta.* 37**.** 2573-2580.

Kirchmeyer, S. and Reuter, K. (2005) Scientific Importance, Properties and Growing Applications of Poly(3,4-Ethylenedioxythiophene). *Journal of Materials Chemistry.* 15**.** 2077-2088.

Lu, X. Q., Liao, T. L., Ding, L., Liu, X. H., Zhang, Y., Cheng, Y. and Du, J. (2008) Interaction of Quercetin with Supported Bilayer Lipid Membranes on Glassy Carbon Electrode. *International Journal of Electrochemical Science.* 3**.** 797-805.

Melato, A. I., Viana, A. S. and Abrantes, L. M. (2008) Different Steps in the Electrosynthesis of Poly(3,4-Ethylenedioxythiophene) on Platinum. *Electrochimica Acta.* 54**.** 590-597.

Oliveira-Brett, A. M., Brett, C. M. A. and Silva, L. A. (2002) An Impedance Study of the Adsorption of Nucleic Acid Bases at Glassy Carbon Electrodes. *Bioelectrochemistry.* 56**.** 33-35.

Richardson-Burns, S. M., Hendricks, J. L., Foster, B., Povlich, L. K., Kim, D. H. and Martin, D. C. (2007) Polymerization of the Conducting Polymer Poly(3,4-ethylenedioxythiophene) (PEDOT) Around Living Neural Cells. *Biomaterials.* 28**.** 1539-1552.

Sundfors, F., Bobacka, J., Ivaska, A. and Lewenstam, A. (2002) Kinetics of Electron Transfer between $Fe(CN)_6^{3-/4-}$ and Poly(3,4-ethylenedioxythiophene) Studied by Electrochemical Impedance Spectroscopy. *Electrochimica Acta.* 47**.** 2245-2251.

Yang, J., Yang, T., Feng, Y. and Jiao, K. (2007) A DNA Electrochemical Sensor Based on Nanogold-Modified Poly-2,6-pyridinedicarboxylic Acid film and Detection of PAT Gene Fragment. *Analytical Biochemistry.* 365**.** 24-30.

Zykwinska, A., Domagala, W. and Lapkowski, M. (2003) ESR Spectroelectrochemistry of Poly(3,4-ethylenedioxythiophene) (PEDOT). *Electrochemistry Communications.* 5**.** 603-608.

CHAPTER 7

ALL-SOLID-STATE ION-SELECTIVE ELECTRODES BASED ON PEDOT DOPED WITH BULKY ANIONS

7.1 Introduction

Potentiometric measurements are attractive due to the possibility of miniaturisation. It is relatively easy to make small size, portable and low cost instrumentation for potentiometric measurements. In conventional potentiometric ion sensor or ion-selective electrode (ISE), the ion-to-electron transduction takes place at the internal reference electrode (Ag/AgCl) (**Equation (7.1)**) that is immersed in the inner filling solution (**Figure 7.1a**).

$$\mathrm{AgCl}\,(s) + \mathrm{e}^- \rightleftharpoons \mathrm{Ag}\,(s) + \mathrm{Cl}^- \qquad \textbf{(7.1)}$$

The selectivity of ISE is based on the ionophore immobilised in the ion-selective membrane (ISM). The interest in the development of ISEs has increased significantly as the limit of detection of conventional ISE can be lowered to picomolar level (Sokalski *et al.*, 1997) as the ion fluxes in the membrane are controlled by using buffer solution in order maintain a low activity of primary ion in the inner filling solution (**Figure 7.2**). However, the use of inner filling solution could be a serious limitation in developing a durable, robust, easy to miniaturise and maintenance free ISE due to the limit of temperature range in sensor operation that can give rise to undesired ionic fluxes in the membrane. The all-solid-state ISE (ASSISE) without internal filling solution is one of the best alternatives (Nikolskii and Materova, 1985) to fulfill these criteria. However, the fabrication of ASSISE needs careful design of solid contact between the ISM and electronic conductor (*e.g.* glassy carbon, gold and platinum) (Nikolskii and Materova, 1985).

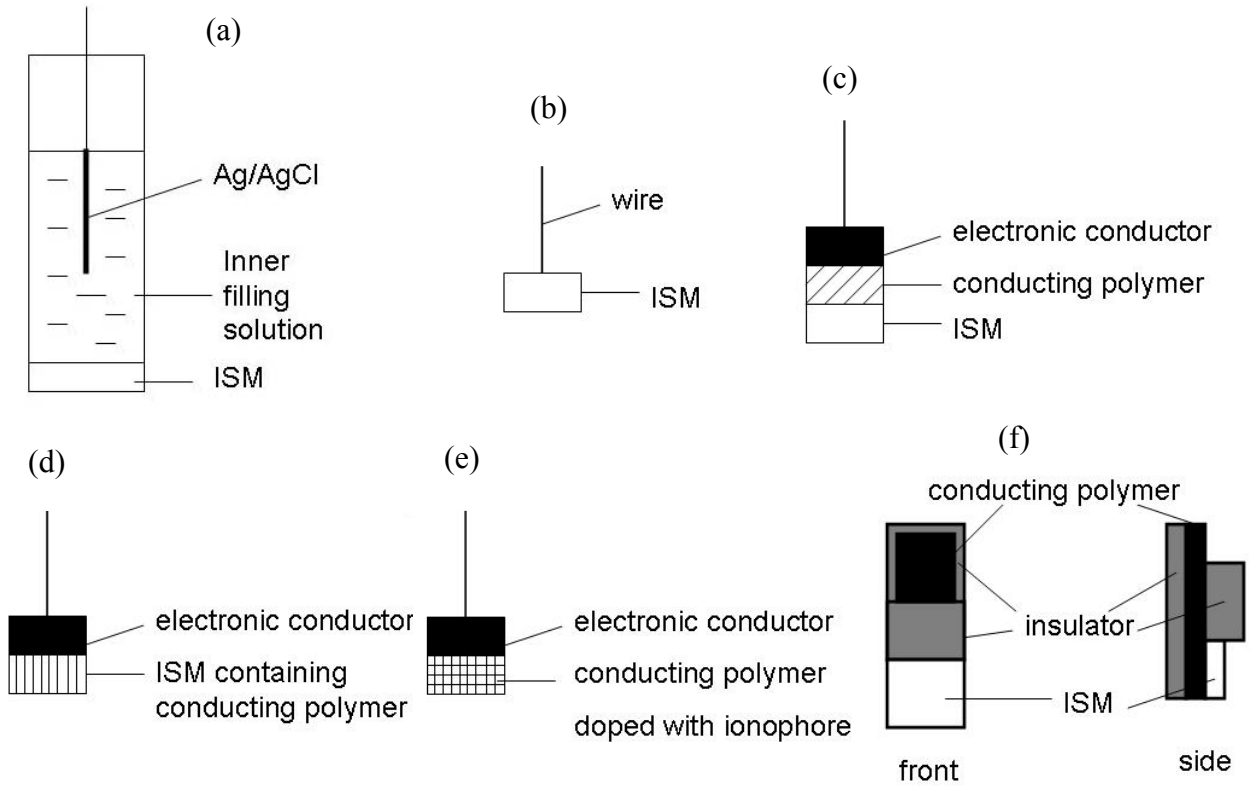

Figure 7.1: (a) Conventional ISE; (b) coated-wire electrode (CWE); (c-e) solid-state ion-selective electrode: (c) CP as a transducer (d) CP incorporated with ISM (single piece all-solid state) (e) CP doped with ionophore (f) all-plastic electrode. CP: conducting polymer. ISM: ion-selective membrane.

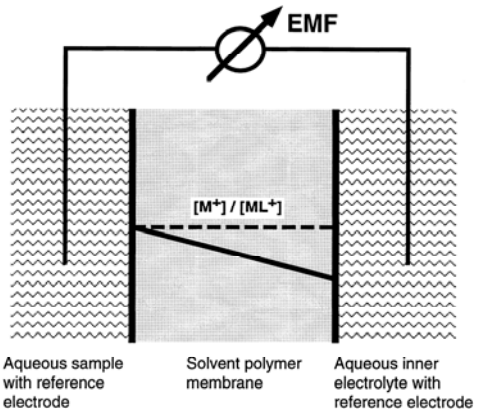

Figure 7.2: Schematic showing the setup and concentration profiles in ion-selective membrane at steady state. In conventional systems (dashed line), slight disturbances induce a flow of M^+ toward the sample, thus biasing its activity at the corresponding membrane surface. This is prevented by the gradient (solid line) (Sokalski *et al.*, 1997).

The so called coated-wire electrode (CWE) (**Figure 7.1b**) was the first concept put forward to obtain simple and robust ASSISEs (Cattrall and Freiser, 1971). CWEs have shown to produce linear response ranges and selectivities comparable with the conventional ISE (Cattrall and Freiser, 1971, Cattrall and Hamilton, 1984). However, this simple set up has major drawbacks such as irreproducibility and drift in the electrode potential due to the poorly defined ion-to-electron transduction (blocked interface) between ionically conducting ISM and electronic conductor (Buck, 1980).

In a conventional ISE, the membrane is in contact with two solutions *i.e.* symmetric configuration (**Figure 7.3a**). The transduction signal in the membrane takes place by ion transfer not by electron transfer. Thus, highly plasticized PVC membranes have been used in order to obtain a sufficiently high mobility in the membrane. A typical PVC-based membrane contains about 66% plasticiser (Bakker *et al.*, 1997). On the other hand, in ASSISE, the ion-to-electron transduction process is asymmetric (**Figure 7.3b**) which involves transfer of ion and electron at the membrane|solution and electronic conductor|membrane interface, respectively.

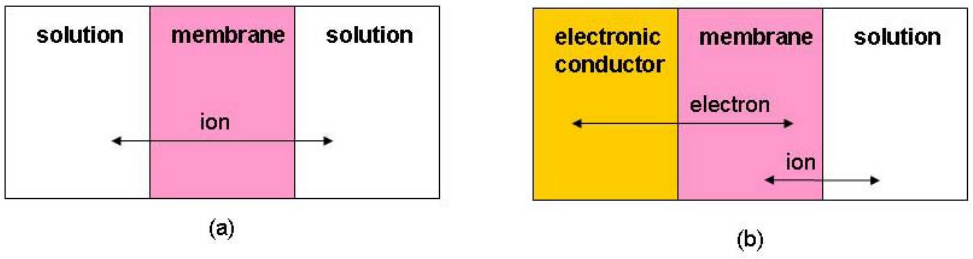

Figure 7.3: Schematic diagram of charge transport (a) symmetric (conventional ion-selective electrode) and (b) asymmetric (all-solid-state ion-selective electrode) (Bobacka *et al.*, 1999) .

Since the fundamental concept in solid-state ISEs is a well-defined pathway for ion-to-electron transduction, much effort has been put into improving the stability of the potential by placing a mediator between the electronic conductor and ISM such as hydrogel (Vandenvlekkert *et al.*, 1988), self-assembled monolayers (Fibbioli *et al.*, 2000,

Fibbioli *et al.*, 2002) and redox polymers (Hauser *et al.*, 1995). However, hydrogel-contact ISEs have some drawbacks due to water uptake/release and resulting volume changes of the hydrogel layer (Lindner *et al.*, 1993). Another approach to solid-state ISEs is based on the modification of the coated-wire electrodes by introducing an intermediate layer of suitable redox and ion-exchange properties between the electronic conductor and the ISM (Nikolskii and Materova, 1985). According to Fibbioli *et al.* (2000), even the application of a monolayer of redox-active compound allows a well-defined pathway for ion to electron transduction. However, a monolayer has the limitation that it has inherently low redox capacitance (C_{redox}). For asymmetric process (ion-to-electron transduction), high redox capacitance is required in order to minimize the polarisability of the solid contact (**Equation (7.2)**) (Bobacka, 1999). The C_{redox} is related to potential drift ($\Delta E/\Delta t$) and the current (i) (**Equation (7.2)**).

$$\frac{\Delta E}{\Delta t} = \frac{i}{C_{redox}} \qquad \textbf{(7.2)}$$

The problems described above prompted the interest in the use of conducting polymers (CPs) as ion-to-electron transducers. CP-based potentiomeric ion sensors were reported for the first time by Dong *et al*. (1988a). In the early reports after the discovery of CPs, the applications were focused on the use of CPs as membranes for potentiometric sensors which is alternative to classical ISM (Bobacka *et al.*, 2003). However, CPs were found unsuitable as an alternative membrane due to interference caused by the presence of redox reactants in solution (Bobacka *et al.*, 1994a, Michalska *et al.*, 1995, Michalska *et al.*, 2001), poor ionic selectivity of the CP membranes (Cadogan *et al.*, 1992a, Cadogan *et al.*, 1992b, Michalska and Lewenstam, 2000) and pH changes (Michalska and Maksymiuk, 1999, Michalska *et al.*, 1995, Qian *et al.*, 1993).

On the other hand, CPs have shown to be a promising material as solid contacts to fabricate ISE free from internal filling solution (Bakker *et al.*, 1997), due to the ionic and electronic conductivity of this material. These unique properties allow the CP to transduce an ionic signal into an electronic signal. The electrical conductivity is due to

formation of charge carriers in the polymer backbone as described in **Chapter 2**. The use of CP as a transducer has overcome the problem of the blocked interface as charge transfer can occur reversibly at both interfaces *i.e.* CP|ISM interface (ion transfer) and electronic conductor|CP interface (electron transfer). Since the first literature reported on this type of configuration (Cadogan *et al.*, 1992a), many studies have been carried out to study in depth this approach.

In general, two approaches can be used to construct the CP-based ASSISEs. A CP can be placed between the electronic conductor and ISM (**Figure 7.1c**) or dissolved in the ISM (so-called single piece all-solid-state electrode (SPISE)) (**Figure 7.1d**). In the first approach, the CP is electropolymerised on the surface of electronic conductor, then coated with ISM. In this approach, the CP acts as the ion-to-electron transducer (solid contact) and the ion selectivity is determined by the ISM. The system is schematically depicted in **Figure 7.4**. In this system, ion transfer occurs reversibly at both ISM|solution and CP|ISM interfaces. The ionic signal is converted to electronic signal by CP film and the electron transfer occurs at electronic conductor|CP interface.

The principle of ion-to-electron transduction (**Equation (7.3)**) of CP is quite similar to the mechanism of the process at the internal reference electrode of the conventional or hydrogel-contact ISE. This type of ISE uses the high selectivity properties of ionophore-based membranes combined with the ion exchange and redox properties of conducting polymers. This type of ASSISE was initially reported using polypyrrole (PPy) by Cadogan *et al*. (1992a). Bobacka *et al*. have used a number of CPs, such as poly(3-octylthiophene) (POT) (Bobacka *et al.*, 1994b), polypyrrole (PPy) (Bobacka, 1999), and poly(3,4-ethylenedioxythiophene) (PEDOT) (Bobacka *et al.*, 2002) for the construction of this type of ASSISE.

$$M^+A^- + e^- \rightleftharpoons M + A^- \qquad \textbf{(7.3)}$$

where:

M^+ metal ion (e.g Ag^+) or oxidised conducting polymer

M metal (e.g Ag) or neutral conducting polymer

A^- anion (e.g. Cl^-)

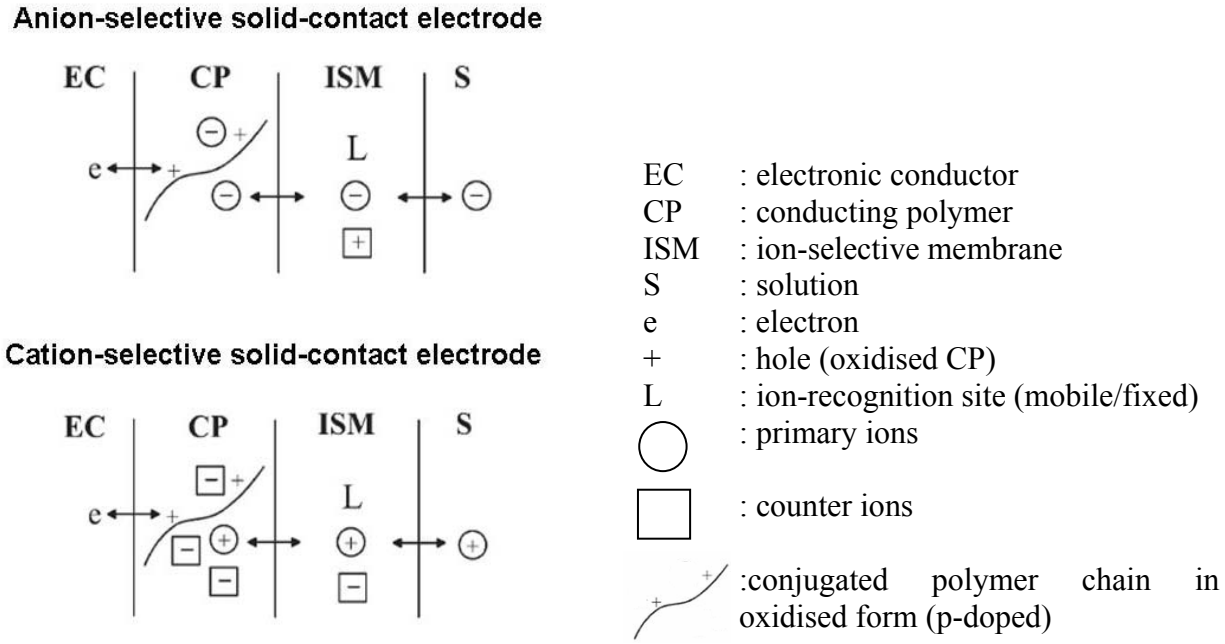

Figure 7.4: Principle of solid-contact ISEs based on conducting polymer as ion-to-electron transducer (Bobacka, 2006).

The latter approach (SPISE) requires the CP to be soluble in tetrahydrofuran (THF) or any other organic solvent that is commonly used as a solvent to dissolve the membrane components during the preparation of plasticized PVC-based ISEs. This configuration makes the construction of ISE simpler and has a potential for mass production. In this concept, the CP is dispersed in the ISM and the ion sensor can easily be prepared in one step either by solution casting, dip coating or spin coating. As a result, the CP can be physically integrated within the ISM and the composition of the membrane can be controlled accurately. However, the CP may affect the selectivity of the ISE depending on the quantity of the CP in the membrane (Bobacka *et al.*, 1995, Lindfors *et al.*, 1999).

Bobacka *et al*. (1995) have succeeded in applying this SPISE concept to making Li^+ and Ca^{2+} electrodes. They studied two soluble CPs *i.e.* poly(3-octylthiophene) (5-25% w/w) in its undoped state and PAn (protonated) doped with bis(2-ethyl)hydrogen phosphate (1-2% w/w). The calibration curves revealed near-Nernstian responses and no redox interference was observed as the concentration of CP was low. It was also found that the incorporation of PAn in the Ca^{2+} membrane improved the stability compared to CWE without the presence of CP in the membrane phase (Bobacka *et al.*, 1995, Lindfors *et al.*, 1996). For Li^+ sensors, the reproducibility of the potential measured was significantly improved by the incorporation of 1% and 2% PAn. It was also observed that 1% PAn improved the sensitivity towards Li^+ but deteriorated when 2% PAn was used in comparison to Li coated-wire electrode (Lindfors *et al.*, 1999). Thus, the optimum amount of PAn in ISM appeared to be 1% even though the amount was low. Both approaches have shown to improve the long term potential stability compared to coated wire (Bobacka *et al.*, 1995, Lindfors *et al.*, 1999).

Both concepts of ASSISE explained above use a plasticized PVC containing ionophore that governs the selectivity behaviour of the ISE and the CP acts as an ion-to-electron transducer. Another possibility to make CP-based ASSISE is the incorporation of an ion-recognition site (ionophore) directly into the conducting polymer matrix (**Figure 7.1e**). The principle of this system is shown in **Figure 7.5**. The incorporation of ionophore can be obtained by doping the CP with metal-complexing ligands (Migdalski *et al.*, 1996) or by covalent binding of ion recognition sites (Garnier, 1989, Marsella and Swager, 1993, Youssoufi *et al.*, 1994) to the conjugated polymer chain. The main challenge of this configuration is to enhance the ion selectivity and at the same time the redox response of CP has to be suppressed. In order to optimise the ion recognition and transduction processes, this approach requires precise and careful control of both electronic and ionic transports of the membrane. Therefore, it seems this concept is still a long way from practical use in chemical sensors.

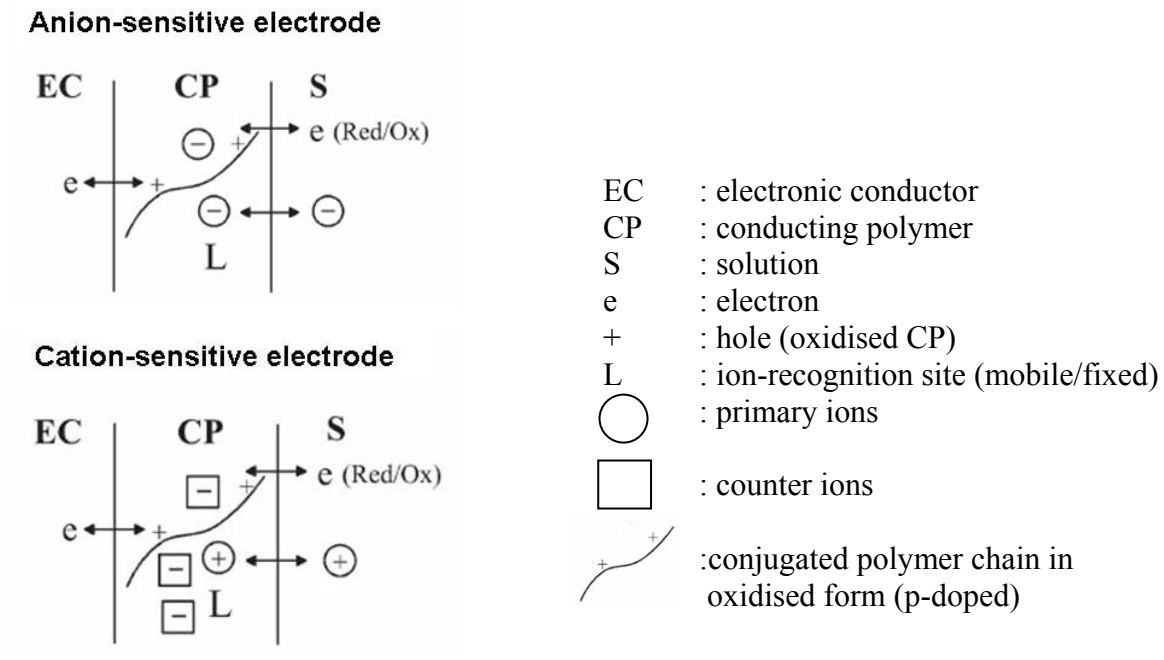

Figure 7.5: Principle of solid-contact ISEs based on conducting polymer as sensing membrane (Bobacka, 2006).

The cost of production of ASSISE based on CP can be lowered by eliminating the use of common electronic conductors (carbon, gold etc). This approach has been proposed by Michalska *et al*. (2004a) using ASS sensors solely based on polymeric materials (**Figure 7.1f**). This concept is called 'all-plastic electrode' as it only consists of synthetic materials. This configuration makes this ISE very flexible, relatively low cost and easy to miniaturise. This sensor was obtained by casting an aqueous suspension of PEDOT doped with poly(4-styrenesulfonate) ions (PEDOT-PSS, Baytron P) onto an insulating plastic substrate. So far, this type of electrode have been used for Ca^{2+} (Michalska and Maksymiuk, 2004a), K^{+} (Michalska and Maksymiuk, 2004a) and Cu^{2+} (Michalska *et al.*, 2005) sensors. The conducting polymer layer served both as electrical contact and as ion-to-electron transducer.

Sundfors *et al.* (2006) has shown that fabrication of solid-state ion selective microelectrodes is also possible. A recessed electrode of gold wire was prepared before being coated by PEDOT/PSS. The remaining cavity was then filled by either a potassium

or a calcium-selective cocktail. These ion-selective microelectrodes have been shown to have similar potentiometric characteristics as conventional electrodes.

It is expected that ASSISE based on CP without the present of liquid phase will result in lower detection limits (Bakker and Pretsch, 2002). However, from the literature cited, this phenomenon does not occur. Nikolskii and Materova (1985) have identified three conditions to obtain a stable ISE with a solid internal contact.

- Reversible transition from ionic to electronic conductivity
- Sufficiently high exchange currents in comparison with the current passed during measurements
- No side reactions parallel to the main electrode reaction.

The first condition can be fulfilled by CPs as they can behave as ion-to-electron transduction. Some CPs have also shown to have large redox capacitance resulting from the reversible oxidation/reduction of the polymer film with simultaneous ion transfer (doping) that can satisfy the second condition.

It is known that ISMs are oxygen permeable (Cattrall *et al.*, 1975, Hulanicki and Trojanowicz, 1976) and it is worth investigating the factors that could influence the potential stability of ISEs. The third condition will be fulfilled if CP does not interact with gases such as O_2 and CO_2 that may cross the ISM. However, Li and Qian (1993) has shown that potential of CPs may be influenced by the O_2/H_2O redox couple. CO_2 could also interfere by changing the pH at the CP solid contact (Dong *et al.*, 1988b, Maksymiuk *et al.*, 2000). These side reactions may result in instability of the potential of the ISEs. Based on the criteria mentioned above, PEDOT was found to be a suitable as a solid contact as it has low sensitivity to O_2 and CO_2 (solution pH changes) compared to PPy (Vázquez *et al.*, 2002). It is also found that high capacitance of PEDOT that acts as ion-to-electron transducer stabilise the electrode potential (Bobacka, 1999).

CPs can be electropolymerised in aqueous solution with bulky molecules as doping anions such as polystyrene sulfonate (PSS) (Groenendaal *et al.*, 2000) and hyaluronic acid (HA) (Asplund *et al.*, 2008, Collier *et al.*, 2000). PSS (**Figure 7.6a**) is a surfactant that was found to facilitate the electropolymerisation process (Tamburri *et al.*, 2009). HA (also called hyaluronan) is a glucosaminoglycan that is present in the intercellular matrix of most vertebrates and in neural tissue. It is a linear polymer that consists of alternating disaccharide units of D-glucuronic acid and N-acetyl-D-glucosamine, linked by alternating β-1,4 and β-1,3 glycosidic bonds (**Figure 7.6b**). It has been shown that potentiometric responses of ASSISE based on CP can be relatively simply tailored. CPs doped with small and easily exchangeable anions behaved as anion sensitive, whereas polymer film containing immobolised bulky anions usually give cationic potentiometric responses (Dong and Che, 1991, Hulanicki and Michalska, 1995, Migdalski *et al.*, 1999). In this work, PEDOT doped with bulky anion *i.e.* PSS and HA were prepared on glassy carbon and the cationic potentiometric responses were investigated. The performance of ion-selective microelectrodes based on PEDOT/PSS as solid contact was also studied for measurements in real samples.

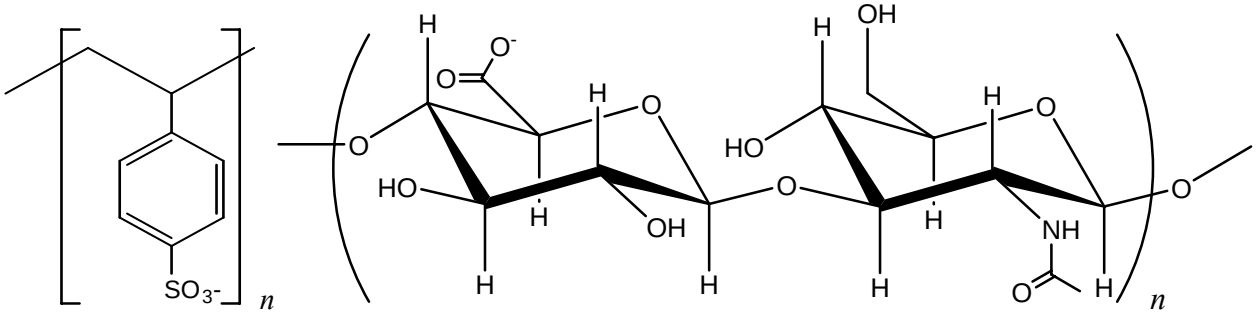

Figure 7.6: Chemical structure of (a) poly(styrenesulfonate) (PSS) and (b) hyaluronic acid (HA).

7.2 Experimental

7.2.1 Chemicals and Reagents

Hyaluronic acid sodium salt from *streptococcus equi*, potassium chloride (KCl), potassium hydroxide (KOH) and plant agar were obtained from Sigma, UK. Poly(sodium 4-styrenesulfonate), (NaPSS) (M_w ~70,000), 3,4-ethylenedioxythiophene (EDOT), calcium chloride ($CaCl_2$) and sodium chloride (NaCl), chlorotrimethylsilane were obtained from Aldrich, UK. Lithium chloride (LiCl) and magnesium chloride ($MgCl_2$) were purchased from BDH. Tetrahydrofuran (THF) was obtained from Fisher, UK. Poly(vinyl chloride) (PVC), 2-nitrophenyl octyl ether (*o*-NPOE), dioctyl sebacate (DOS), calcium ionophore ETH1001, potassium ionophore I (valinomycin), sodium ionpohore X and potassium tetrakis (4-chlorophenyl borate) (KTpClPB) were supplied from Fluka, UK. All chemicals were used as received without any further purification. Carbon fibres were obtained from Specialty Materials (Massachusetts, USA) while borosilicate glass capillaries were obtained from Harvard Apparatus Ltd. Murashige and Skoog (MS) medium was purchased from Melford. *Arabidopsis thaliana* seeds were kindly provided by Prof Marc Knight from Biological and Biomedical Science, University of Durham.

7.2.2 Preparation of Polymer Films

An 0.01 M EDOT aqueous solution was prepared using an ultrasonic bath followed by stirring for 3 h. This solution was then used to prepare 5 mg/mL NaPSS and 1 mg/mL HA. Low concentration of HA was used as a high viscosity of the HA solution will be formed as a result of the formation of hydrogen bond in aqueous solution.

Glassy carbon (GC) (Bioanalytical System Inc.), Ag/AgCl (3.5 M KCl) and Pt plate was used as working electrode, reference electrode and counter electrode, respectively. GC electrodes were cleaned by hand-polished on microcloth pad with aqueous alumina slurry 0.05 μm followed by thorough rinsing with deionised water. The

electrode was then cleaned ultrasonically in deionised water for a few minutes to remove any trace alumina from the surface.

All polymerisations were made using a multichannel potentiostat, model VMP (Perkin-Elmer Instruments). PEDOT films were obtained by galvanostatic electrochemical polymerisation from aqueous solution at current density of 0.2 mA/cm^2 for 600 s and yielded 120 mC/cm^2. The obtained PEDOT doped with PSS (or HA) were rinsed with deionised water to remove any unreacted monomer. The morphology of polymer films was analysed by Hitachi SU70 (Hitachi High Technologies) and the topography of the polymer films was studied with atomic force microscopy (AFM) (Nanoscope IV scanning probe microscope controller, Digital Instruments Inc., Santa Barbara, CA). For AFM measurements, the polymers films were prepared on ITO electrode (Pilkington, UK). The measurements were performed using tapping mode in ambient condition.

For deposition of PEDOT on carbon fibre, a copper wire was attached to carbon fibre using silver epoxy and it was connected to the potentiostat. A Ag/AgCl/ (3.5 M KCl) and platinum flag were used as reference and counter electrodes, respectively.

7.2.3 Fabrication of Ion-Selective Electrode on GC Electrodes

ASSISEs were prepared by fabricating the ion selective membrane on the surface of GC/PEDOT electrode. The calcium-selective membrane contained (in wt %) 1.3% ETH 1001, 0.5% KTpClPB, 65.6% *o*-NPOE and 32.6% PVC; total 200 mg of membrane components were dissolved in 3 mL of THF. For the sodium-selective membrane, the ETH 1001 was replaced by sodium ionophore X. In the case of potassium-selective membrane, the composition (in wt %) was 1.3 % valinomycin, 0.5 % KTpClPB, 65.6 % DOS and 32.6% PVC.

The electrodes with coated electropolymerised polymer films were inverted and 20 µL of THF solution of plastic PVC based membrane components was pipetted on top

of the conducting polymers. The electrodes were then protected from any contamination. After overnight evaporation of the membrane solvent, ASSISEs were conditioned in 0.1 M solution of primary ion (chloride salt) in the absence of galvanostatic polarisation (open circuit) at least 1 day prior to use or applying galvanostatic polarisation by anodic current of 5×10^{-8} A for 6 h.

7.2.4 Fabrication of Ion-selective Microelectrodes

Borosilicate glass capillaries were cleaned with HNO_3 solution followed by rinsing thoroughly with distilled water. The capillaries were then dried in oven at 105 °C. Micropipettes were prepared from dried capillaries using a puller (Sutter Instrument Co. model P-97). The size of the micropipette obtained was measured microscopically (Philip XL30 SEM, Philips/FEI). In order to make the surface of inner wall hydrophobic, it was silanized using chlorotrimethylsilane. This procedure was performed by filling the micropipette with chlorotrimethylsilane using a syringe. The silanized micropipettes were allowed to dry overnight in the oven. The tip of micropipette was filled with ion-selective membrane followed by inserting PEDOT coated carbon fibre (**Figure 7.7a**). The carbon fibre was dipped into the membrane solution about 300 – 500 μm (**Figure 7.7b**) and left overnight. The prepared ion-selective micropipettes were conditioned in 0.1 M solution of primary ion (chloride salt) at least 1 day prior to use. **Figure 7.8** shows the schematic diagram of the ISEs used in this study.

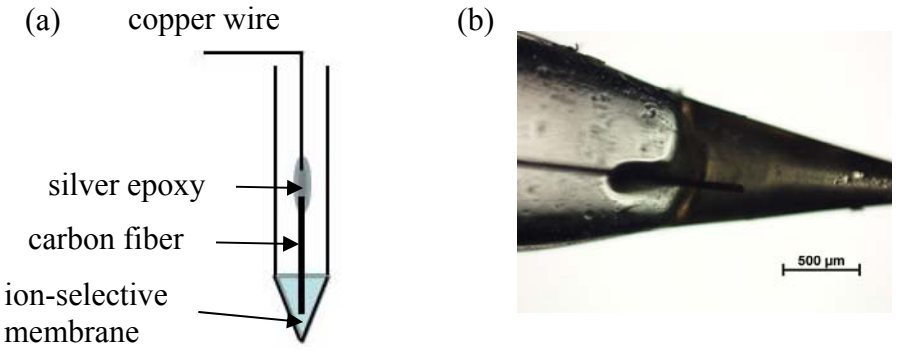

Figure 7.7: (a) Schematic diagram of ion-selective microelectrode (b) image of carbon fibre dipped into the ion-selective membrane.

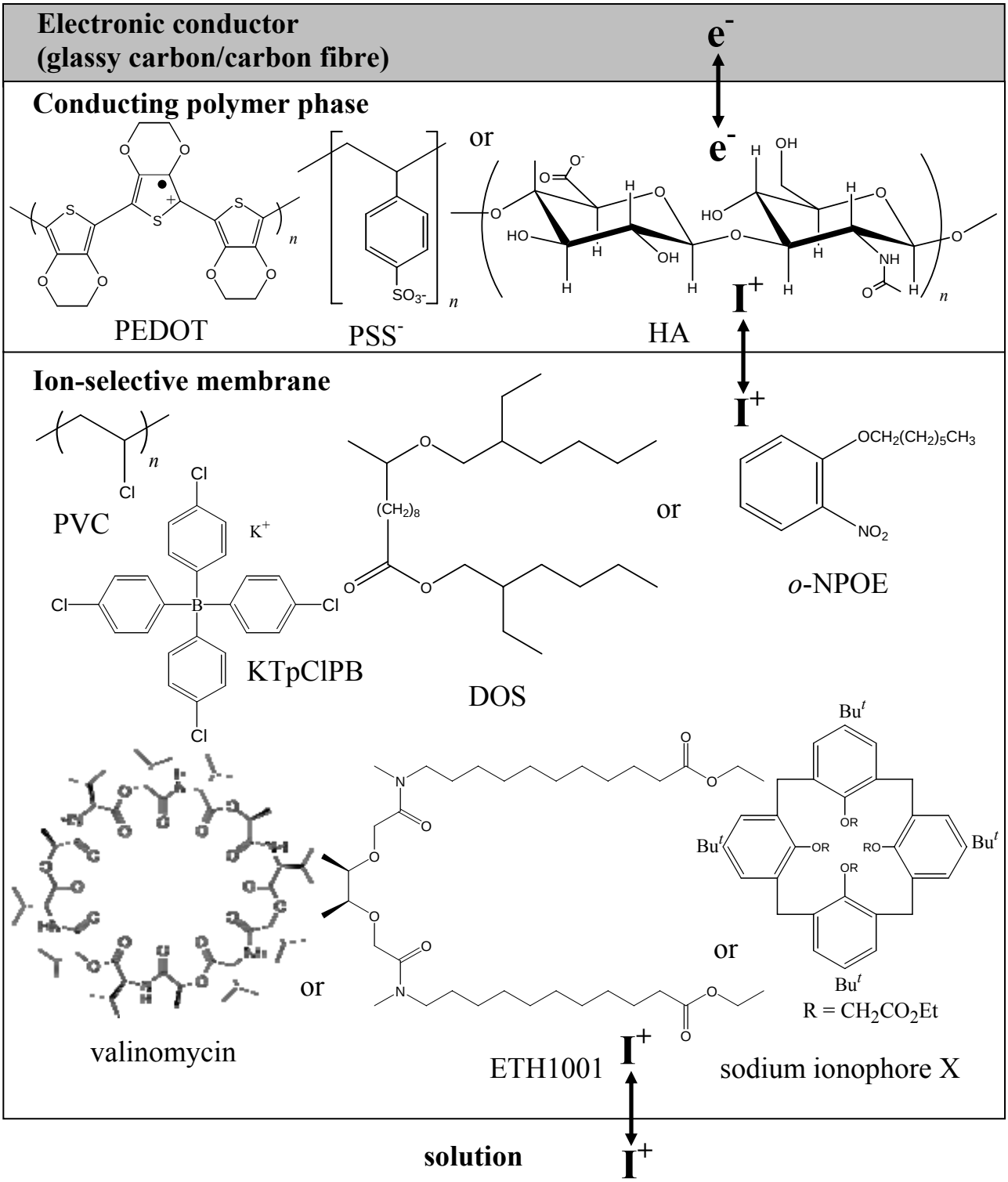

Figure 7.8: Schematic presentation of the electrodes studied in this work, showing the principle of ion-to-electron transduction. I^+ = primary ion.

7.2.5 Potentiometric Measurements

Figure 7.9 shows the set up for the calibration of ISEs using a constant dilution technique as proposed by Horvai (1976). The system consists of constant volume cell where the ISEs were placed. The reference cell was filled with 3.5 M KCl and had a frit that allows contact with the 'washing solution'. The potentiometric measurements were performed with digital multimeter (Thurly Thandar Instruments model 1705) connected to a computer for data acquisition. The reference electrode was a Ag/AgCl. The peristaltic system (Minipuls3, Gilson Inc) was used to obtain constant dilution of the calibrating solutions.

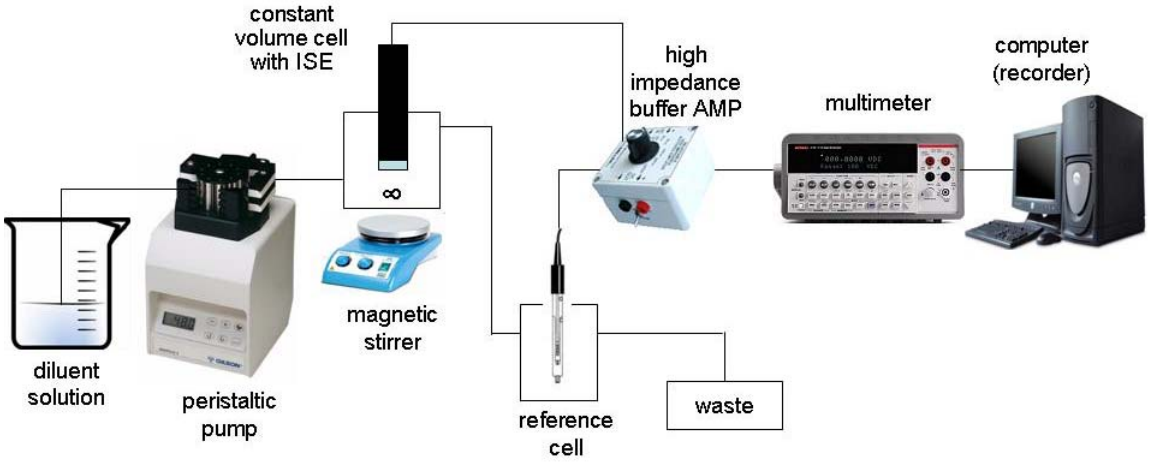

Figure 7.9: Set up for calibration using flow through system.

For a constant volume of flow through cell, a solution contain ion A at concentration C_o can be diluted by passing through a solution without ion A and the concentration of ion A can be calculated.

Let 'C' be the concentration of ion A at any point of time '*t*'

∴ amount of ion A present in constant volume cell = VC

∴ rate of change of the amount of ion A $= \frac{dC}{dt}(VC)$

$$= V\frac{dC}{dt} \qquad \textbf{(7.4)}$$

In a well mixed cell:

rate of accumulation = rate in – rate out + generation

$$V\frac{dC}{dt} = 0 - qc + 0 = -qC$$

$$\frac{dC}{C} = -\frac{q}{V}dt$$

$$\int_{C_O}^{C}\frac{dC}{C} = -\frac{q}{V}\int_{t_o}^{t}dt$$

$$\ln\left(\frac{C}{C_o}\right) = -\frac{q}{V}\left(t - t_o\right)$$

$$C = C_o \exp\left[-\frac{q}{V}\left(t - t_o\right)\right] \qquad \textbf{(7.5)}$$

where:

C concentration at time 't' (M)

C_o initial concentration (M)

t time (s)

t_o initial time (s)

q rate of flow (mL/sec)

V constant volume (mL)

For the calibration of Ca^{2+}-selective electrodes, the constant volume cell was filled with 0.1 M $CaCl_2$ with 0.1 M KCl as a constant ionic background. For K^+-electrodes and Na^+-electrodes, 0.1 M NaCl and LiCl was used as the background solution, respectively. The potential readings were taken until a stable reading was obtained before flowing through the diluent. The activity coefficients were calculated according to Debye-Hückel theory (Meier, 1982):

$$\log \gamma_{\pm} = \frac{-\mathrm{A}\left|z_{+}z_{-}\right|\sqrt{I/I^{\theta}}}{1 + \mathrm{B}\sqrt{I/I^{\theta}}} + \mathrm{C}I \qquad \textbf{(7.6)}$$

where:

A constant value (0.5108 at 25 °C in water)

$|z_+ z_-|$ absolute product of valencies (*i.e.* 1 for uni-univalent electrolytes and 2 for di-univalent electrolytes)

I ionic strength (mol dm^{-3})

I^{θ} 1 mol dm^{-3}

B empirical parameter

C empirical parameter

Electrolyte	Parameter	
	B	C
LiCl	1.3354	0.10790
NaCl	1.4255	0.02626
KCl	1.2796	0.00393
$MgCl_2$	1.7309	0.05195
$CaCl_2$	1.5800	0.04570

The ionic strength (I) was calculated using **Equation (7.7)**:

$$I = \frac{1}{2}\Sigma c_i z_i^2 \qquad \textbf{(7.7)}$$

where:

I ionic strength (mol dm^{-3})

c_i concentration of the ion i (mol dm^{-3})

z_i charge of ion i

The selectivity coefficient was determined by fixed interference method (**Equation (7.8)**) with a constant ionic background of 0.1 M KCl, NaCl, LiCl, $MgCl_2$ or $CaCl_2$. The limit of detection was determined by the method recommended by IUPAC (Buck and Lindner, 1994).

$$K_{A,B}^{pot} = \frac{a_A}{a_B^{Z_A/Z_B}} \quad \textbf{(7.8)}$$

where:

$K_{A,B}^{pot}$ potentiometric selectivity coefficient for ion B with respect to the principal ion A

a_A activity of A obtained from extrapolation of linear portion of emf *vs* logarithm of activity of the primary ion a_A

a_B activity of interfering ion B

z_A charge number: an integer with sign and magnitude corresponding to the charge of primary ion A

z_B charge number: an integer with sign and magnitude corresponding to the charge of interfering ion B

7.2.6 Cyclic Voltammetry

The cyclic voltammetric measurements were performed using a multichannel potentiostat model VMP (Perkin-Elmer Instruments). GC/PEDOT/PSS and GC/PEDOT/HA were used as working electrodes. Pt plate and Ag/AgCl (3.5 M KCl) electrodes were used as counter electrode and reference electrode, respectively. All measurements were performed using a cell with a three-electrode system in deaerated 0.1 M KCl at room temperature.

7.2.7 Measurement in Real Samples

7.2.7.1 Ca^{2+} Measurements For *Arabidopsis Thaliana* Roots

Arabidopsis plants were grown in petri dishes containing MS medium and 0.8% plant agar at 21 °C with 16 h photoperiod (**Figure 7.10a**). The roots were used when four to six-weeks old. The roots were obtained by gripping the green parts of the plant and pulling them out using tweezers. The roots were then washed by distilled water and transferred to 10^{-4} M LiCl solution. The Ca^{2+}-selective microelectrode was placed close to the roots surface (**Figure 7.10b**). The calcium measurements were carried by means of chronoamperometric technique. The temperature was controlled using a cryostat bath (Haake GH) filled with 90% water and 10% ethanol (w/w). The absolute temperature was measured using a thermocouple placed in the solution.

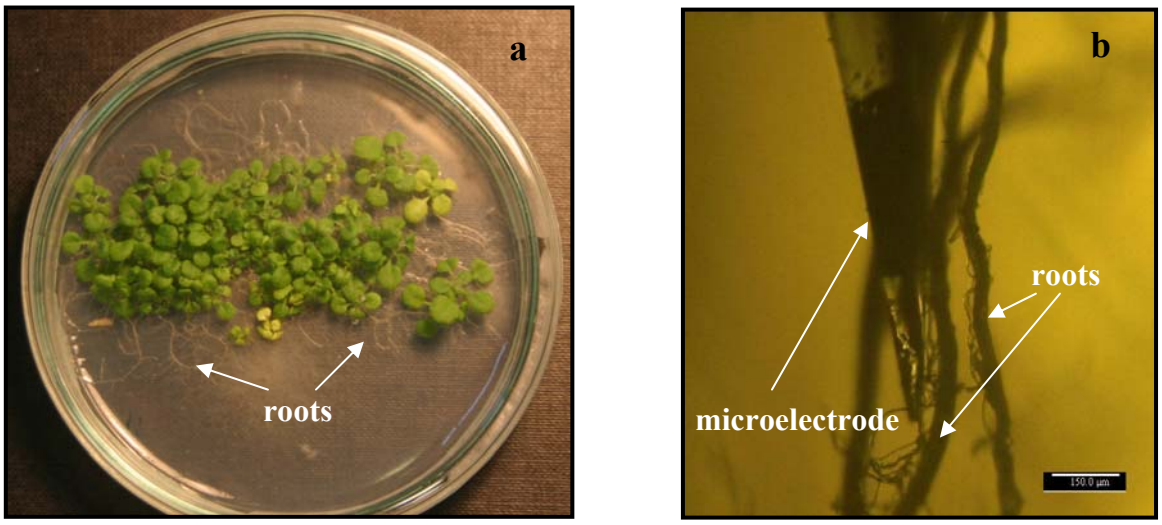

Figure 7.10: (a) *Arabidopsis thaliana* grown in petri dish and (b) typical microelectrode-roots arrangement for calcium and potassium measurements.

7.2.7.2 K^+ Measurement For *Arabidopsis Thaliana* Roots

The roots were washed with distilled water before placing into 1 mL of 10^{-4} M LiCl. The K^+-microelectrode was brought close (37.5 ± 2 μm) to the roots surface as described for calcium measurement. After 5 min, NaCl was added to give a total concentration of 50 mM. The changes of extracellular potassium concentration were measured using a chronoamperometric technique.

7.3 Results and Discussion

7.3.1 Electropolymerisation of PEDOT on GC Electrodes

In this study, GC electrode was chosen as it was found to be the most stable and superior compared to other substrates for the construction of ISE based on CP (Bobacka *et al.*, 1994b, Sun *et al.*, 2000). PEDOT was chosen as solid contact because of its low oxidation potential (Groenendaal *et al.*, 2000) as reported in **Chapter 5** and good potential stability (Bobacka, 1999). PEDOT was electrodeposited at a low current density (0.2 mA/cm^2) due to the low solubility of the EDOT monomer in aqueous solution. Prior to electrodeposition of PEDOT, the solution was stirred for at least 2 h to ensure the dissolution of EDOT monomer.

The chronopotentiometric curves recorded during the galvanostatic electropolymerisation of EDOT in NaPSS and HA on a GC electrode are shown in **Figure 7.11**. These electrodes will hereafter be called as GC/PEDOT/PSS and GC/PEDOT/HA. The galvanostatic method was applied as it is a convenient way to control the amount of electroactive material on the electrode (Asplund *et al.*, 2008). The amount of the polymer deposited on the electrode is proportional to the charge injected during the polymerisation. The thickness of the polymer films were found to be 0.77 μm, by assuming 2.25 electrons/monomer and the film density of 1 g cm^{-3} (Bobacka *et al.*, 2000).

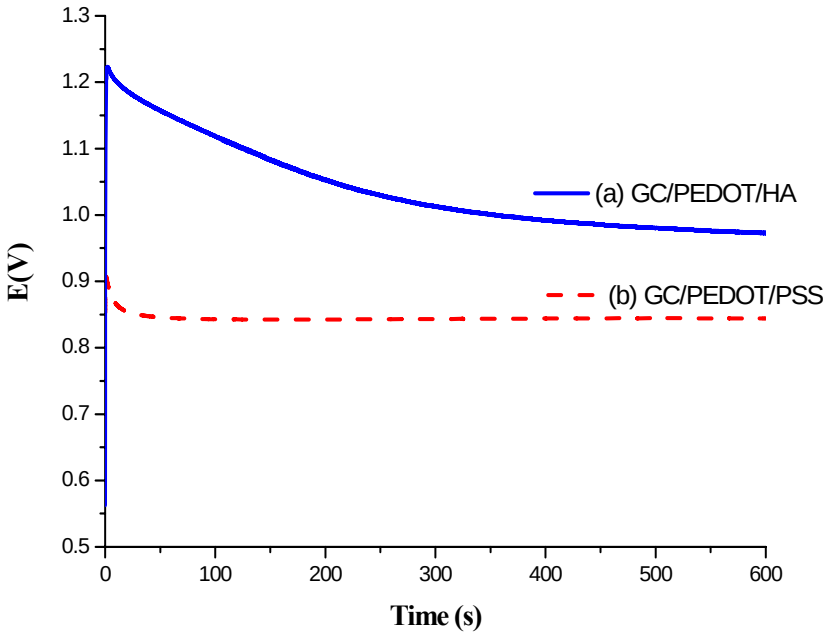

Figure 7.11: Chronopotentiometric curves obtained during galvanostatic polymerisation of EDOT containing (a) HA and (b) NaPSS in aqueous solution.

During the electropolymerisation, the potential initially increases until a peak potential (E_{max}) is reached followed by a decrease to a steady state potential (E_{ss}) over the remaining time. These potential values are tabulated in **Table 7.1**. The result showed that these two anions strongly influence the electropolymerisation of EDOT. It was found that polymerisation took place at lower potential and reached a steady state potential faster for solution containing NaPSS than HA. This is due to the properties of sulfonate group (PSS surfactant) that enhance solubility of EDOT monomer (Patil *et al.*, 1987) and facilitates the electropolymerisation as reported by other studies (Groenendaal *et al.*, 2000, Tamburri *et al.*, 2009).

Table 7.1: Peak potential and steady state potential.

Electrode	E_{max} **(V)**	E_{ss} **(V)**
PEDOT/HA	1.22	0.97
PEDOT/PSS	0.91	0.84

7.3.2 Surface Characterisation of PEDOT Coated Glassy Carbon

SEM and AFM measurements were used to study more details of the surface morphology and topography of the polymer films. **Figure 7.12** shows the images of PEDOT/PSS and PEDOT/HA which found that the polymer films obtained were evenly distributed. The higher magnification images (inset) revealed the cauliflower-like structure of the polymer films and it was observed that PEDOT containing HA had larger grain structure than PEDOT/PSS.

The topographic images of AFM showed that the polymer films prepared by galvanostatic methods were smoother compared to polymer films prepared by potentiodynamic methods (**Chapter 5**). It was found that PEDOT/HA had higher roughness (76 ± 6 nm) compared to PEDOT/PSS (22 ± 4 nm). Similar finding were also observed by Paczosa-Bator *et al.* (2006).

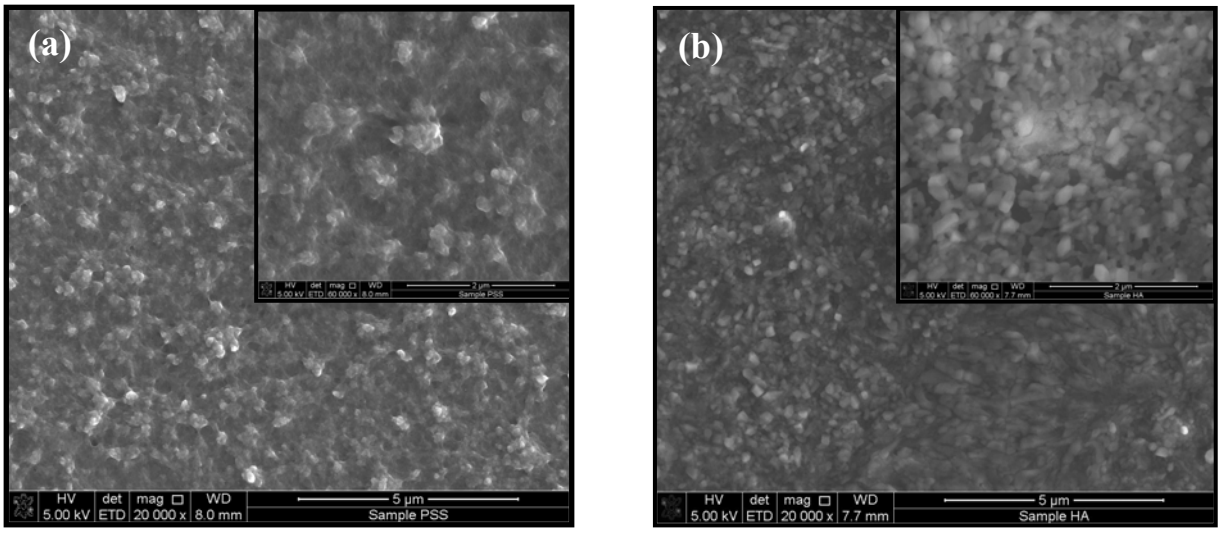

Figure 7.12: SEM images of (a) PEDOT/PSS and (b) PEDOT/HA.

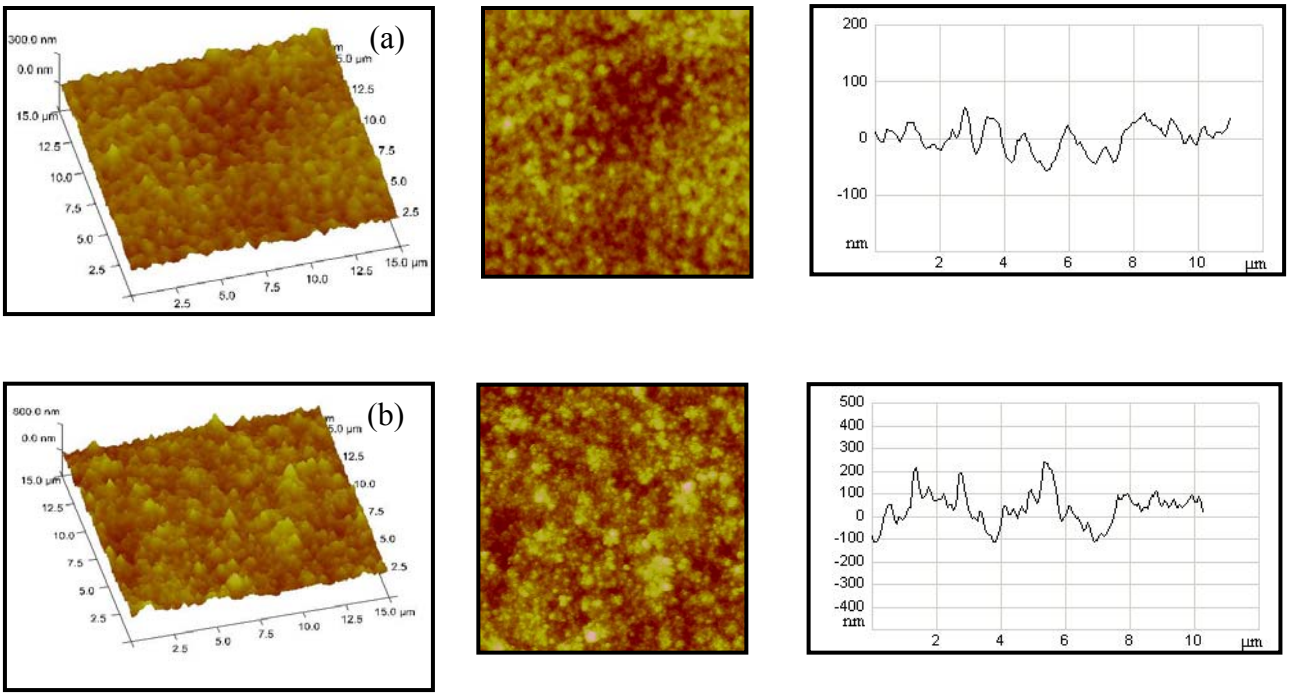

Figure 7.13: AFM images of PEDOT prepared in aqueous solution containing 0.1 M: (a) NaPSS (RMS: 22 ± 4 nm) (b) HA (RMS: 76 ± 6 nm). 3-dimensional topographic image (left), topview (middle) and typical roughness profile (right).

Table 7.2: Surface roughness.

Sample	Surface roughness (nm)*
PEDOT/PSS	22 ± 4
PEDOT/HA	76 ± 6

*Average of 3 measurements at each sample and at least two samples for each material.

7.3.3 Effect of Galvanostatic Conditioning

After the electropolymerisation of PEDOT doped with PSS or HA, the electrodes were coated with three different ISMs (*i.e.* Ca^{2+}, K^+ or Na^+-selective membrane). These electrodes will hereafter be denoted as GC/PEDOT/PSS-Ca^{2+}, GC/PEDOT/HA-Ca^{2+}, GC/PEDOT/PSS-K^+, GC/PEDOT/HA-K^+, GC/PEDOT/PSS-Na^+ and GC/PEDOT/HA-Na^+. **Figure 7.14** shows the potential *vs* time recorded during the galvanostatic

conditioning of these electrodes for 6 h. In all cases, the potential in the initial stage increased steadily, but further contact in conditioning solutions had little effect on the potential recorded. It was observed that PEDOT containing HA took less time (4 h 30 min – 5 h 16 min) to reach stable potential compared to PEDOT doped with PSS (4 h 47 min – 5 h 41 min). These results suggest that PEDOT/HA is able to reach stable potential slightly faster than PEDOT/PSS. It was also observed that only membranes containing calcium *i.e* GC/PEDOT/PSS-Ca^{2+} and GC/PEDOT/HA-Ca^{2+} reached stable potential values. This could be due to the divalent ions are more strongly attracted to HA (Cowman *et al.*, 1996) and PSS than monovalent ions.

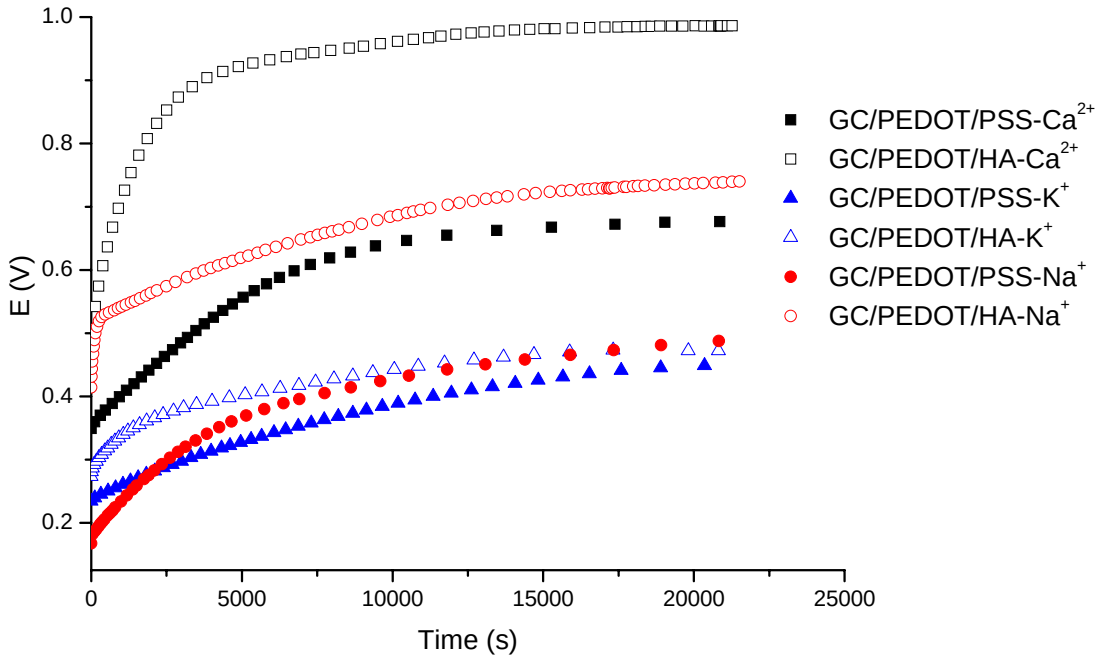

Figure 7.14: Potential *vs* time dependences recorded over galvanostatic conditioning of GC/PEDOT/PSS-Ca^{2+}, GC/PEDOT/HA-Ca^{2+}, GC/PEDOT/PSS-K^+, GC/PEDOT/HA-K^+, GC/PEDOT/PSS-Na^+, GC/PEDOT/HA-Na^+.

7.3.4 Ca^{2+}-selective Electrodes

Potentiometric measurements results from ion-exchange processes occurring at the ISM|solution interface. This process is relatively fast and accompanied by a relatively slow processes of charging and discharging of the polymer film (Dumańska and Maksymiuk, 2001, Michalska *et al.*, 2003).

Some as-prepared conducting polymers have been suggested as being protonated (Pei and Qian, 1992, Qian *et al.*, 1993). The formation of protonated conducting is thought to be as a result of releasing of H^+ from monomer during the polymerisation. Some of these H^+ (associated with counterions) are then considered to be retained in the conducting polymer (Pei and Qian, 1992). Upon contacting with solutions, spontaneous discharging of polymer phase occurs as a result of deprotonation of the conducting polymers (Krivan *et al.*, 2003, Michalska and Maksymiuk, 1998) followed by the release of mobile doping anion to maintain the electroneutrality. Alternatively, incorporation of cation from solution has to occur (Michalska *et al.*, 1997b) for a polymer film containing an immobilised bulky doping anion. In high electrolyte activity, this spontaneous discharging process dominates compared to charging due to the accessibility of electrolyte cations (Dumańska and Maksymiuk, 2001, Michalska and Maksymiuk, 2004b). This process can still take place for polymer film coated with cation-selective membrane permeable to water and oxygen (Lindfors and Ivaska, 2004, Michalska *et al.*, 2003) (**Figure 7.15a**). As pointed out by previous study (Michalska and Hall, 1999), regardless of the ion-exchange properties of polymer film (either cation or anion exchanging), only cations can be exchanged with solution via cation-selective membrane. The spontaneous discharging process relates to decrease of positive charge in the conducting polymer phase that requires uptake of cations from solution.

On the other hand, in solutions of low electrolyte activity, polymers in neutral state can be spontaneously oxidised (charging) by dissolved oxygen present in a solution (**Figure 7.15b**). This process can occur due to the permeability properties of ISM to electrolyte ions, water and oxygen. The rate of discharging process is low due to limited

ion activity. The spontaneous charging process is accompanied by release of cation from polymer film to the solution, resulting in a decrease of cations in the CP film. However, the prevailing process, either discharging or charging is also dependent on the availability of ions (in the polymer film and the solution) and the rate of these processes depends on the concentration of the available ions. These two processes can occur even for long period of conditioning under open circuit condition. The oxidation state of the polymer film can slowly change and the membrane equilibrium will continuously readjusted accordingly to the oxidation state of the polymer. This process would result in a potential drift.

(a) at high electrolyte activity in solution

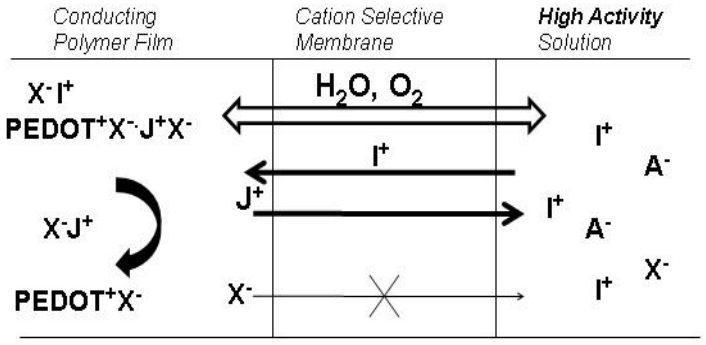

(b) at low electrolyte activity in solution

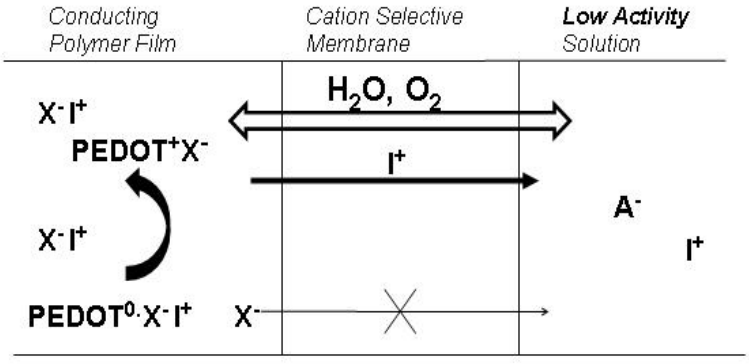

$PEDOT^+$: oxidised form
$PEDOT^0$: neutral form
X^- : doping anions
J^+ : interferent (e.g H^+)
I^+ : primary ions
A- : anion

Figure 7.15: The schematic representation of the spontaneous conducting polymer discharging and charging occurring in electrolyte of (a) high and (b) low activity.

Figure 7.16 shows the open circuit potentiometric calibrations recorded for ASS Ca^{2+}-selective electrodes with PEDOT as solid contact. The data obtained from calibration curves are tabulated in **Table 7.3**. According to IUPAC, the slopes were calculated from the linear part of the calibration curves and the detection limit was obtained as crossection of the extrapolated linear calibration curve with the part of characteristic independent of changes of log of activity of electrolyte (Buck and Lindner, 1994). The theoretical slopes (Nersntian response) for mono and divalent cations are 59.16 and 29.58 mV dec^{-1} at 25 °C, respectively (Buck and Lindner, 1994).

All Ca^{2+}-selective electrodes were characterized with linear responses within the activity range from 10^{-1} to 10^{-4} M (**Figure 7.16**), with the slope close to Nernstian response (**Table 7.3**). For activity of electrolyte lower than $10^{-4.5}$ M, the potential values for all four electrodes were unaffected by the changes of the solution activity. This behaviour is attributed to the constant reversible exchange of ions from the membrane phase to the solution (Mathison and Bakker, 1998, Sokalski *et al.*, 1997).

Lindner and co-workers (Lindner *et al.*, 1999, Pergel *et al.*, 2001) have proposed galvanostatic polarisation to adjust the ion fluxes through the ISM phase. The discharging process can be compensated by applying anodic current in order to control the amount of primary ion in the polymer film and local fluctuation of the electrolyte activity (Dumańska and Maksymiuk, 2001, Michalska *et al.*, 2003, Michalska and Maksymiuk, 2004b). Stable potential can be recorded if the applied current is relatively small and does not affect the overall oxidation state of the polymer film, but only compensates the spontaneous process of the conducting polymer phase. It could be expected that if the incorporation of primary ion is prevented, the linear responses range is extended and lower limit of detection would be observed (Michalska, 2005). If the applied anodic current not only compensates the spontaneous process but also affect the oxidation state of the polymer film, super-Nersntian response would be observed (Michalska, 2005). In contrast, if cathodic current is applied, the discharge process will be enhanced and the effect of lowering the limit of the detection would not be observed due to the more incorporation of primary ion into the polymer film.

As can be seen in **Figure 7.16**, the potential values obtained for Ca^{2+}-selective electrodes applying anodic current of 5×10^{-8} A during conditioning were shifted to more positive values. This anodic current value was chosen based on the work carried out by Michalska (2005) in order to compensate the spontaneous process. This shift is due to the ohmic drop caused by the applied current. This observation is more pronounced for PEDOT doped with PSS. As pointed out by Michalska (2005), this anodic current applied to Ca^{2+}-selective electrode (PPy as solid contact) should produce an extended linear range, however, this phenomenon was not observed in this study. This could be associated with the difference properties of PEDOT and PPy for compensating the spontaneous process. However, the limit of the detection (LOD) of GC/PEDOT/PSS/Ca^{2+} ($10^{-4.07}$ M) conditioned by applying anodic current was slightly improved compared to the Ca^{2+}-selective electrode conditioning in open circuit condition ($10^{-3.49}$ M).

The selectivity coefficient values for the four Ca^{2+}-selective electrodes are illustrated in **Table 7.3**. The selectivity coefficients for Ca^{2+} with respect to K^+, Na^+ and Li^+ were in the range of -1.13 to -1.84 and the log $K^{pot}_{Ca^{2+},Mg^{2+}}$ was > -2. These selectivity coefficient values were compared to the values obtained by Lindfors and Ivaska (2000) for ASS-polyaniline Ca^{2+}-selective electrode using the same neutral carrier ($\log K^{pot}_{Ca^{2+},j}$: -1.7 ($j = K^+$), -1.8 ($j = Na^+$), -1.7 ($j = Li^+$) and -2 ($j = Mg^{2+}$)). The values are similar as observed in this study within the range of experimental error. These results show that the interference by Mg^{2+} is likely to be negligible for practical use.

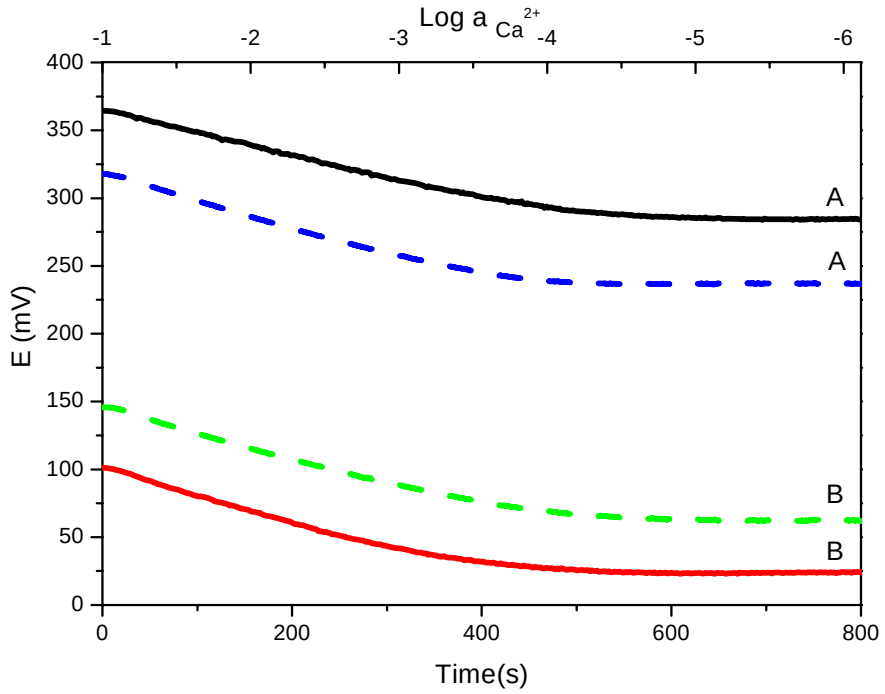

Figure 7.16: Calibration curves of GC/PEDOT/PSS-Ca^{2+} (solid line) and GC/PEDOT/HA-Ca^{2+} (dashed line) conditioning in 0.1 M $CaCl_2$ under (A) applying anodic current 5×10^{-8} A (B) open circuit recorded in $CaCl_2$ solution with 0.1 M KCl as ionic background.

Table 7.3: Response properties of Ca^{2+}-selective electrodes based on PEDOT polymer films.

Electrode	Conditioning	Slope (mV dec^{-1})	LOD	Log $K^{pot}_{Ca^{2+},j}$ (SD: ± 0.1)			
				$j = K^+$	$j = Na^+$	$j = Li^+$	$j = Mg^{2+}$
GC/PEDOT/PSS/Ca^{2+}	5×10^{-8} A	29.40 ± 0.72	$10^{-4.07}$	-1.84	-1.13	-1.50	-2.45
GC/PEDOT/PSS/Ca^{2+}	open circuit	36.32 ± 0.87	$10^{-3.49}$	-1.26	-1.27	-1.39	-2.41
GC/PEDOT/HA/Ca^{2+}	5×10^{-8} A	37.98 ± 0.43	$10^{-3.44}$	-1.21	-1.24	-1.53	-2.22
GC/PEDOT/HA/Ca^{2+}	open circuit	34.02 ± 1.09	$10^{-3.78}$	-1.55	-1.30	-1.18	-2.33

7.3.5 K^+-selective Electrodes

Figure 7.17 shows the open circuit potentiometric characteristics of ASS K^+-selective electrodes and the data are tabulated in **Table 7.4**. GC/PEDOT/PSS/K^+ conditioned in open circuit has shown the best performance and was characterised with a linear dependence of potential on the logarithm of potassium activity within the range from 10^{-1} to $10^{-3.5}$ M (slope 58.93 ± 0.58 mV/dec, R^2 = 0.9994). For activity lower than $10^{-4.5}$ M, the potentials recorded were independent of K^+ activity. Upon applying anodic current (5×10^{-8} A) to the GC/PEDOT/PSS/K^+ to compensate the spontaneous charging process, the slope of linear range decreased (47.44 mV dec^{-1}) but the limit of detection slightly improved (**Table 7.4**), which is similar to the phenomena observed for Ca^{2+}-selective electrodes..

CP layer that initially shows anion exchange behaviour can be tailored to be used as cation exchange after being covered by cation-selective membrane, as the mobile anions are trapped in the CP layer and only cation cations can be exchanged with solution via cation-selective membrane (Michalska and Hall, 1999). Previous studies have shown that anionic-exchanging membrane PPy(Cl) film (Dong *et al.*, 1988b, Michalska *et al.*, 2002) can also be used as solid contact for the fabrication of a K^+-selective electrode upon coating the polymer film with potassium-selective membrane (Michalska *et al.*, 1997a). However, the potential of PEDOT as solid contact was found to be more stable (Bobacka, 1999) and was less sensitive to O_2 and CO_2 (changes in pH of solution) compared to PPy (Vázquez *et al.*, 2002). This is the reason PEDOT has been chosen in this study.

It was noted that the selectivity coefficients for GC/PEDOT/PSS/K^+ pretreated galvanostatically applying 5×10^{-8} A, were slightly improved (**Table 7.4**) compared to GC/PEDOT/PSS/K^+ conditioned in the absence of polarisation. However, these selectivity coefficient values (**Table 7.4**) were lower than reported in literature (Bobacka, 1999) ($\log K^{pot}_{K^+,j}$: -4.2 (j = Na^+), -5.4 (j = Ca^{2+}), -5.4 (j = Li^+) and -5.7 (j = Mg^{2+})). This could be attributed to the low concentration of the ion-exchanging polymeric doping

anion, PSS used in this work. It has been reported that increasing the amount of PSS anion in the polymer layer can induce more effective binding of potassium ion in the transducer contact phase, resulting in improvement of the linear response range and selectivity (Michalska and Maksymiuk, 2004a). However, it was interesting that all K^+-selective electrodes still exhibited good K^+ selectivity even in the presence of a high background concentration of Na^+, Ca^{2+}, Li^+ and Mg^{2+}. The most promising results were obtained for divalent cation interferences. The effect observed can be related to the properties of PEDOT layer and is important for clinical analysis. Some data could not be determined such as the LOD and log $K^{pot}_{K^+,j}$ for GC/PEDOT/HA/K^+ conditioning in open circuit due to the two differing gradients. This is probably attributable to two different ion-exchange mechanisms.

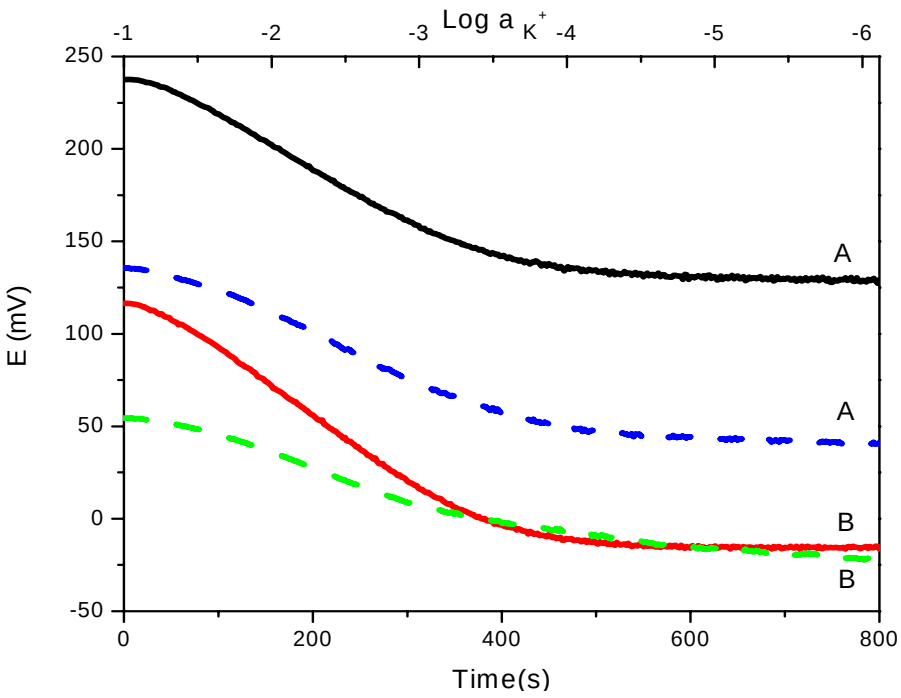

Figure 7.17: Calibration curves of GC/PEDOT/PSS-K^+ (solid line) and GC/PEDOT/HA-K^+ (dashed line) conditioning in 0.1 M KCl under (A) applying anodic current 5×10^{-8} A (B) open circuit recorded in KCl solution with 0.1 M NaCl as ionic background.

Table 7.4: Response properties of K^+-selective electrodes based on PEDOT polymer films.

Electrode	Conditioning	Slope (mV dec^{-1})	LOD	Log $K^{pot}_{K^+,j}$ (SD: ± 0.1)			
				$j = Na^+$	$j = Ca^{2+}$	$j = Li^+$	$j = Mg^{2+}$
GC/PEDOT/PSS/K^+	5×10^{-8} A	47.44 ± 0.61	$10^{-3.37}$	-2.26	-2.84	-2.12	-2.80
GC/PEDOT/PSS/K^+	open circuit	58.93 ± 0.58	$10^{-3.0}$	-1.89	-2.83	-2.03	-2.49
GC/PEDOT/HA/K^+	5×10^{-8} A	40.10 ± 0.54	$10^{-3.54}$	-2.43	-3.13	-2.24	-
GC/PEDOT/HA/K^+	open circuit	31.73 ± 0.15	-	-	-	-	-

7.3.6 Na^+-selective Electrodes

In the next experiments, potentiometric responses of ASS Na^+-selective electrodes were investigated and the results are presented in **Figure 7.18**. Linear responses were obtained within the activity range $10^{-1.0}$ to ~$10^{-3.5}$ M for all electrodes except for GC/PEDOT/HA-Na^+ conditioning in open circuit. However, only PEDOT containing PSS showed slopes close to Nernstian responses. The best sensitivity for K^+-selective electrode with a slope of 59.20 ± 0.49 mV/dec (R^2 = 0.9993) was obtained with GC/PEDOT/PSS/Na^+ determined in the concentration range 10^{-1}-10^{-3} M.

As can be seen in **Table 7.5**, the slope of linear range for GC/PEDOT/PSS/Na^+ conditioned by applying anodic current (5 × 10^{-8} A) to compensate the spontaneous discharging process decreased but the limit of detection improved. Contrasting phenomena were observed for Na^+-selective electrode containing PEDOT doped with HA as solid contact, in which the slope of linear range improved but the limit of detection decreased. Similar findings were observed for Ca^{2+} and K^+-selective electrodes. These results indicate that the nature of the doping anions have a strong influence on the performance of the ASSISE using PEDOT as solid contact.

The calculated value of logarithm of potentiometric selectivity coefficient, $\log K^{\text{pot}}_{\text{Na}^+,j}$ with respect to K^+, Ca^{2+} and Li^+ and Mg^{2+} (**Table 7.5**) were comparable with values reported in the literature with the same ionophore (Cadogan *et al.*, 1989) ($\log K^{\text{pot}}_{\text{Na}^+,j}$: -1.9 ($j$ = K^+), -2.5 (j = Ca^{2+}), -2.5 (j = Li^+) and <-6 (j = Mg^{2+})). It was observed that for each electrode, the selectivity towards divalent cations was higher compared to monovalent ions, which is similar as observed for ASS K^+-selective electrodes.

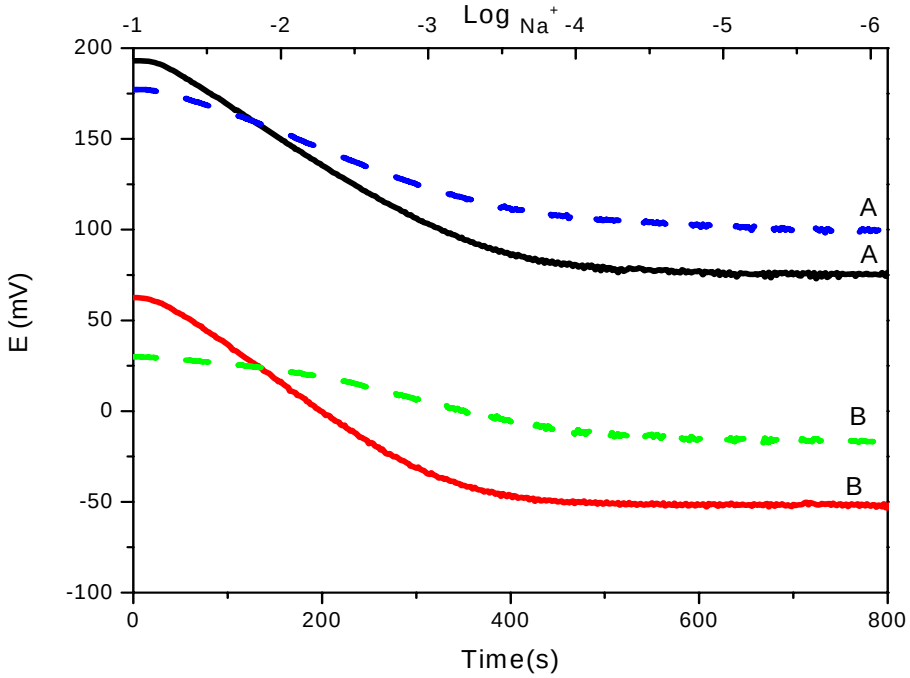

Figure 7.18: Calibration curves of GC/PEDOT/PSS-Na^+ (solid line) and GC/PEDOT/HA-Na^+ (dashed line) conditioning in 0.1 M NaCl under (A) applying anodic current 5×10^{-8} A (B) open circuit recorded in NaCl solution with 0.1 M LiCl as ionic background.

Table 7.5: Response properties of Na^+-selective electrodes based on PEDOT polymer films.

Electrode	Conditioning	Slope (mV dec^{-1})	LOD	Log $K^{pot}_{Na^+,j}$ (SD: ± 0.1)			
				$j = K^+$	$j = Ca^{2+}$	$j = Li^+$	$j = Mg^{2+}$
GC/PEDOT/PSS/Na^+	5×10^{-8} A	51.37 ± 1.11	$10^{-3.48}$	-1.74	-2.91	-2.38	-2.73
GC/PEDOT/PSS/Na^+	open circuit	59.20 ± 0.49	$10^{-3.13}$	-1.82	-2.51	-2.03	-2.52
GC/PEDOT/HA/Na^+	5×10^{-8} A	32.94 ± 0.37	$10^{-3.42}$	-1.63	-2.91	-2.32	-2.93
GC/PEDOT/HA/Na^+	open circuit	19.91 ± 0.48	$10^{-3.84}$	-	-3.26	-2.74	-

Since the doping ions are negatively charged, it is expected that cations can be attracted to it. As it can be seen in **Table 7.3 - Table 7.5**, for the electrodes containing PEDOT/HA as a solid contact, only Ca^{2+} electrodes were characterised with slopes close to Nernstian responses. The observed effect could be attributed to effective binding of Ca^{2+} by the hyaluronate ions (Cowman *et al.*, 1996) incorporated in the transducer layer during the electrodeposition. In contrast, both monovalent and divalent ions have the same binding capacities to PSS, which is determined by the charge stoichiometry (Li *et al.*, 2003).

7.3.7 Cyclic Voltammograms of PEDOT/PSS and PEDOT/HA

CV measurements were carried out in order to investigate the capacitance properties of PEDOT/PSS and PEDOT/HA. As can been seen in **Figure 7.19**, the capacitance of PEDOT/PSS is much higher compared to PEDOT/HA. The capacitance values ($C = i/v$; i = charging current at steady state, v = scan rate) estimated from CV were 1.76 mF and 0.08 mF for PEDOT/PSS and PEDOT/HA, respectively. As described by Bobacka (1999), a sufficiently high bulk (redox) capacitance of the solid contact (conducting polymer) is required to obtain a stable electrode potential of the ASSISE. This could be the reason why ASSISE based on PEDOT/PSS as solid contact showed better performance and potential stability than PEDOT/HA even at low activity.

Based on the potentiometric and cyclic voltammetric measurements, electrodes PEDOT/PSS were found to be superior to PEDOT/HA. As a result, for fabrication of ion-selective microelectrodes, PEDOT/PSS is used as solid contact and electrodes yielding near-Nernstian calibrations were used.

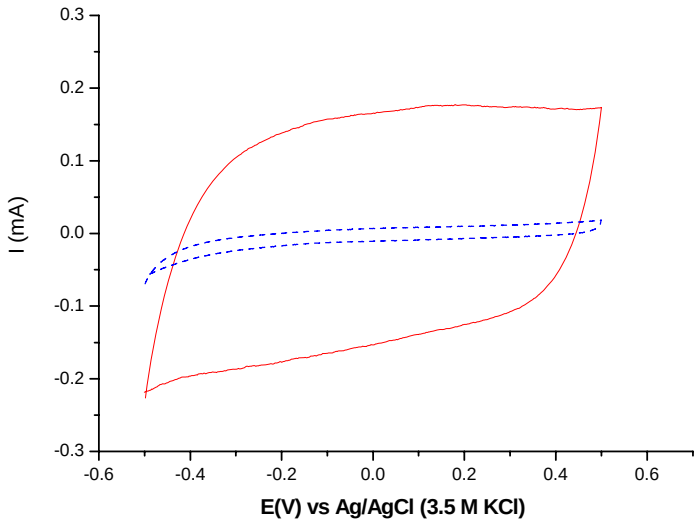

Figure 7.19: Cyclic voltammograms of GC/PEDOT/PSS (solid line) and GC/PEDOT/HA (dotted line) recorded in deaerated 0.1 M KCl at 100 mVs^{-1}.

7.3.8 SEM of Micropippette and Carbon Fibre

Ion-selective microelectrodes were prepared in order to monitor the behaviour of plant roots (*Arabidopsis thaliana*) subjected to temperature stress. In this study, Ca^{2+} and K^{+}-selective microelectrodes were prepared for the application of real sample measurements. The fabrication of micropipettes that has been described in experimental section (**Section 7.2.4**) was analysed by scanning electron microscopy. As shown in **Figure 7.20**, the size of the micropipette tip was found to be 14.1 ± 0.3 µm.

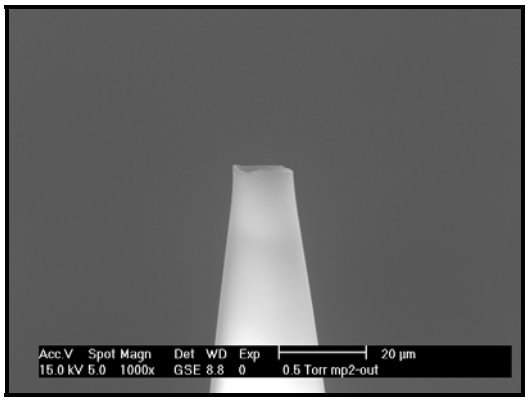

Figure 7.20: SEM image of the micropipette tip.

Figure 7.21 shows the SEM images of an uncoated and PEDOT/PSS coated carbon fibre. The size of the uncoated carbon fibres was confirmed to be 33.5 ± 2.5 mm (inset **Figure 7.21a**). The surface of uncoated fibre was smooth and become rough upon deposition of PEDOT/PSS (**Figure 7.21b**). The PEDOT/PSS showed granular structure and even distribution on the surface of carbon fibre.

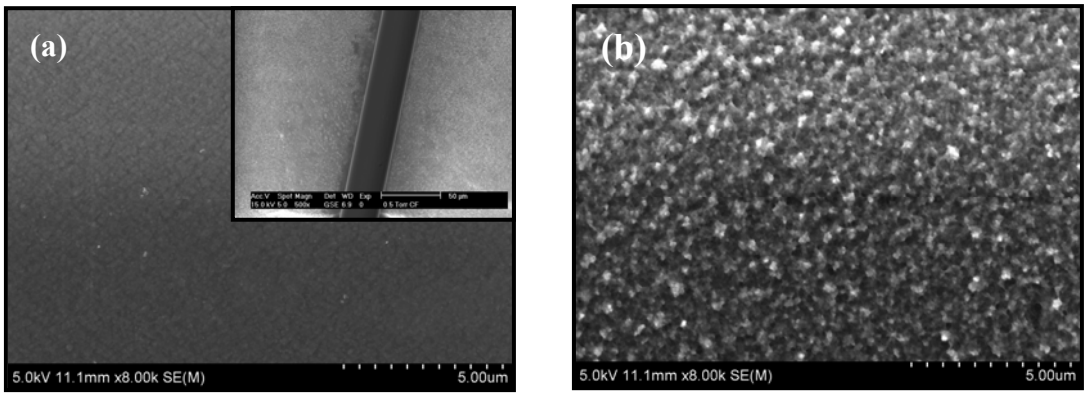

Figure 7.21: SEM image of (a) uncoated carbon fibre and (b) PEDOT/PSS coated carbon fibre.

7.3.9 Ion-selective Microelectrode

7.3.9.1 Effect of Temperature of Ca^{2+}-selective Microelectrode

Calibration curves for Ca^{2+}-selective microelectrodes at different temperatures are displayed in **Figure 7.22**. Based on the Nernst equation, the slope of calibration curve would change with temperature, at the rate of 3.4% per 10 °C. It was shown that the electrode exhibits good Nernstian response in the temperature range studied (0 – 25 °C). These data indicate that this electrode can be used to measure calcium at low temperatures.

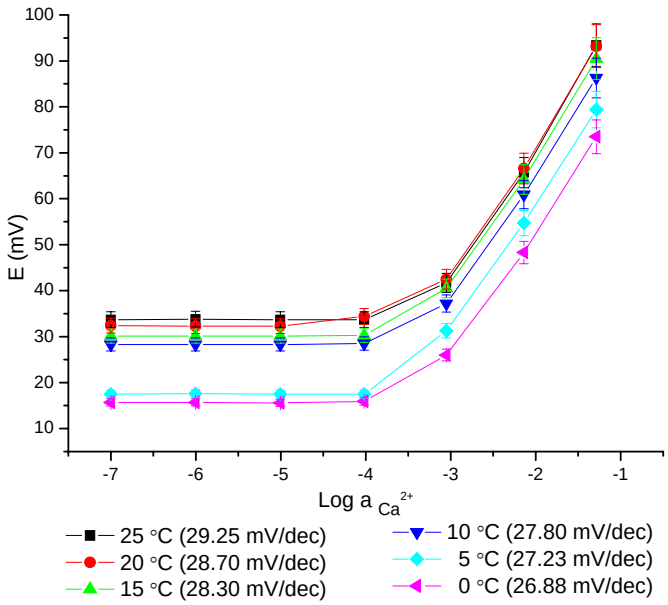

Figure 7.22: Calibration curves of Ca^{2+}-selective microelectrode at different temperatures in $CaCl_2$ solution with 0.1 M KCl as ionic background. Values in parentheses refer to the slope of linear range.

The standard cell potentials (E^0_{cell}) at different temperatures were determined from the calibration curve as the intercepts at log a Ca^{2+} = 0. The values were used to determine the isothermal temperature coefficients (dE^0/dt) using the following equation (Antropov, 1972):

$$E^0_{cell} = E^0_{cell\,(25°C)} + \left(\frac{dE^0}{dt}\right)_{cell} (t - 25) \qquad \textbf{(7.9)}$$

The slope of the straight line (**Figure 7.23**) obtained represents the isothermal coefficient of the electrode, amounting to 0.0009 V/°C. The small value of dE^0/dt indicates a good thermal stability of the electrode within the temperature range studied.

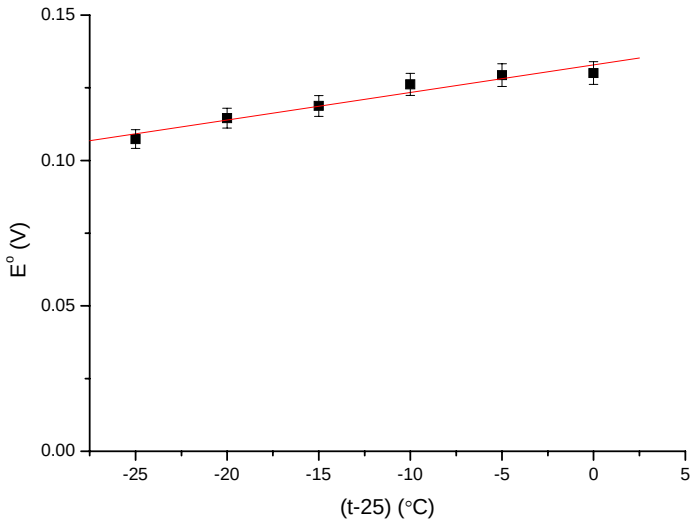

Figure 7.23: Plot of E^0 *vs* (t-25).

The selectivity coefficients (log $K^{pot}_{Ca^{2+},j}$) determined by fixed interference method were as follows: j = K^+ (-1.86), Na^+ (-1.43), Li^+ (-2.00) and Mg^{2+} (-1.63). These results are comparable with the data obtained by Lindfors and Ivaska (2000) using a membrane containing the same neutral carrier (log $K^{pot}_{Ca^{2+},j}$: -1.7 (j = K^+), -1.8 (j = Na^+), -1.7 (j = Li^+) and -2 (j = Mg^{2+})).

7.3.9.2 Ion Amperometry

Since ISE has been studied mainly using potentiometric measurements, less attention has been focused on ion amperometric measurements. The fundamental concept of ion amperometry is the transfer of ions across an interface. This concept allows the detection redox of inactive species (e.g calcium). The transfer of ions across an interface can be investigated by various electrochemical techniques, such as cyclic voltammetry.

An ion-selective membrane can still be considered as an organic liquid phase (Oesch and Simon, 1980) because the diffusion coefficients of dissolved components (*e.g*

ionophore) are in the order of 10^{-7} to 10^{-8}cm^2 s^{-1}. A liquid-liquid interface of two immiscible solutions will be formed when an ISE is placed in an aqueous solution. This set-up allows the exploration of ion transfer at the liquid-liquid interface by means of amperometric sensor.

In order to evaluate the performance and applicability of the electrode as an ion-amperometric sensor, cyclic voltammetric and chronoamperometric measurements were performed. The cyclic voltammetric measurements were carried out using a 3-electrode system as shown in **Figure 7.24**. Agar gel (5%) was prepared with 0.1 M $CaCl_2$ solution and placed in an electrochemical cell. The working electrode *i.e.* the Ca^{2+}-selective microelectrode was placed close to the surface of the agar gel. For the potassium measurement, the $CaCl_2$ solution and Ca^{2+}-selective microelectrode were replaced by a 0.1 M KCl solution and K^+-selective microelectrode, respectively. The measurements were carried out immediately after 10^{-4} M LiCl solution was placed on top of the agar gel.

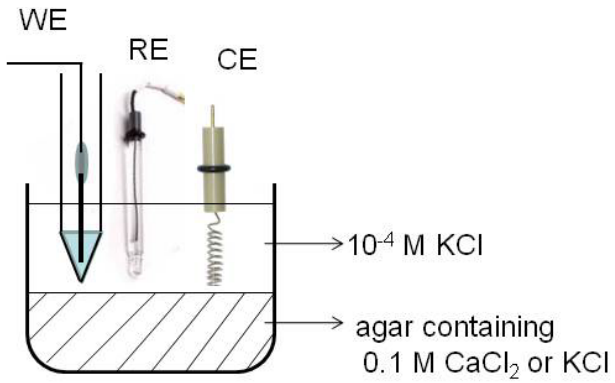

Figure 7.24: Ion amperometric measuremet set-up.

As can been seen in **Figure 7.25**, there was no observable peak in the background measurement in 10^{-4} M LiCl solution. In contrast, one obvious peak centred at 1.3 V was observed in the presence of agar gel containing calcium (**Figure 7.25a**). In the case of agar gel containing potassium, the peak current was at 1.25 V. Calcium (or potassium) concentration gradient was formed after background solution (10^{-4} M LiCl) was added on

top of agar gels. Thus, the observable peaks are attributed to the transport of calcium and potassium ions from the solution to the ion-selective membrane. The peaks observed were not sigmoidal in shape as expected due a larger micropipette tip and the formation of membrane particle after filling the micropipette with ion-selective membrane solution.

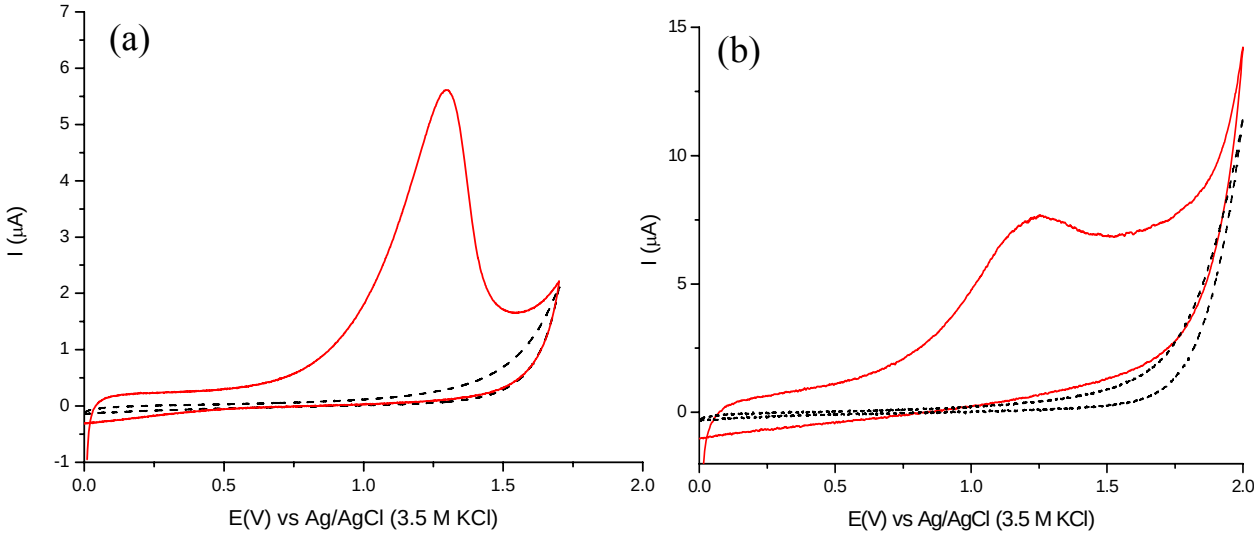

Figure 7.25: (a) Cyclic voltammogram of Ca^{2+}-selective microelectrode in 10^{-4} M KCl solution (dashed line) and in the presence of $CaCl_2$ in 10^{-4} M KCl (solid line). (b) Cyclic voltammogram of K^+-selective microelectrode in 10^{-4} M LiCl solution (dashed line) and in the presence of KCl in 10^{-4} M LiCl (solid line). Sweep rate: 50 mVs^{-1}.

Figure 7.26 shows the response of the Ca^{2+}-selective microelectrode and K^+-selective microelectrode to $CaCl_2$ and KCl, respectively in aqueous solutions at different concentrations. A constant potential of 1.35 V (Ca^{2+}) or 1.3 V (K^+), which is just slightly beyond the peak current in cyclic voltammetric measurement (**Figure 7.25**) was applied. As can been seen, the current increases as the concentration of $CaCl_2$ (or KCl) increases. The reproducibility of the measurements was obtained from five repeated injections and the electrodes showed highly reproducible with a relative standard deviation (RSD) of

3.9% and 4.7% for Ca^{2+}- and K^{+}-selective microelectrodes, respectively. These results were used to plot the calibration curve (current *vs* concentration) as shown in the inset of **Figure 7.26**. The current values were obtained from the peak currents.

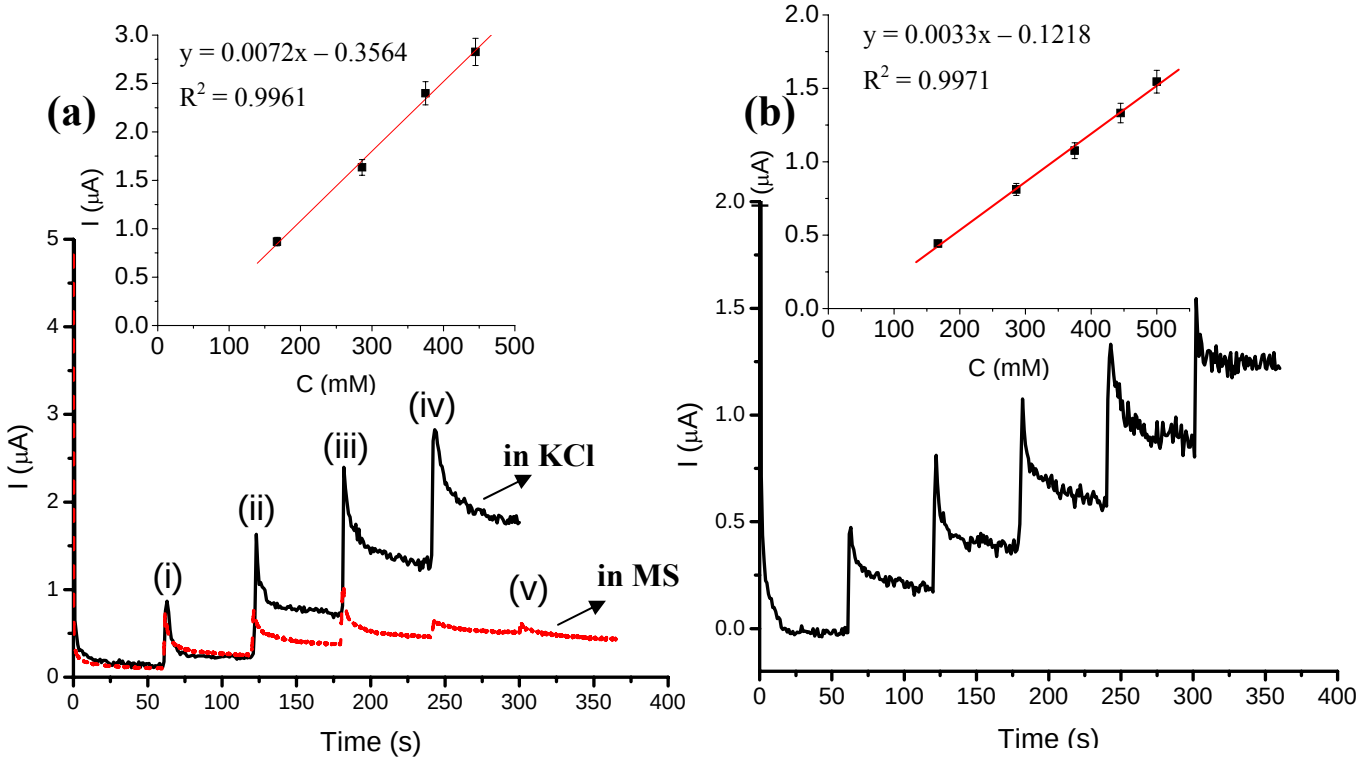

Figure 7.26: Chronoamperogram recorded by injection of (a) $CaCl_2$ and (b) KCl at different concentrations (i) 167 mM (ii) 286 mM (iii) 375 mM (iv) 445 mM and (v) 500 mM. Inset: calibration curve.

Measurements in MS medium were also carried out for comparison (**Figure 7.26a**). It was found that the current increased until the concentration of $CaCl_2$ become 375 mM before decreasing significantly. However, the increase in current was not as high as the measurement performed in LiCl solution. This is due to the presence of EDTA in MS medium that might form a complex with calcium ion (Bachra *et al.*, 1958). This finding shows that MS medium is not suitable to be used as a background solution for calcium measurements.

7.3.9.3 Detection of Calcium

In this work, *Arabidopsis thaliana*, commonly studied in plant biology (Lew, 1998, Shabala *et al.*, 2006) was chosen as a model for detection of calcium in real sample. It is known that Ca^{2+} plays an important element in plant cells as a secondary messenger in many signalling pathways including plant stress response (Orrenius *et al.*, 2003). The intracelullar concentration of Ca^{2+} in a cell is normally very low (10^{-7} M), while the extracellular concentration is quite high (about 10^{-3} M).

It has been demonstrated that cold stress induced the elevation of cytosolic free calcium concentration (Plieth *et al.*, 1999) and it is expected that the extracellular free Ca^{2+} concentration would change as well. **Figure 7.27** shows a spike upon rapid cooling (dT/dt = 0.16 °C/s) the solution in the presence of *Arabidopsis* roots, indicating the transient elevation of calcium concentration. The amount of calcium release can be estimated from calibration curve (inset **Figure 7.26a**) and it was found to be 92.36 ± 0.12 mM. The measurements showed an acceptable reproducibility with RSD of 3.37%. In contrast, there was no increase in current in the absence of roots (**Figure 7.27**).

According to Plieth *et al*. (1999), the effect of temperature change on *Arabidopsis thaliana* roots is mainly dependent on the cooling rate rather than the absolute temperature. The increase in cytosolic free calcium concentration is mainly initiated by Ca^{2+} influx through the plasma membrane and by Ca^{2+} release from internal store (vacuole and endoplasmic reticulum) (Knight *et al.*, 1996). In order to ensure that calcium release only occurs upon rapid cooling, a control experiment at gradual reduction in temperature (dT/dt = 0.01 °C/s) was carried out. The same result as in the absence of roots upon rapid cooling was observed *i.e.* no observable spike (inset **Figure 7.27**), confirming the calcium release was due to rapid cooling.

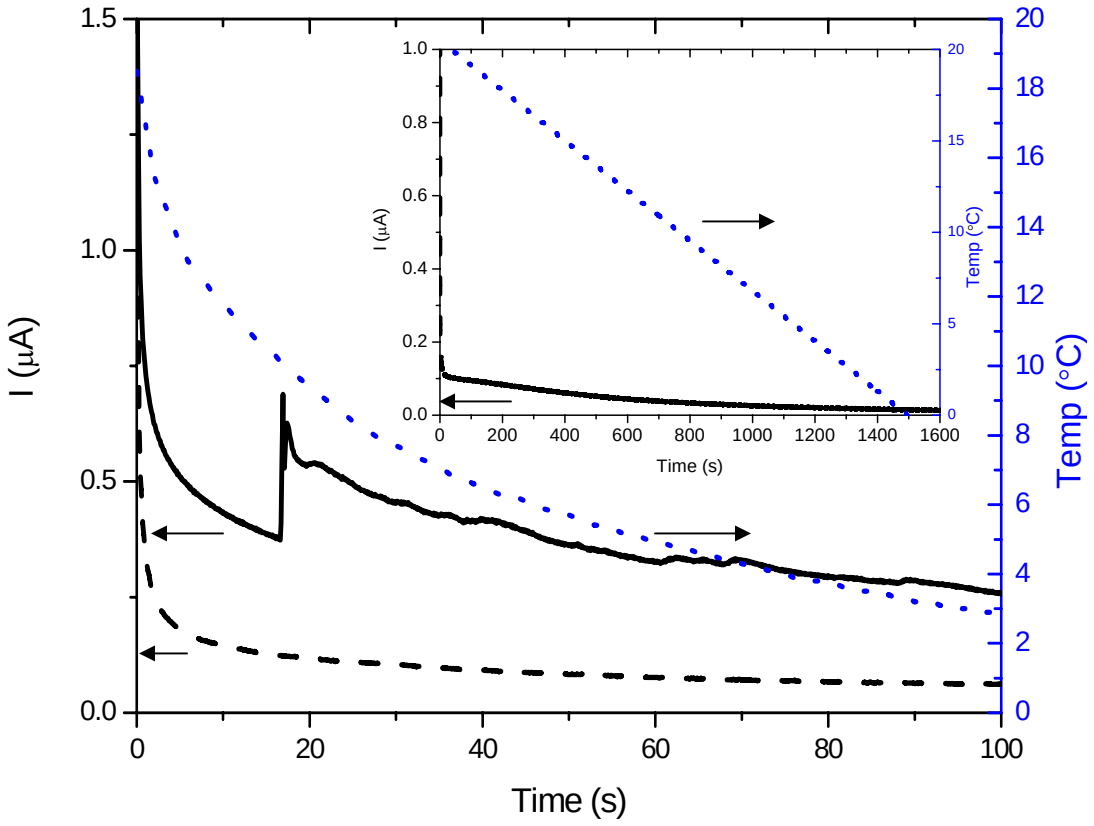

Figure 7.27: Chronoamperogram recorded at rapid cooling rate (d*T*/d*t* = 0.16 °C/s) in the absence of *Arabidopsis thaliana* roots (dashed line), in the presence of the roots (solid line) and temperature profile (dotted line). Inset: chronoamperogram recorded at slow cooling rate (~ d*T*/d*t* = 0.01 °C/s). The arrows pointed to the scale used (Y-axis) for each plot. Potential of Ca^{2+}-selective microelectrode: 1.35 V.

7.3.9.4 Detection of Potassium

Another approach to study the changes of ion content of plant cells is through salinity stress. It is well known that sodium toxicity causes negative impact on the production of food in agriculture throughout the world. As a result, many studies have been carried out to detect and decrease the toxicity. In this study, K^+-selective microelectrode was prepared and used to detect the K^+ efflux from *Arabidopsis thaliana* roots. The selectivity coefficients ($K^{pot}_{K^+,j}$) of the electrode were as follows: j = Na^+ (-2.27), Ca^{2+} (-2.54), Li^+ (-2.11) and Mg^{2+} (-2.53). These selectivity values were lower than reported by Bobacka (1999) due to the low concentration of PSS used in this work.

In order to detect potassium, the same concept used earlier for Ca^{2+}-selective microelectrode was applied *i.e.* ion amperometric sensing by applying a constant potential at 1.3 V, which is slightly beyond the peak current in the cyclic voltammetric measurement (**Figure 7.25b**). An immediate rise in current occurred after adding 50 mM NaCl to the roots (**Figure 7.28d**) and the current gradually decreased before reaching steady state current (after ~ 2 min). The high current seen at the beginning of the chronoamperometric measurements (**Figure 7.28**) was due to the charging current. The dramatic increase in current was due to the K^+ efflux from the roots (Shabala *et al.*, 2006) and the amount was 42.55 ± 0.58 mM (based on calibration curve in **Figure 7.26b**). This finding is in good agreement with Cuin *et al.* (2003) who showed a reduced amount of potassium in the cytosol from 68 to 15 mM (leaf epidermal cells of barley) by addition of high amount of NaCl (200 mM). The results of five measurements under the same conditions in this study showed a RSD of 1.35%, showing a good reproducibility. Shabala *et al*. (2006) reported that NaCl-induced K^+ efflux was initiated by Na^+ influx. This Na^+ influx caused the depolarisation of plasma membrane (Shabala, 2003) and the K^+ efflux may originate from depolarisation-activated K^+ channels (DAPCs).

The result obtained can be supported by control experiments. As can been seen in **Figure 7.28c,** there was no increase in current in the presence of roots without adding the

NaCl. Another control experiment was carried out by injecting 50 mM into background solution *i.e.* LiCl. A slight increase in current was observed upon injecting NaCl, but it can be neglected as the current did not dramatically rise as shown in the presence of roots (**Figure 7.28b**) and the current recovered after ~ 2.5 min. It has also been shown that salt stress resulted in a rapid reduction of cytosolic free K^+ concentration (Carden *et al.*, 2003, Shabala *et al.*, 2006). This finding has proven the phenomenon of K^+ efflux by imposing NaCl stress. The K^+ efflux and accumulation of Na^+ in cytosol due to Na^+ influx, resulting decline in cytosolic K^+ and Na^+ ratio and eventually cell death (Shabala *et al.*, 2006).

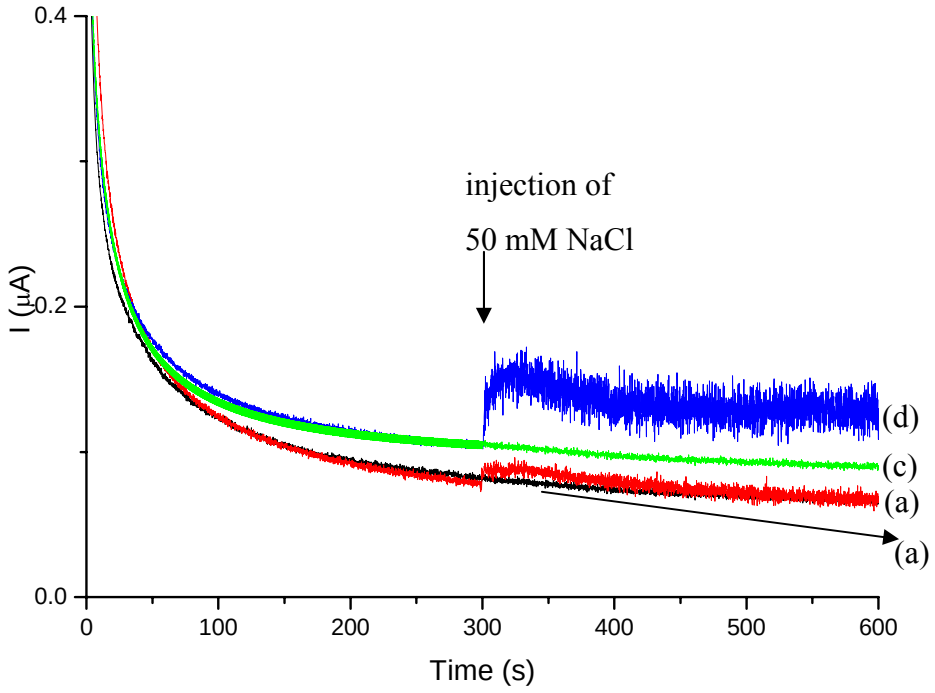

Figure 7.28: Chronoamperogram of K^+-selective microelectrode (a) in 10^{-4} M LiCl and (b) injection of 50 mM NaCl to 10^{-4} M LiCl in the absence of *Arabidopsis* roots; (c) in 10^{-4} M LiCl and (d) injection of 50 mM NaCl to 10^{-4} M LiCl in the presence of *Arabidopsis* roots. Potential of Ca^{2+}-selective microelectrode: 1.3 V

7.4 Conclusions

ASS Ca^{2+}-, K^{+}- and Na^{+}-selective electrodes based on PEDOT as solid contact have been prepared in this study. PEDOT/PSS has shown to be the better solid contact compared to PEDOT/HA and the performance was comparable to the conventional inner-filling electrode. The application of Ca^{2+} and K^{+}-selective microelectrode based on PEDOT to measure calcium and potassium ion in *Arabidopsis thaliana* roots has been demonstrated in this work. The Ca^{2+}-selective microelectrode was shown to be stable at different temperatures, even at low temperature. This property allows the use of this electrode for measurement of calcium under cold-stress conditions in plants.

References

Antropov, L. I. (1972) *Theoritical Electrochemistry.* Moscow, Mir.

Asplund, M., Von Holst, H. and Inganas, O. (2008) Composite Biomolecule/PEDOT Materials For Neural Electrodes. *Biointerphases.* 3**.** 83-93.

Bachra, B. N., Dauer, A. and Sobel, A. E. (1958) The Complexometric Titration of Micro and Ultramicro Quantities of Calcium in Blood Serum, Urine, and Inorganic Salt Solutions. *Clin Chem.* 4**.** 107-119.

Bakker, E., Buhlmann, P. and Pretsch, E. (1997) Carrier-Based Ion-Selective Electrodes and Bulk Optodes. 1. General Characteristics. *Chemical Reviews.* 97**.** 3083-3132.

Bakker, E. and Pretsch, E. (2002) The New Wave of Ion-Selective Electrodes. *Analytical Chemistry.* 74**.** 420A-426A.

Bobacka, J. (1999) Potential Stability of All-Solid-State Ion-Selective Electrodes Using Conducting Polymers As Ion-to-Electron Transducers. *Analytical Chemistry.* 71**.** 4932-4937.

Bobacka, J. (2006) Conducting Polymer-Based Solid-State Ion-Selective Electrodes. *Electroanalysis.* 18**.** 7-18.

Bobacka, J., Alaviuhkola, T., Hietapelto, V., Koskinen, H., Lewenstam, A., Lamsa, M., Pursiainen, J. and Ivaska, A. (2002) Solid-Contact Ion-Selective Electrodes For Aromatic Cations Based on π-Coordinating Soft Carriers. *Talanta.* 58**.** 341-349.

Bobacka, J., Gao, Z. Q., Ivaska, A. and Lewenstam, A. (1994a) Mechanism of Ionic and Redox Sensitivity of p-Type Conducting Polymers: Part 2. Experimental Study of Polypyrrole. *Journal of Electroanalytical Chemistry.* 368**.** 33-41.

Bobacka, J., Ivaska, A. and Lewenstam, A. (1999) Plasticizer-Free All-Solid-State Potassium-Selective Electrode Based on Poly(3-Octylthiophene) and Valinomycin. *Analytica Chimica Acta.* 385**.** 195-202.

Bobacka, J., Ivaska, A. and Lewenstam, A. (2003) Potentiometric Ion Sensors Based on Conducting Polymers. *Electroanalysis.* 15**.** 366-374.

Bobacka, J., Lewenstam, A. and Ivaska, A. (2000) Electrochemical Impedance Spectroscopy of Oxidized Poly(3,4-Ethylenedioxythiophene) Film Electrodes in Aqueous Solutions. *Journal of Electroanalytical Chemistry.* 489**.** 17-27.

Bobacka, J., Lindfors, T., Mccarrick, M., Ivaska, A. and Lewenstam, A. (1995) Single-Piece All-Solid-State Ion-Selective Electrode. *Analytical Chemistry.* 67**.** 3819-3823.

Bobacka, J., Mccarrick, M., Lewenstam, A. and Ivaska, A. (1994b) All Solid-State Poly(Vinyl Chloride) Membrane Ion-Selective Electrodes with Poly(3-Octylthiophene) Solid Internal Contact. *Analyst.* 119**.** 1985-1991.

Buck, R. P. (1980) Ion Selective Electrodes IN FREISER, H. (Ed.) *Analytical Chemistry.* New York. Plenum.

Buck, R. P. and Lindner, E. (1994) Recommendations for Nomenclature of Ion-Selective Electrodes (IUPAC Recommendations 1994). *Pure and Applied Chemistry.* 66**.** 2527-2536.

Cadogan, A., Gao, Z. Q., Lewenstam, A., Ivaska, A. and Diamond, D. (1992a) All-Solid-State Sodium-Selective Electrode Based on a Calixarene Ionophore in a Poly(vinyl chloride) Membrane with a Polypyrrole Solid Contact. *Analytical Chemistry.* 64**.** 2496-2501.

Cadogan, A., Lewenstam, A. and Ivaska, A. (1992b) Anionic Responses of Electrochemically Synthesized Polypyrrole Films. *Talanta.* 39**.** 617-620.

Cadogan, A. M., Diamond, D., Smyth, M. R., Deasy, M., Mckervey, M. A. and Harris, S. J. (1989) Sodium-Selective Polymeric Membrane Electrodes Based on Calix[4]arene Ionophores *Analyst.* 114**.** 1551-1554.

Carden, D. E., Walker, D. J., Flowers, T. J. and Miller, A. J. (2003) Single-Cell Measurements of The Contributions of Cytosolic Na^+ and K^+ to Salt Tolerance. *Plant Physiology.* 131**.** 676-683.

Cattrall, R. W., Drew, D. M. and Hamilton, I. C. (1975) Some Alkylphosphoric Acid Esters for Use in Coated-Wire Calcium-Selective Electrodes : Part I. Response Characteristics *Analytica Chimica Acta.* 76**.** 269-277.

Cattrall, R. W. and Freiser, H. (1971) Coated Wire Ion Selective Electrode. *Analytical Chemistry.* 43**.** 1905-1906.

Cattrall, R. W. and Hamilton, I. C. (1984) Coated-Wire Ion-Selective Electrodes. *Ion-Selective Electrode Reviews.* 6**.** 125-172.

Collier, J. H., Camp, J. P., Hudson, T. W. and Schmidt, C. E. (2000) Synthesis and Characterization of Polypyrrole-Hyaluronic Acid Composite Biomaterials for Tissue Engineering Applications. *Journal of Biomedical Materials Research.* 50**.** 574-584.

Cowman, M. K., Hittner, D. M. and Federdavis, J. (1996) ^{13}C-NMR Studies of Hyaluronan: Conformational Sensitivity to Varied Environment. *Macromolecules.* 29**.** 2894-2902.

Cuin, T. A., Miller, A. J., Laurie, S. A. and Leigh, R. A. (2003) Potassium activities in cell compartments of salt-grown barley leaves. *Journal of Experimental Botany.* 54**.** 657-661.

Dong, S. J. and Che, G. L. (1991) An Electrochemical Microsensor for Chloride. *Talanta.* 38**.** 111-114.

Dong, S. J., Sun, Z. H. and Lu, Z. L. (1988a) A New Kind of Chemical Sensor Based on a Conducting Polymer Film. *Journal of the Chemical Society-Chemical Communications.* 993-995.

Dong, S. J., Sun, Z. S. and Lu, Z. L. (1988b) Chloride Chemical Sensor Based on An Organic Conducting Polypyrrole Polymer. *Analyst.* 113**.** 1525-1528.

Dumańska, J. and Maksymiuk, K. (2001) Studies on Spontaneous Charging/Discharging Processes of Polypyrrole in Aqueous Electrolyte Solutions. *Electroanalysis.* 13**.** 567-573.

Fibbioli, M., Bandyopadhyay, K., Liu, S. G., Echegoyen, L., Enger, O., Diederich, F., Buhlmann, P. and Pretsch, E. (2000) Redox-Active Self-Assembled Monolayers as Novel Solid Contacts for Ion-Selective Electrodes. *Chemical Communications.* 339-340.

Fibbioli, M., Bandyopadhyay, K., Liu, S. G., Echegoyen, L., Enger, O., Diederich, F., Gingery, D., Buhlmann, P., Persson, H., Suter, U. W. and Pretsch, E. (2002) Redox-Active Self-Assembled Monolayers for Solid-Contact Polymeric Membrane Ion-Selective Electrodes. *Chemistry of Materials.* 14**.** 1721-1729.

Garnier, F. (1989) Functionalized Conducting Polymers - Towards Intelligent Materials. *Angewandte Chemie-International Edition in English.* 28**.** 513-517.

Groenendaal, B. L., Jonas, F., Freitag, D., Pielartzik, H. and Reynolds, J. R. (2000) Poly(3,4-Ethylenedioxythiophene) and Its Derivatives: Past, Present, and Future. *Advanced Materials.* 12**.** 481-494.

Hauser, P. C., Chiang, D. W. L. and Wright, G. A. (1995) A Potassium-Ion Selective Electrode with Valinomycin Based Poly(vinyl chloride) Membrane and a Poly(vinyl ferrocene) Solid Contact. *Analytica Chimica Acta.* 302**.** 241-248.

Horvai, G., Toth, K. and Pungor, E. (1976) A Simple Continuous Method for Calibration and Measurement with Ion-Selective Electrodes. *Analytica Chimica Acta.* 82**.** 45-54.

Hulanicki, A. and Michalska, A. (1995) All-Solid-State Chloride-Selective Electrode with Poly(pyrrole) Solid Contact. *Electroanalysis.* 7**.** 692-693.

Hulanicki, A. and Trojanowicz, M. (1976) Calcium-Selective Electrodes with PVC Membranes and Solid Internal Contacts. *Analytica Chimica Acta.* 87**.** 411-417.

Knight, H., Trewavas, A. J. and Knight, M. R. (1996) Cold Calcium Signaling in Arabidopsis Involves Two Cellular Pools and a Change in Calcium Signature After Acclimation. *Plant Cell.* 8**.** 489-503.

Krivan, E., Visy, C. and Kankare, J. (2003) Deprotonation and Dehydration of Pristine PPy/DS Films during Open-circuit Relaxation: An Ignored Factor in Determining The Properties of Conducting Polymers. *Journal of Physical Chemistry B.* 107**.** 1302-1308.

Lew, R. R. (1998) Immediate and Steady State Extracellular Ionic Fluxes of Growing Arabidopsis Thaliana Root Hairs under Hyperosmotic and Hypoosmotic Conditions. *Physiologia Plantarum.* 104**.** 397-404.

Li, W. J., Teasdale, P. R., Zhang, S. Q., John, R. and Zhao, H. J. (2003) Application of a Poly(4-Styrenesulfonate) Liquid Binding Layer for Measurement of Cu^{2+} and Cd^{2+} with the Diffusive Gradients in Thin-Films Technique. *Analytical Chemistry.* 75**.** 2578-2583.

Li, Y. F. and Qian, R. Y. (1993) Stability of Conducting Polymers from the Electrochemical Point-of-View *Synthetic Metals.* 53**.** 149-154.

Lindfors, T., Bobacka, J., Lewenstam, A. and Ivaska, A. (1996) Impedance Spectroscopic Study on Single-Piece All-Solid-State Calcium-Selective Electrode Based on Polyaniline. *Analyst.* 121**.** 1823-1827.

Lindfors, T. and Ivaska, A. (2000) All-Solid-State Calcium-Selective Electrode Prepared of Soluble Electrically Conducting Polyaniline and Di(2-Ethylhexyl)phosphate with ETH1001 as Neutral Carrier. *Analytica Chimica Acta.* 404**.** 101-110.

Lindfors, T. and Ivaska, A. (2004) Stability of The Inner Polyaniline Solid Contact Layer in All-solid-state K^+-Selective Electrodes Based on Plasticized Poly(vinyl chloride). *Analytical Chemistry.* 76**.** 4387-4394.

Lindfors, T., Sjoberg, P., Bobacka, J., Lewenstam, A. and Ivaska, A. (1999) Characterization of a Single-Piece All-Solid-State Lithium-Selective Electrode Based on Soluble Conducting Polyaniline. *Analytica Chimica Acta.* 385**.** 163-173.

Lindner, E., Cosofret, V. V., Ufer, S., Johnson, T. A., Ash, R. B., Nagle, H. T., Neuman, M. R. and Buck, R. P. (1993) In Vivo and In Vitro Testing of Microelectronically Fabricated Planar Sensors Designed for Applications in Cardiology. *Fresenius Journal of Analytical Chemistry.* 346**.** 584-588.

Lindner, E., Gyurcsanyi, R. E. and Buck, R. P. (1999) Tailored Transport Through Ion-Selective Membranes for Improved Detection Limits and Selectivity Coefficients. *Electroanalysis.* 11**.** 695-702.

Maksymiuk, K., Bobacka, J., Ivaska, A. and Lewenstam, A. (2000) Coupled Redox and pH Potentiometric Responses of Electrodes Coated with Polypyrrole. *Analytical Letters.* 33**.** 1339-1360.

Marsella, M. J. and Swager, T. M. (1993) Designing Conducting Polymer-Based Sensors: Selective Ionochromic Response in Crown Ether-Containing Polythiophenes. *Journal of the American Chemical Society.* 115**.** 12214-12215.

Mathison, S. and Bakker, E. (1998) Effect of Transmembrane Electrolyte Diffusion on the Detection Limit of Carrier-Based Potentiometric Ion Sensors. *Analytical Chemistry.* 70**.** 303-309.

Meier, P. C. (1982) Two-Parameter Debye-Huckel Approximation for the Evaluation of Mean Activity Coefficients of 109 Electrolytes. *Analytica Chimica Acta.* 136**.** 363-368.

Michalska, A. (2005) Improvement of Analytical Characteristic of Calcium Selective Electrode with Conducting Polymer Contact. The Role of Conducting Polymer Spontaneous Charge Transfer Processes and Their Galvanostatic Compensation. *Electroanalysis.* 17**.** 400-407.

Michalska, A., Dumańska, J. and Maksymiuk, K. (2003) Lowering the Detection Limit of Ion-Selective Plastic Membrane Electrodes with Conducting Polymer Solid Contact and Conducting Polymer Potentiometric Sensors. *Analytical Chemistry.* 75**.** 4964-4974.

Michalska, A., Hulanicki, A. and Lewenstam, A. (1997a) All-Solid-State Potentiometric Sensors for Potassium and Sodium Based on Poly(pyrrole) Solid Contact. *Microchemical Journal.* 57**.** 59-64.

Michalska, A., Ivaska, A. and Lewenstam, A. (1997b) Modeling Potentiometric Sensitivity of Conducting Polymers. *Analytical Chemistry.* 69**.** 4060-4064.

Michalska, A. and Lewenstam, A. (2000) Potentiometric Selectivity of p-Doped Polymer Films. *Analytica Chimica Acta.* 406**.** 159-169.

Michalska, A. and Maksymiuk, K. (1998) On The pH Influence on Electrochemical Properties of Poly(pyrrole) and Poly(N-methylpyrrole). *Electroanalysis.* 10**.** 177-180.

Michalska, A. and Maksymiuk, K. (1999) The Specific Influence of Hydrogen Ions on Poly(pyrrole) Potentiometry. *Electrochimica Acta.* 44**.** 2125-2129.

Michalska, A. and Maksymiuk, K. (2004a) All-Plastic, Disposable, Low Detection Limit Ion-Selective Electrodes. *Analytica Chimica Acta.* 523**.** 97-105.

Michalska, A. and Maksymiuk, K. (2004b) Conducting Polymer Membranes for Low Activity Potentiometric Ion Sensing. *Talanta.* 63**.** 109-117.

Michalska, A., Maksymiuk, K. and Hulanicki, A. (1995) On the Nature of the Potentiometric Response of Polypyrrole in Acidic Solutions. *Journal of Electroanalytical Chemistry.* 392**.** 63-68.

Michalska, A., Nadrzycka, U. and Maksymiuk, K. (2001) The Modelled and Observed Transition from Redox to Ionic Potentiometric Sensitivity of Poly(pyrrole). *Electrochimica Acta.* 46**.** 4113-4123.

Michalska, A., Ocypa, M. and Maksymiuk, K. (2005) Highly Selective All-Plastic, Disposable, Cu^{2+}-Selective Electrodes. *Electroanalysis.* 17**.** 327-333.

Michalska, A., Walkiewicz, S., Maksymiuk, K. and Hall, E. A. H. (2002) Potentiometric Responses of Poly(pyrrole) Films Surface Modified by Nafion. *Electroanalysis.* 14**.** 1236-1244.

Michalska, A. J. and Hall, E. A. H. (1999) Inducing a Cationic Response in Poly(pyrrole) Films. *Electroanalysis.* 11**.** 756-762.

Migdalski, J., Blaz, T. and Lewenstam, A. (1996) Conducting Polymer-Based Ion-Selective Electrodes. *Analytica Chimica Acta.* 322**.** 141-149.

Migdalski, J., Blaz, T. and Lewenstam, A. (1999) Electrochemical Deposition and Properties of Polypyrrole Films Doped with Calcion Ligands. *Analytica Chimica Acta.* 395**.** 65-75.

Nikolskii, B. P. and Materova, E. A. (1985) Solid Contact in Membrane Ion-Selective Electrodes. *Ion-Selective Electrode Reviews.* 7**.** 3-39.

Oesch, U. and Simon, W. (1980) Life Time of Neutral Carrier Based Ion-Selective Liquid-Membrane Electrodes. *Analytical Chemistry.* 52**.** 692-700.

Orrenius, S., Zhivotovsky, B. and Nicotera, P. (2003) Regulation of Cell Death: The Calcium-Apoptosis Link. *Nature Reviews Molecular Cell Biology.* 4**.** 552-565.

Paczosa-Bator, B., Migdalski, J. and Lewenstam, A. (2006) Conducting Polymer Films as Model Biological Membranes - Electrochemical and Ion-Exchange Properties of Poly(pyrrole) Films Doped with Asparagine and Glutamine. *Electrochimica Acta.* 51**.** 2173-2181.

Patil, A. O., Ikenoue, Y., Wudl, F. and Heeger, A. J. (1987) Water-Soluble Conducting Polymers. *Journal of the American Chemical Society.* 109**.** 1858-1859.

Pei, Q. B. and Qian, R. Y. (1992) Electrode-potentials of Electronically Conducting Polymer Polypyrrole. *Electrochimica Acta.* 37**.** 1075-1081.

Pergel, E., Gyurcsanyi, R. E., Toth, K. and Lindner, E. (2001) Picomolar Detection Limits with Current-Polarized Pb^{2+} Ion-Selective Membranes. *Analytical Chemistry.* 73**.** 4249-4253.

Plieth, C., Hansen, U. P., Knight, H. and Knight, M. R. (1999) Temperature Sensing by Plants: The Primary Characteristics of Signal Perception and Calcium Response. *Plant Journal.* 18**.** 491-497.

Qian, R. Y., Pei, Q. B. and Li, Y. F. (1993) Proton Doping of Reduced Polypyrrole. *Synthetic Metals.* 61**.** 275-278.

Shabala, S. (2003) Regulation of Potassium Transport in Leaves: from Molecular to Tissue Level. *Annals of Botany.* 92**.** 627-634.

Shabala, S., Demidchik, V., Shabala, L., Cuin, T. A., Smith, S. J., Miller, A. J., Davies, J. M. and Newman, I. A. (2006) Extracellular Ca^{2+} Ameliorates NaCl-Induced K^+ Loss from Arabidopsis Root and Leaf Cells by Controlling Plasma Membrane K^+-Permeable Channels. *Plant Physiology.* 141**.** 1653-1665.

Sokalski, T., Ceresa, A., Zwickl, T. and Pretsch, E. (1997) Large Improvement of the Lower Detection Limit of Ion-Selective Polymer Membrane Electrodes. *Journal of the American Chemical Society.* 119**.** 11347-11348.

Sun, X. X., Sun, L. Z. and Aboul-Enein, H. Y. (2000) Internal Solid Contact Electrode for the Determination of Salbutamol Sulfate in Pharmaceutical Formulation. *Electroanalysis.* 12**.** 853-857.

Sundfors, F., Bereczki, R., Bobacka, J., Toth, K., Ivaska, A. and Gyurcsanyi, R. E. (2006) Microcavity Based Solid-Contact Ion-Selective Microelectrodes. *Electroanalysis.* 18**.** 1372-1378.

Tamburri, E., Orlanducci, S., Toschi, F., Terranova, M. L. and Passeri, D. (2009) Growth Mechanisms, Morphology, and Electroactivity of PEDOT Layers Produced by Electrochemical Routes in Aqueous Medium. *Synthetic Metals.* 159**.** 406-414.

Vandenvlekkert, H. H., Kloeck, B., Prongue, D., Berthoud, J., Hu, B., Derooij, N. F., Gilli, E. and Decrousaz, P. (1988) A pH-ISFET and An Integrated pH-Pressure Sensor with Back-Side Contacts. *Sensors and Actuators.* 14**.** 165-176.

Vázquez, M., Bobacka, J., Ivaska, A. and Lewenstam, A. (2002) Influence of Oxygen and Carbon Dioxide on the Electrochemical Stability of Poly(3,4-ethylenedioxythiophene) Used as Ion-to-Electron Transducer in All-Solid-State Ion-Selective Electrodes. *Sensors and Actuators B-Chemical.* 82**.** 7-13.

Youssoufi, H. K., Yassar, A., Baiteche, S., Hmyene, M. and Garnier, F. (1994) Designing Polypyrrole-Based Sensors: Selective Electrochemical Cation in Aza Crown Ethers. *Synthetic Metals.* 67**.** 251-254.

CHAPTER 8

CHIRAL ACID SELECTIVITY DISPLAYED BY PEDOT ELECTROPOLYMERISED IN THE PRESENCE OF CHIRAL MOLECULES

8.1 Introduction

Chirality (handedness) is a property of nonsuperimposability of an object on its mirror image and is a common property found in nature such as hands, feet and shoes. These objects have right- and left-handedness and are not superimposable on each other. A pair of molecules that possesses this property are called enantiomers. A sample is enantiomerically pure if only one enantiomer is present. Enantiomers are optically active as they can rotate the plane of polarisation and each rotates in the opposite direction. The enantiomer causing a clockwise rotation of the plane-polarised light is called the dextrorotatory (+)- or *d*-isomer, while that causing an anti-clockwise rotation is termed the levorotatory (-)- or *l*-isomer. *Dextro* and *levo* are latin prefixes for "to the right" and "to the left", respectively. An achiral compound does not rotate the plane of polarisation and it is optically inactive.

In chemistry, chiral properties are associated with certain organic molecules, biological compounds and inorganic salts. In living organisms, most of the important molecules are chiral such as amino acids, sugars, proteins and nucleic acids. These chiral molecules are very important because biological systems show homochirality and tend to favour one enantiomer of a chiral molecule over the other. This is the reason why only L-amino acid and D-glucose are absorbed into our body. Homochirality (one-handedness) refers to a group of molecule having the same sense of chirality. This term is commonly applied to biological macromolecules such as proteins and deoxyribonucleic acids (DNA). Protein molecules are constructed from a set of amino acids. All amino acids are chiral

(except of glycine) and they can exist in two mirror image forms. However, in proteins, amino acids exist in their left-handed form. Similarly nucleic acids contain all right-handed sugars. The origin of this phenomenon is not well understood but it is essential to form the right shape of protein and double helix structure of DNA in order to function effectively (Wade, 2002).

The importance of chirality is also seen in the high number of chiral compounds used in the pharmaceutical industries such as drugs (Mohan *et al.*, 2009). Many drugs molecules are chiral and usually only one enantiomer may perform the desired task, the other enantiomer may be inactive or even toxic. The chiral interactions exist due to the different stereochemistry of biologically active chiral molecules. Thus, each enantiomer may react differently when in a chiral environment such as in the body. Drug receptors are protein (chiral environment) and will bind one enantiomer of drugs better than the other. A similar effect occurs for receptors located on the exterior of nerve cells in the nose. These receptors are able to perceive and differentiate the estimated 10,000 smells to which they are exposed (Bruice, 2004). For instance, (*R*)-(−)-carvone is found in spearmint oil and (*S*)-(+)-carvone is the main constituent of caraway seed oil. These two enantiomers have different odours because each enantiomer fits into different receptor (Bruice, 2004).

There are a few types of chirality in molecules namely central chirality, planar chirality, axial chirality and helical chirality. The most important forms of chirality in this study are those of central chirality and helical chirality. Central chirality is related to a tetrahedral atom bonded to four different substituents. Helical chirality refers to a helical molecule that can adopt either right- or left-handed twist. This chirality is commonly found in biopolymers such as DNA and proteins (Wade, 2002). Circular dichroism (CD) spectroscopy is one of the techniques used to characterise chiral molecules. This technique measures the difference in molar extinction coefficients when passing left and right hand circularly polarized light through a sample of the compound ($\Delta\varepsilon = \varepsilon_L - \varepsilon_R$). Enantiomeric molecules exhibit mirror imaged CD spectra of opposite sign. This technique has proved to be a powerful tool for probing polymer chain conformations, including chiral conducting

polymer. CD spectroscopy can also be used to study molecular interactions. For instance, this technique can determine whether protein-protein or protein-ligand interactions can alter the conformation of protein. Any conformational changes will result in a spectrum which will differ from the sum of the individual components.

A few methods have been developed for chiral recognition such as high-performance liquid chromatography (HPLC) (Aneja *et al.*, 2010) and electrochemical detection (Trojanowicz and Kaniewska, 2009). HPLC is commonly used for the separation of two enantiomers by having a chiral stationary phase in a column. This technique is laborious, requires several chemical pretreatments for a sample and is time-consuming. However, electrochemical sensors based on chiral electrodes has become the subject of interest for chiral recognition studies (Bates *et al.*, 1992, Bates *et al.*, 1994, Trojanowicz and Kaniewska, 2009) due to advantages such as simple set-up, relative speed of use and cost effectiveness compared to chromatographic techniques. In addition, electrochemical sensors exhibit high enantioselectivity, sensitivity and accuracy (Ozoemena *et al.*, 2005).

The use of conducting polymer (CP) modified electrodes as chiral electrodes gives some advantages such as the polymer films are readily on the surface of the electrode after electropolymerisation and a high conductivity of the polymer film enhances the electron transfer and allows the preparation on electrodes of large surface to volume ratio. The properties of electrodeposited CPs can be tailored by choosing suitable dopants for certain applications. Several approaches can be used to induce chirality in CP such as covalently bonded chiral substituent on the monomer as a side chain (Elsenbaumer *et al.*, 1985) and doping with a chiral dopant (Goto and Akagi, 2006). The first report of the preparation of chiral CPs was by Elsenbaumer *et al.* (1985) via electropolymerisation of pyrrole monomers bearing chiral substituents covalently bonded to the N atom of pyrrole (**Figure 8.1**). Since then there have been several reports of the introduction of optically active moieties to achiral polymers (Kane-Maguire and Wallace, 2010). Amongst the many CPs, poly(3,4-ethylenedioxythiophene) (PEDOT) has attracted the most interest due to its high environmental stability (Vázquez *et al.*, 2002, Yamato *et al.*, 1995) compared to commonly

used CPs such as polyaniline (PAn) and polypyrrole (PPy). Chiral PEDOTs were initially reported by Caras-Quintero and Bäuerle (2004) by substituting different chiral moieties at the ethylene bridge. However, the approach to introduce chirality in CP via synthesis of chiral monomers is tedious and expensive. Alternatively, a simple method of doping the conducting polymer with chiral dopants can be utilised.

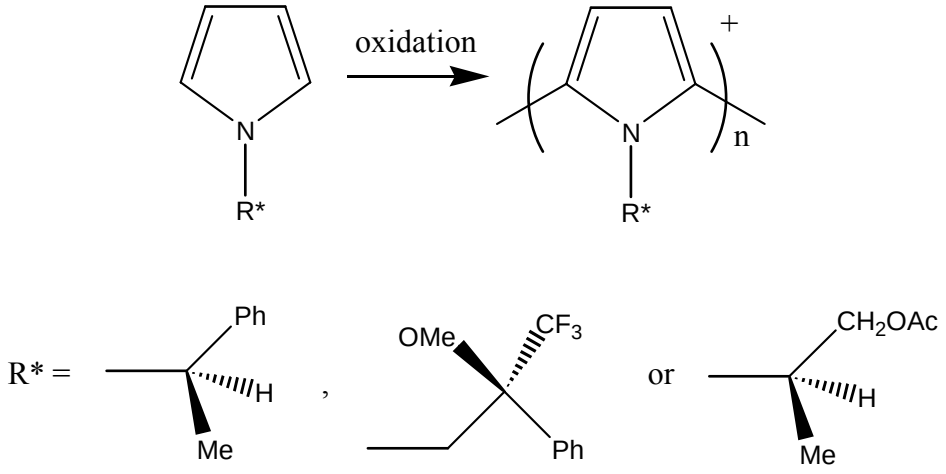

Figure 8.1: Electropolymerisation of pyrrole bearing chiral substituents (Elsenbaumer *et al.*, 1985).

The introduction of chirality in conducting polymers via the incorporation of optically active dopant anions is less well explored compared to monomers bearing chiral substituents. Aboutanos *et al.* (2000) have studied the electropolymerisation of pyrroles in the presence of camphorsulfonic acid, tartaric acid and mandelic acid enantiomers. The PPy-camphorsulfonic acid formed was found to be weakly active but both PPy- tartaric acid and PPy- mandelic acid were mildly optically active. Recently, Fu *et al.* (2011) has demonstrated a novel strategy for the recognition of mandelic acid enantiomers in the presence of metal ion (Zn^{2+}) on L-cysteine self-assembled on gold electrode. The recognition was based on the enantioselective formation of Zn complexes with mandelic acid enantiomers.

In this work, chiral selectors were prepared by electropolymersing PEDOT using two approaches; either by electropolymersing PEDOT in the presence of chiral anions such as anionic collagen and hyaluronic acid (HA) or by electropolymerising in a chiral environment provided by the helical polymer hydroxypropyl cellulose (HPC) (Goto and Akagi, 2006), with perchlorate as the dopant ion. Both anionic collagen and HA are negatively charged and have intrinsic chiral properties. Collagen is a fibrous protein found in muscle, bones and tendons, and consists of three polypeptide chains, each possessing left-handed helicity, which has been used previously as a chiral agent (Kataky and Zawawi, 2010). The three polypeptide chains coil together into a right-handed triple helix structure (**Figure 8.2**). The polypeptide chains in collagen mainly consist of glycine and proline residues. Hydrogen bonding between the N-H and C=O groups of adjacent chains is important for maintaining the fibrous structure. HA (**Figure 8.3**) is a glucosaminoglycan that present in the intercellular matrix of most vertebrates and in neural tissue. It has multiple chiral centres that consists of alternating disaccharide units of D-glucuronic acid and N-acetyl-D-glucosamine, linked by alternating β-1,4 and β-1,3 glycosidic bonds. These chiral anions can be regarded as chiral dopants. HPC (**Figure 8.4**) is an ether of cellulose that is soluble both in water and polar organic solvent. In water, it forms a right-handed helical nematic liquid crystal (N*-LC) structure (Werbowyj and Gray, 1984). Electropolymerisation is carried out with perchlorate as the dopant ion with HPC forming a chiral nematic phase for inducing chiral alignment during electropolymerisation. Optically active PEDOT with HPC (chiral environment) has been previously reported (Goto and Akagi, 2006) but the enantioselective properties have not been investigated.

In this work, the enantioselective properties of the chiral PEDOT assembled by the above methods were examined in the presence of enantiomers of mandelic acid (**Figure 8.5**) using electrochemical techniques. This work may provide a way forward for chiral extraction and detection.

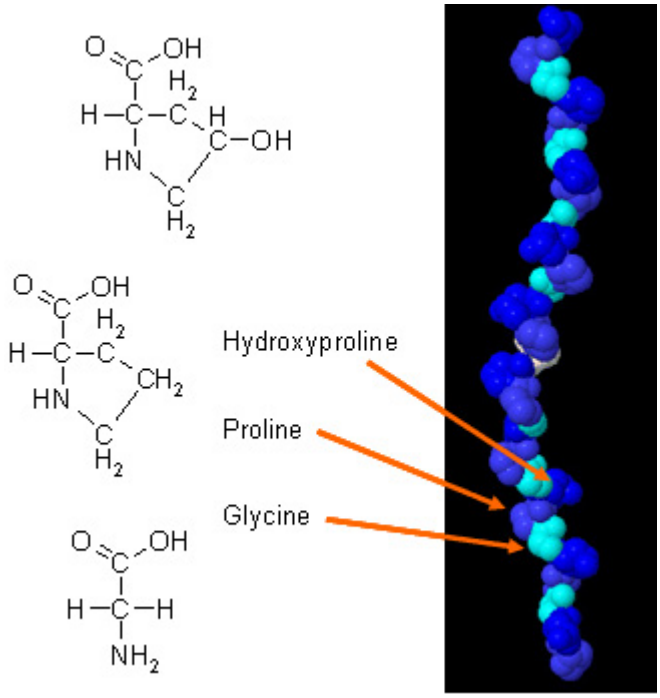

Figure 8.2: Structure of triple helix collagen and the structural formula.

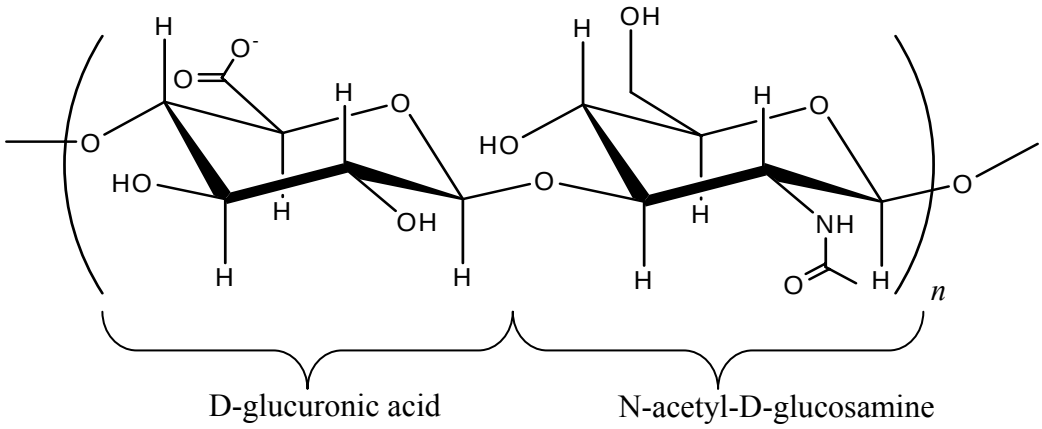

Figure 8.3: Structure of hyaluronic acid (HA).

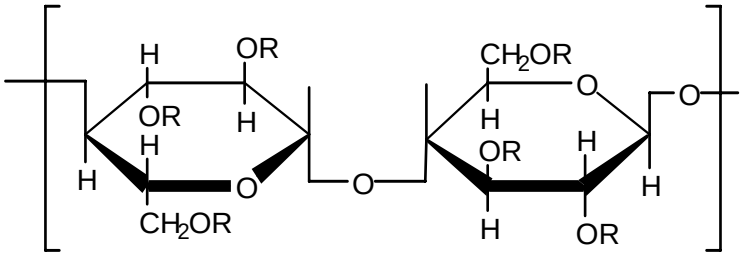

Figure 8.4: Structure of hydroxypropyl cellulose (HPC).

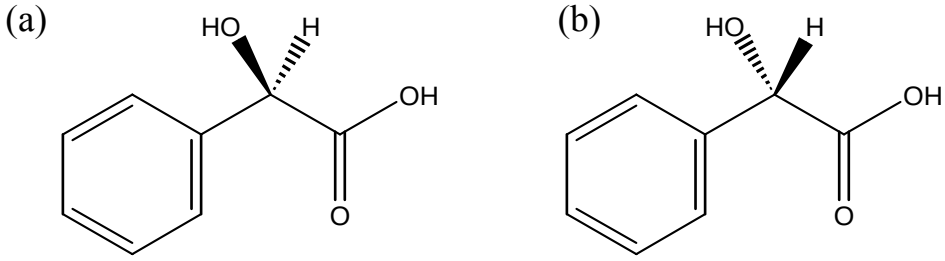

Figure 8.5: Chemical structure of (a) (*R*)-(−)- and (b) (*S*)-(+)-mandelic acid.

8.2 Experimental

8.2.1 Chemicals and Reagents

(*R*)-(−)-mandelic acid, (*S*)-(+)-mandelic acid, hyaluronic acid (HA) sodium salt from *streptococcus equi*, collagen from rat tail, hydroxypropyl cellulose (HPC), potassium chloride (KCl), 3,4-ethylenedioxythiophene (EDOT) and potassium hydroxide (KOH) were obtained from Aldrich, UK. Hydrochloric acid and tetrabutylammonium perchlorate (TBAP) were supplied from Fisher and Fluka, UK, respectively. All chemicals were used as received without any further purification.

8.2.2 Instrumentation and Electropolymerisation

Glassy carbon (GC) electrodes (Bioanalytical System Inc.) were used as a substrate for depositing PEDOT. The GC electrodes were polished with alumina slurry (0.05 μm) before electropolymerisation. The electrode was then cleaned ultrasonically in deionised water for a few minutes to remove any trace alumina from the surface. The electrochemical polymerisations of EDOT and voltammetry measurements were carried out using a multichannel potentiostat model VMP (Perkin-Elmer Instruments). The electropolymerisation of EDOT with chiral molecules (collagen, HA and HPC) were performed in one-compartment three-electrode electrochemical cell. A Ag/AgCl (3.5 M KCl) and a Pt plate were used as reference and counter electrode, respectively. PEDOT was deposited on the GC electrode by galvanostatic electropolymerisation of 0.01 M EDOT in 1 mg/mL collagen, 65 wt% HPC or 1 mg/mL HA. For the electropolymerisation containing HPC, 0.1 M TBAP was used as supporting electrolyte (Goto and Akagi, 2006). A constant current density of 0.2 mA/cm^2 was applied for 600 s. After the electropolymerisation, the electrodes were rinsed with distilled water to remove unreacted EDOT. The deconvolutions of the peaks from voltammetric measurements were performed using OriginPro 7.5 (OriginLab Corporation, USA).

The morphology of polymer films was analysed by Hitachi SU70 (Hitachi High Technologies) and the topography of the polymer films was studied with atomic force microscopy (AFM) (Nanoscope IV scanning probe microscope controller, Digital Instruments Inc., Santa Barbara, CA). For SEM and AFM measurements, the polymers films were prepared on ITO coated glass. The measurements were performed using tapping mode in ambient condition.

8.3 Results and Discussion

8.3.1 Surface Characterisation

Scanning electron microscopy (SEM) was carried out in order to study the surface morphology of the conducting polymer films on ITO coated glass. The electropolymerised films revealed very diverse structures. PEDOT/collagen (**Figure 8.6a**) showed a granular structure whereas PEDOT/HA (**Figure 8.6b**) revealed a cauliflower-like structure. The SEM image of PEDOT/HA is similar to the cauliflower-like structure of PEDOT/PSS (**Chapter 7**). The size of the cauliflower structure is larger (2.5 μm) compared to PEDOT/PSS (1. 5 μm). PEDOT-HPC/ClO_4 (**Figure 8.6c**), on the other hand showed very fine well-ordered structures, in agreement with the findings of Goto and Akagi (Goto and Akagi, 2006), who reported PEDOT-HPC/ClO_4 as an optically active polymer with electrochromic properties. This morphology is different from the SEM images of other PEDOTs, which commonly exhibits rough, porous and cauliflower-like structure as discussed in Chapter 5 and 7. This is probably due to the chiral liquid crystal structure provided by HPC (Goto and Akagi, 2006).

The AFM studies revealed that PEDOT/collagen had granular morphology (**Figure 8.7a**) which was consistent with the SEM micrograph (**Figure 8.6a**). In addition, PEDOT/collagen showed the roughest surface (RMS roughness of 243 ± 2 nm) compared to the PEDOT/HA (RMS: 76 ± 6 nm) and PEDOT-HPC/ClO_4 (RMS: 46 ± 3 nm). It is clearly seen that different, well-distributed microstructures are obtained by these electropolymerisation methods. Such observations have been reported previously by Ivaska and co workers (Han *et al.*, 2007).

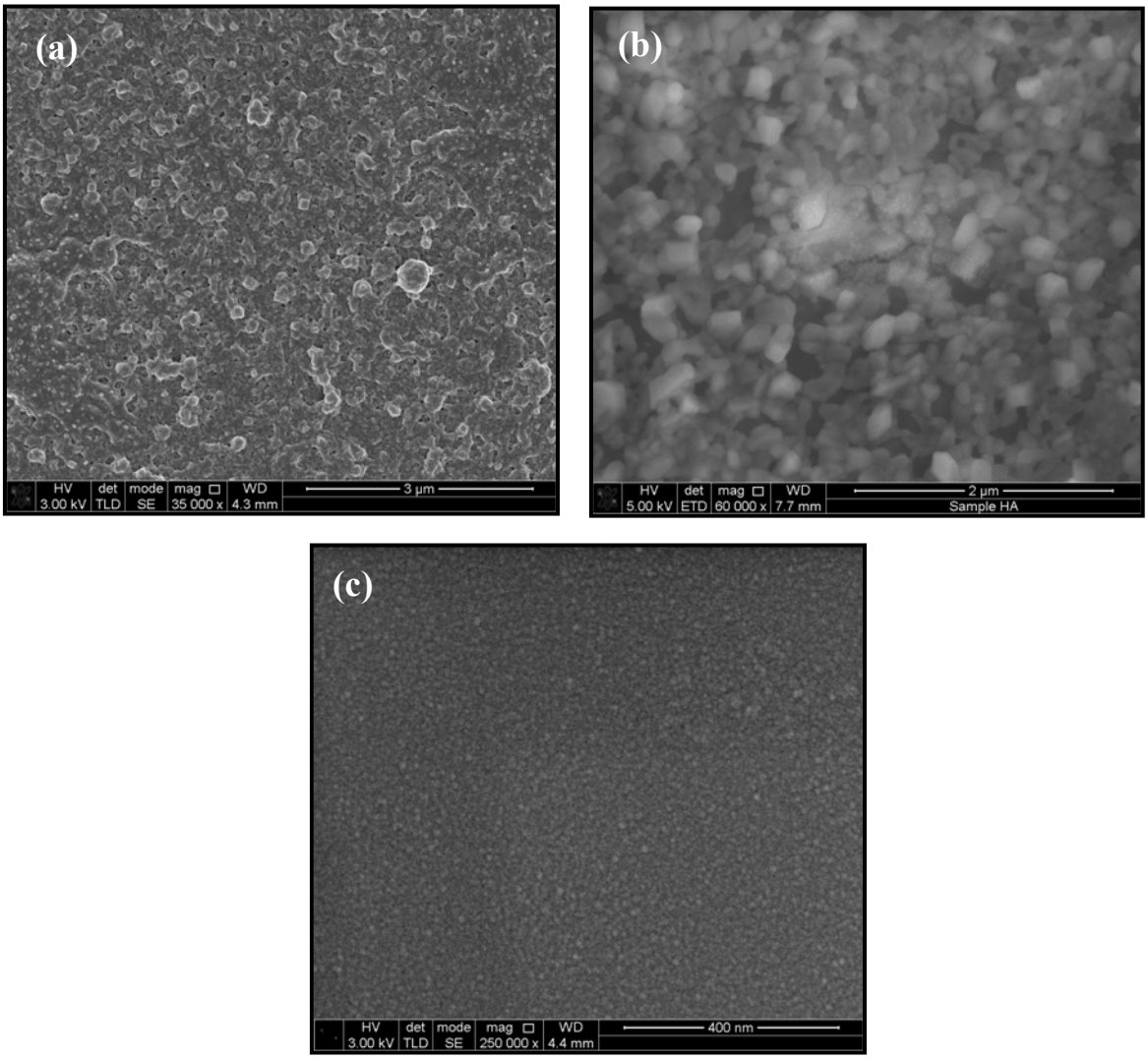

Figure 8.6: SEM images of (a) PEDOT/collagen, (b) PEDOT/HA and (c) PEDOT-HPC/ClO_4.

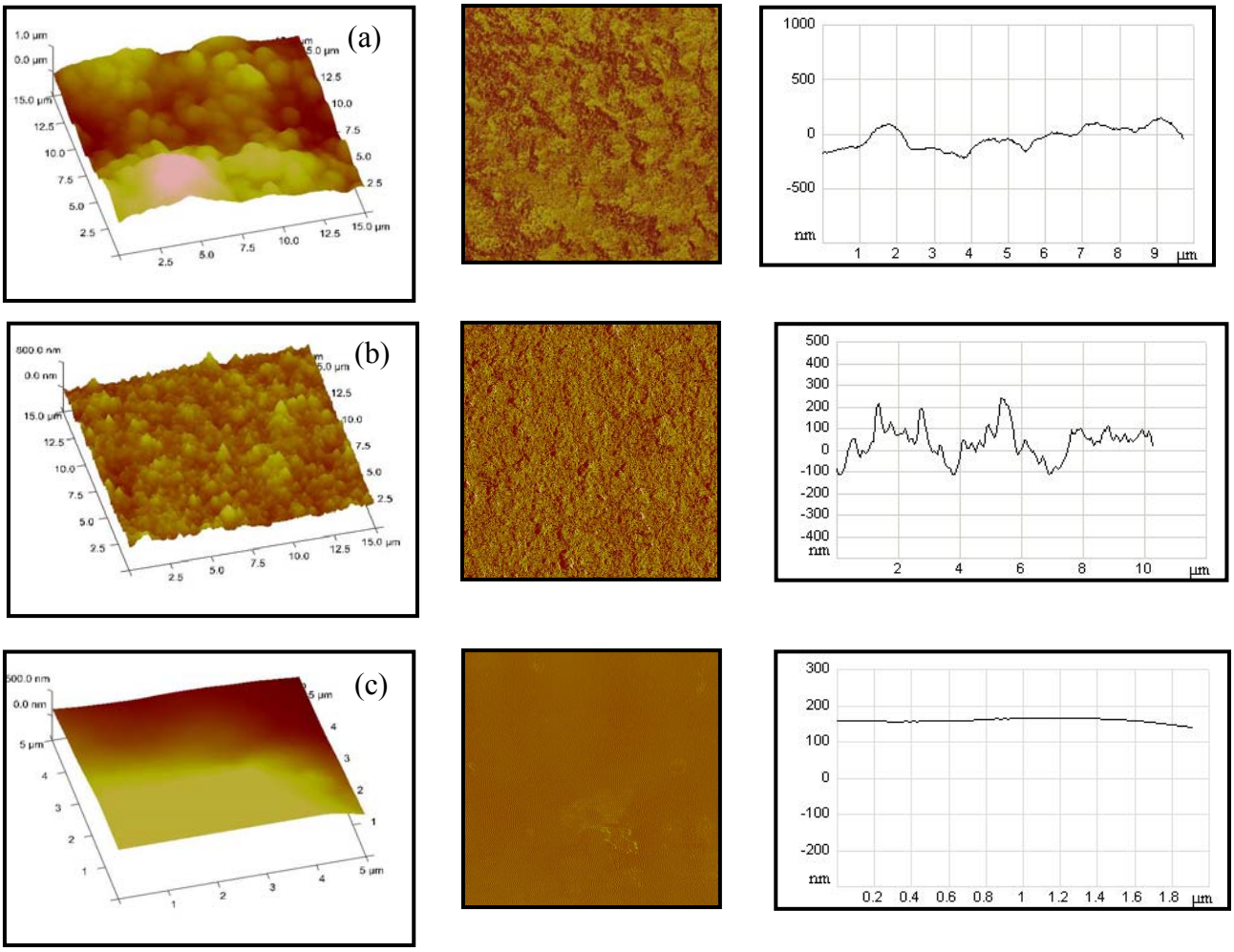

Figure 8.7: AFM image of (a) PEDOT/collagen (RMS: 243 ± 2 nm) (b) PEDOT/HA (RMS: 76 ± 6 nm) (c) PEDOT-HPC/ClO_4 (RMS: 46 ± 3 nm). 3-dimensional (left), phase imaging (middle) and typical roughness profile (right).

8.3.2 Enantioselectivity of Chiral PEDOT

In this present work, PEDOT/collagen, PEDOT/HA and PEDOT-HPC/ClO_4 hybrids, were used as enantioselective composites for the detection of chiral anions using the enantiomers of mandelic acid as an example. In order to verify the enantioselectivity of PEDOT/collagen, PEDOT/HA and PEDOT-HPC/ClO_4, the cyclic voltammograms recorded in 100 mM KCl containing 1 mM (*R*)-(−)-mandelic acid and (*S*)-(+)-mandelic acid were compared. As can been seen in **Figure 8.8a**, anodic and cathodic peaks were

observed for PEDOT/collagen in the presence of (*R*)-(−)-mandelic acid. In contrast, no observable peak was found for (*S*)-(+)-mandelic acid. This observation reveals strong enantioselective recognition between the two mandelic acid enantiomers.

Initial observations using cyclic voltammograms were further analysed using square wave voltammetry, which is much more sensitive technique. A striking evidence in chiral discrimination appeared as a well-defined peak at 298 mV for (*R*)-(−)-mandelic acid in comparison to (*S*)-(+)-mandelic acid (**Figure 8.8b**)**.** Similar results were also observed for PEDOT/HA (288 mV, **Figure 8.9a**) and PEDOT-HPC/ClO_4 (298 mV, **Figure 8.9b**). These results clearly indicate the existence of chiral interactions between the composites and the chiral anion, (*R*)-(−)-mandelic acid. The comparison of the square wave voltammograms (**Figure 8.10**) showed a significantly high current observed with (*R*)-(−)-mandelic acid for PEDOT-HPC/ClO_4 (45.25 μA) compared to the PEDOT/collagen (17.48 μA) and PEDOT/HA (18.36 μA) chiral sensors.

There are several reports on the distribution of reduced and oxidised species of conducting polymers on electrode surfaces. This is clearly illustrated in Li and Imae's paper (Li and Imae, 2004) showing the existence of dual mode of ion-exchange in the redox process of PEDOT films. **Figure 8.11** and **Figure 8.12** depict the speciation of mandelic acid at different pHs and the possible interactions of the PEDOT/collagen, PEDOT/HA and PEDOT-HPC/ClO_4 films (*vide infra*). The results obtained show that (*R*)-(−)-mandelic acid interact with PEDOT/collagen, PEDOT/HA and PEDOT-HPC/ClO_4 in a stereoselective manner and suggests that the opposite enantiomer is sufficiently inhibited in its ingress to prohibit redox reaction. This deduction was also confirmed by control experiment using a bare glassy carbon electrode (**Figure 8.10**). This result revealed that the chiral sensors possess excellent chiral discrimination between (*R*)-(−)- and (*S*)-(+)-mandelic acid.

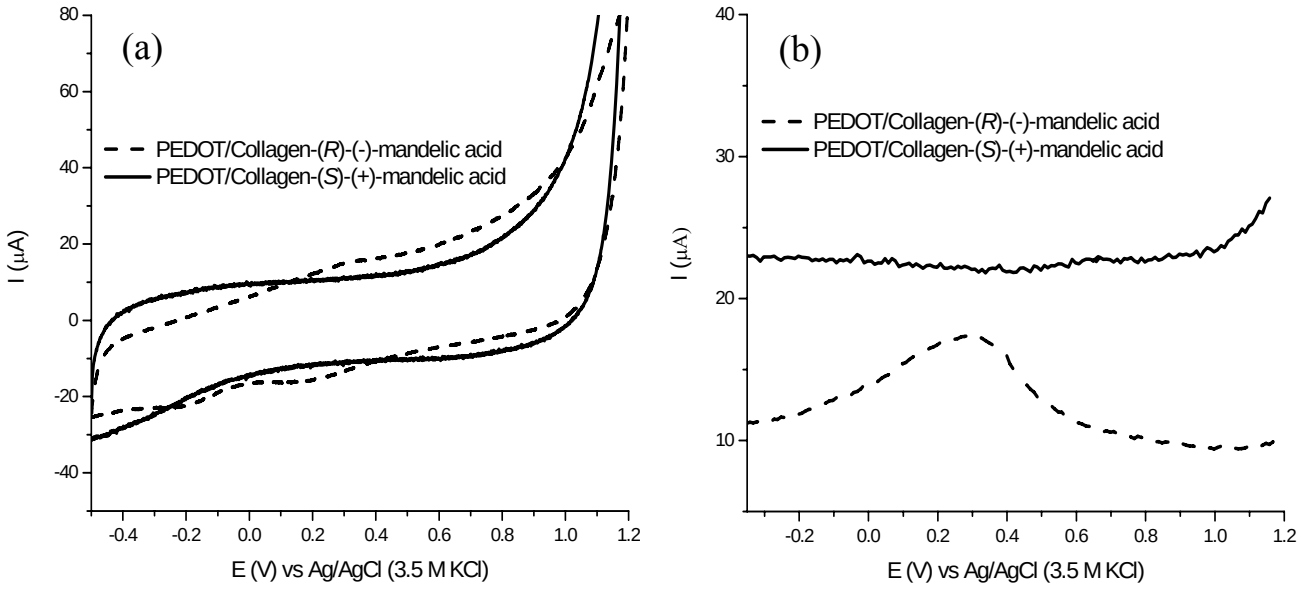

Figure 8.8: (a) Cyclic voltammograms and (b) square-wave voltammograms of PEDOT/collagen in 100 mM KCl containing 1 mM (*R*)-(−)-mandelic acid (dashed line) and 1 mM (*S*)-(+)-mandelic acid (solid line).

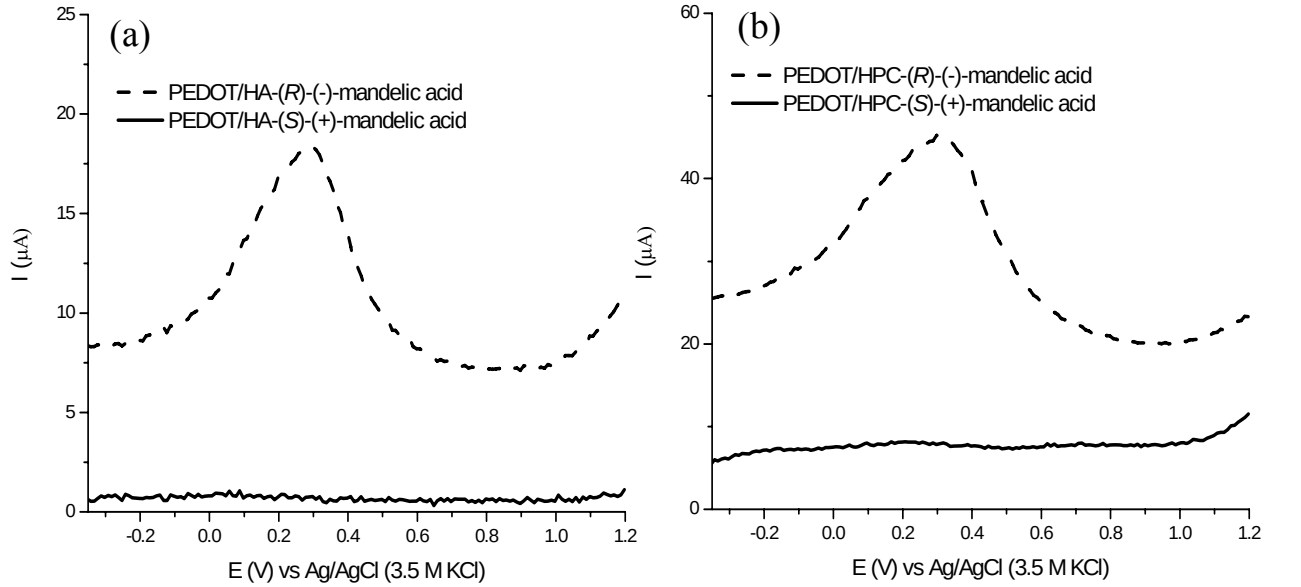

Figure 8.9: Square-wave voltammograms of (a) PEDOT/HA and (b) PEDOT-HPC/ClO_4 in 100 mM KCl containing 1 mM (*R*)-(−)-mandelic acid (dashed line) and 1 mM (*S*)-(+)-mandelic acid (solid line).

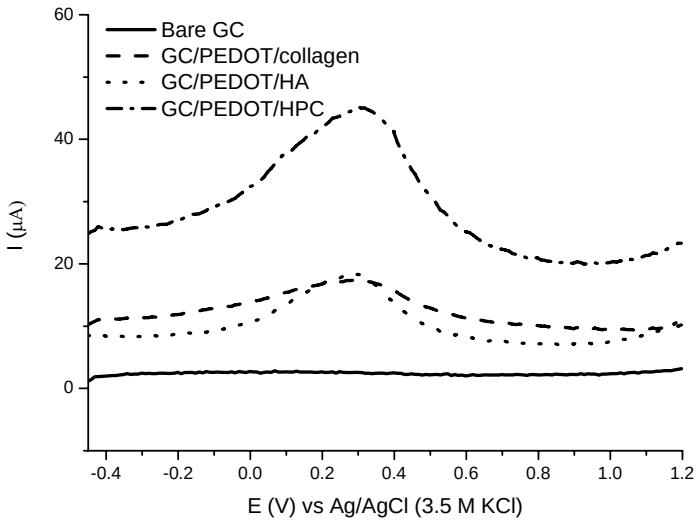

Figure 8.10: Comparison of square-wave voltammograms of PEDOT electropolymerised with different chiral molecules in 100 mM KCl containing 1 mM (*R*)-(−)-mandelic acid.

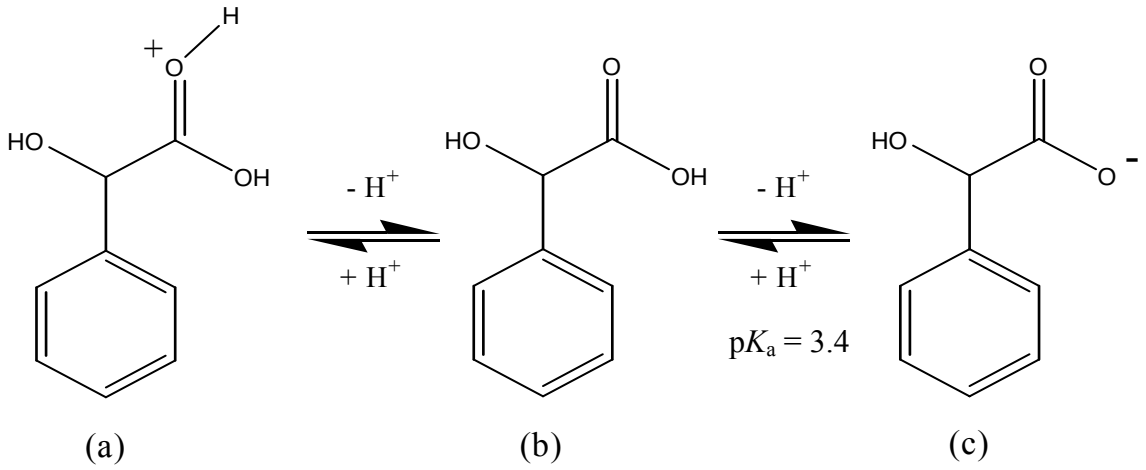

Figure 8.11: Structure of mandelic acid: (a) protonated form (HMA^+) (b) neutral form (MA) and (c) deprotonated form (MA^-).

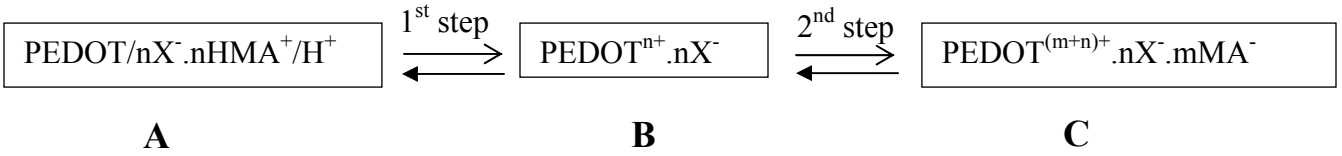

Figure 8.12: Scheme depicting the cation and anion exchange processes for PEDOT films. 1st step denotes the movement of cations into the anion doped film (B) giving the observed cationic response (A) and 2nd step denotes the movement of any anionic species into the film when the doped polymer has any excess cationic sites (C). HMA^+ = protonated form of mandelic acid. MA^- = deprotonated form of mandelic acid. X^-: doping anion.

8.3.3 Effect of pH

Further investigations were carried out to understand the origin of the chiral interactions by studying the speciation of the mandalate ion. This was done by adjusting the pH of solutions containing 1 mM enantiomers of mandelic acid (pK_a=3.4) by using 0.1 M HCl or 0.1 M KOH. The peaks were then deconvoluted and compared with square wave voltammogams of the background solutions *i.e* without the mandelic acid enantiomers. Thus, we were able to identify the transfer of protons (H^+) and (*R*)-(−)-mandelic acid.

At pH 2, the peak potentials were found at 398 mV (PEDOT/collagen), 398 mV (PEDOT/HA) and 368 mV (PEDOT-HPC/ClO_4) (**Figure 8.13**). At this pH (3.83% dissociated-determined by Henderson-Hasselbalch equation), mandelic acid will be primarily in the protonated form (**Figure 8.11a**). Peak 2 (at 140, -21 and -49 mV) are clearly due to the transfer of protons (H^+) whereas peak 1 at 327, 360 and 330 mV for PEDOT/collagen (**Figure 8.14a**), PEDOT/HA (**Figure 8.16a**) and PEDOT-HPC/ClO_4 (**Figure 8.18a**), respectively, may be attributable to the transfer of the protonated (*R*)-(−)-mandelic acid (HMA^+). The most pronounced peak is observed for the PEDOT-HPC/ClO_4 composite (**Figure 8.13**) with a peak current of 35.25 μA compared to 5.70 μA and 12.92 μA for PEDOT/collagen and PEDOT/HA, respectively.

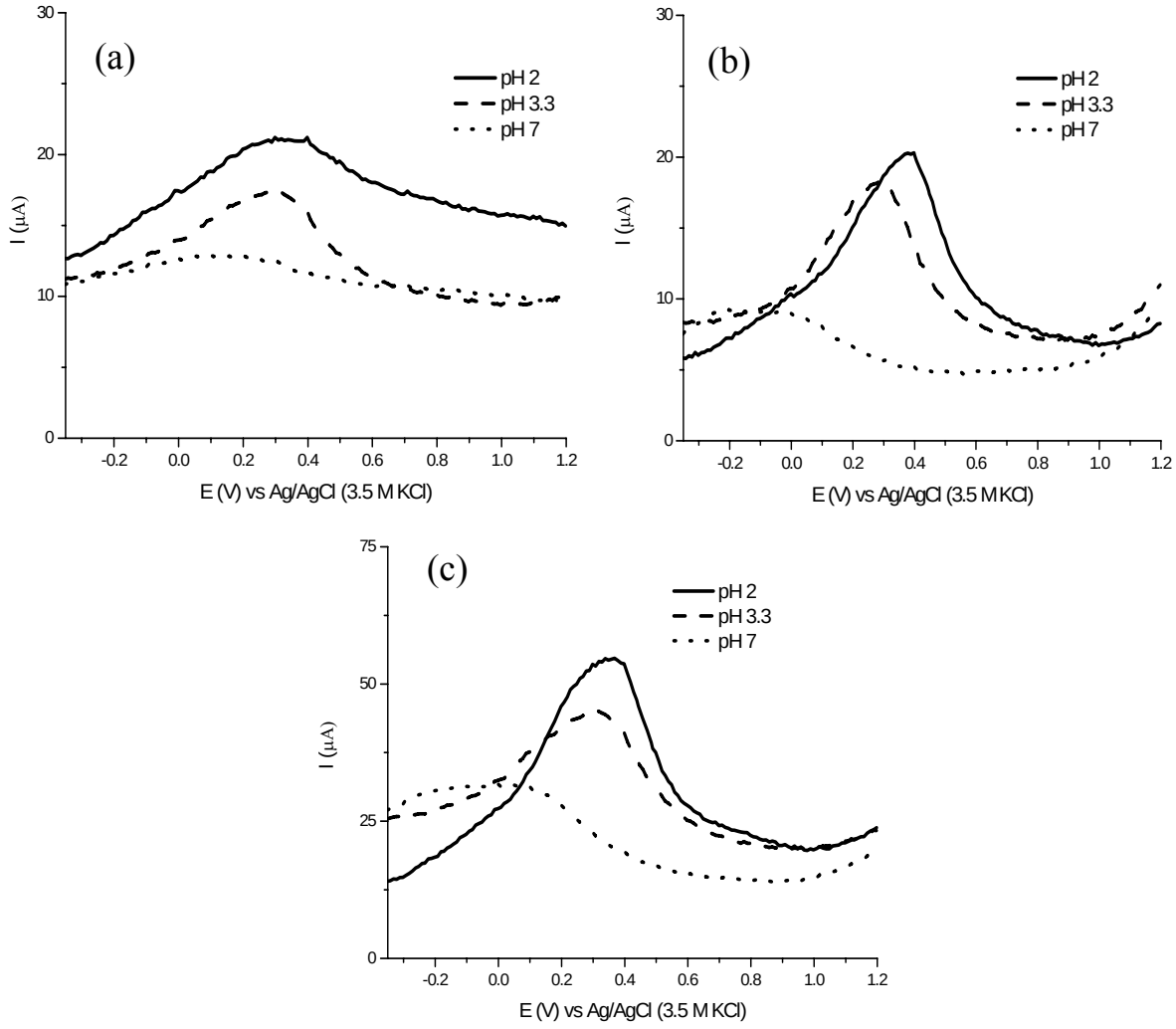

Figure 8.13: Square wave voltammograms of (a) PEDOT/collagen, (b) PEDOT/HA and (c) PEDOT-HPC/ClO_4 in 100 mM KCl containing (*R*)-(−)-mandelic acid at different pHs.

At pH 3.3 (44.27% dissociated), the transfer of protons and (*R*)-(−)-mandelic acid is still evident. However, the currents attributed to peak 1 in each case are lowered to 4.22, 9.14 and 19.32 μA for PEDOT/collagen (**Figure 8.14b**), PEDOT/HA (**Figure 8.16b**) and PEDOT-HPC/ClO_4 (**Figure 8.18b**), respectively.

As the pH moves to more basic (pH 7, 99.97% dissociated), the peak potentials shifted to more negative values *i.e.* 198 mV, -52 mV and -22 mV for PEDOT/collagen,

PEDOT/HA and PEDOT-HPC/ClO_4, respectively. In addition, the current responses at this pH were significantly suppressed (**Figure 8.13**).

Related to the scheme in **Figure 8.12**, the first step is due to the movement of cationic species H^+ and HMA^+ from the anionic polymer film B. This phenomenon was observed at pH 2 and 3.3, as discussed above. The second step denotes the movement of any anionic species (MA^-) into the PEDOT film B when the doped polymer has any excess cationic sites. This is probably explains the weak interaction between chiral PEDOT hybrids and the deprotonated form of mandelic acid (MA^-, **Figure 8.11c**) at pH 7.

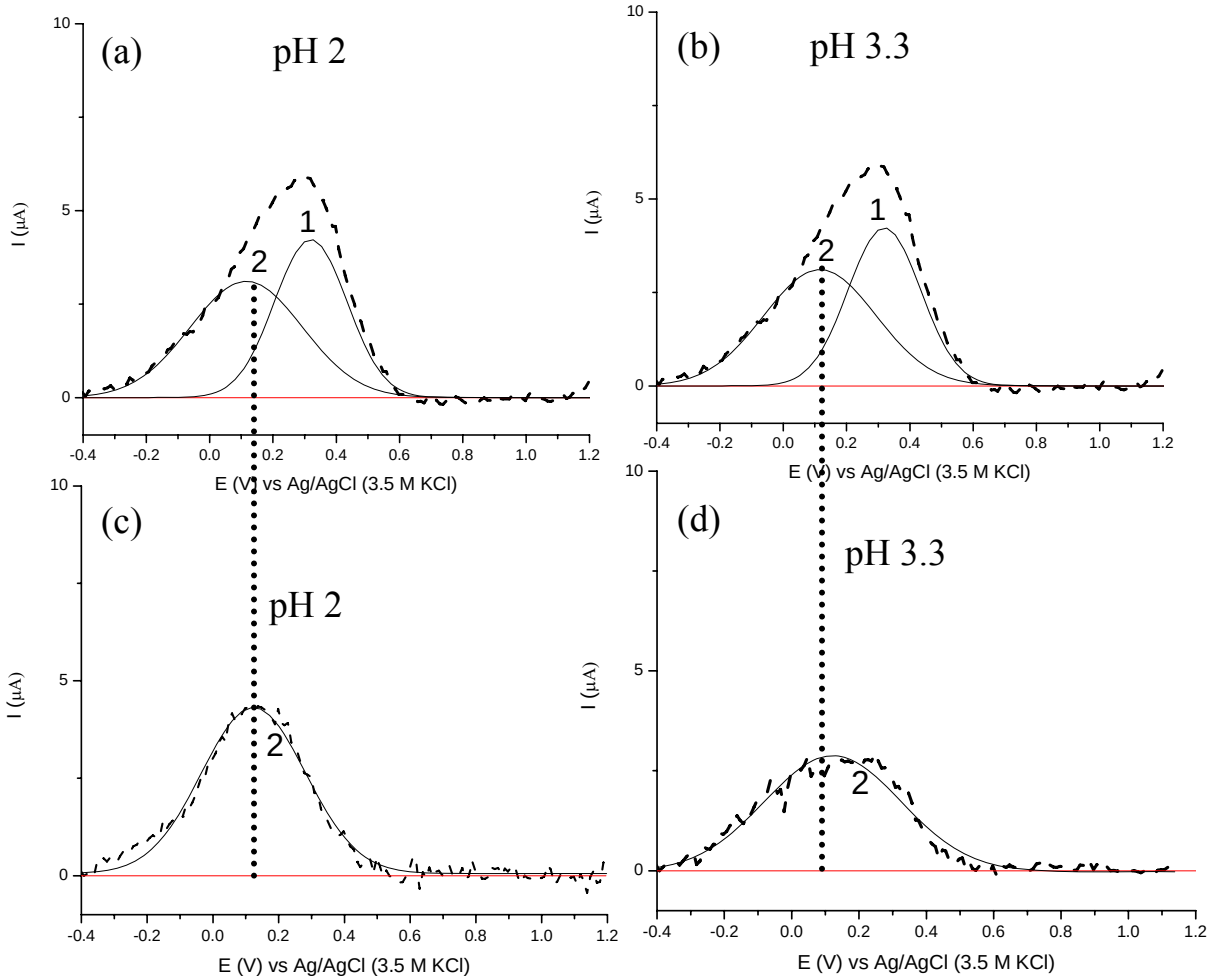

Figure 8.14: Deconvoluted square wave voltammograms of PEDOT/collagen in: (a and b) 100 mM KCl containing (*R*)-(−)-mandelic acid; (c and d) background solution at pH 2 and pH 3.3.

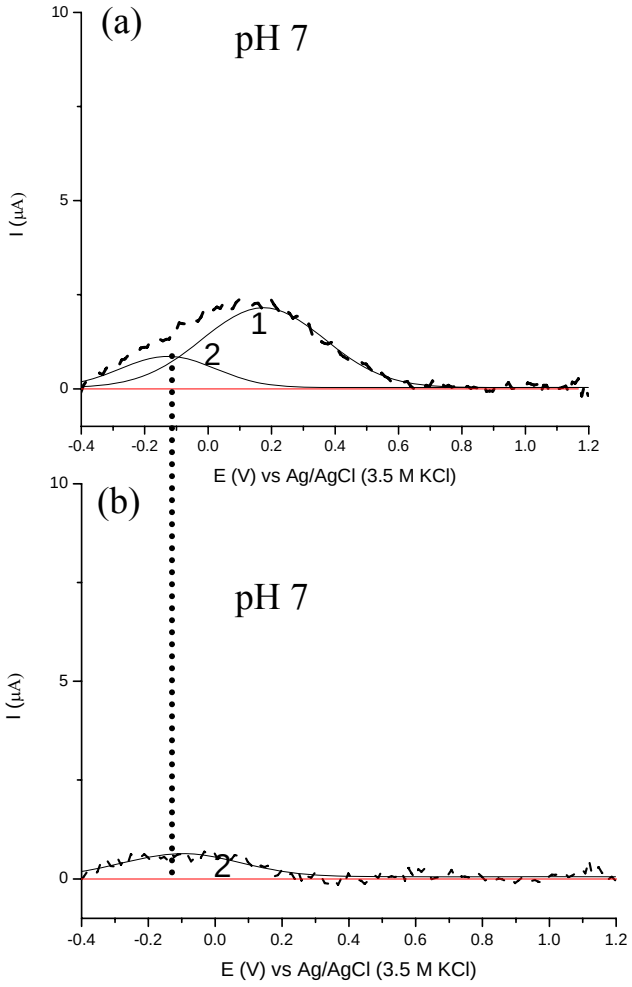

Figure 8.15: Deconvoluted square wave voltammograms of PEDOT/collagen in: (a) 100 mM KCl containing (*R*)-(−)-mandelic acid and (b) background solution at pH 7.

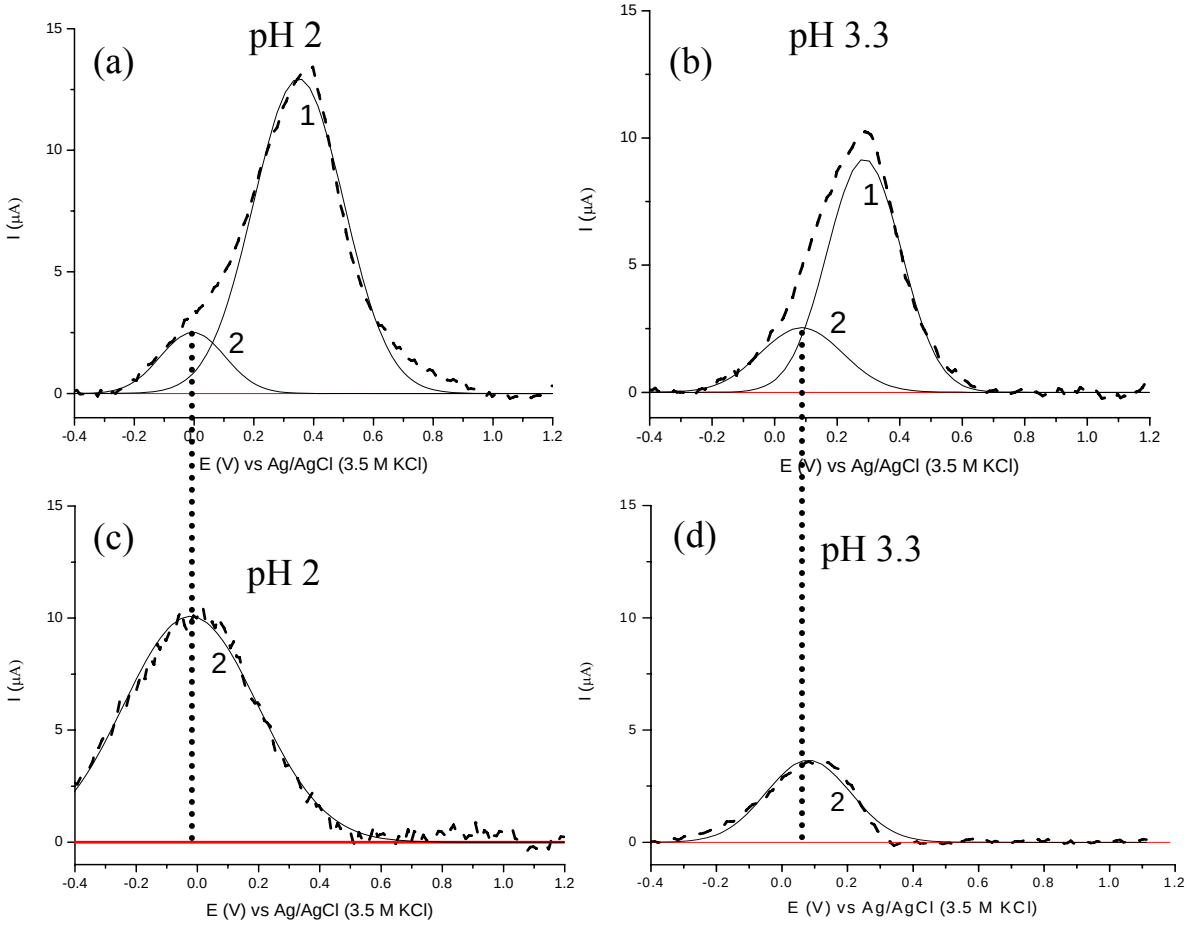

Figure 8.16: Deconvoluted square wave voltammograms of PEDOT/HA in: (a and b) 100 mM KCl containing (*R*)-(−)-mandelic acid; (c and d) background solution at pH 2 and pH 3.3.

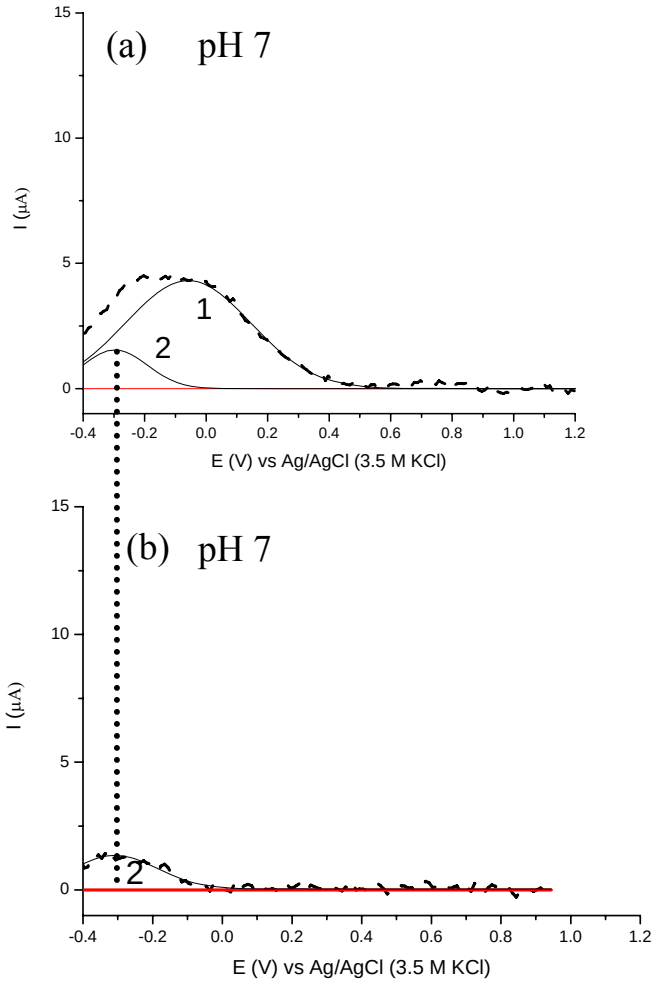

Figure 8.17: Deconvoluted square wave voltammograms of PEDOT/HA in: (a) 100 mM KCl containing (*R*)-(−)-mandelic acid and (b) background solution at pH 7.

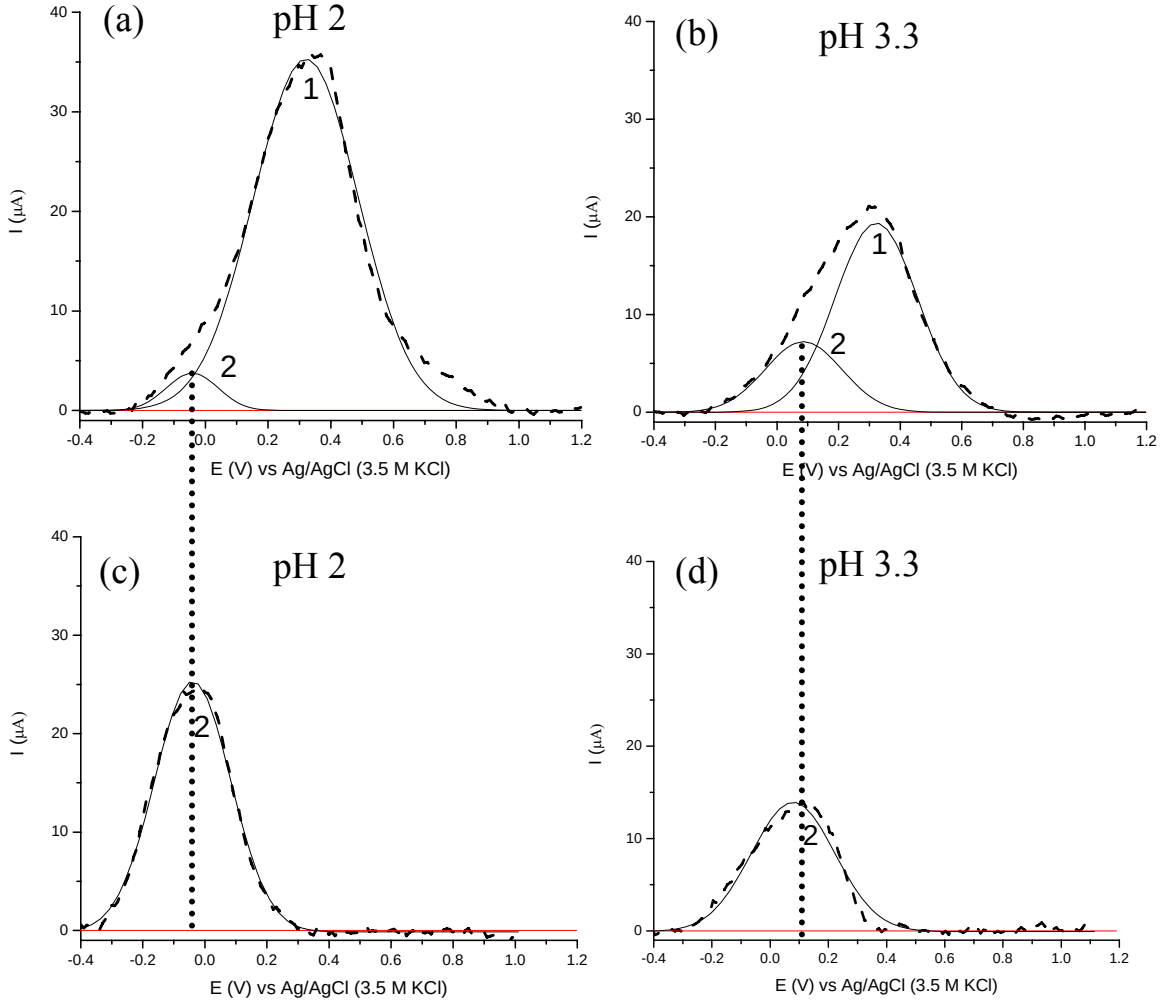

Figure 8.18: Deconvoluted square wave voltammograms of PEDOT-HPC/ClO_4 in: (a and b) 100 mM KCl containing (*R*)-(−)-mandelic acid; (c and d) background solution at pH 2 and pH 3.3.

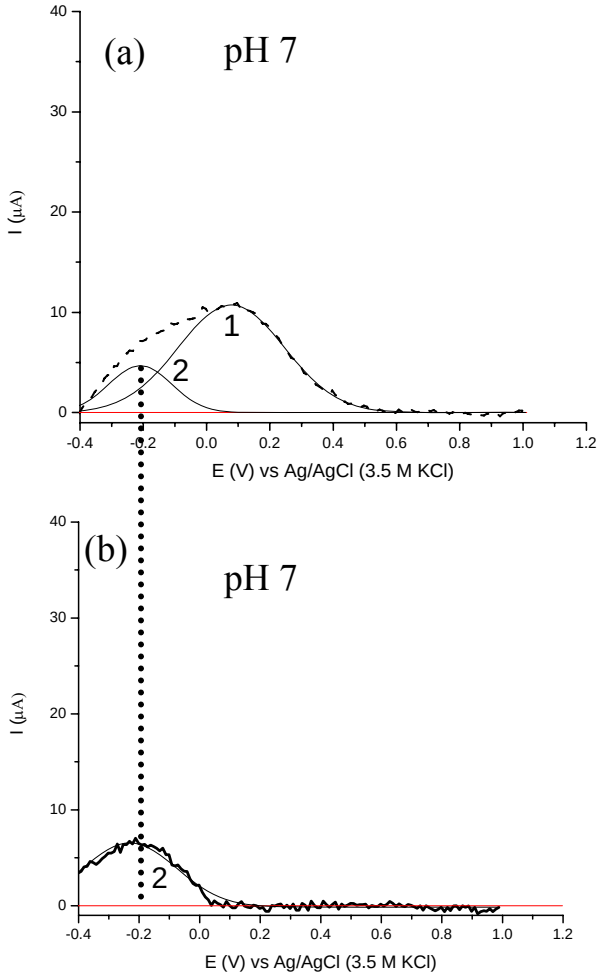

Figure 8.19: Deconvoluted square wave voltammograms of PEDOT-HPC/ClO_4 in: (a) 100 mM KCl containing (*R*)-(−)-mandelic acid and (b) background solution at pH 7.

8.4 Conclusion

Chiral discrimination and separation of chiral acids, using PEDOTs electropolymerised with different chiral molecules *i.e.* collagen, hyaluronic acid and hydroxypropyl cellulose is demonstrated using (*R*)-(−)- and (*S*)-(+)-mandelic acid. Speciation studies at pHs below and above pK_a of the acid revealed the transfer of protons and the chiral transfer of protonated acid between solution and chiral PEDOT modified electrode.

References

Aboutanos, V., Akhtar, P., Kane-Maguire, L. A. P. and Wallace, G. G. (2000) Optically Active Polypyrroles Containing Chiral Dopant Anions. *Australian Journal of Chemistry.* 53**.** 83-87.

Aneja, R., Luthra, P. M. and Ahuja, S. (2010) High-Performance Liquid Chromatography Separation of Enantiomers of Mandelic Acid and Its Analogs on A Chiral Stationary Phase. *Chirality.* 22**.** 479-485.

Bates, P. S., Kataky, R. and Parker, D. (1992) A chiral sensor based on a peroctylated [small alpha]-cyclodextrin. *Journal of the Chemical Society, Chemical Communications.* 153-155.

Bates, P. S., Kataky, R. and Parker, D. (1994) Chiral sensors based on lipophilic cyclodextrins: interrogation of enantioselectivity by combined NMR, structural correlation and electrode response studies. *Journal of the Chemical Society, Perkin Transactions 2.* 669-675.

Bruice, P. Y. (2004) *Organic Chemistry.* (Fourth Ed ed.). Prentice Hall.

Caras-Quintero, D. and Bäuerle, P. (2004) Synthesis of The First Enantiomerically Pure and Chiral, Disubstituted 3,4-Ethylenedioxythiophenes (EDOTs) and Corresponding Stereo- and Regioregular PEDOTs. *Chemical Communications.* 926-927.

Elsenbaumer, R. L., Eckhardt, H., Iqbal, Z., Toth, J. and Baughman, R. H. (1985) Chiral Metals: Synthesis and Properties of a New Class of Conducting Polymers *Molecular Crystals and Liquid Crystals.* 118**.** 111-116.

Fu, Y., Wang, L., Chen, Q. and Zhou, J. (2011) Enantioselective recognition of chiral mandelic acid in the presence of Zn(II) ions by l-cysteine-modified electrode. *Sensors and Actuators B: Chemical.* 155**.** 140-144.

Goto, H. and Akagi, K. (2006) Optically Active Electrochromism of Poly(3,4-Ethylenedioxythiophene) Synthesized by Electrochemical Polymerization in Lyotropic Liquid Crystal of Hydroxypropyl Cellulose/Water: Active Control of Optical Activity. *Chemistry of Materials.* 18**.** 255-262.

Han, D., Yang, G., Song, J., Niu, L. and Ivaska, A. (2007) Morphology of Electrodeposited Poly(3,4-Ethylenedioxythiophene)/Poly(4-Styrene Sulfonate) Films. *Journal of Electroanalytical Chemistry.* 602**.** 24-28.

Kane-Maguire, L. A. P. and Wallace, G. G. (2010) Chiral Conducting Polymers. *Chemical Society Reviews.* 39**.** 2545-2576.

Kataky, R. and Zawawi, R. M. (2010) Modification of the chiral selectivity of D-glucose oxidase and L-lactate oxidase in a collagen matrix. *Physical Chemistry Chemical Physics.* 12**.** 9183-9187.

Li, C. and Imae, T. (2004) Electrochemical and optical properties of the poly(3,4-ethylenedioxythiophene) film electropolymerized in an aqueous sodium dodecyl sulfate and lithium tetrafluoroborate medium. *Macromolecules.* 37**.** 2411-2416.

Mohan, S. J., Mohan, E. C. and Yamsani, M. R. (2009) Chirality and Its Importance in Pharmaceutical Field- An Overview. *International Journal of Pharmaceutical Sciences and Nanotechnology.* 1**.** 309-316.

Ozoemena, K. I., Stefan, R.-I., Staden, J. F. V. and Aboul-Enein, H. Y. (2005) Enantioanalysis of *S*-perindopril using Different Cyclodextrin-based Potentiometric Sensors. *Sensors and Actuators B: Chemical.* 105**.** 425-429.

Trojanowicz, M. and Kaniewska, M. (2009) Electrochemical Chiral Sensors and Biosensors. *Electroanalysis.* 21**.** 229-238.

Vázquez, M., Bobacka, J., Ivaska, A. and Lewenstam, A. (2002) Influence of Oxygen and Carbon Dioxide on the Electrochemical Stability of Poly(3,4-ethylenedioxythiophene) Used as Ion-to-Electron Transducer in All-Solid-State Ion-Selective Electrodes. *Sensors and Actuators B-Chemical.* 82**.** 7-13.

Wade, L. G. (2002) *Organic Chemistry.* Pearson Academic.

Werbowyj, R. S. and Gray, D. G. (1984) Optical Properties of Hydroxypropyl Cellulose Liquid Crystals. I. Cholesteric Pitch and Polymer Concentration. *Macromolecules.* 17**.** 1512-1520.

Yamato, H., Ohwa, M. and Wernet, W. (1995) Stability of Polypyrrole and Poly(3,4-ethylenedioxythiophene) for Biosensor Application. *Journal of Electroanalytical Chemistry.* 397**.** 163-170.

CHAPTER 9

CONCLUSIONS AND FUTURE WORK

9.1 Conclusions

Poly(3,4-ethylenedioxythiophene) (PEDOT) was chosen in this study as this polymer is reported to be the most chemically stable polymer to date due to the presence of two O-electron donating groups at the position 3 and 4 of thiophene that stabilise the structure of PEDOT (Groenendaal *et al.*, 2000). In addition, two PEDOT derivatives *i.e* poly(3,4-propylenedioxythiophene) (PProDOT) and poly(3,3-dibenzyl-3,4-propylenedioxythiophene) (PDBPD) were compared and the physical and electrochemical properties of these polymers were thoroughly examined.

Initially, extensive studies on the characterisation of the electropolymerised polymers were carried out. Fundamental understanding of the properties of conducting polymer is very crucial before any application can be implemented. The work presented in this thesis has shown that PEDOT and its derivatives *i.e*. PProDOT and PDBPD can be successfully electropolymerised in a non-aqueous solution (acetonitrile) and deposited on electronic conductors such as glassy carbon (GC) and indium-tin-oxide (ITO) electrodes. A subtle change in the monomer such as using ProDOT with a seven membered ring instead of an EDOT with six membered ring and introduction of phenyl substituents DBPD can hugely affect the physical and electrical properties of the film. The nature of the film, particularly its thickness and electrical properties also depends on the substrate on which it is deposited. The morphological studies have revealed that conducting polymers deposited on ITO electrodes and GC electrodes appear to be similar. The roughness and porosity of the films formed affect their wettability, giving wettabilities in the order PEDOT > PProDOT > PDBPD.

PEDOT was also electropolymerised using cyclic voltammetry in aqueous solutions GC and ITO electrodes. The films formed were of poor quality, particularly in solutions containing KCl. This observation is believed to result from the fact that the EDOT monomer is only partially dissolved in aqueous solution. However, PEDOT prepared in aqueous $LiClO_4$ solutions produced better morphology as the ClO_4^- is more lipophilic than Cl^- which helps the dispersion of EDOT in an aqueous solution (Gemene *et al.*, 2007). Bulky molecules *i.e.* poly(sodium 4-styrenesulfonate) and hyaluronic acid (HA) which can be immobilised in polymer matrix were also used as doping anions in order to give cationic potentiometric responses in the fabrication of all-solid-state ion-selective electrodes (ASSISEs). The findings reveal that PEDOT doped with PSS in aqueous solution was shown to be superior to PEDOT doped with HA as a solid contact for the fabrication of ASSISEs.

The interfacial charge transfer behaviour of the polymer film modified electrodes was studied using cyclic voltammetry (CV) and electrochemical impedance spectroscopy (EIS). The CV measurements in monomer free solutions have shown that the doping process and the transport of ions occur at the conducting polymer film|solution interface at characteristic potentials depending on the hydrophobicity of the polymer films. Electrochemical impedance spectroscopy (EIS) has proven to be a powerful technique for studying the interfacial properties and demonstrating that the charge transfer properties vary with the film thickness and porosity. These fundamental studies are crucial for the numerous applications of these films. The investigation has also revealed that conducting polymers prepared by galvanostatic methods were smoother than potentiodynamic methods.

Two novel applications of sensor based on PEDOT were demonstrated:

1. All-solid-state ion-selective microelectrodes based on PEDOT/PSS for monitoring extracellular calcium and potassium activities upon plant stress.

2. Chiral sensors using PEDOT containing chiral molecules (hyaluronic acid, hydroxycellulose or collagen) have indicated the ability to discriminate between (*R*)-(−)- and (*S*)-(+)-mandelic acid.

In conclusion, this is the first time detailed, extensive and comparative characterisation of EDOT and its derivatives, ProDOT and DBPD have been carried out (Sulaiman and Kataky, 2012). The all-solid-state ion-selective electrodes in amperometric mode are very suitable for the measurement of well-defined and reproducible Ca^{2+} and K^{+} transients in plants. (Sulaiman *et al.*, 2012). The chiral sensors based on PEDOT can also be used for chiral recognition and separation.

Due to time restraints other applications could not be explored. However, this work has laid the foundation for future work on all-solid-state sensors in bioanalysis, biomedical and environmental applications.

9.2 Future Work

The future direction of this research includes the fabrication of ASSISE with PEDOT containing ion recognition. This approach could be carried out by introducing substituents containing an ion recognition site to the backbone of PEDOT chain or doping the PEDOT with dopant containing an ion recognition site. This approach could eliminate the use of ion-selective membranes. Another possibility is to fabricate ASS ion-selective microelectrode arrays for analysing multiple analyte simultaneously. Further application of PEDOT chiral sensors to other chiral molecules such as tartaric acid and propranolol could be investigated. Comparison of the heterogeneous rate constant (k_o) values for the polymer film modified electrodes on ferri/ferrocyanide by curve fitting using DigiElch software could also be carried out.

References

Gemene, K. L., Shvarev, A. and Bakker, E. (2007) Selectivity Enhancement of Anion-Responsive Electrodes by Pulsed Chronopotentiometry. *Analytica Chimica Acta.* 583**.** 190-196.

Groenendaal, B. L., Jonas, F., Freitag, D., Pielartzik, H. and Reynolds, J. R. (2000) Poly(3,4-Ethylenedioxythiophene) and Its Derivatives: Past, Present, and Future. *Advanced Materials.* 12**.** 481-494.

Sulaiman, Y. and Kataky, R. (2012) Effect of Monomer Modifications On The Physical Properties of Electropolymerised PEDOT Films. *Journal of The Electrochemical Sociecty.* 159**.** F1-F9.

Sulaiman, Y., Knight, M. R. and Kataky, R. (2012) Non-invasive Monitoring of Temperature Stress in *Arabidopsis Thaliana* Roots, using Ion Amperometry. *Analytical Methods.*